Chemistry of *peri*-Naphthoindigo and Analogous Compounds

A Thesis Submitted in Partial Fulfilment of the Requirements for the Degree

of

Doctor of Philosophy

by

Rashmi Jyoti Das

Roll no 136122033

Department of Chemistry

Indian Institute of Technology, Guwahati

Guwahati-781039

Thesis supervisor

Dr. Kingsuk Mahata

Department of Chemistry

Indian Institute of Technology, Guwahati

Guwahati-781039

Dedicated to family and friends

"All knowledge that the world has ever received comes from the mind; the infinite library of the universe is in our own mind."
-Swami Vivekananda

Declaration

I do hereby declare that the research work embodied in this thesis entitled "**Chemistry of *peri*-Naphthoindigo and Analogous Compounds"** has been carried out by me under the supervision of **Dr. Kingsuk Mahata** in the Department of Chemistry, Indian Institute of Technology Guwahati, Assam-781039, India.

In keeping with the general practice of reporting scientific observations, due acknowledgements have been made wherever the work described is based on finding of other investigators.

Guwahati Rashmi Jyoti Das

17th May 2019

Acknowledgement

I would like to take this opportunity to express my earnest gratitude to my thesis supervisor Dr. Kingsuk Mahata. Without his continuous optimism, enthusiasm, encouragement and support this work would hardly reach its novelty. I am grateful for the opportunity of working under his guidance. His sincerity towards critical thinking and the effort will always be my inspiration to work on what I believe.

I would also like to express my sincere gratitude to the doctoral committee: Prof. Parameswar Krishnan Iyer, Dr. Sumana Dutta and Dr. Shyam Prosad Biswas for their insightful comments and encouragement, also for the hard questions which incented me to widen my research from various perspectives.

I thank Department of Chemistry, Central Instruments Facility, IIT Guwahati for allowing me to use the necessary instrumental service for my Ph.D work. I am thankful to the people associated with the smooth running of our laboratory and instrumental facilities. I would also like to acknowledge IIT Guwahati for the financial assistance during the course.

I am definitely thankful to all the fellow lab mates past and present for keeping their calm in the laboratory even when there was literal chaos. I specially thank Indraneel and Tirupati for their support and help during the preparation of this thesis.

Finally, I am taking this opportunity to acknowledge my family and friends. I am thankful towards my parents for their immense belief in me throughout this and my life in general. Last but not the least; I thank Ms. Trinayanee, Hiranaya Jyoti, Hemanta Gogoi, and Shiromoni Bhuyan for bearing with my moods throughout. It's been almost six years since this journey began in July 2013. No matter where I go from here, the things I learned in this campus will always remain with me.

Indian Institute of Technology Guwahati

Dr. Kingsuk Mahata
Assistant Professor
Department of Chemistry
Guwahati, Assam -781039

Phone: +91-361-258-3308
Fax: +91-361-258-2349
Email: kingsuk@iitg.ernet.in

Certificate

This is to certify that Ms. Rashmi Jyoti Das has been working under my supervision since July 2013. I am forwarding her thesis entitled "**Chemistry of *peri*-Naphthoindigo and Analogous Compounds"** being submitted for the Ph. D degree of this institute. I certify that she has fulfilled all the requirements according to the rules of the institute, and regarding the investigations described in this thesis. This work has not been submitted elsewhere for a degree.

Guwahati
2019

Dr. Kingsuk Mahata
Supervisor

Table of Contents

Synopsis

1. Introduction

The ancient dye indigo has been used as brilliant source for blue colour over centuries. Because of its high photo-stability and characteristic colour indigo was and still is produced industrially. As of 2011, annual commercial production of indigo is 50,000 tons.[1] Besides application as textile dye, indigoids have also been used as food colorants, pigments for contact lenses, and ambipolar organic semiconductor.[2] Indigo has also been used as ligand for various metal-complexes.[3] Because of diverse applications, various synthetic modifications have been carried out on indigo to tune the properties. Normally, this is done in two different ways. On one hand, the outer phenyl rings have been substituted at 4-to-7 positions by different groups like halogens, alkyl, cyano etc.[4] On the other hand, modifications of the "H-chromophore" have been reported by replacing one or two N-H group(s) with N-R, oxygen, sulfur, and selenium. All these modifications led to generation of wide variety of ring-[4] and N-substituted indigoids[5], oxindigo[6], thioindigo[7], and selenoindigo[8] dyes (Figure 1).

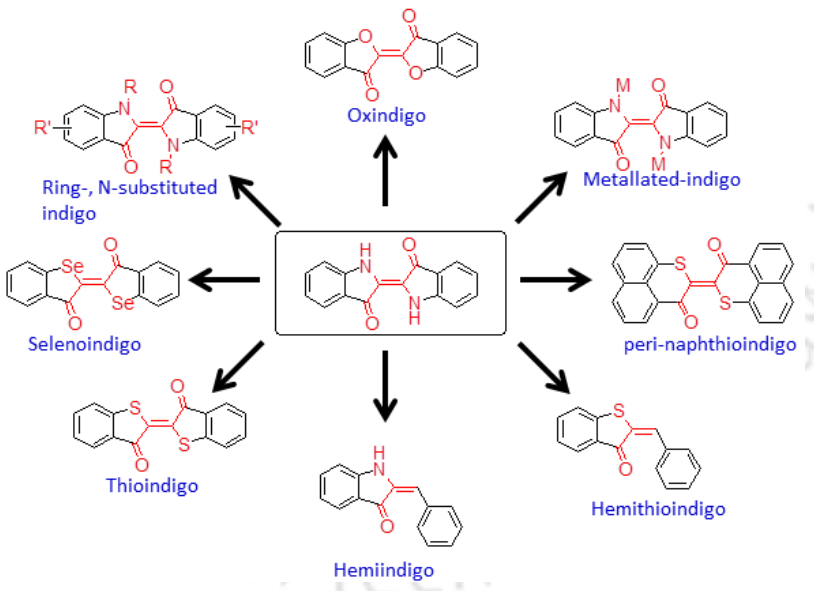

Figure 1. Structure of indigo and its analogues.

The synthetic alternations not only produce new molecules, but exhibit exciting properties. For examples, photochromism have been reported on N,N'-disubstituted indigos and thioindigo dyes. Partial modification of the chromophore directed to generation of hemiindigo[9] and hemithioindigo[10]. The synthetic alternations not only produce new molecules, but exhibit exciting properties. Hemiindigos are known to show bistable photoswitching at biooptical window. Owing to the vast range of

structural modifications and multidisciplinary applications of the same, the "century old" indigo is still a fascinating molecule to work with. and quest for new indigoid is an expanding field of research.

1.1 Research objective

In pursuit for new indigoid structures, installation of the parent H-chromophore of indigo sandwiched into the *peri*-positions of two naphthalene moieties would result into *peri*-naphthoinigo (PNI) (Figure 2). In fact, the structure of PNI was proposed first time in a U.S. patent in 1977 by R. A. Nathan and his co-workers.[11] Another theoretical report by Zhang *et. al*,[12] predicted PNI to show better performance as ambipolar organic semiconductor material than indigo. Encouraged by these reports and prospective of the molecule the primary goal of this thesis work was to synthesize PNI and investigation of its various molecular properties. We also wanted to explore other possibilities such as self-sorting with other naphthalene based dyes. Presence of chromophore as well as two naphthalene rings also presents with possibilities towards further modification of the structure.

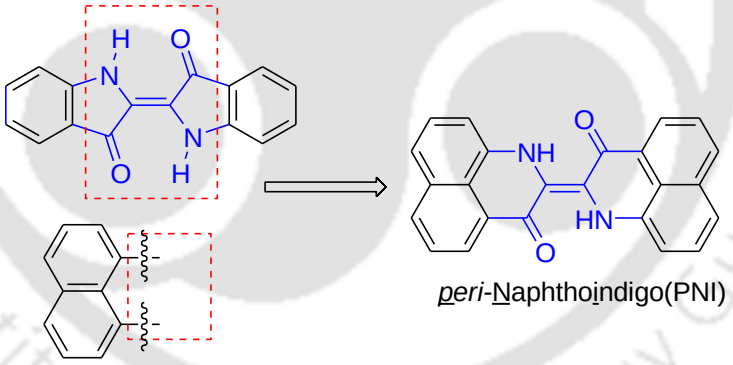

Figure 2: Structure of *peri*-Naphthoindigo.

1.2 Research summary

Chapter 2 in the thesis contains a brief discussion of synthetic trials went into this compound. The fundamental impact of steric as well as electronic control imposed on 1,8-*peri* positions of naphthalene resulted into success of the specified reaction condition.

Chapter 3 comprises of investigation on the photophysical, aggregation, electrochemical and halochromic behaviour of the synthesized molecule. Discrete knowledge of such molecular properties is useful towards development of application the dye.

Successful utilization of various co-self-assembly processes to prepare heteromeric aggregates with PNI comprises the discussions included in Chapter 4. Installation of AIEE to the generated co-aggregates, along with presence of FRET process and dual emission is a benchmark attained in this chapter.

Chapter 5 is a compilation of attempts towards derivatization of PNI. Multiple new structures based on PNI, generated via metal-complex formation and substitution of the dye adds characteristic features to this new dye's chemistry.

Finally, chapter 6 is a note on the achieved goals and their future possibilities. The experimental details of all the procedures along with synthetic, spectroscopic as well as other details are included in chapter 7 of the thesis.

2. Result and discussion

Chapter 2. Synthesis and characterization of PNI

The synthesis of PNI was proven to be challenging. Many analogous methods, known for indigo synthesis, have been tried using appropriate starting materials. However, all attempts were turned out to be unsuccessful. Finally, PNI was synthesized successfully in single step from 8-nitro-1-acetylnaphthalene (**2**) using B_2pin_2 and KF in ethanol (Scheme1).[13] The formation of PNI occurs via reductive cyclization of the enol form of 8-nitro-1-acetylnaphthalene, followed by dimerization and oxidation. Keeping the probable mechanistic pathway in mind, the reaction condition was optimized by changing solvents, bases and reagents. The best combination was found to be B_2pin_2 and KF in ethanol under aerial atmosphere. The structure of the dye was established by using a combination of high-resolution mass spectrometry (HRMS), 1D and 2D NMR, IR spectroscopy. Unlike indigo, PNI was found to exist in mono-enol isomer.

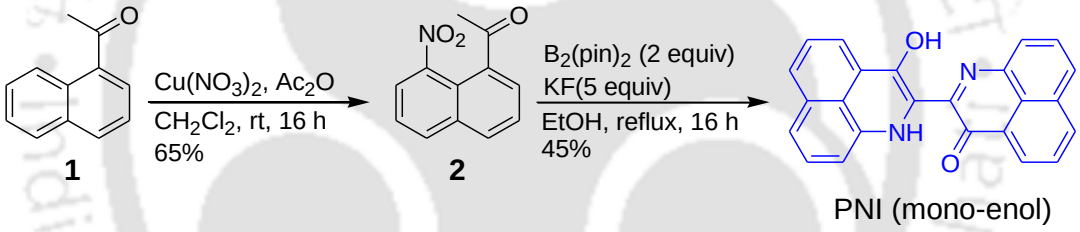

Scheme 1. Synthetic route of PNI.

Table 1. Effects of solvent and base on **PNI** synthesis.

entry	base	solvent	yield (%)[a]
1	KF	EtOH	21[b]
2	**KF**	**EtOH**	**65**
3	Cs_2CO_3	EtOH	55
4	K_2CO_3	EtOH	55
5	CsF	EtOH	25
6	NaOH	EtOH	trace
7	^{t}BuOK	EtOH	trace
8	AcOK	EtOH	10
9	KF	1,4-dioxane	trace
10	KF	MeOH	trace
11	KF	toluene	trace

Chapter 3. Photophysical, aggregation, electrochemical and halochromic behavior of PNI

Detailed studies on photophysical, electrochemical, aggregation and halochromic properties of PNI were done. Compared to the phenyl analogue, PNI exhibits a red shifted stronger absorption maxima. The dye shows very strong (ε = 29390 $M^{-1}cm^{-1}$) absorption band with maxima varying from 611 nm (in acetonitrile, blue solution) to 632 nm (in chloroform, turquoise solution). Steady state emission of PNI was observed in the near infra-red (NIR) region with maxima at around 736 nm (chloroform). Similar to indigo, the relative quantum yield of PNI was found to be low (0.003 in THF). Solvent dependent UV-vis spectroscopic investigations didn't show any significant change in absorption behavior, suggesting its existence in the mono-enol form in all solvents.

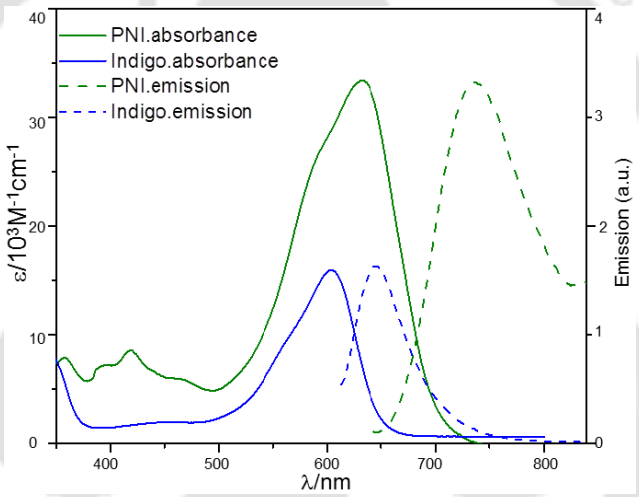

Figure 3. Absorption and emission spectra of PNI and indigo in $CHCl_3$.

The aggregation property of PNI was explored by changing solvent and concentration. The dye underwent multiple self-assembly processes in DMSO as well as DMSO-water mixtures. However the high concentration demand for the process in DMSO, limited the scope for photophysical investigation. The self-assembly process was installed at low concentration using a polar solvent combination of DMSO-water (1:9 v/v). Formation of self-assembled structures via π-π interaction of the naphthyl rings was evident from the FESEM images of the aggregate. The most intriguing case of aggregation was observed in a mixture of THF and hexane (1:9 v/v). Formation of rigid microcrystalline cuboid architectures, result into vibronic decoupling of the absorption behaviour followed by emission enhancement. Morphological investigation using FESEM suggested the generation of uniform cuboid morphology via a combination of intermolecular H-bonding and π- π stacking.

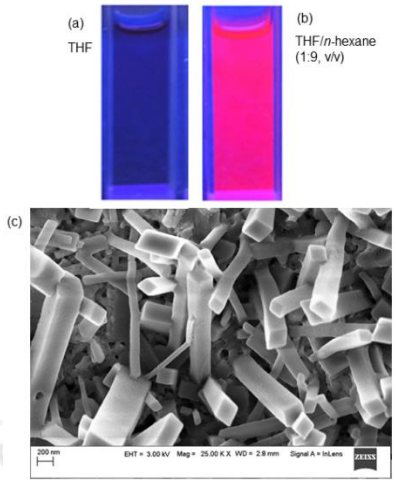

Figure 4. (a) PNI in THF, (b)AIEE of PNI in a solvent mixture of THF/ *n*-hexane(v/v = 1/9), (c) FESEM image of PNI aggregates obtained from a solvent mixture of THF/ *n*-hexane(v/v = 1/9).

PNI undergoes oxidation and reduction at 0.30 V and –0.58 V (vs Fc/Fc^{+}) respectively. From the electrochemical data, the HOMO-LUMO energy gap was calculated to be 0.88 eV. Compared to the indigo, the HOMO-LUMO gap was found to be lower. In acidic pH PNI was halochromic in nature. Addition of acid (e.g. CF_3CO_2H, HCl etc.) to an acetonitrile solution resulted in visible colour change from blue to green. The process of halochromism was also established from spectroscopic (UV/vis and ^1H NMR) measurements. In acetonitrile, upon acidification, absorption maxima of PNI shifted bathochromically to 681 nm from 611 nm with increase in color intensity (ε = 56815 $M^{-1}cm^{-1}$). Such bathochromic shift associate with protonation is known in indigo and other dyes. Protonation process is reversible and the initial spectrum can be recovered simply by addition of base (NaOH, NH_4OH). Halochromism process was observed in other solvent (chloroform, dioxane).

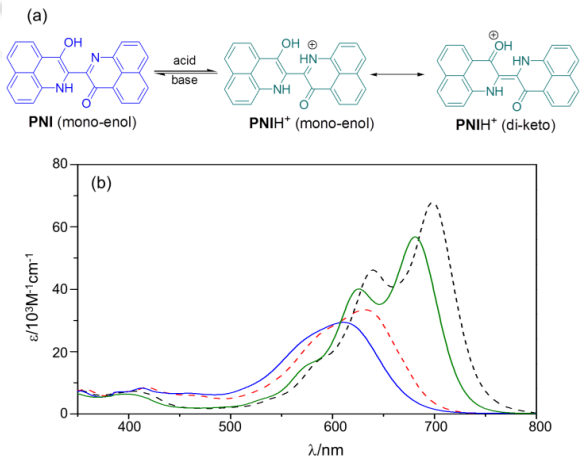

Figure 5. (a) Halochromism of PNI. (b) Absorption spectra (293 K, c ≈ 10^{-5} $molL^{-1}$) of PNI in chloroform (red, dash), acetonitrile (blue, solid), and $PNIH^{+}$ in chloroform (black, dash), acetonitrile (olive, solid).

Chapter 4. Self-sorted co-assembly of PNI and 1,8-naphthalimide based dyes

Self-sorting in self-assembly processes is an excellent tool for construction of complex supramolecular structures in a multi-component mixture. Utilizing the design principles of artificial self-sorting, two 1,8-naphthalimide based dyes (H-NMI, NH_2-NMI) were prepared. These bulky imide-containing dyes were used to prepare heteromeric co-aggregates with PNI (Figure 6a). PNI undergoes social self-sorting with both H-NMI and NH_2-NMI in a solvent mixture of THF/*n*-hexane (v/v = 1:9) to form long ribbon shaped morphologies (Figure 6b). In case of PNI/H-NMI co-aggregate, emission enhancement was observed for PNI while H-NMI remained non-emissive. But, mutual enhancement of emission was achieved in the co-aggregate between NH_2-NMI and PNI. Increments in steady state emission intensities were calculated to be 28% for the imide and more than 400% for PNI. In addition to successful merger of social self-sorting with AIEE, spectral overlap between the emission of NH_2-NMI and the absorption of PNI enabled FRET from the imide to PNI. The resultant co-aggregate of PNI/NH_2-NMI was also dual emissive in nature when excited at 410 nm. Such vibrant features obtained due to self-sorting holds the possibility of adding advantages in many applications that requires proper tuning of photophysical behaviour. The photophysical characteristics of the multi-component assemblies (broad absorption band with emission in the NIR region) can also be useful for efficient light-energy harvesting.

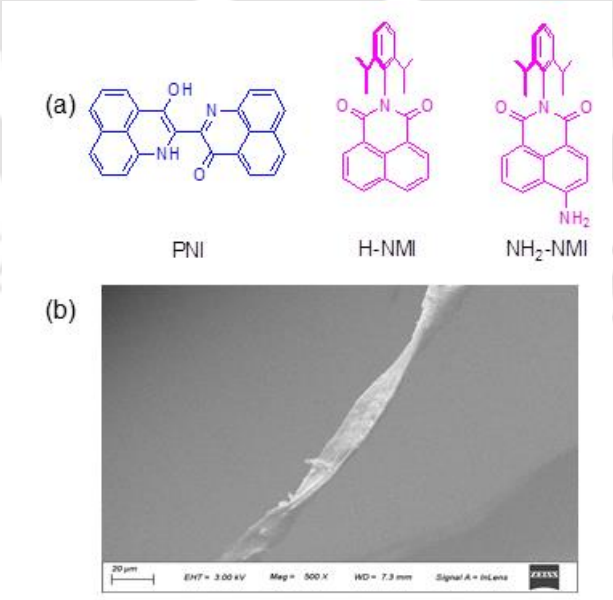

Figure 6. (a) Dye molecules used for self-sorting processes; (b) FESEM image of a co-aggregate formed between PNI and H-NMI.

Chapter 5. Derivatives of PNI

Various modifications on PNI have been described in this chapter. The dye was found to be a bidentate ligand and produced 2:1 (PNI:Pd) complex. The coordination compound was characterized by a combination of mass spectrometry and ^{1}H-NMR spectroscopy. Although four different complexes are possible, only one was produced in the reaction. Theoretical investigation along with ^{1}H-NMR spectroscopy suggested **Pd2** (Figure 7) to be the most stable structure. Compared to PNI, the complex shows red shifted absorption maxima. The emission property quenched completely after metallation.

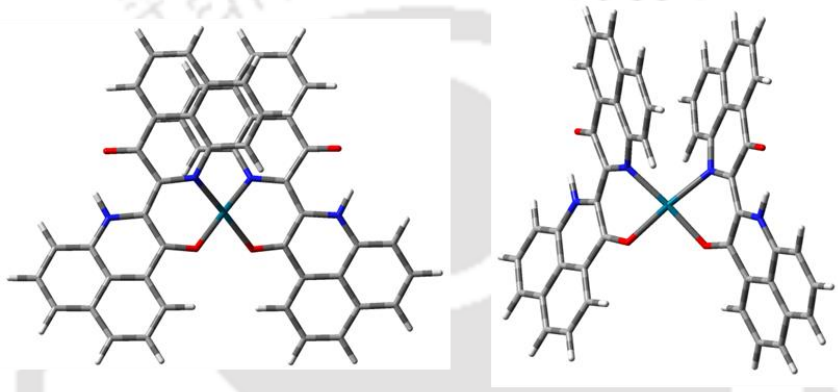

Figure 7. Energy optimized structures of palladium complex of PNI.

Alkylation of PNI was attempted with various alkyl halides. Most of the reactions were found to be unfruitful. Instead of the desired N-alkylated and/or O-alkylated product(s), decomposition of PNI was observed when NaH was used as base. Characterization of the dissociation product confirmed formation of N-substituted lactam (Scheme 2). Such kind of dissociation is common in indigoids under various conditions.

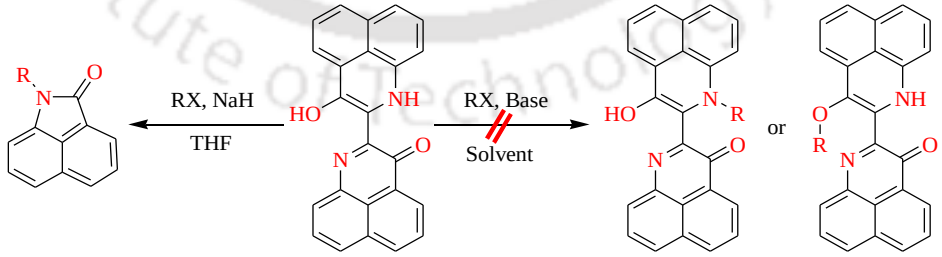

Scheme 2. Synthetic attempts for substitution of chromophoric unit of PNI.

Effect of substitution in the naphthalene rings was explored by targeting synthesis of Br-PNI (Scheme 3). The compound was prepared from 1-bromonaphthalene in three steps. Bromo substitution decreased solubility and limited its characterization by NMR spectroscopy. However, its structure was established by HRMS. Compared to PNI, the

substituted dye exhibited red shifted absorption maxima (642 nm) in chloroform. The substituted dye was also found to halochromic. Spectral changes are found to be similar with the parent molecule (Figure 8). Bromo substituted PNI exhibited photoluminescence in the NIR region with maxima at 753 nm (chloroform).

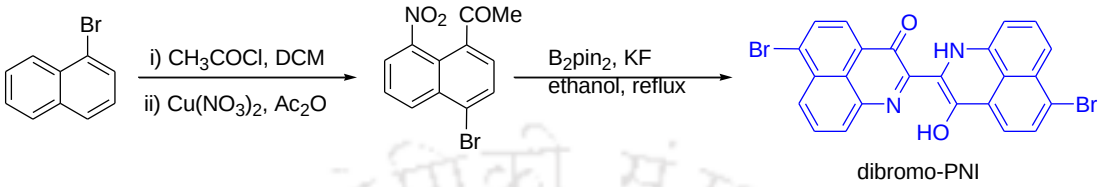

Scheme 3. Synthetic route of brominated-PNI.

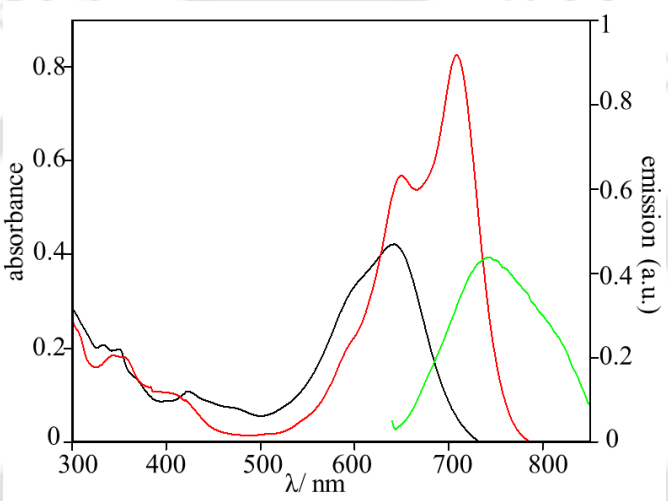

Figure 8. Absorption spectra of dibromo-PNI (black), dibromo-PNI-H^+ (red) and emission spectrum of dibromo-PNI (green) in chloroform.

Chapter 6. Conclusion and Future prospective

In summary, PNI was successfully synthesized from 8-nitro-1-acetylnaphthalen and characterized using a combination of HRMS, NMR and IR spectroscopic techniques. Change in surrounding of chromophore marks huge difference in property as well as in synthetic difficulty. Unlike other indigoids, the isolated dye was identified as the mono-enol isomer of PNI. Successful installation of molecular processes like AIEE, halochromism and social self-sorting makes PNI a promising candidate for multiple applications. Further derivatization of the dye provides the possibility for a diverse library of dye molecules.

References

1. L. K. Wolf, *Chem. Eng. News*, **2011**, *89*, 44.
2. (a) K. H. Ferber, *J. Environ. Pathol., Toxicol. Oncol.* **1987**, *7*, 73-83; (b) A. G. Newsome, C. A. Culver, R. B. van Breemen, *J. Agric. Food Chem.* **2014**, *62*, 6498−6511; (c) M. Irimia-Vladu, E. D. Głowacki, P. A. Troshin, G. Schwabegger, L. Leonat, D. K. Susarova, O. Krystal, M. Ullah, Y. Kanbur, M. A. Bodea, V. F. Razumov, H. Sitter, S. Bauer, N. S. Sariciftci, *Adv. Mater*. **2012**, *24*, 375-380; (d) E. D. Głowacki, G. Voss, N. S. Sariciftci, *Adv. Mater*. **2013**, *25*, 6783-6800; (e) M. Gsänger, D. Bialas, L. Huang, M. Stolte, F. Würthner, *Adv. Mater*. **2016**, *28*, 3615-3645.
3. (a) J.-Y. Wu, C.-H. Chang, P.Thanasekaran. C.-C. Tsai, T.-W. Tseng, G.-H. Lee, S.-M. Peng, K.-L. Lu, *Dalton. Trans.* **2008**, 6110-6112; (b) D. Bhattacharya, C.-H. Chang, Y.-H. Cheng, L. –L. Lai, H.-Y. Lu, C.-Y. Lin, K.-L. Lu, *Chem. Eur. J.* **2012**, *18*, 5275-5283; (c) P. Mondal, A. Das, G. K. Lahiri, *Inorg. Chem.* **2016**, *55*, 1208-1218; (d) P. Mondal, M. Chatterjee, A. Paretzki, K. Beyer, W. Kaim, G. K. Lahiri, *Inorg. Chem.* **2016**, *55*, 3105-3116; (e) D. V. Konarev, L. V. Zorina, S.S. Khasanov, A. F. Shestakov, A. M. Fatalov, A. Otsuka, H. Yamochi, H. Kitagawa, R. N. Lyubovskaya, *Inorg. Chem.* **2018**, *57*, 583-589; (f) M. Chatterjee, P. Ghosh, K. Beyer, A. Paretzki, J. Fiedler, W. Kaim, G.K. Lahiri, *Chem. Asian J.* **2018**, *13*, 118-125.
4. (a) P. Friedländer, *Ber. Dtsch. Chem. Ges*. **1909**, *42*, 765-770; (b) J. C. Duff, *J. Chem. Soc., Trans.* **1914**, *105*, 2182-2186; (c) I. T. Shadi, B. Z. Chowdhry, M. J. Snowden, R. Withnall, *Chemm. Commun*. **2004**, 1436-1437.
5. (a) C. R. Giuliano, L. D. Hess, J. D. Margerum, *J. Am. Chem. Soc*. **1968**, *90*, 587-594; (b) A. Nuñez, T. Hollebeek, M. M. Labes, *J. Am. Chem. Soc.* **1992**, *114*, 4925-4926; (c) D. Farka, M. Scharber, E. D. Głowacki, N. S. Sariciftci, *J. Phys. Chem. A* **2015**, *119*, 3563-3568; (d) C.-Y. Huang, A. Bonasera, L. Hristov, Y. Garmshausen, B. M. Schmidt, D. Jacquemin, S. Hecht, *J. Am. Chem. Soc.* **2017**, *139*, 15205-15211.
6. (a) K. Fries, A. Hasselbach, *Ber. Dtsch. Chem. Ges.* **1911**, *44*, 124-128; (b) R. Stoermer, K. Brachmann, *Ber. Dtsch. Chem. Ges*. **1911**, *44*, 315-319; (c) F. Bruin, F. W. Heineken, M. Bruin, *J. Org. Chem*. **1963**, *28*, 562-564; (d) H. Langhals, B. Wagner, *Angew. Chem. Int. Ed.* **1996**, *35*, 1016-1019.
7. (a) P. Friedländer, *Ber. Dtsch. Chem. Ges.* **1906**, *39*, 1060-1069; (b) L. Dinescu, R. P. Lemieux, *Adv. Mater*. **1999**, *11*, 42-45; (c) D. Jacquemin, J. Preat, V. Wathelet, M. Fontaine, E. A. Perpète, *J. Am. Chem. Soc.* **2006**, *128*, 2072-2083; (d) R. Rondão, J. S. Seixas de Melo, *J. Phys. Chem. C* **2013**, *117*, 603-614; (e) M. Dittmann, F. F. Graupner, B. Maerz, S. Osterling, R. de Vivie-Riedle, W. Zinth, M. Engelhard, W. Lüttke, *Angew. Chem. Int. Ed.* **2014**, *53*, 591-594; (f) G. Boice, B. O. Patrick, R. McDonald, C. Bohne, R. Hicks, *J. Org. Chem*. **2014**, *79*, 9196-9205.

8. (a) D. R. Ross, J. Blanc, F. J. Matticoli, *J. Am. Chem. Soc.* **1970**, *92*, 5750-5752; (b) H. Bauer, K. Kowski, H. Kuhn, W. Lüttke, P. Rademacher, *J. Mol. Struct.* **1998**, *445*, 277-286; (c) R. Gerke, L. Fitjer, P. Müller, I. Usón, K. Kowski, P. Rademacher, *Tetrehedron* **1999**, *55*, 14429-14434.

9. (a) C. Petermayer, S. Thumser, F. Kink, P. Mayer, H. Dube, *J. Am. Chem. Soc*. **2017**, *139*, 16060-16067; (b) C. Petermayer, H. Dube, *Acc. Chem. Res.* **2018**, *51*, 1153-1163.

10. (a) S. Wiedbrauk, B. Maerz, E. Samoylova, A. Reiner, F. Trommer, P. Mayer, W. Zinth, H. Dube, *J. Am. Chem. Soc.* **2016**, *138*, 12219-12227; (b) F. Kink, M. Collado, S. Wiedbrauk, P. Mayer, H. Dube, *Chem. Eur. J.* **2017**, *23*, 6237-6243; (c) L. A. Huber, K. Hoffmann, S. Thumser, N. Böcher, P. Mayer, H. Dube, *Angew. Chem., Int. Ed.* **2017**, *56*, 14536-14539; (d) J. E. Zweig, T.R. Newhouse, *J. Am. Chem. Soc.* **2017**, *139*, 10956-10959.

11. R. A. Nathan, R. E. Schwerzel, A. H. Adelman, R. E. Wyant, U.S. Patent, 4004572, 1977.

12. S.-F. Zhang, X.-K. Chen, J.-X. Fan, A.-M. Ren, *Org. Electron.* **2015**, *24*, 12-25.

13. K. Yang, F. Zhou, Z. Kuang, G. Gao, T.G. Driver, Q. Song, *Org. Lett.* **2016**, *18*, 4088-4091.

List of Abbreviations

General terminology

NMR	Nuclear magnetic resonance
FESEM	Field emission scanning electron microscope
HRMS	High resolution mass spectrometry
IR spectroscopy	Infra -red spectroscopy
Uv-vis	Ultra violet and visible spectroscopy
XRD	X-ray diffraction
HOMO	Highest occupied molecular orbital
LUMO	Lowest unoccupied molecular orbital
FRET	Forster resonance energy transfer
AIEE	Aggregation induced enhanced emission
ESIPT	Excited state intramolecular proton transfer
MOF	Metal-organic framework
SCC	Supramolecular coordination complex
DSSC	Dye sensitized solar cell
NIR	Near infra-red

Mathematical Symbols

λ	Wave length
ϕ_F	Fluorescence quantum yield
ϵ	Molar extinction co-efficient
f_w	Volume fraction of water
f_h	Volume fraction of hexane

Units

V	Volt
eV	Electron Volt
µm	Micro meter
nm	Nano meter
ppm	Parts per million
Hz	Hertz

K	Kelvin
^{o}C	Degree celsius

Chemical symbols

DCM	Dichloromethane
THF	Tetrahydrofuran
DMF	N,N'-dimethyl formamide
MeCN	acetonitrile/methyl cyanide
DMSO	dimethyl sulfoxide
$CHCl_3$	Chloroform
^{t}BOC	tert-Butyloxycarbonyl
^{t}Bu	tert-Butyl

Chapter 1
Introduction

1.1 Foreword

Indigo is known as one of the most light-stable organic dyes with a characteristic blue color. On account of its presence in nature and longevity, indigo is a molecule often linked with mysticism whose synthesis triggered the beginning of modern chemical industry.[1] The roots of development of modern chemistry principally emerged from the historical dye chemistry.[2] Although the journey of indigo started as dyeing agent, the fascinating molecule has been used in many other areas including organic electronic, food industry etc. in recent time. Because of such diverse applications, indigo and its derivatives have created interest among the scientific community towards extensive and systematic exploration of chemical and physical properties of these molecules. The historical dye indigo has impacted the course of socio-economic as well as scientific evolution into the present state of human civilization. It also emphasized the potential of a small molecule in modern applications. Another noteworthy observation in this search was the ubiquity of the 1,8-positions of the naphthalene ring and its impact towards realization of a molecular structure that has been imaginary for decades.

1.2 History of indigo

Indigo dyeing is recognized as one of the oldest known biotechnologies in the course of civilization. As evident from multiple archaeological evidences the practice of indigo dyeing dates back to 4000 BC and was mastered in diverse forms by civilizations in Asia, Europe, and the Americas.[3,4,5] The name “indigo” was termed in the ancient Greece based on its origin from the river-valleys of Indus, where traces of the Indian-Harappan civilization were found. Unlike other colors of the visible spectrum with multiple natural sources, indigo was the only available blue dye for textiles. Because of this, all through the past cultures indigo

dyed garments were particularly valuable and were considered as symbol of wealth and power.[4] Bio-originated indigo was extracted from the plants *Indigofera tinctoria* and *Isatis tinctoria*. The 'true' indigo plant *Indigofera tinctoria* was of Indian origin and contained 30 times more indigo precursor compared to the other plant known commonly known as Dyers' Woad in the Europe.[6]

Figure 1. (a) *Indigofera tinctoria,* the tropical plant-source of indigo; (b) the "Madonna in the Rose Bower" by Stephan Lochner (ca. 1410–1451); (c) a scrap of indigo-dyed fabric between 5,585 and 5,848 years old.

From these plants indigo was prepared from glycosidic precursors named indican, a chemical entity with an indoxyl ring attached to a sugar molecule. The biochemical starting point of such molecules is amino acid tryptophan. Bio-chemical synthesis of indigo starts with fermentation of the raw indigo plant matter to accomplish an enzymatic cleavage of the glycosidic precursor. The resultant molecule indoxyl, then undergoes oxidative dimerization in presence of aerobic oxygen to produce a highly-insoluble blue indigo mass.[7]

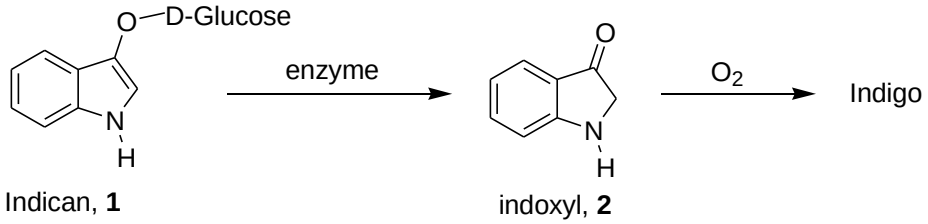

Scheme 1. Natural synthetic route to indigo from indican (glycosidic precurssor) in *Indigofera tictoria*.

Indigo is a water insoluble dye. However, for dyeing purpose it is reduced to water soluble leuco form. The reduced indigo readily penetrates the textile fibres dipped into the solution of leuco indigo, called vat. Once the textile is taken out of the dye bath, re-oxidation of the leuco indigo produced insoluble blue indigo in presence of air. In this process the indigo dye trapped inside the textile fibres produce blue dyed textile. This process is known as vat dying. The chemical reduction of indigo in pre-modern times was achieved either using sugar fermentation producing NADH or by using metals like zinc as reducing agents. The economic impact of natural-origin indigo reflects deep into the world history. In the Middle Ages woad was extensively cultivated in Europe and at the same time small volumes of the indigo pigment from *Indigofera* was imported from India. In the 18th century, with expansion of the British colonization, higher quality indigo from India, derived from the plant *Indigofera tinctoria*, was imported to Europe. As a result, the European woad-industry started to sink and India became the major exporter of natural-origin indigo. According to reports in 1897, 6,000 tonnes of natural indigo were produced.[2] Prior to that, in 1853, at the time of the Californian gold-rush, Levi Strauss set up a wholesale business of haberdashery in San Francisco. He produced special canvas pants for the gold-diggers. In 1873, Levi Strauss obtained a patent for his designs. His products gained huge acceptance and over time particularly the indigo-coloured denim became the "blue jeans".[2] In modern times, indigo is the most produced dyestuff world-wide due to its use in blue jeans. In the meantime, the on-going pursuit for economically viable and superior quality dye-stuff saw an incredible breakthrough with Adolf von Baeyer's success in indigo synthesis as well as structure elucidation of the dye.[8] Successful commercialization of synthetic indigo by BASF based on Baeyer's work followed by necessary modifications developed by Karl Heumann and Jhon Pfleger resulted into a market dominated by synthetic indigo which eventually took over the nature-origin product.[2]

1.3 Structure elucidation and first chemical synthesis of indigo

The first documented work on indigo was done by Otto Paul Unverdorben (1806–1873) in 1826 to elucidate the structure of the dye. Unverdorben attempted distillation of indigo with lime and obtained aniline. Under milder conditions the same methodology produced anthranilic acid. On continuation of these findings, the most important degradation reaction of indigo was performed in 1841 by Otto Linné Erdmann (1804-1869) and Auguste Laurent (1807–1853), who oxidized it with nitric acid to yield isatin.[2] This state of knowledge was further explored by Adolf von Baeyer as he started his work on indigo in 1865 at Berlin University. At this stage, the critical question regarding the dye structure was the connectivity and position of oxygen atom in indigo. On reduction of isatin with zinc in presence of HCl, Baeyer isolated dioxindole. Further reduction of this compound with sodium amalgam resulted oxindole. Finally, distillation of oxindole with Zn-dust in a stream of H_2 resulted into formation of indole. Baeyer confirmed his results via total synthesis of these degradation products oxindole, isatin and indole.

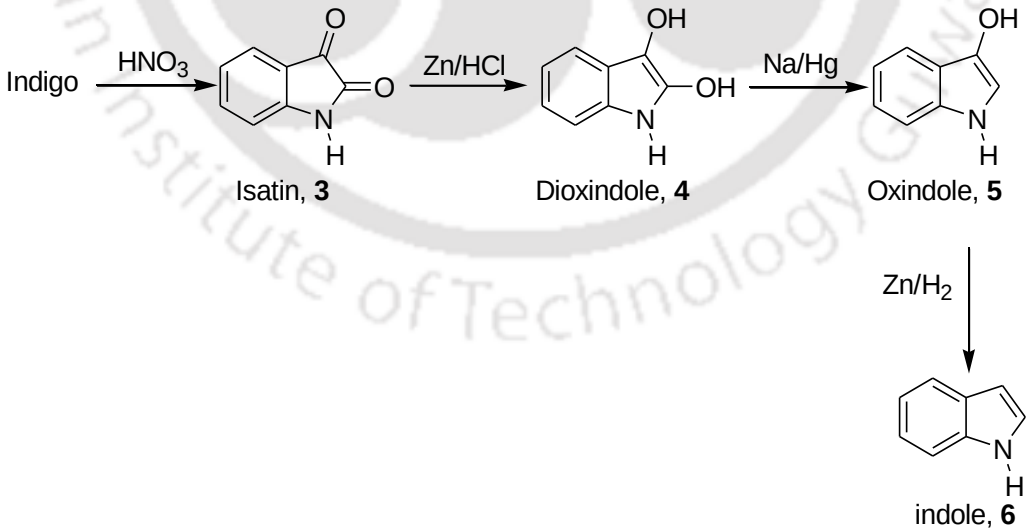

Scheme 2. Degradation products of indigo.

The final piece of the puzzle was solved after isolation of urinary indicant in 1879 by Baumann and Tiemann. This potassium salt of indoxyl sulphate upon acid hydrolysis formed indoxyl and underwent spontaneous oxidation to indigo in air. Based on these critical observations, Baeyer proposed the structure of indigo in 1883.[9] But, he was unable to assign the *cis*- or *trans*- nature of the dye. In 1928, the question on the *cis*/*trans*-isomer on solid-state indigo was resolved by Reis and Schneider using X-ray crystallography.[10] In 1905 Baeyer was awarded with Nobel Prize for his contribution in indigo-chemistry.[8]

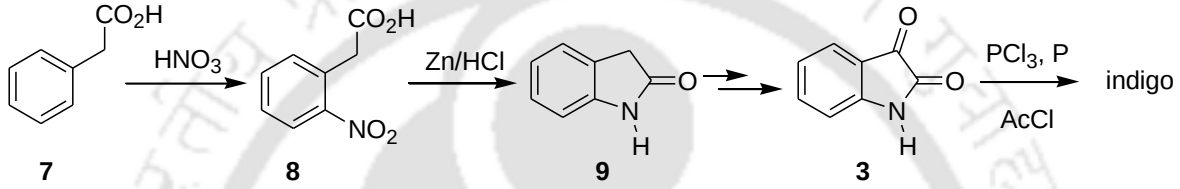

Scheme 3. First synthetic procedure for indigo developed by Adolf von Baeyer in 1878.

Much before its structure was proposed, the dye was synthesized by Baeyer in the laboratory in 1878 using phenyl acetic acid as the starting material.[11]As his journey with indigo continued, in 1882 Baeyer and Drewsen developed the first commercially viable synthetic route for indigo from *o*-nitrobenzaldehyde. This one-pot reaction is popularly known as the Baeyer-Drewsen method of indigo synthesis.[12]

1.4 Photophysical properties of indigo

The ubiquity of indigo and its long history of uses and importance lie on its intense blue color combined with high light-fastness. Initial focus in the course of development was on the structure elucidation and commercialization of the dye. After the discovery of Baeyer *et. al.* on commercial synthesis and X-ray crystallography by Reis and Schneider, focus shifted to the origin of blue color and photostability of the dye. In 1908, Paul Friedländer proposed a general structural definition for indigoids using a structural unit consisting of two pairs of

electron donor-acceptor connected via endocyclic double bond.[13] Later on Lüttke et al. proposed that the *trans*-orientation of this donor-acceptor pair, known as H-chromophore, possibly is the origin of the color.

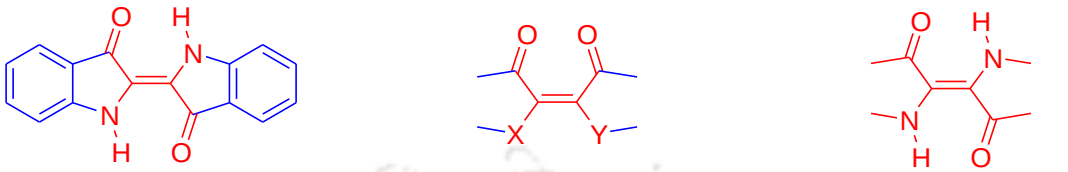

Indigo, **10** general structure of indigoids, **11** H-Chromophore, **12**

Figure 2. Structure of indigo (**10**), general structure of indigoids (**11**) proposed by Paul Friedländer and H-chromophore (**12**).

This doubly cross-conjugated system allows lower energy absorption, and results into the blue color of the dye. This conclusion was reached through a combination of theoretical calculations and syntheses of indigo analogues with different components employing a "stripped down" approach. The absorption behavior of the dye varies with change in physical state of the dye.[14] In vapour phase, the dye appears as red, which changes to blue in dilute solutions of non-polar solvents (λ_{max}= 603 nm, $CHCl_3$). In polar solvents the color changes to blue-green. Aggregated thin film of the dye shows further red shifted maxima (λ_{max}= 702 nm). The justification of such bathochromic shift in its solid state by about 100 nm relative to dilute solutions is found in the strong intermolecular exchange coupling imposed by intermolecular hydrogen bonding that leads to co-facial π-π stacking in solid state.[15] The extent of this bathochromic shift is therefore affected by nature of substituents in the phenyl rings. Indigo with substituents at 4,4'- and 7,7'- positions causes steric hindrance in intermolecular H-bonds formation, hence shows no bathochromic shifts while going from monomeric form to aggregated solid state. In both solid state and in solution, indigoids exist in the *trans*-form. The *trans*-isomer is maintained by intramolecular hydrogen bonding

between adjacent amine and ketone groups. Because of this photoinduced *E-Z* isomerism of indigo is never observed (Figure 3).

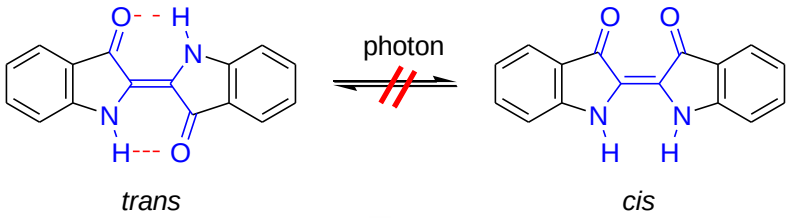

Figure 3. Absence of photoinduced *cis-trans* isomerism in indigo due to intramolecular H-bonding**.**

Indigo is a low emissive dye with a strikingly high photostability. These significant characteristics of the dye are a result of overall radiationless internal conversion in the excited state. The extremely short excited state lifetime and efficient internal conversion occurs through excited state intramolecular proton transfer (ESIPT) mechanism. The excited-state proton transfer is followed by keto-enol tautomerism leading to formation of its isomers **13** and **14** as depicted in Figure 4. Although it is ambiguous whether there occurs single- or double-proton transfer, the theory of proton transfer is widely accepted.

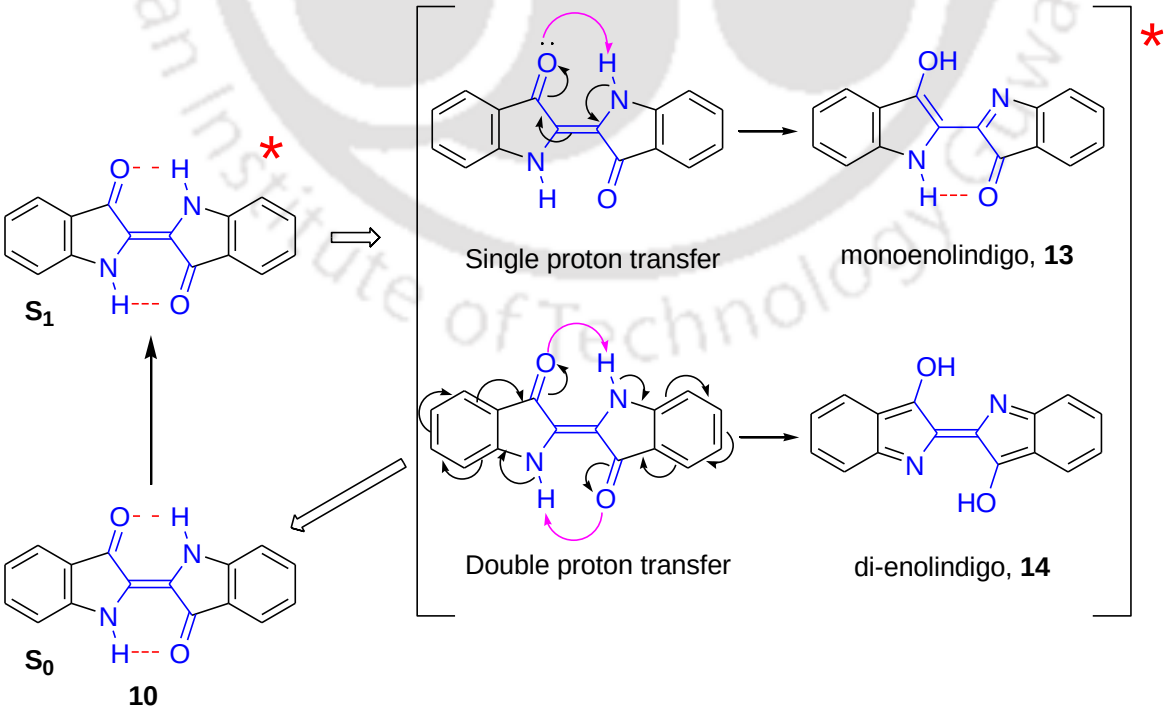

Figure 4. Radiationless deactivation of excited state via proton-transfer in indigo.

Efficient coupling between S_0 and S_1 vibrational modes due to lowered HOMO-LUMO gap favours this highly efficient phenomenon (efficiency 99.99%). The photo-excited state is thus deactivated without photoluminescence. As a result, the emission occurs in only low quantum yield.[16] The theory of excited state proton transfer mechanism leading to low fluorescence emission is a well-known phenomenon for other compounds as well. The fact that other indigoid derivatives with S, O or Se heteroatoms or acylated or alkylated amine nitrogen are highly fluorescent also supports the theory. Absence of H-bonding parameters in these indigoids enhances the photoluminescence emission intensity. These molecules can also undergo photochemical *cis-trans* isomerism (Figure 5a). Further increase in emission intensity can also be achieved by removing the scope of *cis-trans* isomerism. Structural restriction imposed around the central double bond would limit the pathways of energy consumption in the excited state. For example, the dye cibalackrot (Figure 5b), produced via the condensation of phenylacetyl chloride with indigo is highly fluorescent (Φ_f = 0.69, DMF).

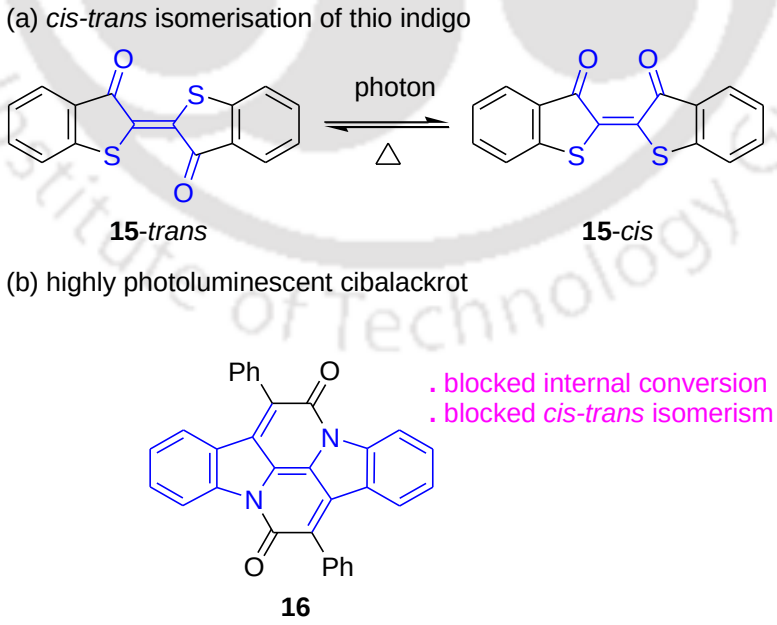

Figure 5. Effect of removing intramolecular H-bonding from indigo analogues and indigo derivatives.

A proper understanding of photophysical properties of indigo is also crucial for understanding the fading process of the natural-dye when used as pigments in paintings (artworks). Researchers have shown that the central double bond of the H-chromophore acts as a photoprotector. In general the chromophoric double bond of indigo is very stable, displaying photo-degradation quantum yields with below 10^{-6} under dry and closed condition. However, photo-degradation quantum yield increases to 10^{-4}-10^{-3} in presence of oxygen-based radicals or reducing species. Such degradation of the dye under UV-vis light is a well-known fact. Isatin was found to be the major product generated after photo-degradation of indigo. Based on the studies in DMF, dichloromethane[17] and solid matrixes, it was proposed that isatin was produced via reaction between an indigo molecule and an indigo radical, generated via initial attack at central double bond.

The redox chemistry of indigo plays an important role in its application as vat dye. The first step of dyeing process involves generation of water-soluble reduced-form. This reduction process of indigo to its leuco-form represents an important type of industrial process. In this context, in depth knowledge of the redox chemistry of the dye is essential.

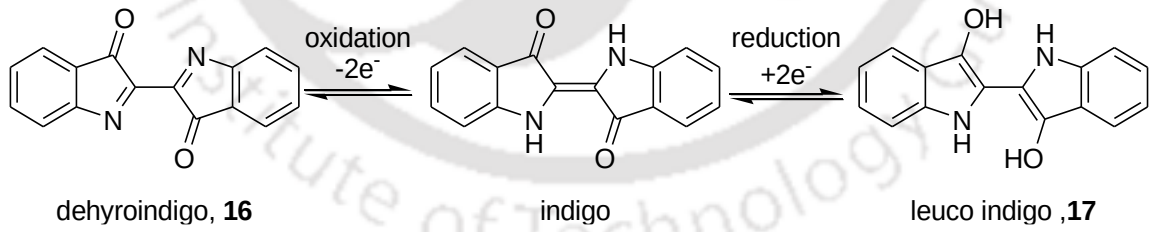

Figure 6. Redox chemistry of indigo.

Redox behavior of indigo, investigated using cyclic voltammetry technique, shows two reversible peaks at –1.1 V and 0.6 V with respect to Ag/AgCl. Two-electron reduction (Figure 6) leads to the formation of leuco-indigo, while oxidation generates dehydroindigo. From the obtained electrochemical data, the energy gap between highest occupied molecular

orbital (HOMO) and lowest unoccupied molecular orbital (LUMO) was calculated to be 1.7 eV. As established from experimental evidence followed by DFT approximation, the HOMO is located in the central double bond and the amine nitrogen; whereas the carbonyl oxygen along with the central double bond carries the LUMO. The donor group raises the energy of the HOMO while the electron acceptor lowers the LUMO essentially decreasing the HOMO-LUMO bandgap.[18]

The comparison between the photophysical properties of the leuco-indigo and indigo revealed that the radiation less rate constant in the leuco forms are lower than that of its keto form. As a result, fluorescence and triplet-state formation are much more prominent means of deactivation channels for the singlet excited state in the case of the leuco forms. The larger fluorescence quantum yield (Φ_f) values in the leuco forms can also be associated with some degree of rotation around the central C−C bond. These differences witnessed between the two forms suggest that the distinguished photo-stability of the keto forms of indigo is not present with the reduced species, leuco.

1.5 Derivatives of indigo

After the industrial revolution involving indigo, there were significant efforts among the scientific community to prepare derivatives of the blue dye. Modifications were done in the benzene ring as well as on the H-chromophore. Such alterations provided new indigoid with exciting properties like better charge transportation capability, photochromism and molecular switching. Based on the nature of substitutions, the derivatives of indigo can be classified into two categories; 1) substitution at the outer phenyl rings at 4-to-7 positions by different groups like halogens, alkyl, cyano, alkoxy etc., 2) modifications of the H-chromophore via

substitution of one or two N-H group(s) with N-R, treatment of the carbonyl with amine to form imine or by connecting the electron donor NH-group with the electron acceptor carbonyl via a electroactive backbone to produce bay-annulated indigoids. All these modifications led to generation of wide variety of ring- and N-substituted indigoids with exciting properties.

1.5.1 Ring-Substituted indigo

The change in property of phenyl-substituted indigoids depends upon the nature (size, electron donating or electron withdrawing capability) of the substituting group, as well as the position and degree of substitution at the phenyl rings. Besides indigo, 6,6'-dibromoindigo commonly known as Tyrian purple is the only other naturally occurring indigoid dye. Similar to its parent dye this compound too has a rich history of application as a textile dye. Unlike indigo, the natural origin of Tyrian purple is very limited. In ancient times this dye was produced from secretions of various species of snails found in the Atlantic and Mediterranean coasts.[19] The chemical structure of this dye was first identified by Paul Friedländer in 1909.[13] The first synthesis of this dye from 4-bromo-2-nitrobenzaldehyde was reported by Sachs and Kempf in 1903.[20] Besides Tyrian purple another derivative of indigo with a long standing history is indigo carmine. This disulphonated species of indigo was prepared from treatment of the dye with sulphuric acid.[21] The major difference obtained via this treatment is the solubility. Indigo and Tyrian purple are water insoluble, while indigo carmine is soluble in water due to the ionic character. As substitutions occur only at the peripheral position of the phenyl rings, solubility of indigoids can also be varied by using other functional groups.

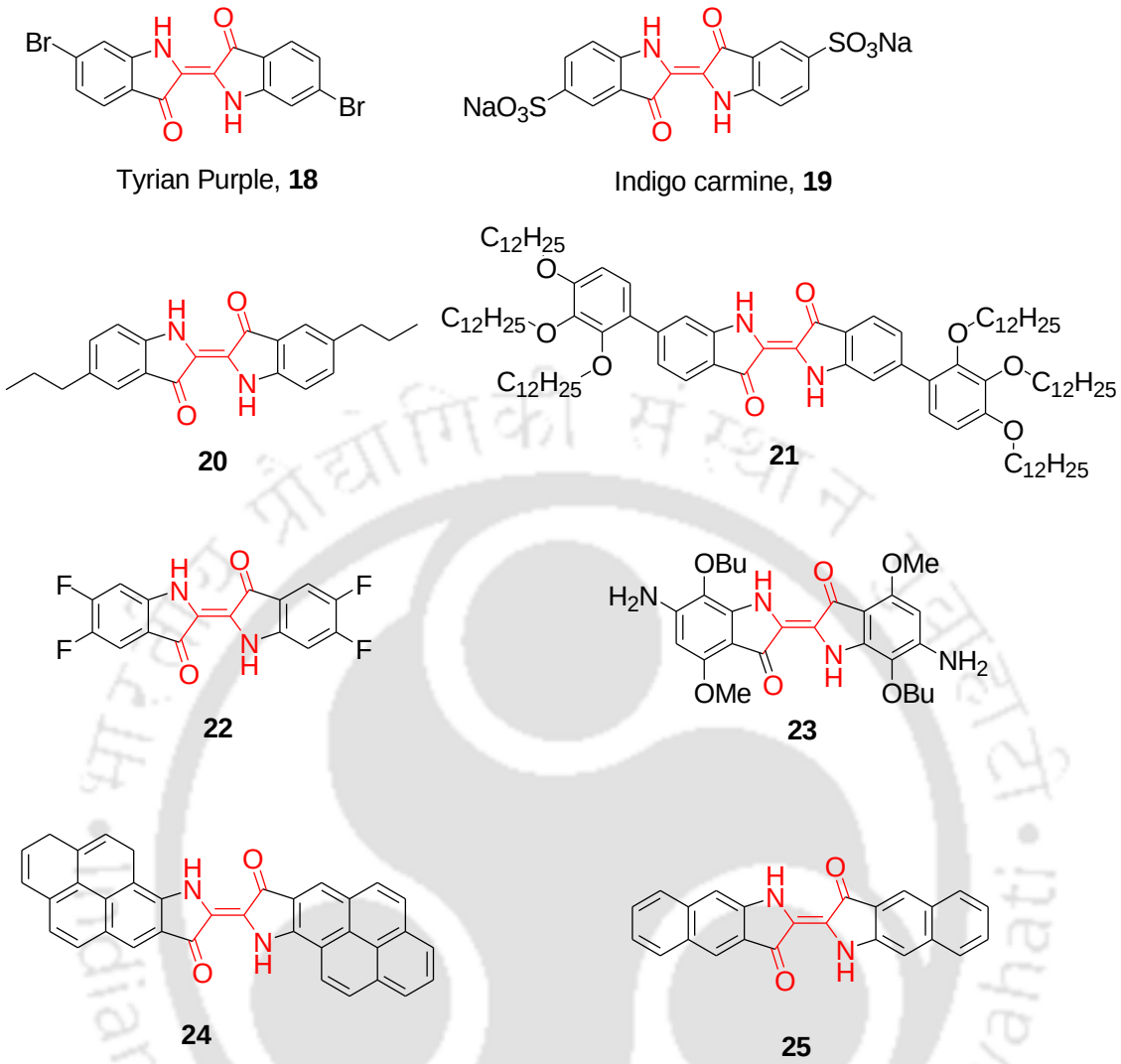

Figure 7. Representative examples of ring-substituted indigoids.

For example, dialkylated-indigo at 5,5'-positions with propyl and butyl group shows solubility in chloroform and 1,2-dichlorobenzene, which are 65-89 times higher as compared to the parent indigo.[22] Replacements of the benzene ring with other aromatic systems have also been reported. Installation of the indigoid-chromophore into extended π-systems pyrene and naphthalene rings resulted into novel indigoids **24** and **25** respectively.[23] Effect of substitution on the optoelectronic properties of indigoids is a well-studied area for researchers driven by the constant urge for proper understanding of structure-property relationship. The absorption spectra of 6,6'-dihalogenated indigoid shows blue shifts in comparison with the

parent indigo. The dibromo derivative (**18**) shows absorption maxima at 550 nm in chloroform.[19] The degrees of these shifts are in order of increased electronegativity of the halogen substituents: F > > Cl ~ Br. On the other hand, substitution by electron deficient functional groups like CF_3, NO_2 and CN at 6,6'-positions results into a red shifted absorption maxima.[24,27] An opposite effect is observed when substitution is carried out at 5,5'-positions. Electron-donating groups like alkyl or amine (e.g. **20**) cause a bathochromic shift, while electron deficient CF_3, NO_2 and CN induce a hypsochromic shift. The photophysical properties of ring-substituted indigoids also depend upon the degree of substitution. Di-substituted indigoids are much like the parent dye presenting a mirror image relationship between absorption and emission behaviour. On increasing the number to tetra or hexa-substitution, the absorption spectra becomes broader while the emission peak gets sharp. This results into loss of the mirror image relationship of the respective spectra. Depending upon the number and nature of substituents, this approach can produce molecules with absorption maxima as high as ~740 nm (compound **23,** DMF solution). In case of tetrafluoroindigo **22,** the absorption maximum (586 nm) lies, in between the maxima of 5,5'-bisfluorinated compounds (525 nm) and 6,6'-bisfluorinated (618 nm) analogue.[25] The indigoids with extended conjugation resulted into red shifted absorption behavior (**24**, λ_{abs}/ 687 nm, ethyl acetate) of the indigoids. The most interesting fact was noticed in case of naphthyl analogue **25**. While all other derivatives of indigo exist as *trans*-indigoids, compound **25** was isolated as *cis*-indigoid. The *trans*-isomer of the same could be generated photochemically. Significant difference was observed between the two isomers. In case of *cis*-indigoid, destabilization of the π-conjugation resulted into high energy absorption maxima at 540 nm in dioxane. The *trans*-form displayed longer wavelength absorption maxima (672 nm, dioxane) due to extensive π-conjugation.

The electrochemical properties of the derivative show remarkable dependency on the nature of electronic effect of the substitution. Introduction of electron rich substituents like halogens at the 6,6'-positions stabilizes the HOMO without affecting the LUMO located on the carbonyl of the H-chromophore. But, with electron withdrawing groups like of CF_3, NO_2 and CN significant changes are observed in the reduction potential of the dye. A shift of LUMO towards benzene rings caused by polarization induced by the electron deficient substituents results in a lower LUMO, with overall decline in its redox potential. Substitution by chlorine and bromine atoms to the indigo core at 5,5'-positions affects mostly HOMO energies of the resulting compounds, while LUMO levels remain unchanged compared to indigo. However, fluorine substitution at these positions induces an increase in reduction potential without affecting the oxidation potential of the parent dye. An overall decrease in redox potential is observed in presence of alkyl chains at 5,5'-position. These electron rich groups increase the energy of the highest occupied molecular orbital, while reducing the energy of the lowest unoccupied molecular orbital.

One crucial property of an organic molecule for its application in organic electronics is its charge-transport behavior. The two naturally occurring indigoids, indigo and Tyrian purple mainly serves as p-type ambipolar semiconductor with charge mobility of 0.01 cm^2/Vs for indigo and upto 0.04 cm^2/Vs for bromo derivative depending upon the dielectric gate used in the OFET device.[26] However, the corresponding chloro and fluoro-derivatives along with other electron deficient substituents exhibited purely n-type behavior. It is reasonable to assume that the presence of electron withdrawing substituents in the indigo core, increases the barrier for the hole injection and facilitates the electron injection. Experimental evidences obtained by P. A. Troshin and his co-workers also revealed that, introduction of strong electron withdrawing substituents lower the LUMO energy of the indigo core to yield improved stability of n-channel OFETs under ambient conditions. [27]

Indigo has also been used as chromophoric core to synthesize symmetrically bis-substituted derivatives with long peripheral alkyl chains to produce novel chromophoric liquid crystals (compound **21**). As reported by Jan H. Porada and Dirk Blunk, long chain alkoxy substituted phenyl rings attached to 5,5' or 6,6'-positions of indigo forms phasmidic mesogens.[28] Smectic or nematic liquid crystalline phases could also be generated by bring additional halogen at the 7,7' -positions.[29]

1.5.2 N-substituted indigo

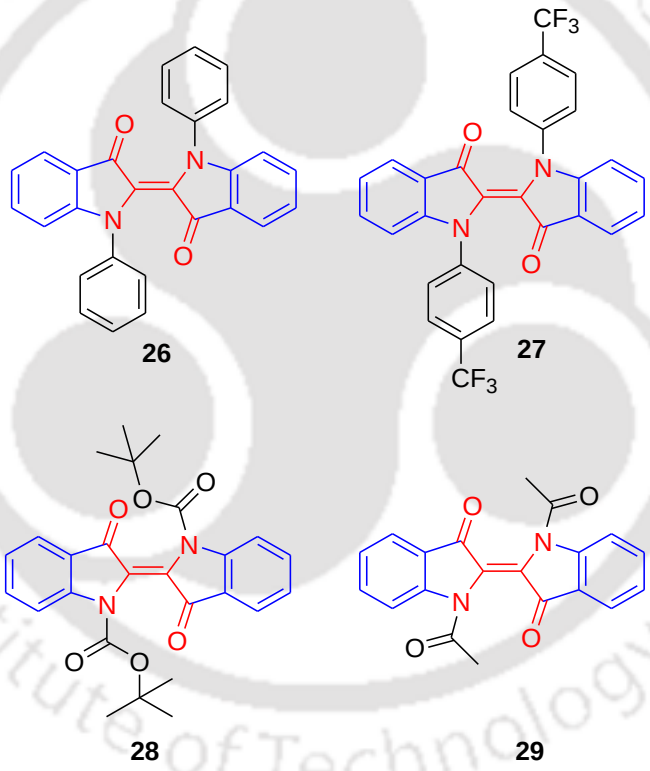

Figure 8. N-substituted indigoids.

Replacement of one or both the imide protons with acyl, alkyl and phenyl resulted into a wide variety of N-substituted indigoids. The major structural difference between such indigoids and indigo is the lack of hydrogen bonding. Depending upon the nature of the substituents, significant deviation in planarity had also been observed. A combination of lack of H-

bonding and planarity caused improved solubility in N-substituted indigoids. Low emission quantum yield of indigo is associated with its ESIPT property. Absence of such quenching mechanism causes significant improvement in photoluminescence intensity of the derivatives. Introduction of di-*tert*-butyldicarbonate (**28**) at the N-H resulted in twisted structure with many torsional configurations. Restriction in intramolecular motion (RIM) in the crystallized state caused improved photoluminescence emission.[30] Another intriguing property of N-substituted indigoids is their facile photo-induced *cis-trans* isomerism. The thermal lifetime of the photo-stationary state could be manipulated simply by changing the substituents. Installation of electron-withdrawing substituents on the N-aryl moiety was found to be an effective way to enhance the thermal stability of the Z-isomers. For example, the thermal half-life of the *cis*-form of compound **27** was found to be 81 min, while compound **26** shows a half-life of 3.1 min only.[31b] Many of the N-substituted indigoids show photoswitching behavior in the bio-optical window (650-1100 nm),[31] which is demanding for various applications.

1.5.3 Bay-annulated indigo

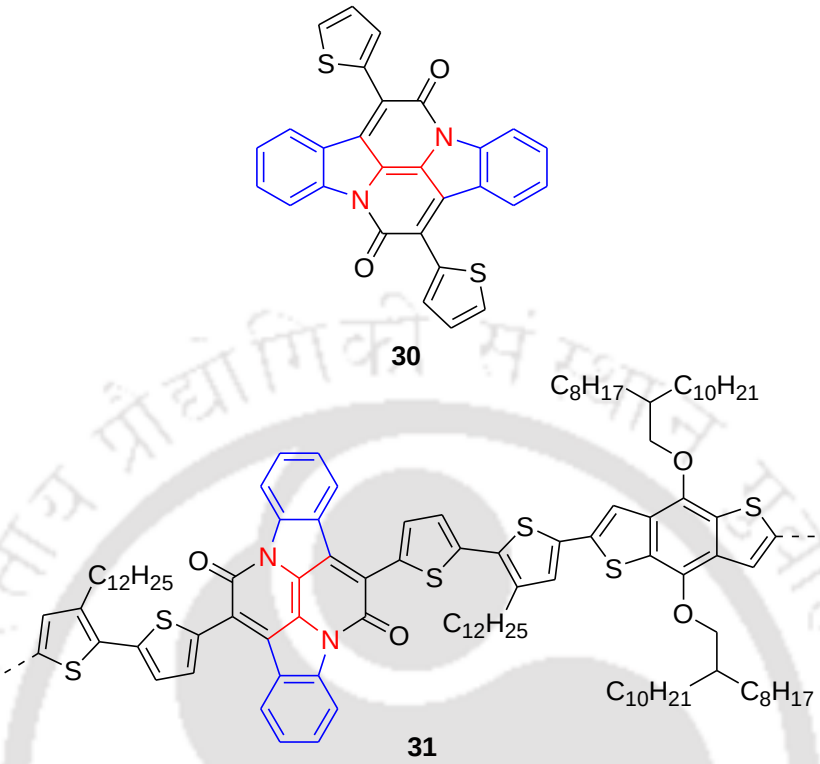

Figure 9. Bay-annulated indigo**, 30** and a polymer containing BAI, **31**.

One-step functionalization of indigo dye via the condensation with acetyl chloride derivatives results into the formation of bay-annulated indigo (BAI). Similar to indigo, BAI contains two pairs of donor-acceptor moieties and display absorption in the longer wavelength region of visible spectrum. The electron donor tertiary amine and acceptor carbonyl groups are located in two fused lactams. BAIs are molecules with restricted intramolecular rotations along the indigoid C=C bond. Some BAIs are utilized for the preparation of novel donor−acceptor small molecules and polymers and often exhibits low-lying LUMO energy levels and small HOMO−LUMO gaps. Field effect transistors based on BAI-containing polymers show excellent ambipolar transporting behaviour, with the hole and electron mobility reaching 1.5 and 0.41 $cm^2\ V^{-1}\ s^{-1}$, respectively.[32] BAIs are also used as a building block for near-infrared sensitive, push–pull type conjugated polymers that can be used as a photo-detector.[33]

1.5.4 Nindigo (indigodiamine)

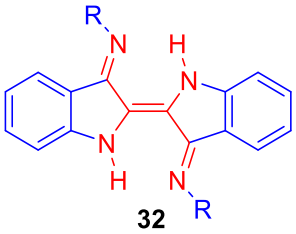

32

R = Ph, *p*tol, ^{t}Bu etc.

Synthesis of indigodiamine-compounds, known as nindigo, was first reported by R. G. Hicks and his co-workers in 2010.[34] The conversion of carbonyl groups into imine causes enhanced solubility of nindigos. The resultant imine groups are very good donor and nindigos can act as both bidentate and *bis*-(bidentate) ligands. A wide variety of mono- and di-nuclear metal-complexes have been prepared using such molecules. By tuning the steric and electronic nature of the imines, a diverse range of nindigos have been reported. The protonated form of the molecule undergoes reversible *cis-trans* isomerization.[35]

1.6 Applications of indigo and its derivatives

1.6.1 Application as textile dye

Indigo and its derivatives are organic compounds that have comparatively low acute toxicity.[36] Indigo is synthesized chemically or can be extracted from plant sources (e.g. woad and *Indigofera tictoria*). The dye shows high chemical and physical stability (high melting point 390°C).[37] Another important aspect of the dye is its long-wavelength absorption maxima in a comparatively small π-conjugated system. On the contrary, other blue dyes like azo-dyes or anthraquinone consist of extended conjugation. The most significant property of indigo is however its high light-fastness property. The primary use of indigo is as a dye for cotton yarn, in the production of denim cloth for blue jeans. It is also used for dyeing wool

and silk.[7b] As of 2011, annual commercial production of indigo is 50,000 tons.[38] Apart from indigo, Tyrian purple was also used a nature-originated vat dye used for textile dyeing.

Figure 10. Textile dyed with indigo and Tyrian purple.

1.6.2 Application as pigments and coloring agents in other areas

Indigo serves an excellent source of blue color not only in the textile industry, but also in many other applications. For instance, pure indigo can be finely ground and mixed as water-color, tempera, or oil paint. Plant-derived indigo is used as a natural food colorant and been used as pigments for contact lenses.[39] Indigo carmine is another derivative of the dye to be used as FDA approved food colorant.[40]

1.6.3 Application of indigoids as ambipolar semiconductor

The most intriguing modern day application of indigo and its derivatives is established towards the development of sustainable organic electronics. Application of indigo and some of its analogous dyes as organic semiconductors was first proposed in a Japanese patent in 2006.[41] Indigo was shown as a promising sustainable semiconductor material, exhibiting balanced ambipolar transport in OFETs and good performance in inverter circuits.[42] Indigo exhibits high performance ambipolar transport with balanced charge mobility of 0.01 cm^2/Vs in organic field effect transistors. Further improvements of charge mobility as well as

solubility, stability are achieved in other indigoid-based OFETs.[43] For example, Tyrian purple (**16**) can show charge mobility upto 0.4 cm^2/Vs. Introduction of phenyl groups at 5,5'-positions causes excellent and well-balanced ambipolar transistor properties in the indigo derivative. Hole and electron mobilities of 5,5'-diphenylindigo are found to be 0.56 and 0.95 $cm^2\ V^{-1}\ s^{-1}$ respectively. The enhanced performance is attributed to the extended π–π overlap of the phenyl groups as well as the characteristic packing.[44] Further modifications like introduction of strong electron withdrawing substituents to the indigo core improves the stability of n-channel OFETs under ambient conditions. Along with enhanced charge mobility, the lifetime of OFETs based on 6,6'-*bis*(trifluoromethyl)indigo and 5,5',6,6'-tetrafluoroindigo (60 days in aerobic condition) are considerably higher than that of indigo.[27] Indigo and its derivatives have also found their place in the field of nanostructured dye sensitized solar cells (DSSCs). Organic photovoltaic devices based on indigo-based dyes exhibit medium to high power conversion efficiency. Indigo is a molecule of very low solubility in common organic solvents. The low solubility profile makes it difficult to prepare thin-film, necessary for applications in organic electronics. A strategic design to ease the process of making indigo thin-films is to prepare a more soluble ^{t}BOC-protected structure. Thin films produced via spin casting of ^{t}BOC-protected indigo are then used as an active layer in organic solar cells, where the indigo pigment acts as an electron acceptor. Thermal regeneration of the dye in the thin film via deprotection causes photoinduced charge transfer between indigo and the other polymeric layers of the solar-cell.[45]

1.6.4 Application of indigoids as ligand for metal complexation

Uses of indigo as a ligand for synthesis of metal complexes add another aspect towards versatility of the dye in multi-disciplinary application. The metallation of indigo can be realized in varying binding modes resulting into different classes of redox-active organic

chromophores with modified photophysical, redox and structural behavior. The non-innocent redox active form (H_2L) of the dye had been utilized to form organometallic complexes using Cr[46], Ru[47], Re[48], Pd[49] etc. The dye has been used as bidentate as well as *bis*(bidentate) ligand. Several binding modes are available for both cases.

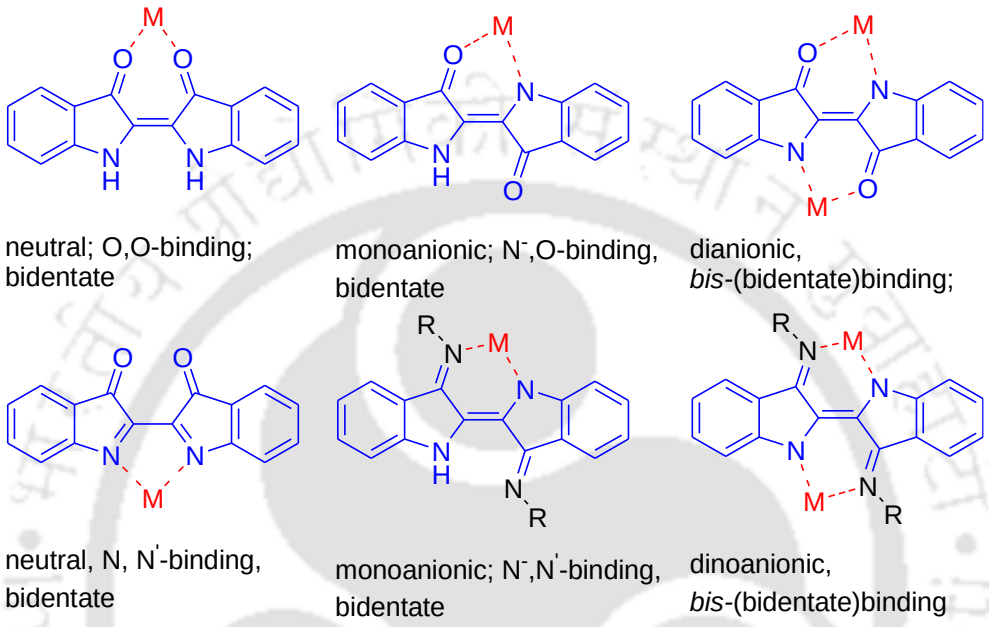

Figure 11. Different binding modes of indigo, dehydroindigo and ninindigo in a metal complex.

The dye can acts as bidentate ligands via neutral O,O-coordination or monoanionic O,N^--coordination. In case of *bis*(bidentate) behavior, the coordination occur through O,N^- atoms. Indigo also exhibits binding capability in its oxidized form dehydroindigo, which acts as neutral bidentate ligands via N,N-coordination.[50] Partial modification of the chromophoric unit by changing the carbonyl to imine forms nindigo compounds. Several bindings modes are known for nindigos as well as shown in Figure 11. Utilizing such diverse range of binding modes and motifs, large number of metal-complexes, metallo-supramolecular architectures have been prepared. For example, indigo has been used to prepare triangular metalloprism with Re(I). Absorption in the NIR region of the assembly shows potential in electrochromic

switching.[51] Metallation of nindigo resulted into a new class of bridging ligands with tuneable steric and electronic control by changing the substituent at the imine nitrogen.[52]

1.6.4 Application of indigoids as photoswitch materials

Indigo exists in a stable *trans*- planar configuration with strong intramolecular H-bonding. This strong H-bonding present in both solution and solid state of the dye is responsible for the unattainable *cis-trans* transformation.

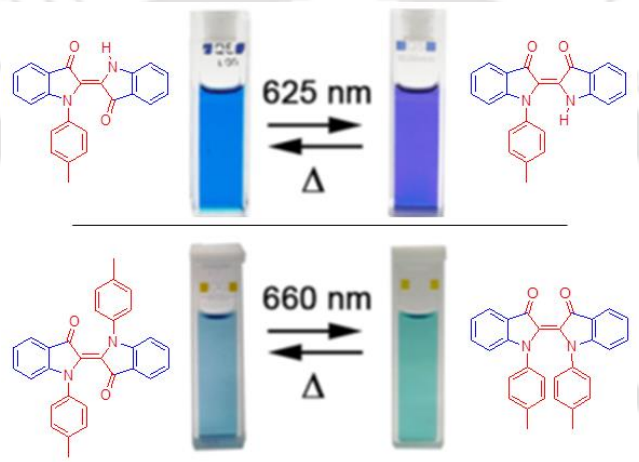

Figure 12. Mono- and bis-arylated indigo photoswitches with red-light responsiveness.

But, once the suitable modification was done to nullify or minimize the strength of this intramolecular bond, indigoids are found be very suitable in the field of molecular switches due to very efficient photoisomerization. For example, N,N'-disubstituted or N-monosubstituted indigoids undergoes photo-induced transformation from *trans*- to their corresponding *cis*-isomer. The stability of the isomers and rate of interconversion are dependent on the nature of substituents. Installation of electron-withdrawing substituents on the N-aryl moieties of N,N'-disubstituted indigos enhance the thermal stability of the Z-isomers. Depending on the nature of substituents, some derivatives even absorb in the red

region of the spectrum. The photoswitching property in the bio-optical window makes them attractive candidates for various applications in life science.[53] Stimuli-controlled *cis-trans* isomerism also makes them suitable in various applications in material science.

1.7 Analogous compounds of indigo

Indigo-analogous compound are a range of indigoids with modifications at the chromophore unit of the dye. When the electron donor amine groups of the H-chromophore are replaced by hetero atoms like S, O and Se indigo-analogues namely thioindigo, oxindigo and selenoindigo are formed. Modification of the chromophore can also be done by replacing one half of the cross-conjugated structure with a phenyl moiety to form hemiindigo. Similar modification can be done at the thioindigo to get hemithioindigo. Along with the chromophore modification of thioindigo, changing the connectivity from *ortho*-in benzene rings to the *peri*-positions of the naphthyl rings gives *peri*-naphthothioindigo.

1.7.1 Hemiindigo

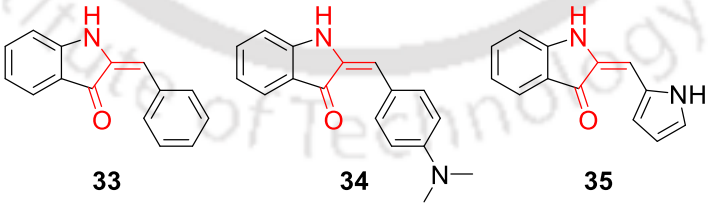

Figure 13. Examples of hemiindigos.

Hemiindigos consist of an indigo fragment and a half-part of stilbene sharing a common central double bond. It was first described by Adolf von Baeyer in 1883 naming the compounds "indogenide" as it was obtained from condensation of indoxylic acid and

aldehydes.[9] Hemiindigo are compounds with high solubility in common organic solvents. Depending upon the nature of non-indigoid substituent part, these molecules can undergo different photo-induced transformations like E-Z isomerization, [2+2] cycloadditions etc. In modern times this long-standing molecules with almost quantitative photoisomerization rate have been established as highly bistable photoswitching material at the biooptical window.[54]

1.7.2 Thioindigo

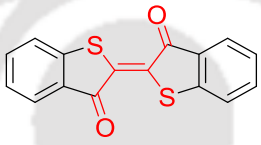

36

The synthesis of thioindigo was first published by Fierz-David and Blangey in 1924. The stable *trans*-form shows an intense fluorescence emission with quantum yield of ~0.72 (in benzene) upon excitation at its absorption maximum of 544 nm (in benzene).[55] Due to the absence of hydrogen bonds, a photoinduced *cis-trans* isomerisation is possible making it an excellent candidate for molecular photoswitches. The absorption behavior of the *cis*-conformer is more energy demanding similar to other indigoids that exhibit this conformer. Thioindigo is also used as a red-vat dye for textile coloring.

1.7.3 Hemithioindigo

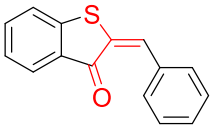

37

Hemithioindigo (HTI) compounds are hybrid chromophores in which a central photoisomerizable double bond connects a thioindigo part with a stilbene part. The boom in

their recent popularity is a result of their efficient photoswitching properties. In recent times, a huge number of compounds (different at the non-indigoid fragment) have been reported and studied for their functional behaviours as molecular photoswitches, molecular motors etc.[56]

1.7.4 Oxindigo

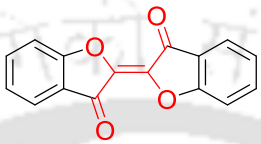

38

The first synthetic report on yellow colored oxindigo (**38**) dates back to 1908.[57] This molecule in its benzene solution exhibits an absorption maximum of 413 nm in *trans*-configuration and an absorption maximum at 396 nm in *cis*-configuration. Oxindigo does not easily form a vat and is not very stable, specifically in a water-alcoholic alkaline solution degradation of the molecule occur via opening of the cumarone ring. This makes it an unfit candidate for vat dyeing. Oxindigo has extreme low solubility in common organic solvents except xylene and benzene.[58]

1.7.5 Selenoindigo

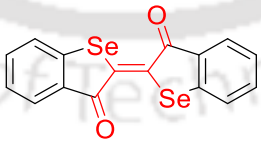

39

Selenoindigo (**39**) is a violet colored compound and capable of photo-induced *cis-trans* transformation due to the obvious absence of intermolecular H-bonding. In toluene it shows an absorption maximum of 562 nm for its *trans*- conformer, while the higher energy *cis* isomer has absorption maxima of 485 nm in toluene.[59]

1.7.6 *Peri*-naphthothioindigo (PNT)

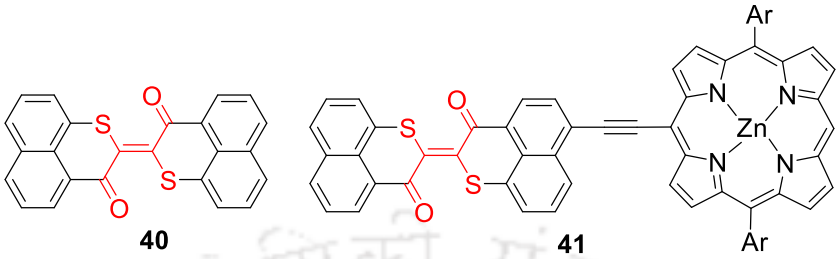

Peri-naphthothioindigo (**40**) is a photochromic molecule, that undergoes reversible photoisomerization between a yellow *cis*-conformer ($\lambda_{max/absorbance}$ = 484 nm) and a purple *trans*-conformer ($\lambda_{max/absorbance}$ = 595 nm). The stable *trans*- form converts to the *cis*- with a conversion quantum yield of 0.027 in toluene and 0.062 in PMMA. The reversible characteristic of this phenomenon is evident from the quantum efficiency of *cis*- to *trans*-conversion of ~0.27–0.85 in toluene and ~0.17–0.68 in PMMA. The highest conversion efficiency of this (*cis*- to *trans*-) thermodynamically slow process occurs in the vicinity of its λ_{max} of 484 nm. *trans*-PNT has a strong fluorescence quantum yield, 0.14 (toluene) and 0.16 (PMMA). But *cis*-PNT is non-emissive in nature.[60] Structural modifications to a porphyrin-perinaphthothioindigo conjugate (**41**) also shows efficient two photon absorption and demonstrated the switching of a PNT moiety via both two-photon excitation and one-photon irradiation. This efficient and reversible property of photoswitching between fluorescent and non-fluorescent forms makes it a successful material for many applications in imaging and 3D-data storage.[61]

1.8 Objective

Despite continuous efforts devoted to their development, dyes with high chemical and photochemical stability, high molar absorption coefficients, high fluorescence quantum yields, large Stokes shifts, and tuneable absorption/emission properties are still fewer in number. On account of its structural diversity and application indigo dye is still an attractive molecule in scientific community. The growing opportunities of applications based on indigoids, drive the quest for new structures to an expanding field of research. In the continuous effort towards new-indigoids, even unsuccessful attempts were made to realize an all carbon indigoid system.[62] Inspired by these, a fascinating modification in this route would be installation of the basic H-chromophore of indigo sandwiched into the *peri*-positions of two naphthalene molecules to make *peri*-naphthoindigo (PNI) (Figure 14).

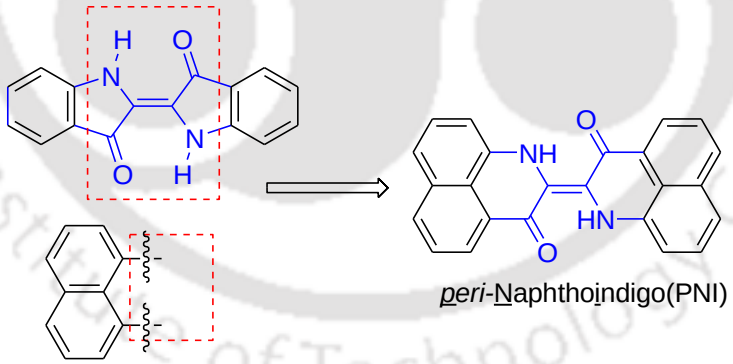

Figure 14: Structure of *peri*-naphthoindigo.

The structure of PNI was proposed first time in a U.S. patent in 1977 by R. A. Nathan and his co-workers.[63] A theoretical report by Zhang et. al,[64] which predicted better performance of PNI than indigo as ambipolar organic semiconductor material, also predicted a diketo isomer of PNI.

The primary goal of this thesis work was to design a synthetic route for PNI. As chapter 2 unveils the synthetic trials went into this compound, the fundamental impact of steric as well as electronic control imposed by the basic organic skeletal like the naphthyl moiety will be discussed. Upon fruitful synthesis, isolation and characterization of the targeted molecule will sum up the foundation of this course.

In a next step, the focus is directed towards investigation of photophysical, aggregation, electrochemical and halochromic behavior of the synthesized molecule. These studies will serve as a tool for further modification and utilization of the dye.

In an attempt to utilize the various molecular processes suitable for indigo-type compounds, molecular self-assembly along with the prospect of self-sorted structures will be investigated with PNI and some other molecules.

At last but not the least, the aspect of PNI derivatization will be explored to gain an access to a new class of molecules, followed by investigation of their electronic as well as molecular behaviors.

1.9 References

1. M. M. Sousa, C. Miguel, I. Rodrigues, A. J. Parola, F. Pina, J. S. Seixas de Melo, M. J. Melo, *Photochem. Photobiol. Sci.* **2008**, *7*, 1353-1359.
2. B. Schaefer, *Natural Products in the Chemical Industry* **2014**, *XVIII*, 13-22, ISBN: 978-3-642-54460-6.
3. J. C. Splitstoser, T. D. Dillehay, J. Wouters, A. Claro, *Sci. Adv. 2* **2016**, *2*, e1501623.
4. R. Prasad, *Ind. J. Hist. Sci.* **2018**, *53*, 296-301.
5. M. Seefelder, *Indigo in culture, Science, and Technology* Ecomed, Landsberg, Germany, **1994**.
6. P. Garcia-Macias, P. John, *J Agric. Food Chem.* **2004,** *52*, 7891-7896.
7. (a) D. R. Waring G. Hallas *The chemistry and application of dyes New York: Plenum Press*, **1990**. 2-9; (b) J. Wisniak, *Ind. J. Hist. Chem.* **2004**, *39*, 75-100; (c) Y. Minami, H. Takao, T. Kanafuji, K. Miura, M. Kondo, I. Hara-Nishimura, M. Nishimura H. Matsubara, *H. Plant Cell Physiol*. **1997**, *38*, 1069-1074.

8. (a) R Huisgen, *Angew. Chem. Int. Ed.* **1986**, *25*, 297-311; (b) A. de Meijire, *Angew. Chem. Int. Ed.* **2005**, *44*, 7836-7840.

9. A. von Baeyer, *Ber. Dtsch. Chem. Ges*. **1883**, *16*, 2188-2204.

10. A. Reis, W. Schneider, *Z. Kristallog.* ***1928***, **68**, 543-546.

11. A. von Baeyer, *Ber. Dtsch. Chem. Ges*. **1878**, *11*, 1228-1229.

12. A. von Baeyer, V. Drewsen, *Ber. Dtsch. Chem. Ges.* **1882**, *15*, 2856-2864.

13. P. Friedlaender, *Ber. Deutsch. Chem. Ges*. **1909**, *42*, 765-770.

14. (a) S. E. Sheppard, P. T. Newsome, *J. Am. Chem. Soc*. **1942**, *64*, 2937-2946; (b) M. Wyman, J. Weinstein , *J. Org.Chem*. **1956**, *78*, 2387-2390; (c) A. R. Monahan, J. E. Kuder, *J. Org. Chem.* **1972**, *37*, 4182-4184.

15. A. Amat, F. Rosi, C. Miliani, A. Sgamellotti, S. Fantacci, *J. Mol. Struct*. **2011**, *993*, 43-51.

16.(a) T. Kobayashi, P. M. Rentzepis, *J. Chem. Phys.* **1979** , *70*, 886;(b) I. Iwakura, A. Yabushita, T. Kobayashi, *Bull. Chem. Soc. Jpn*. **2011**, *84*, 164-171; (c) S. Yamazaki, L. Sobolewski, W. Domcke, *Phys. Chem. Chem. Phys.* **2011**, *13*, 1618-1628 .

17. P. Novotná, J. J. Boon, J. van der Horst, V. Pacáková, *Color. Technol.* **2003**, *119*, 121-127.

18. (a) M. Klessinger, W. Lüttke, *Tetrahedron* **1963**, *19*, 315-335; (b) W. Lüttke , H. Hermann , M. Klessinger , *Angew. Chem. Int. Ed.* **1966**, *5*, 598-99; (c) L. Serrano-Andrés, B. O. Roos, *Chem. Eur. J.* **1997**, *3*, 717-725; (d) D. Jacquemin, J. Preat, V. Wathelet, E. A. Perpète, *J. Chem. Phys*. **2006**, *124*, 74104-74112;

19. (a) C. Cooksey, *Molecules* **2001**, *6*, 736-769; (b) J. L. Wolk, A. A. Frimer, *Molecules* **2010**, *15*, *5473-5508.*

20. F. Sachs, R. Kempf, *Ber. Deutsch. Chem. Ges*. **1903**, *36*, 3299-3303.

21. J. R. Bailey, J. Travis, *Dyes Pigments* **1985**, *6*, 135-154.

22. M. Watanabe, N. Uemura, S. Ida, H. Hagiwara, K. Goto, T. Ishihara, *Tetrahedron* **2016**, *72*, 4280-4287.

23. (a) T. M. Ivanova, G. M. Ostapchuk, L. B. Shagalov, V. N. Berdyugin, *Chem. Heterocycl. Compd.* **1981**, *17*, 360-363; (b) S. Selvi, S.-C. Pu, Y. -M. Cheng, J.-M. Fang, P. -T. Chou, *J. Org. Chem*. **2004**, *69*, 6674-6678.

24. (a) P. W. Sadler, *J. Org. Chem.*, **1956**, *21*, 316-318; (b) M. Lamsabhi, C. A. Escobar, P. Perez, *J. Phys. Org. Chem*. **2005**, *18*, 1161-1168.

25. J. S. seixas de Melo, R. Randão, H. D. Burrows, M. J. Melo, S. Navaratnam, R. Edge, G. Voss, *ChemPhysChe*, **2006**, *7*, 2303-2311.

26. Y. Kanbur , M. Irimia-Vladu , E. D. Głowacki , G. Voss , M. Baumgartner , G. Schwabegger , L. Leonat , M. Ullah , H. Sarica , S. Erten-Ela , R. Schwödiauer , H. Sitter , Z. Küçükyavuz , S. Bauer , N. S. Sariciftci , *Org. Electron.* **2012**, *13*, 919-924.

27. I. V. Klimovich, L. I. Leshanskaya, S. I. Troyanov, D. V. Anokhin, D. V. Novikov, A. A. Piryazev, D. A. Ivanov, N. N. Dremova, P. A. Troshin, *J. Mater. Chem. C* **2014**, *2*, 7621-7631.

28. J. H. Porada, D. Blunk, *J. Mater. Chem*. **2010**, *20*, 2956–2958.

29. J. H. Porada, J. -M. Neudörfla, D. Blunk, *New J.Chem.* **2015**, *39*, 829-8301.

30. (a) J. Weinstein, G. M. Wyman, *J. Am. Chem. Soc.* **1956**, *78*, 4007-4010; (b) C. Yang, Q. T. Trinh, X. Wang, Y Tang, K. Wang, S. Huang, X. Chen, S. H. Mushrifa, M. Wang, *Chem. Commun.* **2015**, *51*, 3375-3378; (c) C.-Y. Huang, A. Bonasera, L. Hristov, Y. Garmshausen, B. M. Schmidt, *J. Am. Chem. Soc*. **2017**, *139*, 15205-15211.

31. M. Hammerich, C. Schütt, C. Stähler, P. Lentes, F. Röhricht, R. Höppner, R. Herges, *J. Am. Chem. Soc.* **2016**, *138*, 13111-13114.

32. (a) B. He, A. B. Pun, D. Zherebetskyy, Y. Liu, F. Liu, L. M. Klivansky, A. M. McGough, B. A. Zhang, K. Lo, T P. Russell, L. Wang, Y. Liu, *J. Am. Chem. Soc*. **2014**, *136*, 15093−15101; (b) J. Zhu, T. Li, K. Shi, J. Wang, Y. Lin, G. Yu, X. Zhan *J. Polym. Sci., Part A: Polym. Chem.* **2017**, *56*, 213-220.

33. F. Verstraeten, S. Gielen, P. Verstappen, J. Kesters, E. Georgitzikis, J. Raymakers, D. Cheyns, P. Malinowski, M. Daenen, L. Lutsen, K. Vandewalad, W. Maes *J. Mater. Chem. C* **2018**, *6*, 11645-11650.

34. S. R. Oakley, G. Nawn, K. M. Waldie, T. D. MacInnis, B. O. Patrickb, R. G. Hicks, *Chem. Commun.* **2010**, *46*, 6753-6755.

35. E. C. Nicholls-Allison, G. Nawn, B. O. Patrick, R. G. Hicks, *Chem. Commun.* **2015**, *51*, 12482-12485.

36. K. H. Ferber, *J. Environ. Pathol. Toxicol. Oncol*. **1987**, *7*, 73-83.

37. J. R. Mckee, M. Zanger, *J. Chem. Ed.* **1991**, *68*, A242-A244.

38. L. K. Wolf, *Chem. Eng. News* 2011, *89*, *44*.

39. (a) S. Wahyuningsih, A. H. Ramelan, D. K. Wardani, F. N. Aini, P. L. Sari, B. P. N. Tamtama, Y. R. Kristiawan, *IOP Conference Series: Materials Science and Engineering* **2017**, *193*, 012048 (1-6); (b) P. Doshi, J. Fox, P. Bently, J. Patel, C. Kulkarni, S. Halbe, Hananiah Dalton, *Tinted lenses and methods of manufacture*, *WO2005036236A2*, *WIPO (PCT)* **2005.**

40.(a) A. G. Newsome, C. A. Culver, R. B. van Breemen, *J. Agric. Food Chem.* **2014**, *62*, 6498-6511; (b) M. Kumar, M. P. Venkatesh, T. M. Pramod Kumar, *Int. J. Pathol. Clin. Res.* **2017**, *9*, 525-533.

41. Y. Hiroyuki, Organic transistors *JP 098454A*, **2008**.

42. (a) M. Imira-Vladu, P. A. Troshin, M. reisinger, L. Shmygleva, Y. Kanbur, G. Schwabegger, M. A. Bodea, R. Schwödiauer, A. Mumyatov, J. W. Fergus, V. Razumov, H. Sitter, N. S. Sariciftci, S. Bauer, *Adv. Funct. Mater.* **2010**, *20*, 4069-4076; (b) M. Imira-Vladu, E. D. Glowacki, P. A.

Troshin, G. Schwabegger, L. Leonat, D. K. Susarova, O. Kyshtal, M. Ullah, Y. Kanbur, M. A. Bodea, V. Razumov, H. Sitter, S. Bauer, N. S. Sariciftci, *Adv. Mater.* **2012,** *2*, 375-380.

43.(a) E. D. Głowacki, G. Voss, L. Leonat, M. Irimia-Vladu, S. Bauer, N. S. Sariciftci *Isr. J. Chem.* **2012**, *52*, 1-12; (b)E. D. Glowacki, G. Voss, N. S. Saricifti, *Adv. Mater.* **2013**, *25*, 6783-6800; (c) M. Gsänger, D. Bialas, L. Huang, M. Stolte, F. Würthner, *Adv. Mater*. **2016**, *28*, 3615-3645.

44. O. Pitayatanakul, T. Higashino, T. Kadoya, M. Tanaka, H. Kojima, M. Ashizawa, T. Kawamoto, H. Matsumoto, K. Ishikawa, T. Mori, *J. Mater. Chem. C* **2014**, *2*, 9311-9317.

45. E. D. Głowacki, G. Voss, K. Demirek, M. Havlicek, N. Sünger, A. C. Okur, U. Monkowius, J. Gąsiorowski, L. Leonat, N. S. Sariciftci, *Chem. Commun.* **2013**, *49*, 6063-6065.

46. D. V. Konarev, S. S. Khasanov, A. V. Kuzmin, A. F. Shestakov, A. Otsuka, H. Yamochi, G. Saito, R. N. Lyubovskayaa, *Dalton Trans*. **2016**, *45*, 17095-17099.

47. P. Mondal, A. Das, G. K. Lahiri, *Inorg. Chem*. **2016**, *55*, 1208-1218.

48. J.-Y. Wu, C.-H. Chang, P. Thanasekaran, C.-C. Tsai, T.-W. Tseng, G.-H. Lee, S.-M. Peng, K.-L. Lu, *Dalton Trans.* **2008**, 6110-6112.

49. W. Beck, C. Schmidt, R. Wienold, M. Steimunn, B. Wagner, *Angew. Chem. Int. Ed. Engl*. **1989**, *28*, 1529-1531.

50. M. Chatterjee, P. Ghosh, K. Beyer, A. Paretzki, J. Fiedler, W. Kaim, G. K. Lahiri, *Chem. Asian J.* **2018**, *13*, 118-125.

51. G. Nawn, K. M. Waldie, S. R. Oakley, B. D. Peters, D. Mandel, B. O. Patrick, R. McDonald, R. G. Hicks, *Inorg. Chem*. **2011**, *50*, 9826-9837.

52. (a)G. Nawn, R. McDonald, R. G. Hicks, *Inorg. Chem.* **2013**, *52*, 10912-10919; (b) G. Nawn, S. R. Oakley, M. B. Majewski, R. McDonald, B. O. Patrick, R. G. Hicks, *Chem. Sci*. **2013**, *4*, 612-622.

53. (a) Y. Matsumoto, H. Tananka, *Heterocycles* **2003**, *60*, 1805-1810; (b) C. Y. Huang, A. Bonasera, L. Hristov, Y. Garmshausen, B. M. Schmidt, D. Jacquemin, S. Hecht, *J. Am. Chem. Soc*. **2017**, *139*, 15205−15211; (c) C. Petermayer, H. Dube, *Acc. Chem. Res.* **2018**, *51*, 1153-1163.

54. (a) A. R. Katritzky, Q. -L. Li, W. -Q. Fan, *J. Heterocycl. Chem.* **1988**, *25*, 1287-1292; (b) A. D. Laurent, J. -M. Andre, E. A. Perpete, D. Jacquemin, *Chem. Phys. Lett*. **2007**, *436*, 84-88; (c) C. Petermayer, S. Thumser, F. Kink, P. Mayer, H. Dube, *J. Am. Chem. Soc.* **2017**, *139*, 15060-150

55. R. C. Pereira, M. Pineiro, A. M. Galvão, J. S. Seixas de Melo, *Dyes Pigments* **2018**, *158*, 259-266.

56. (a) K. Eggers, T. M. Fyles, P. J. Montoya-Pelaez, *J. Org. Chem.* **2001**, *66*, 2966-2977; (b) C. Thorben, S. Torsten, P. Beate, R. -B. Karola, Z. Wolfgang, *J. Phys. Chem. A* **2008**, *112*, 581-588; (c) A. Gerwien, T. Reinhardt, P. Mayer, H. Dube, *Org.Lett*. **2018**, *20*, 232-236; (d) K. Hoffmann, P. Mayera, H. Dube, *Org. Biomol. Chem*. **2019**, *17*, 1979-1983.

57. K. Fries, G. Fink, *Ber. Dcsch. Ges*. **1908**, *41*, 4271-4284.

58. F. W. Heineken, M. Bruin, F. Bruin, *Tetrahedron* **1963,** *19,* 439-443.

59. (a) D. L. Ross, J. Blanc, F. J. Matticoli, *J. Am. Chem. Soc.* **1970,** *92*, 5750-5752; (b) G. M. Wyman, B. M. Zarnegar, *J. Phys. Chem*. **1977**, *77*, 831-837.

60. (a) K. Fukunishi, M. Kobayashi, A. Morimoto, M. Kuwabara, *Bul. Chem. Soc. Jpn.* **1989**, *62*, 3733-3735; (b) M. Irie, H. Ishida, T. Tsujioka, *Jpn. J. Appl. Phys*. **1999**, *38*, 6114-6117; (c) N. J. Cherepy, R. D. Sanner, *Optical Materials* **2006**, *28*, 1350-1354.

61. J. T. Dy, R. Maeda, Y. Nagatsuka, K. Ogawa, K. Kamada, K. Ohta, Y. Kobuke, *Chem. Commun.***2007**, 5170-5172.

62. S. Yildizhan, H. Hopf, P. G. Jones, *Beilstein J. Org. Chem*. **2015**, *11*, 363-372.

63. R. A. Nathan, R. E. Schwerzel, A. H. Adelman, R. E. Wyant, U.S. Patent, 4004572, **1977**.

64. S.-F. Zhang, X.-K. Chen, J.-X. Fan, A.-M. Ren, *Org. Electron.* **2015**, *24*, 12-25.

Chapter 2

Synthesis and Characterization of *peri*-Naphthoindigo

Abstract*:* *peri*-Naphthoindigo (PNI) was synthesized for the first time from a simple precursor. Installation of the H-chromophore at *peri*-position of naphthalene is very distinctive in terms of synthetic difficulties and property. The common synthetic procedures known for indigo were unsuccessful towards PNI formation. The synthetic protocol developed for PNI was found to be very specific. Contrary to indigo, PNI exists in mono-enol form and has better solubility in common organic solvents than indigo.

2.1 Introduction

The "century old dye" indigo is an excellent example for a longstanding small molecule to find its spot in designing functional organic building blocks.[1] Apart from its traditional applications in the dye industry, in recent times indigo and other indigoids have been used as food colorants, pigments for contact lenses, and ambipolar organic semiconductor.[1,2] Indigo has also been used as ligand for various metal-complexes recently.[3] The origin of popularity and huge applications of indigo over centuries is to be found in its high photostability associated with the "H-chromophore" (Figure 1). In indigo the "H-chromophore" comprises of two cross-conjugated pairs of secondary amine (D = electron donor) and carbonyl (A = electron acceptor).[4] The scope of structural as well as functional tuning of indigo presents a fascinating field of work. Numerous synthetic modifications have been carried out around the H-chromophore. Normally, this is done in two different ways. On one hand, the outer phenyl rings have been substituted by different groups like halogens, alkyl, cyano, alkoxy etc (Figure 1).[5] On the other hand, modifications of the H-chromophore have been reported by replacing one or two N-H group(s).

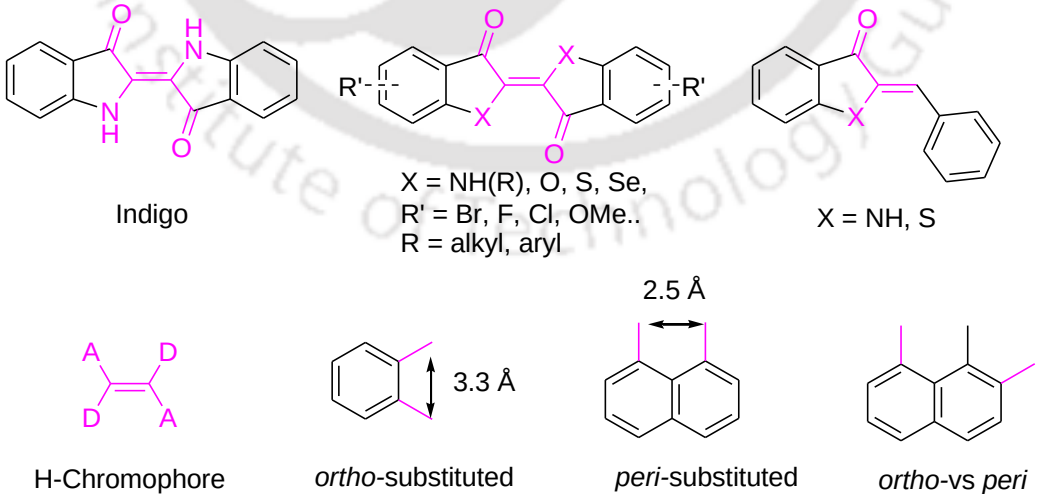

Figure 1. Structure of indigo; structural analogues of indigo; H-chromophore and steric scenarios at *ortho*- vs *peri*-position.

All these modifications led to generation of wide variety of ring- and N- substituted indigoids[6], oxindigo[7], thioindigo[8] and selenoindigo[9] dyes (Figure 1). Partial modification of the chromophore directed towards generation of hemiindigo[10] and hemithioindigo[11]. The synthetic alterations produced new molecules with exciting properties. For examples, photochromism have been reported on N,N'-disubstituted indigos,[6] hemiindigo,[10] hemithioindigo,[11] and thioindigo[8] dyes. Because of these, indigo dye is still an attractive molecule in scientific community[12] and quest for new indigoid is a burgeoning field of research. There was even report about unsuccessful attempts for preparation of all carbon indigoid systems.[13] An exciting and innovative modification along the same route is to install H-chromophore (D = NH, A = carbonyl) at *peri*-position of naphthalene (Figure 2) to make *peri*-naphthoindigo (PNI).

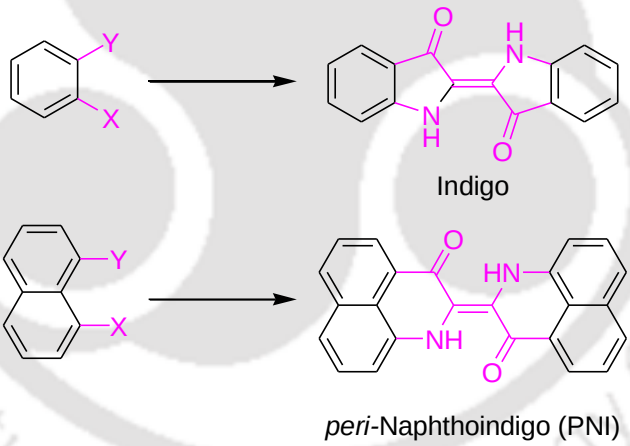

Figure 2. Structural analogy between indigo and PNI.

The 1- and 8-positions of naphthalene are said to be *peri* to each other. The planar geometry of naphthalene with all the bond angles close to 120.8°, results in parallel *exo*-bonds. Except for naphthalene itself (two hydrogen in peri positions), the rigid geometry of naphthalene imparts strain on any other (i.e. non-hydrogen) *peri*-atoms. When two atoms or functional groups are attached to these positions, they are in much closer proximity than similar substituents placed at *ortho*- to each other. In contrast to *ortho*-substituents attached on a

benzene ring and separated by about 3.3 Å, the 1- and 8-positions are relatively close with spatial distance of 2.5 Å, which is within the van der Waals radius for many atoms. This "proximity effect" [14] (Figure 1) results in the appearance of several unique properties of *peri*-substituted naphthalene both in terms of preparation and molecular behaviour. The structure of PNI was proposed first time in a U.S. patent in 1977 by R. A. Nathan and his co-workers claiming it to be a potential candidate for solar energy application.[15] Recently, theoretical calculation by A. M. Ren and his co-workers[16] predicted better performance of PNI than indigo as ambipolar organic semiconductor material. However, the fascinating molecule has never been synthesized. This chapter describes various unsuccessful and successful synthetic attempts, characterization and identification of PNI. Synthesis of PNI was attempted by employing the suitable naphthyl analogues to the phenyl precursors used in indigoid synthesis. Multiple synthetic routes were explored with different starting materials as well as reaction conditions. Synthesis of PNI was proven to be challenging. The outcome was indeed anticipated, as a result of *peri*-effect.

2.2 Synthesis of PNI

2.2.1 Synthetic route 1

One of the very popular methods for indigo synthesis was reported by Baeyer and Drewsen.[17] In this method *o*-nitrobenzaldehyde was treated with acetone in presence of aqueous NaOH. A series of reactions including crossed aldol reaction, cyclization, and dehydration produced the blue dye in single step. A similar strategy was employed for the synthesis of PNI. Accordingly the required precursor 8-nitro-1-naphthaldehyde (**3**) was prepared from 1-naphthaldehyde. Nitration of the aldehyde in presence of H_2SO_4/KNO_3 in dichloromethane

furnished a mixture of 5-nitro and 8-nitro derivative.[18] Chromatographic separation produced compound **3** in 45% yield. The precursor **3** was then treated with similar condition as reported by Baeyer. The reactant **3** was consumed within 15 min and the color of the reaction mixture changed from light yellow to dark reddish.

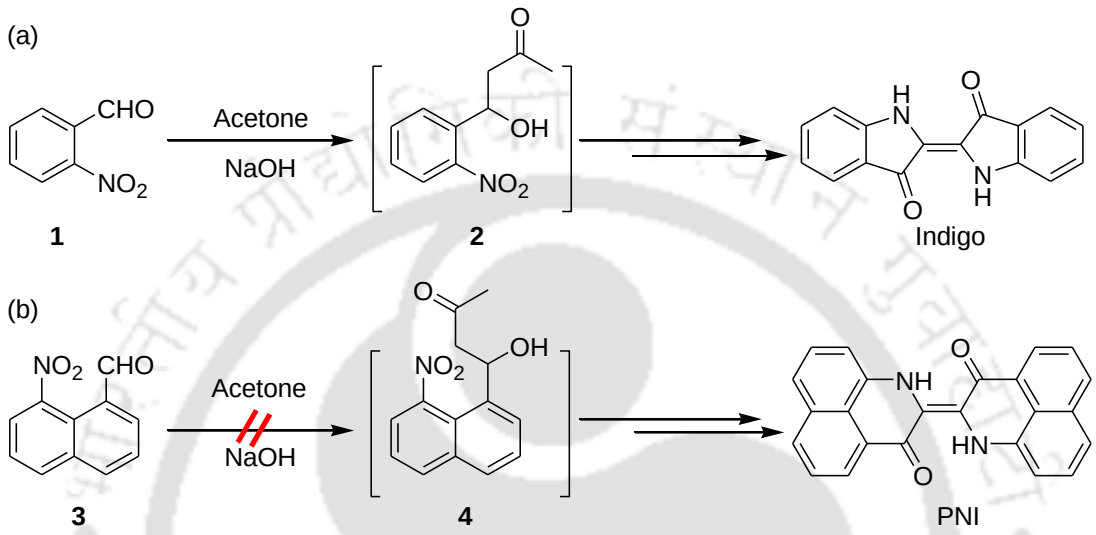

Scheme 1. Synthetic route for indigo (a) and PNI (outline, b) by Baeyer-Drewsen method.

The reaction was terminated after 24 h. The outcome of the reaction was complicated and chromatographic separation was unsuccessful. Greater steric hindrance at *peri*-position compare to *ortho*-position possibly caused such problem. Anticipating such difficulties, the conditions were altered by utilizing refluxing temperature. Despite of the modification and trials for different separation attempts, synthesis of PNI remained unsuccessful. An important intermediate in the reaction sequence of Baeyer-Drewsen method is the formation of cross-aldol adduct **2.** Several reactions pathways are possible from the intermediate.

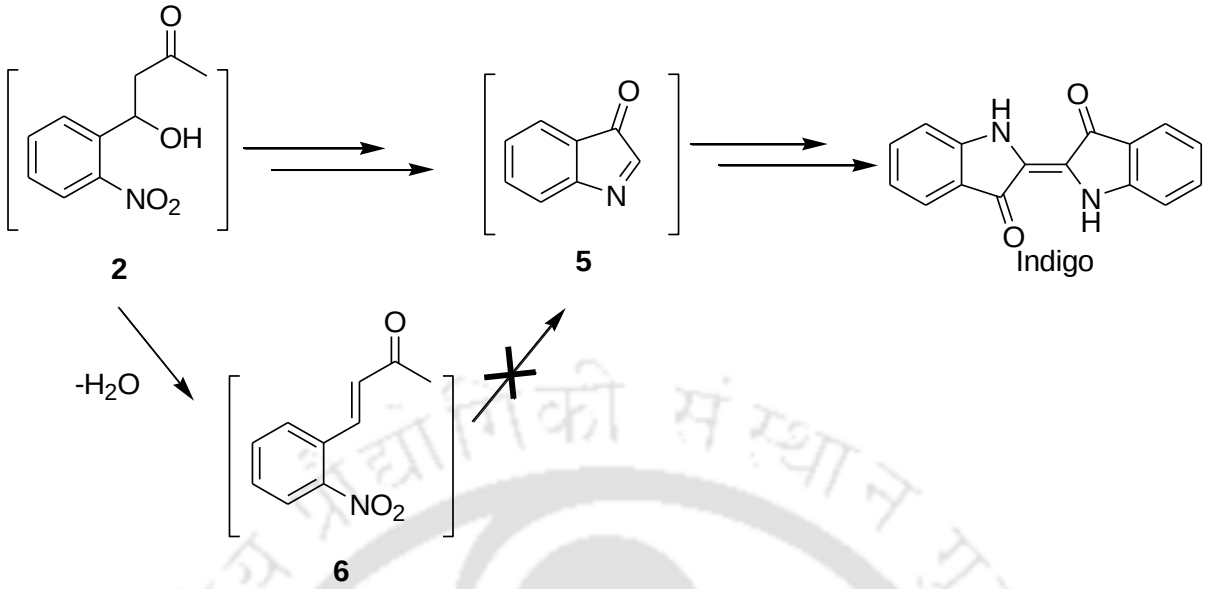

Scheme 2. Aldol-adduct **2** vs dehydrated-aldol product **6**.

Reductive cyclization, followed by dimerization and oxidation led to the formation of desired product. However, an unwanted side reaction is the formation of **6** via dehydration of **2**. The reaction condition should be such that it favors the reductive cyclization and hinder the dehydration process. In pursuit of synthesis of PNI, special attention was given to avoid dehydration of the aldol adduct. Mild reaction-conditions in terms of base strength and solvent polarity, which are known in literature to form cross-aldol adduct were employed. Reaction of **3** with acetone in presence of L-proline in DMSO at room temperature[19] was found to be unsuccessful. Further attempts with $Ba(OH)_2$ as the catalytic reagent at refluxing condition[20] resulted into negligible reactant conversion. Similar results were noticed when the reaction was done using K_2CO_3 in DMSO at refluxing condition.[21] Evidently, all modifications were insufficient to obtain the desired intermediate. Hence, the Baeyer-Drewsen method was not suitable for PNI synthesis.

2.2.2 Synthetic route 2

In the next attempt, Harley-Mason method[22] was used to prepare PNI following the synthetic outline depicted in Scheme 3b. In this procedure a stepwise approach was employed for indigo synthesis from *o*-nitrobenzaldehyde via formation of nitro-aldol adduct **7**.

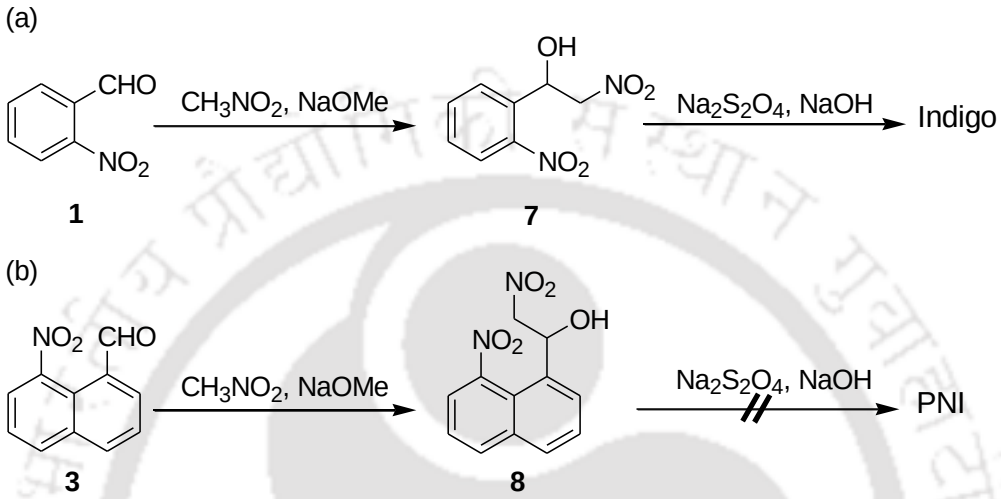

Scheme 3. Synthetic route for indigo (a) and PNI (outline, b) by Harley-Mason method.

Subsequent treatment of 7 with sodium dithionate in presence of sodium hydroxide leads to indigo formation (Scheme 3a) via reductive cyclization followed by dimerization and oxidation in presence of aerial oxygen. To prepare PNI using a similar reaction sequence, precursor **3** was treated with nitromethane in presence of sodium methoxide. Mass spectrometric analysis of the crude reaction mixture indicated formation of compound **8**. The crude yield of the first step was estimated to be 20%. Purification of compound **8** from the nitro-aldol reaction mixture was problematic, and the crude mixture was treated with alkaline sodium dithionite solution to yield PNI. But, this route was also found to be unsuccessful. Since the reaction of crude **8** was problematic, modifications were attempted to make **8** in higher yield. Initial changes were concentrated on reagents known to produce the required nitro-aldol adduct. Treatment of 8-nitro-1-naphthaldehyde with nitromethane in presence of imidazole in water at room temperature[23] did not produce the required product.

Use of Zn(L-proline)$_2$ as catalyst[24] was also turned out to be unsuccessful. Reaction of **4** and nitromethane in presence of ammonium acetate[25] in acetic acid under refluxing condition led to an inseparable mixture. Despite of successive chromatographic separation, isolation of **8** in pure form was not possible. Similar result was observed when potassium hydroxide[26] was used as base in an aqueous solution at 0°C. As all the attempted modifications were insufficient to obtain the desired intermediate, the Henry method was concluded to be unsuitable for PNI synthesis. The failure of this treatment can be explained in terms of the *proximity-effect*[14]of the naphthyl ring. Closer proximity of the functional groups resulted into diminished reactivity of the aldehyde group towards the nitro-aldol reaction. Even the small amount of obtained intermediate could not further proceed towards PNI formation due to different steric orientation from that of the phenyl-analogue.

2.2.3 Synthetic route 3

In 2011, Suzuki *et al.*[27] reported the preparation of indigo via oxidative dimerization of indole (**10**) using Mo(CO)$_6$ and organic peroxide (Scheme 4a). The main precursor indole was synthesized from **1** in two steps as depicted in Scheme 4a. Treatment of *o*-nitrobenzaldehyde and malonic acid in presence of piperidine and picoline yielded cinnamic acid derivative **9**.[28] Successive treatment of **9** with *bis*-(pinacolato)diboron produced **10** via boron-mediated deoxygenative cyclization. Following a similar strategy to realize PNI (as outlined in Scheme 4b), compound **12** was targeted starting from **3**. Reaction of compound **3** with malonic acid and piperidine in picoline resulted into a complex mixture of multiple new products with substantial amount of unreacted **3.** In order to gain an insight on feasibility of this reaction path way, this was followed by attempts to achieve boron-mediated deoxygenative cyclization by B_2pin_2 in presence of KF.[29]

It resulted into a complex mixture of multiple compounds. The crude mixture was treated with $Mo(CO)_6$ and organic peroxide.

(a)

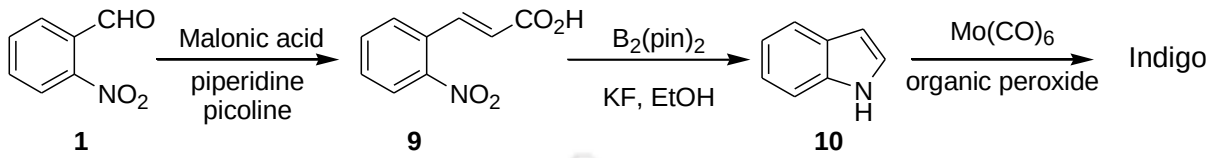

1 **9** **10**

(b)

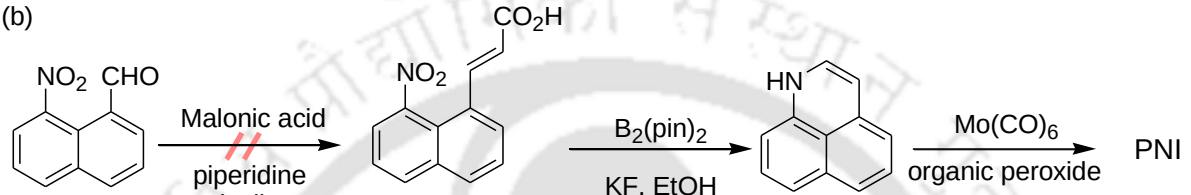

3 **11** **12**

Scheme 4. Synthetic route for indigo (a) and PNI (outline, b) via indole formation.

Prominent changes were observed in appearance and color of the reaction mixture but the changes observed were inconclusive towards PNI formation. Clearly, in this trial, formation of compound **11** was hindered owing to difference in reactivity of compound **3** compared to that of compound **1**. Modifications were attempted by following a microwave assisted reaction of compound **3** with malonic acid.[30] Improvement in reaction efficiency was not significant. Combined the problem of isolation of pure **11** and poor reactivity of the associated intermediate, this procedure was also concluded to be impractical. Accordingly, this synthetic route towards preparation of PNI from compound **3** was dismissed.

2.2.4 Synthetic route 4

In 1909, Paul Friedländer reported a synthesis procedure for 6,6'-dibromoindigo from *p*-aminotoluene via an acetyl-protected-indoxyl intermediate **14**. Later on Joel L. Wolk and Aryeh A. Frimer developed a new approach to synthesize **14.** Ullmann coupling of *o*-bromobenzoic acid and glycine produced **13.** On exposing compound **13** to sodium acetate in

acetic anhydride towards Claisen condensation yielded compound **14**. Successive hydrolysis of **14** in presence of sodium hydroxide produced indigo (Scheme 5a).[31]

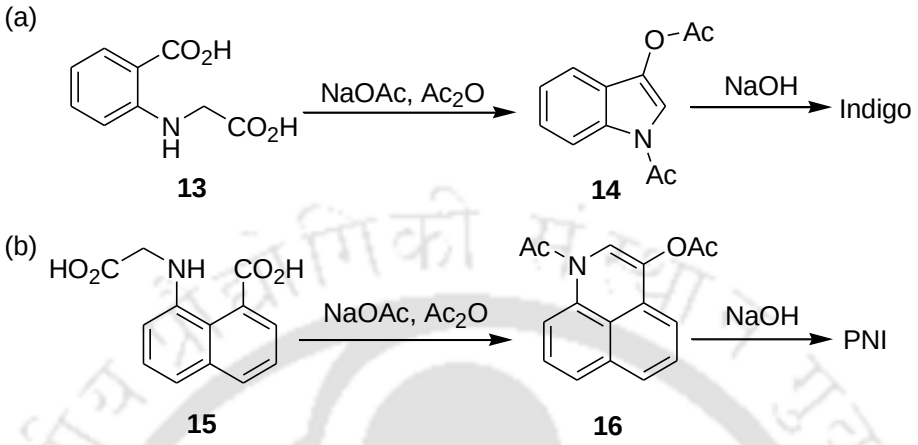

Scheme 5. Synthetic route for indigo (a), PNI (outline, b) via Claisen condensation.

To follow a similar strategy for the PNI, various synthetic efforts have been done to prepare the main precursor **15**. The synthesis started from 1,8-naphthalic anhydride (**17**) and all attempts are summarized in Scheme 6. First, **17** was converted to 8-iodo-1-naphthoic acid (**18**) following a synthetic method reported by Kobuke and his co-workers**.** [32] The naphthoic acid derivative was then treated with glycine in presence of Cu(0) to produce **15.** Although the reactant was consumed, the reaction was found to be proceeded in wrong direction. A complicated mixture of multiple products was produced. Isolation of pure compound from the mixture was not possible. Since single-step preparation of **15** from **18** was problematic, two-step approaches were tested. Compound **20** was synthesized from **18** in 12% yield. However, the conversion of **20** to **15** was found to be unsuccessful. Instead of the desired compound, lactam **22** was produced upon treatment of **20** with bromoacetic acid in presence of potassium carbonate. In next attempt, lactam **19** was prepared from 1,8-naphthalic anhydride[33] and subsequently treated with bromoacetic acid and potassium carbonate to yield

21. The N-substituted lactam **21** was then subjected to basic hydrolysis to prepare the target compound **15.**

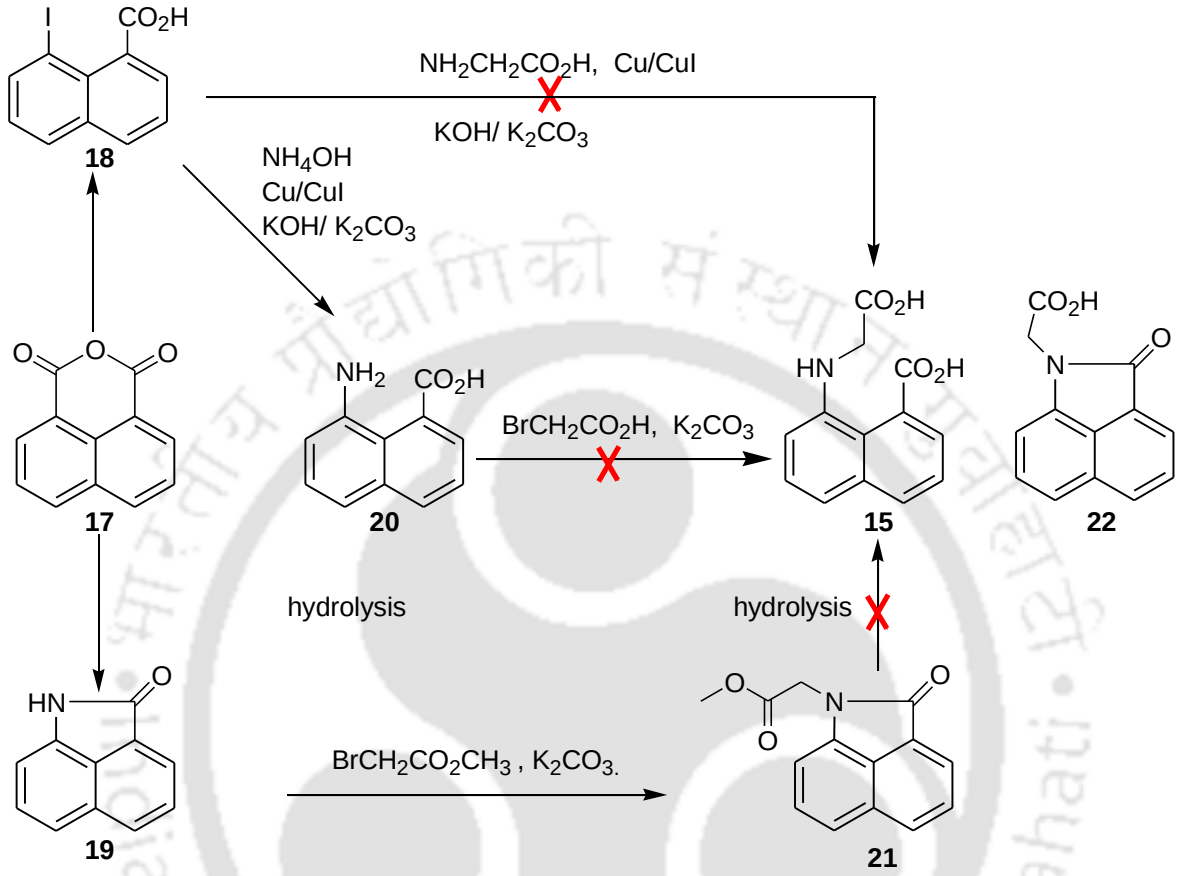

Scheme 6. Synthetic attempts towards compound **15**.

Isolation of the crude reaction mixture followed by thorough characterization using ^{1}H-NMR and HRMS indicated the formation of N-substituted lactam **22** as the major product along with negligible percentage of **15**. Further treatment of the crude mixture for Claisen condensation and successive hydrolysis for PNI synthesis produced an irresolute compound mixture. The synthetic route outlined in Scheme 5 was thus terminated prematurely.

2.2.5 Synthetic route 5

Utilizing aniline as a starting material, Karl Heumann successfully prepared indigo in 1897. In this method aniline was treated with 2-bromo acetic acid to yield N-phenyl glycine (**24**). Reaction of **24** with sodium-amalgam at high temperature led to the formation of **25**, which was subsequently undergone oxidative dimerization to indigo under aerobic condition. Viability of this reaction was immediately recognized by the BASF for industrial scale production of the blue dye.

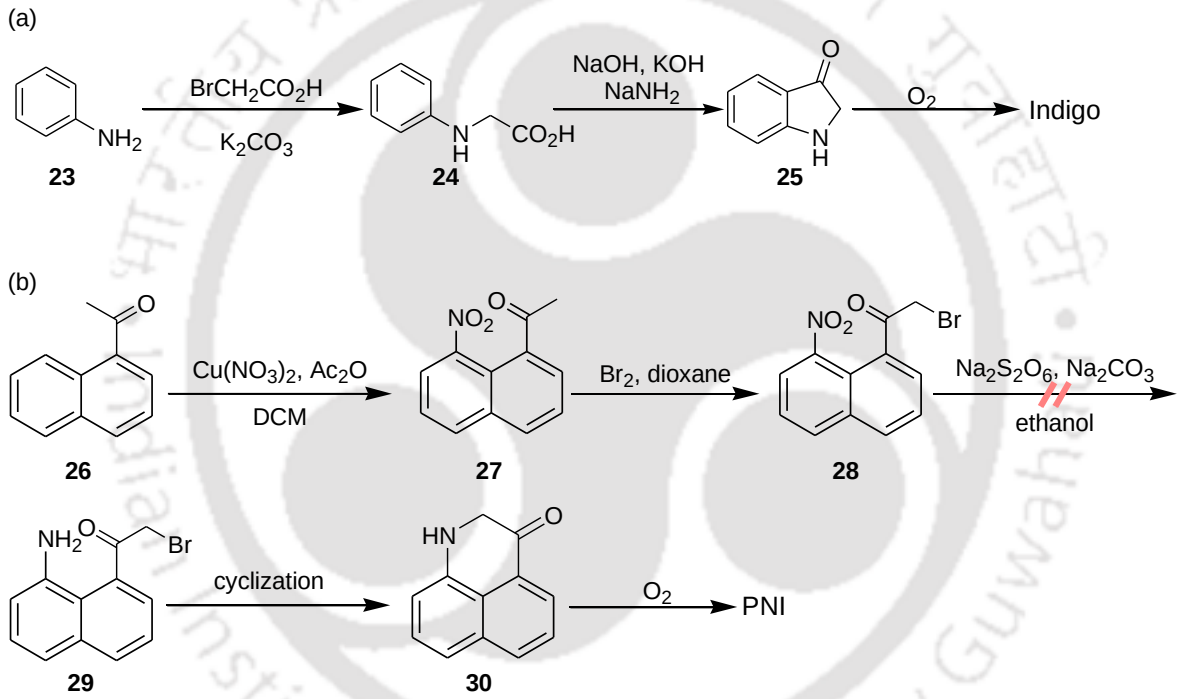

Scheme 7. (a) Heumann-Pfleger method for indigo synthesis. (b) Proposed synthetic route for PNI.

In 1901, Johannes Pfleger modified the cyclization procedure and applied a milder reaction condition by combining sodium hydroxide, potassium hydroxide and sodamide at a lower temperature.[34] To prepare PNI following a similar procedure, a synthetic route involving intermediate **30** was designed. The overall route is summarized in Scheme 7b. The synthesis started via nitration of 1-acetylnaphthalene. Treatment of Nitration of **26** in presence of $Cu(NO_3)_2/Ac_2O$ in dichloromethane furnished a mixture of 5-nitro and 8-nitro derivative.

Chromatographic separation produced the required 8-nitro derivative in 65% yield. Compound **27** was then treated with bromine in dioxane[35] to acquire **28** via aliphatic bromination. The yield was calculated to be 40% from the ^{1}H NMR spectrum of crude reaction mixture. Isolation of pure **28** was problematic and the crude mixture was used as such for next step. Treatment of compound **28** with sodium dithionate did not produce the desired compound 8-amino-1-bromoacetylnaphthalene (**29**).[36] Change in reagent for the reduction process did not improve the situation either and the synthetic route was abandoned without further investigations.

2.2.6 Synthetic route 6

After numerous unsuccessful attempts following procedures known for indigo synthesis, a new strategy was considered for PNI. In 2016, Song *et al.*[29] reported that boron-mediated reductive cyclization could be used to convert 2-nitrostyrene into indole by using ethanolic solution of B_2pin_2 and KF under inert condition (Scheme 8a). A similar reaction of the enol form of **27** can lead to the formation of PNI. Accordingly, 8-nitro-1-acetylnaphthalene (**27**) was refluxed in presence of *bis*-(pinacolato)diboron and KF in ethanol under inert atmosphere. The color of the reaction mixture changed from yellow to dark greenish-blue within 30-45 minutes of refluxing. After continuing the reaction for overnight the crude mixture was isolated and purified by column chromatography. The resulted dark-tarquish solid was significantly soluble in many organic solvents making it suitable for thorough characterization by various analytical techniques viz. high resolution mass spectrometry (HRMS) and NMR spectroscopy. HRMS spectrum of the compound using electrospray ionization (ESI) method showed a peak at m/z = 363.1142, which could be attributed to protonated PNI. Further insight into the structure of PNI was obtained by 1D and 2D NMR,

infrared spectroscopy (IR), and mass fragmentation. It is necessary to mention that PNI can exists in two isomers, mono-enol and di-keto.

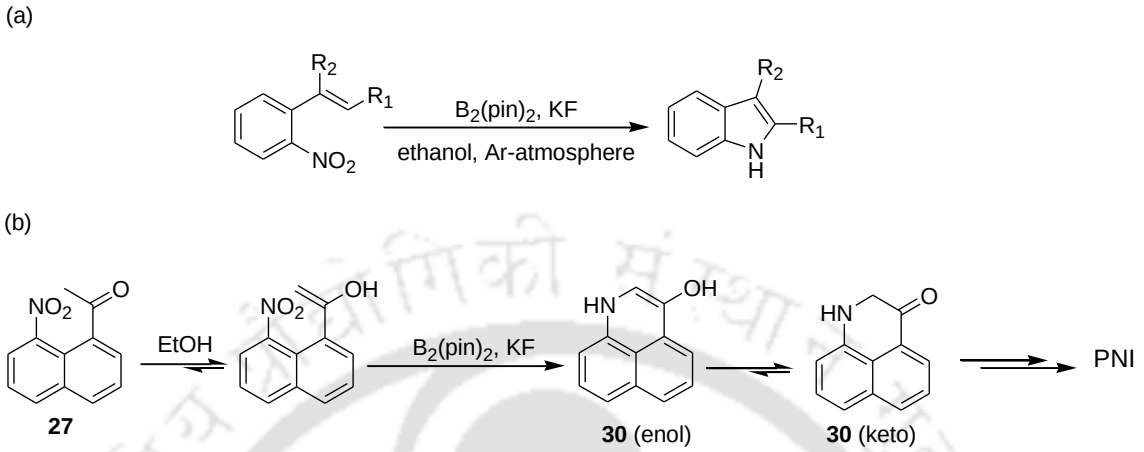

Scheme 8. Reaction outline towards intermediates for PNI synthesis via boron-mediated reductive cyclization.

2.3 Structure elucidation of PNI

Although indigo dye is insoluble in common organic solvent, PNI displays a better solubility profile. PNI has sufficient solubility in chloroform to record ^{1}H and ^{13}C NMR. Considering a diketo-structure, PNI is expected to show six different type aromatic protons along with a secondary amine (–NH) proton signal. Instead, its proton resonance spectrum showed twelve magnetically dissimilar aromatic protons, accompanying a sharp singlet at 7.22 ppm and a broad peak at 12.49 ppm (Figure 3). This observation can only be explained by considering mono-enol form of PNI, in which all aromatic protons are magnetically different. The sharp singlet at 7.22 ppm was assigned to N-H. Presence of hydroxy-group was evident from the broad signal at 12.49 ppm. In order to exclude possibility of mixing of any proton signal of PNI with the residual signal of chloroform, ^{1}H NMR was also recorded in acetone-d_6. The spectrum was found to be similar with the one acquired in $CDCl_3$.

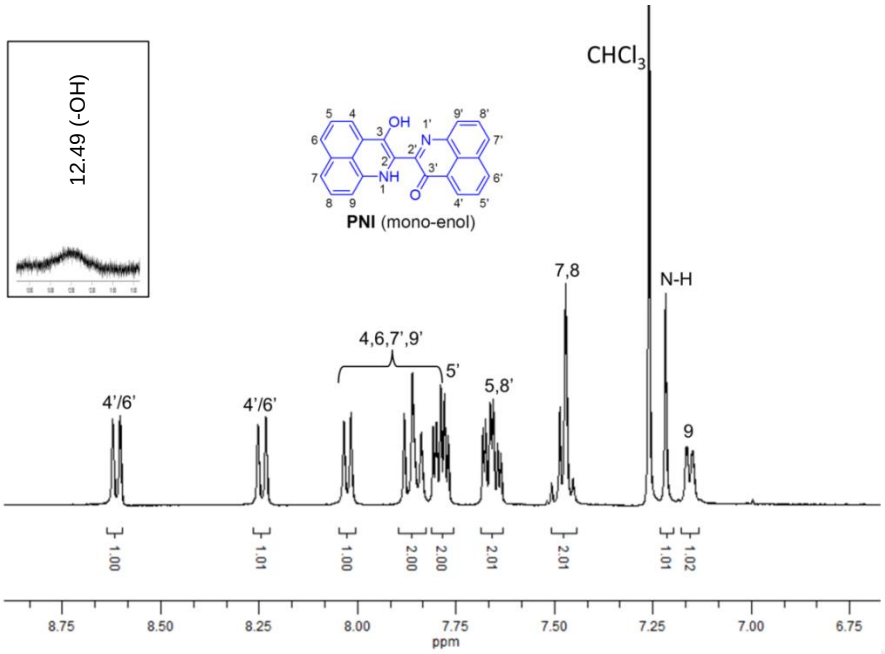

Figure 3. ^{1}H NMR spectrum of PNI (mono-enol) (400 MHz, $CDCl_3$, 295K).

Connectivity of the proton resonances and assignment of the signals was done by measuring ^{1}H-^{1}H correlation spectroscopy (COSY) of PNI.. COSY spectrum of the compound showed cross-peak correlation between the doublet at 7.16 ppm and the multiplets at 7.45-7.52 ppm. Combining 1D and 2D NMR, the peak at most electronically shielded region was assigned to C9-H. The proton resonances of C7,8-H was detected together as multiplet. The down field doublets at 8.24 and 8.61 ppm were associated with C4',6'-H. Their correlated cross peak was observed as a doublet of doublets (dd) at 7.79 ppm and was assigned to C5' proton. Signals for remaining halves of the naphthyl-rings were appeared as merged peaks of four doublets at 7.79, 7.85, 7.87 and 8.03 ppm (4,6,7',9'-H), and two dd at 7.66 ppm (5,8'-H). Their cross peak connectivity was found to be matched perfectly and justified the mono-enol structure of PNI.

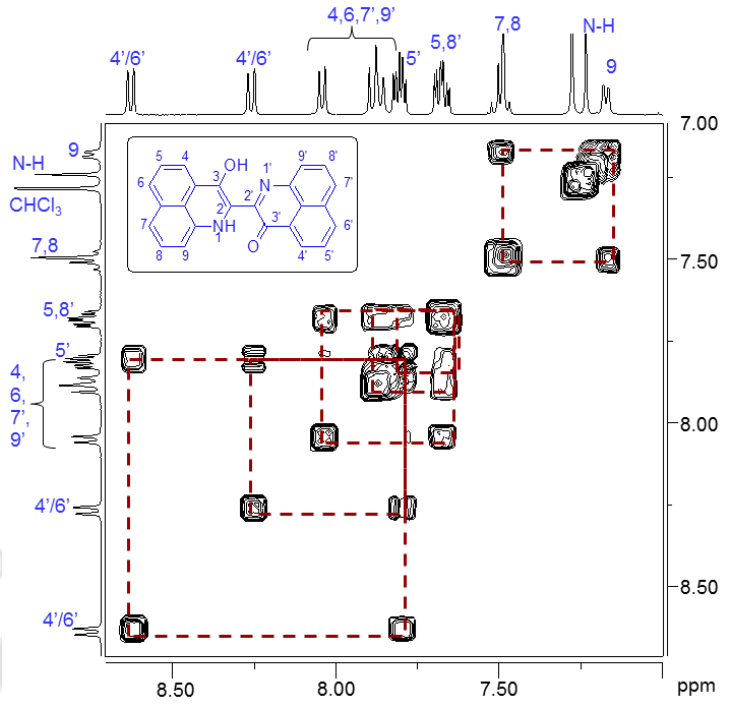

Figure 4. ^{1}H-^{1}H COSY (400 MHz, 295 K) spectrum of **PNI** (mono-enol) in $CDCl_3$.

Further evidence of the mono-enol structure was obtained by studying mass fragmentation. HRMS measurement at high voltage showed a prominent peak at m/z = 347.1179, which could be assigned to protonated PNI without a hydroxyl group. Generation of such fragmented peak is possible if there is hydroxyl group in the dye. Calculated isotopic distribution matched well with the experimentally obtained HRMS data. The observation further approved the presence of PNI in its mono-enol isomer.

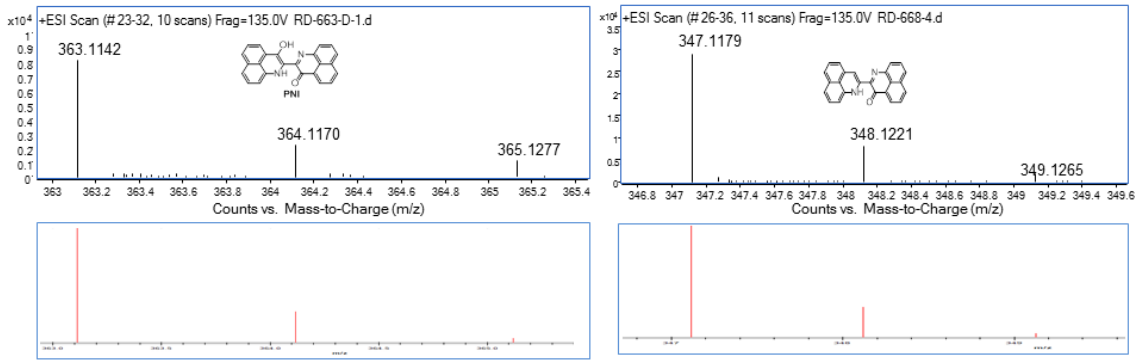

Figure 5. HRMS (ESI) spectrum (acetonitrile) of $[PNI + H]^+$, and $[(PNI - OH) + H]^+$ along calculated isotopic distribution (below, red).

Additional evidence of the suggested mono-enol structure was established from ^{13}C NMR (Figure 6) of PNI. Twenty four magnetically different carbon signals were detected in between 90.8 ppm and 179.5 ppm. The downfield signal present at 179.5 ppm was a clear indication of presence of carbonyl group in the obtained structure. Whereas the up-field signal at 90.8 ppm could be identified as the carbon on the chromophore next to the secondary amine.

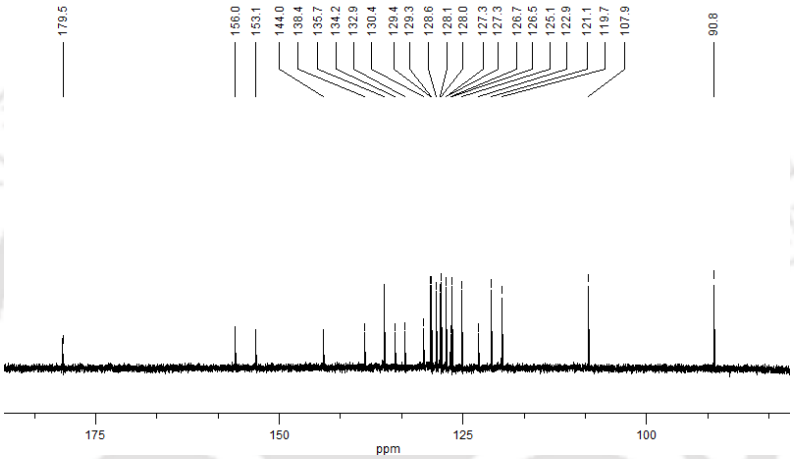

Figure 6. ^{13}C NMR spectrum of **PNI** (150 MHz, $CDCl_3$, 295K).

The structure of PNI was further corroborated using IR spectroscopy. A strong sharp signal at near 1602 cm^{-1} was identified as the stretching vibration of carbonyl functional-group in the chromophore. A very weak signal at around 1068 cm^{-1} was assigned to rocking vibration of C=O. The broad signal at 3440 cm^{-1} with a shoulder was associated with stretching vibration of N-H and O-H. Comparison with IR frequency of PNI to indigo dye[37] reflected on some notable differences. In indigo signals at around 1172, 1126, 1067, 712, and 563 cm^{-1} are distinctive of the five- membered rings formed between the H-chromophore and the phenyl ring. But in PNI peaks at around 1126, 712, and 563 cm^{-1} were completely absent with very weak signals present at around 1172, and 1067 cm^{-1}. This suggested the absence of five-membered ring in PNI and supported the connectivity through *peri-* instead of *ortho-* in the

naphthyl rings. PNI also exhibited peaks at 1515, 1385, 1277, 848 cm^{-1} completely segregated from indigo. Clearly, the IR spectrum of PNI supported the presence of four different functional groups in its cross-conjugated chromophore in terms of distinctive peaks associated with a variety of C-O, C=N, C-N and O-C-C-N connectivity. All other aromatic C-C, C-H, endocyclic double bond, C-N and N-H related signals were also in support of a mono-enol PNI structure. All the analytical data thus unambiguously confirmed the mono-enol form of PNI.

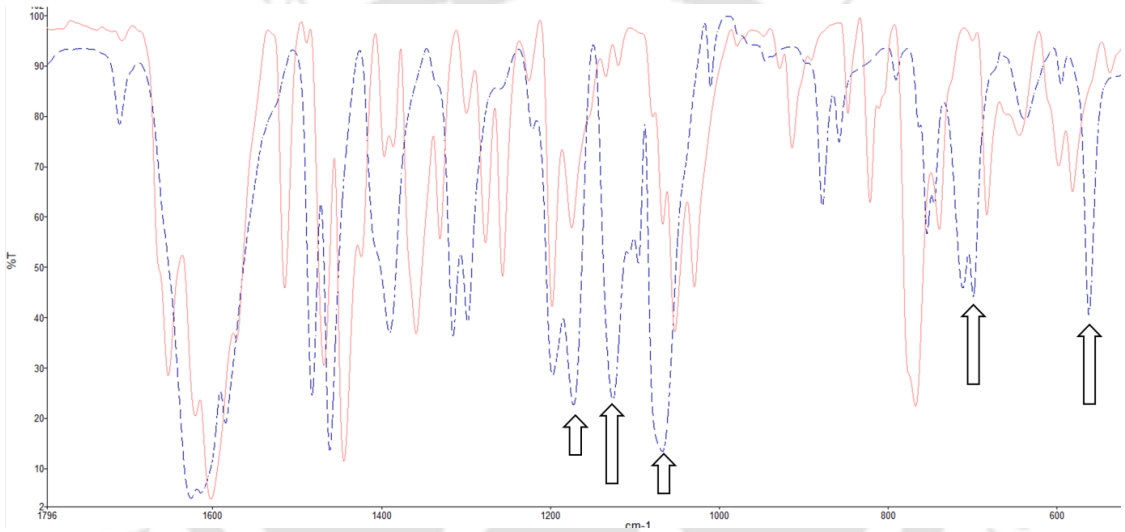

Figure 7. IR(KBr) spectra of PNI (solid, red) and indigo (dash, blue) dye. Differences are marked with arrow.

2.4 Mechanism of PNI formation

The formation of PNI occurred through a series of different reactions. Therefore, attention has been given to understand the mechanism of formation. Mechanistic insight is indeed necessary to get optimum yield and further modification. To get an idea of the plausible intermediates involved in this reaction, the course of the reaction was monitored. After exposing the reactant 8-nitro-1-acetyl naphthalene with the reagents for 30 min, the crude mixture was analysed by mass spectrometry.

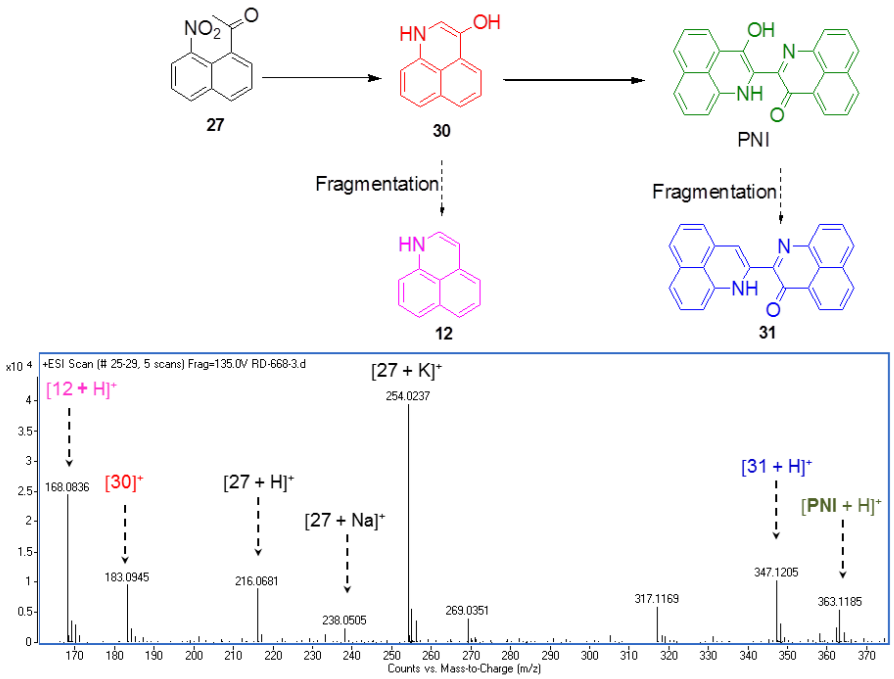

Figure 8. HRMS (ESI) spectrum (in acetonitrile/ethanol 1:1) of crude sample received during preparation of PNI.

In addition to the peaks that are associated with the reactant **27** and the product PNI, two additional peaks were detected at m/z = 168.0836 and 183.0945. The peak at higher m/z was associated with **30,** while the other one can be assigned to **12.** The formation of **12** occurred from **30** via fragmentation. Based on the observations and literature report, the pathway of PNI formation could be briefed as depicted in Scheme 9. The reaction started with reductive cyclization of the enol form of **27**, producing compound **30**. Bis(pinacolato)diboron mediated reductive cyclization occurred in a similar fashion as reported by Song et al.[29]

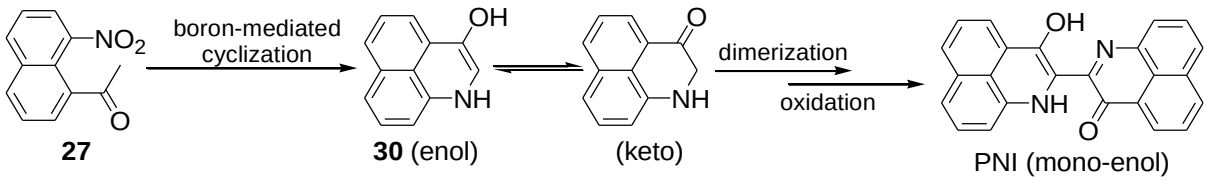

Scheme 9. Plausible mechanism of PNI formation

Dimerization of **30**, followed by oxidation led to the formation of PNI. Preparation of indigo from indoxyl followed a similar route of dimerization followed by oxidation and the mechanistic pathway is well established.[38] A combination of literature report on reductive cyclization by Song et al.,[29] report on dimerization followed by oxidation for the indigo preparation,[38] and HRMS data established the mechanism of PNI formation as summarized in Scheme 9 .

2.5 Optimization of reaction condition

From the mechanistic pathways, it was clear that the formation occurred through a series of reactions including, reductive cyclization, dimerization and oxidation. Enolization of the reactant **27** was also an important step in the reaction sequence. Hence, attention was given to various reaction parameters to get optimum yield. Various solvents were tested to accelerate enolization of **27**. Different reagents have been used to get best condition for reductive cyclization. Reactions were performed in aerobic as well as in inert conditions. Various bases, and reaction temperatures have also been tried. The reductive cyclization occurred only in presence of B_2pin_2/KF. Other reagents, known for similar reactions, were found to be incapable for PNI synthesis. For example, treatment of **27** with $P(OEt)_3/K_2CO_3$[39] did not produce PNI even at 170 ^oC. The reaction was carried out different solvent including non-polar toluene and polar ethanol. Considering the importance of oxidation, the reaction was performed under aerobic as well as inert atmosphere. The yield was improved considerably from 21% in nitrogen-atmosphere to 65% under aerobic atmosphere. However, the yield was decreased to 12% in a pure oxygenic reaction environment. Similar trend was noticed in case of indigo synthesis.[40]

Reaction conditions were also altered by changing base, other condition (Table 1). Best result was received when ethanol was used as solvent and KF as base in air (entry 2, Table 1).

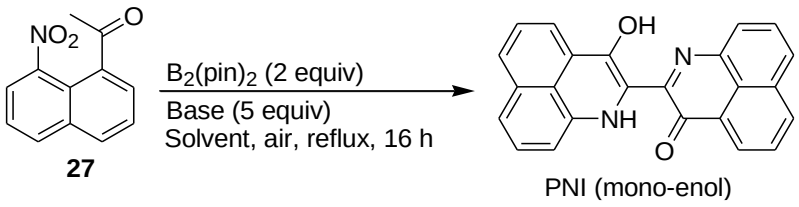

Table 1. Effects of solvent and base on **PNI** synthesis.

entry	base	solvent	yield (%)[a]
1	KF	EtOH	21[b]
2	**KF**	**EtOH**	**65**
3	Cs_2CO_3	EtOH	55
4	K_2CO_3	EtOH	55
5	CsF	EtOH	25
6	NaOH	EtOH	trace
7	^{t}BuOK	EtOH	trace
8	AcOK	EtOH	10
9	KF	1,4-dioxane	trace
10	KF	MeOH	trace
11	KF	toluene	trace

[a]Yields were calculated from NMR measurements. [b]Reaction was carried out under N_2 atmosphere.

In presence of strong bases like NaOH, ^{t}BuOK, the yield decreased significantly to trace amount. Aldol reaction of the keto-form of **27** was possibly the major reaction in presence of NaOH. Applicability of KF, over the other bases like CsF, K_2CO_3 and Cs_2CO_3 could be attributed towards its role in the process of reductive cyclization. This observation was also in line with the observed trend of base sensitivity towards 2-nitrostyrene into indole conversion. On the other hand, successful completion of the reaction towards PNI in alcohol can be attributed to stabilization of enol form of **27**. The polar enol-form was clearly more supported

in ethanol than in 1,4-dioxane or toluene. On the same note, less effectiveness of methanol than ethanol was due its lower boiling-point providing a lower temperature into the reaction. Another interesting fact established was that the reagents and condition for PNI production was very specific. Treatment of *o*-nitroacetophenone with B_2pin_2 and KF in ethanol did not produce indigo at all. Different steric scenario at *peri*-position compared to *ortho*-position known as the proximity-effect was possibly the reason of such outcome. This also purposefully explained the initial failures of the procedures with established reports on indigo-synthesis.

2.6 Geometry optimization

PNI was isolated and identified in its mono-enol form. Contrary to the known indigoid structures bearing a stable diketo isomer, PNI presented a fascinating case for structural studies. A solid state characterization of PNI in its single crystalline form would provide a better light on its structural ubiquity. Unfortunately, even after multiple trials it was not possible to get a proper diffractable single crystal for XRD-studies. The isolated crystals were very thin and dark coloured. In absence of crystal data, the geometry of PNI was optimized theoretically. The single point energy calculations for mono-enol PNI in ground state in the vacuum as well as in chloroform were performed by destiny functional theory (DFT) methods at B3LYP/6-31+G(d,p)[41] level implemented in Gaussian 09.[42] No significant differences have been noticed between the optimized structures in vacuo and in chloroform. A closer look at the bonding parameters of the optimized structure, revealed the effect of steric restrain at the 1,8-*peri* positions of naphthalene skeletal. The most significant observations are the resultant bond-lengths and the bond-angles around the central-

chromophore. The optimized structure also showed that, around C3, C14, C15, C16 substantial deviation occur from the ideal bond angle of 120° for sp^2-carbons.

From DFT, highest occupied molecular orbital (*HOMO*) and lowest unoccupied molecular orbital (*LUMO*) energy levels of frontier orbital were obtained. The charge distribution of the HOMO and the LUMO are depicted in Figure 9. The HOMO and LUMO in PNI are localized primarily over the chromophoric core of the molecule.

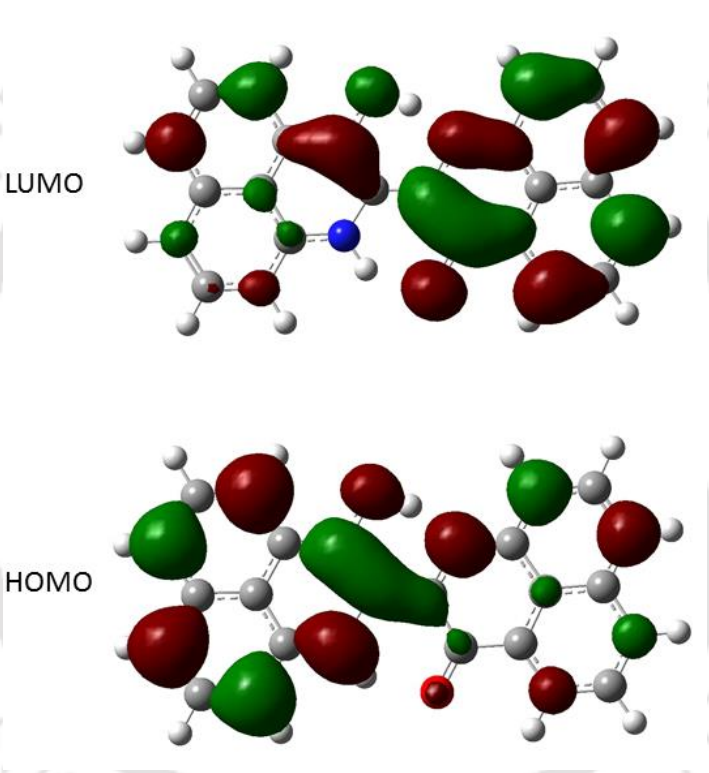

Figure 9. HOMO, LUMO isodensity plots of mono-enol PNI in vacuo and chloroform.

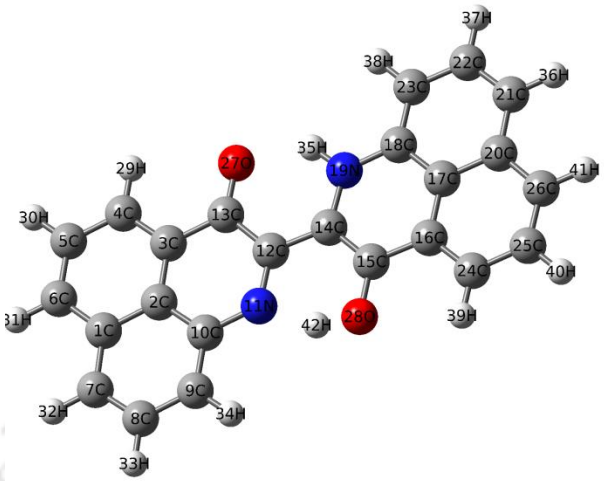

Table 2. Geometry optimized structure and bonding parameters of PNI from DFT.

Bond-length			
Coordinate	Value (Å)	Coordinate	Value (Å)
C1-C2	1.4081	C14-N19	1.403
C1-C6	1.4274	C15-C16	1.466
C1-C7	1.4242	C15-O28	1.362
C2-C3	1.4243	C16-C17	1.427
C2-C10	1.4217	C16-C24	1.388
C3-C4	1.3857	C17-C18	1.423
C3-C13	1.4747	C17-C20	1.407
C4-C5	1.4189	C18-N19	1.389
C5-C6	1.3772	C18-C23	1.386
C7-C8	1.3795	N19-C35	1.050
C8-C9	1.4147	C20-C21	1.426
C9-C10	1.3873	C20-C26	1.424
C10-N11	1.3994	C21-C22	1.379
N11=C12	1.2917	C22-C23	1.4165
C12-C13	1.5008	C24-25	1.4165
C12-C14	1.4768	C25-C26	1.3784
C13=O27	1.2304	O28-H42	0.968
C14=C15	1.376		

Bond angles			
Coordinate	Angle (°)	Coordinate	Angle (°)
C1-C2-C3	120.178	C17-C20-C21	119.126
C2-C3-C4	119.813	C20-C21-C22	120.412
C3-C4-C5	120.012	C21-C22-C23	120.611
C4-C5-C6	120.766	C22-C23-C18	119.732
C5-C6-C1	120.204	C23-C18-C17	120.452
C6-C1-C2	119.017	C17-C16-C24	117.918
C1-C2-C10	120.434	C18-C17-C20	119.660
C2-C10-C9	119.051	C16-C17-C20	121.442
C10-C9-C8	120.680	C16-C24-C25	121.189
C9-C8-C7	121.028	C24-C25-C26	120.711
C8-C7-C1	120.131	C25-C26-C20	119.895
C7-C1-C2	119.094	C26-C20-C17	118.838
C2-C3-C13	118.739	C17-C18-N19	117.610
C2-C10-N11	121.121	C18-N19-C14	125.159
C10-N11-C12	122.171	N19-C14-C15	118.750
N11-C12-C13	121.373	C14-C15-C16	118.763
C3-C2-C10	119.387	C15-C16-C17	120.802
C3-C13-C12	116.204	C16-C17-C18	118.896
C12-C13-27O	122.0902	C14-C15-O28	122.339
N11-C12-C14	117.553	C15-O28-H42	109.721
C13-C12-C14	121.072	C14-C19-C35	117.891
		C12-C14-C15	124.569
		C12-C14-N19	116.678

2.7 Conclusion

In conclusion, changing the position of chromophore from *ortho*-position to *peri*- position made the synthesis challenging compared to that of reported indigoids. Multiple analogous synthetic methods known for indigo and other indigoids were unproductive in case of PNI. In fact, the reaction condition was found to be PNI exclusive. PNI preparation involved a combination of reductive cyclization, dimerization and oxidation reactions. On structural identification of the new dye by a combination of HRMS, NMR and IR spectroscopy it was established that unlike indigo, PNI exists in mono-enol form.

2.8 References

1. E. D. Glowacki, G. Voss, N. S. Sariciftci, *Adv. Mater.* **2013**, *25*, 6783-6800.
2. (a) K. H. Ferber, *J. Environ. Pathol. Toxicol. Oncol.* **1987**, *7*, 73-83; (b) M. Irimia-Vladu, E. D. Głowacki, P. A. Troshin, G. Schwabegger, L. Leonat, D. K. Susarova, O. Krystal, M. Ullah, Y. Kanbur, M. A. Bodea, V. F. Razumov, H. Sitter, S. Bauer, N. S. Sariciftci, *Adv. Mater.* **2012**, *24*, 375-380; (c) A. G. Newsome, C. A. Culver, R. B. van Breemen, *J. Agric. Food Chem.* **2014**, *62*, 6498-6511; (d) M. Gsänger, D. Bialas, L. Huang, M. Stolte, F. Würthner, *Adv. Mater.* **2016**, *28*, 3615-3645.
3. (a) J.-Y. Wu, C.-H Chang, P. Thanasekaran, C.-C. Tsai, T.-W. Tseng, G.-H. Lee, S.-M. Peng, K.-L. Lu, *Dalton. Trans.* **2008**, 6110-6112; (b) D. Bhattacharya, C.-H. Chang, Y.-H. Cheng, L.-L. Lai, H.-Y. Lu, C.-Y. Lin, K.-L. Lu, *Chem. Eur. J.* **2012**, *18*, 5275-5283; (c) P. Mondal, A. Das, G. K. Lahiri, *Inorg. Chem.* **2016**, *55*, 1208-1218; (d) P. Mondal, M. Chatterjee, A. Paretzki, K. Beyer, W. Kaim, G. K. Lahiri, *Inorg. Chem.* **2016**, *55*, 3105-3116; (e) D. V. Konarev, L. V. Zorina, S. S. Khasanov, A. F. Shestakov, A. M. Fatalov, A. Otsuka, H. Yamochi, H. Kitagawa, R. N. Lyubovskaya, *Inorg. Chem,* **2018**, *57*, 583-589; (f) M. Chatterjee, P. Ghosh, K. Beyer, A. Paretzki, J. Fiedler, W. Kaim, G. K. Lahiri, *Chem. Asian J.* **2018**, *13*, 118-125.
4. R. M. Christie, *Biotech. Histochem.* **2007**, *82*, 51-56.
5. (a) P. Friedländer, *Ber. Dtsch. Chem. Ges.* **1909**, *42*, 765-770; (b) J. C. Duff, ***J. Chem. Soc. Trans.*** **1914**, ***105***, 2182-2186; (c) I. T. Shadi, B. Z. Chowdhry, M. J. Snowden, R. Withnall, *Chem. Comm.* **2004**, *0*, 1436-1437; (*d*) J. L. Wolk, A. A. Frimer, *Molecules* **2010**, *15*, 5473-5508; (e) E.

D. Głowacki, G. Voss, K. Demirak, M. Havlicek, N. Sünger, A. C. Okur, U. Monkowius, J. Gąsiorowski, L. Leonat, N. S. Sariciftci, *Chem. Comm.* **2013**, *49*, 6063-6065; (f) I. V. Klimovich, L. I. Leshanskaya, S. I. Troyanov, D. V. Anokhin, D. V. Novikov, A. A. Piryazev, D. A. Ivanov, N. N. Dremova, P. A. Troshin, *J. Mater. Chem. C* **2014**, ***2***, 7621-7631; (g) C. Guo, J. Quinn, B, Sun, Y. Li, *J. Mater. Chem. C* **2015**, *3*, 5226-5232; (h) J. H. Porada, J.-M. Neudörfl, D. Blunk, *New J. Chem.* **2015**, *39*, 8291-8301; (*i*) M. Watanabe, N. Uemura, S. Ida, H. Hagiwara, K. Goto, T. Ishihara, *Tetrahedron* **2016**, *72*, 4280-4287.

6. (a) L. Ettinger, P. Friedländer, *Ber. Dtsch. Chem. Ges.* **1912**, *45*, 2074-2080; (b) J. Weinstein, G. M. Wyman, *J. Am. Chem. Soc.* **1956**, *78*, 4007-4010; (c) C. R. Giuliano, L. D. Hess, J. D. Margerum, *J. Am. Chem. Soc.* **1968**, *90*, 587-594; (d) K. S. Schanze, L. Y. C. Lee, C. Giannotti, D. G. Whitten, *J. Am. Chem. Soc.* **1986**, *108*, 2646-2655; (e) A. Nuñez, T. Hollebeek, M. M. Labes, *J. Am. Chem. Soc.* **1992**, *114*, 4925-4926; (f) M. Sytnyk, E. D. Głowacki, S. Yakunin, G. Voss, W. Schöfberger, D. Kriegner, J. Stangl, R. Trotta, C. Gollner, S. Tollabimazraehno, G. Romanazzi, Z. Bozkurt, M. Havlicek, N. S. Sariciftci, W. Heiss, *J. Am. Chem. Soc.* **2014**, *136*, 16522-16532; (g) C. Yang. Q. T. Trinh, X. Wang, Y. Tang, K. Wang, S. Huang, X. Chen, S. H. Mushrif, M. Wang, *Chem. Commun.* **2015**, *51*, 3375-3378; (h) D. Farka, M. Scharber, E. D. Głowacki, N. S. Sariciftci, *J. Phys. Chem. A* **2015**, *119*, 3563-3568; (i) J. Pina. D. Sarmento, M. Accoto, P. L. Gentili, L. Vaccaro, A. Galvão, J. S. Seixas de Melo, *J. Phys. Chem. B* **2017**, *121*, 2308-2318. (j)C.-Y. Huang, A. Bonasera, L. Hristov, Y. Garmshausen, B. M. Schmidt, D. Jacquemin, S. Hecht, *J. Am. Chem. Soc.* **2017**, *139*, 15205-15211.
7. (a) K. Fries, A. Hasselbach, *Ber. Dtsch. Chem. Ges.* **1911**, *44*, 124-128; (b) R. Stoermer, K. Brachmann, *Ber. Dtsch. Chem. Ges.* **1911**, *44*, 315-319; (c) F. Bruin, F. W. Heineken, M. Bruin, *J. Org. Chem.* **1963**, *28*, 562-564; (d) H. Langhals, B. Wagner, *Angew. Chem., Int. Ed.* **1996**, *35*, 1016-1019.
8. (a) P. Friedländer, *Ber. Dtsch. Chem. Ges.* **1906**, *39*, 1060-1069; (b) L. Dinescu, R. P. Lemieux, *Adv. Mater.* **1999**, *11*, 42-45; (c) D. Jacquemin, J. Preat, V. Wathelet, M. Fontaine, E. A. Perpète, *J. Am. Chem. Soc.* **2006**, *128*, 2072-2083; (d) R. Rondão, J. S. Seixas de Melo, *J. Phys. Chem. C* **2013**, *117*, 603-614; (e) M. Dittmann, F. F. Graupner, B. Maerz, S. Osterling, R. de Vivie-Riedle, W. Zinth, M. Engelhard, W. Lüttke, *Angew. Chem. Int. Ed.* **2014**, *53*, 591-594; (f) G. Boice, B. O. Patrick, R. McDonald, C. Bohne, R. Hicks, *J. Org. Chem.* **2014**, *79*, 9196-9205.
9. (a) D. R. Ross, J. Blanc, F. J. Matticoli, *J. Am. Chem. Soc.* **1970**, *92*, 5750-5752; (b) H. Bauer, K. Kowski, H. Kuhn, W. Lüttke, P. Rademacher, *J. Mol. Struct.* **1998**, *445*, 277-286; (c) R. Gerke, L. Fitjer, P. Müller, I. Usón, K. Kowski, P. Rademacher, *Tetrehedron* **1999**, *55*, 14429-14434.

10. C. Petermayer, S. Thumser, F. Kink, P. Mayer, H. Dube, *J. Am. Chem. Soc.* **2017**, *139*, 16060-16067.
11. (a) S. Wiedbrauk, B. Maerz, E. Samoylova, A. Reiner, F. Trommer, P. Mayer, W. Zinth, H. Dube, *J. Am. Chem. Soc.* **2016**, *138*, 12219-12227; (b) F. Kink, M. P. Collado, S. Wiedbrauk, P. Mayer, H. Dube, *Chem. Eur. J.* **2017**, *23*, 6237-6243; (c) L. A. Huber, K. Hoffmann, S. Thumser, N. Böcher, P. Mayer, H. Dube, *Angew. Chem., Int. Ed.* **2017**, *56*, 14536-14539; (d) J. E. Zweig, T. R. Newhouse, *J. Am. Chem. Soc.* **2017**, *139*, 10956-10959.
12. (a) G. Nwan, K. M. Waldie, S. R. Oakley, B. D. Peters, D. Mandel, B. O. Patrick, R. McDonald, R. G. Hicks, *Inorg. Chem.* **2011**, *50*, 9826-9837; (b) G. Nwan, S. R. Oakley, M. B. Majewski, R. McDonald, B. O. Patrick, R. G. Hicks, *Chem. Sci.* **2013**, *4*, 612-621; (c) E. C. Nicholls-Allison, G. Nawn, B. O. Patrick, R. G. Hicks, *Chem. Commun.* **2015**, *51*, 12482-12485; (d) T. M. Hsu, D. H. Welner, Z. N. Russ, B. Cervantes, R. L. Prathuri, P. D. Adams, J. E. Dueber, *Nat. Chem. Biol.* **2018**, *14*, 256-261.
13. S. Yildizhan, H. Hopf, P. G. Jones, *Beilstein J. Org. Chem.* **2015**, *11*, 363-372.
14. (a)V. Balasubramaniyan, *Chem. Rev.* **1966**, *66*, 567-641; (b) P. Kilian, F. R. Knight, J. D. Woollins, *Chem. Eur. J.* **2011**, *17*, 2302-2328.
15. R. A. Nathan, R. E. Schwerzel, A. H. Adelman, R. E. Wyant, U.S. Patent, 4004572, **1977**.
16. S.-F. Zhang, X.-K. Chen, J.-X. Fan, A.-M. Ren, *Org. Electron.* **2015**, *24*, 12-25.
17. A. Baeyer, V. Drewsen, *Ber. Dtsch. Chem. Ges.* **1882**, *15*, 2856-2864.
18. (a) G. Spiteller, J. Derkosch, *Monatsh. Chem.* **1959**, *90*, 634-644; (b) S. D. Barker, K. Wilson, R. K. Norris, *Aust. J. Chem.* **1995**, *48*, 1969-1979; (c) P. Strazzolini, A. G. Giumanini, A. Runcio, *Tetrahedron Lett.* **2001**, *42*, 1387-1389.
19. B. List, R. A. Lerner, C. F. Barbas, *J. Am. Chem. Soc.* **2000,** *122*, 2395-2396.
20. J. V. Sinisterra , A. Garcia-Raso, J. A. Cabello, J. M. Marinas, *Synthesis* **1984**, *6*, 502-504.
21. L. Gavara, T. Boisse, J. P. Hénichart, A. Daïch, B. Rigo, P. Gautret, *Tetrahedron*, **2010**, *66*, 7544-7561.
22. J. Harley-Mason, *J. Chem. Soc.* **1950**, 2907.
23. M. Phukan, K. J. Borah, R. Borah, *Synth. Commun.* **2008**, *38*, 3068-3073.
24. K. R. Reddy, C. V. Rajasekhar, G. G. Krishna, *Synth. Commun.* **2007**, *37*, 1971-1976.
25 . H. J. Knölker, K. Hartmann, *Synlett.* **1993**, 755-757.
26. R. Ballini, G. Bosica, M. Parrini, *Chem. Lett.* **1999**, 1105-1106.
27. (a) Y. Yamamoto, Y. Inoue, U. Takaki, H. Suzuki, *Bull. Chem. Soc. Jpn.* **2011**, *84*, 82-89; (b) M. Watanabe, N. Uemura, S. Ida, H. Hagiwara, K. Goto, T. Ishihara, *Tetrahedron* **2016**, 72, 4280-4287.

28. T. H. Brown, R. C. Blakemore, G. J. Durant, J. C. Emmett, C. R. Ganellin, M. E. Parsons, D. A. Rawlings, T. F. Walker, *Eur. J. Med. Chem.* **1988**, *28*, 53-62.
29. K. Yang, F. Zhou, Z. Kuang, G. Gao, T. G. Driver, Q. Song, *Org. Lett.* **2016**, *18*, 4088–4091.
30. A. K. Mitra, A. De, N. Karchaudhuri, *Synth. Commun.* **1999**, *29*, 573-581.
31. (a) P. Friedländer, S. Bruckner, G. Deutsch, *Justus Liebigs Ann. Chem.* **1912**, *388*, 23-49; (b) J. L. Wolk , A. A. Frimer, *Molecules* **2010**, *15*, 5561-5580.
32. K. Ogawa, J. Dy, R. Maeda, Y. Nagatsuka, K. Kamada, Y. Kobuke, *J. Porphyr. Phthalocyanines* **2013**, *17*, 821-830.
33. J. Nie, D. D. Dong, Y. Zhang, T. -Y Wang, W. Liu, S. Z. Yi, *Asian J. Chem.* **2014**, *26*, 7329-7336.
34. H. Schmidt, *Chem. unserer Zeit* **1997**, 121-128.
35. I. A. Abdulaeva, L. G. Minyaeva, V. V. Mezheritskii, *Russ. J. Org. Chem.* **2011**, *47*, 384-391.
36. A. V. R. Rao , R. Rao , J. S. Yadav, M. Khagga, *Synth. Commun.* **2013**, *43*, 1661-1667.
37. (a) A. Baran, A. Fiedler, H. Schulz, M. Baranska, *Anal. Methods* **2010**, *2*, 1372-1376; (b) A. Amat, F. Rosi, C. Miliani, A. Sgamellotti, S. Fantacci, *J. Mol. Struct.* **2011**, *993*, 43-51.
38. G. A. Russell, G. Kaupp, *J. Am. Chem. Soc.* **1969**. *91*, 3851-3859.
39. S. Llona-Minguez, M. Desroses, A. Ghassemian, S. A. Jacques, L. Eriksson, R Isacksson, T. Koolmeister, P. Stenmark, M. Scobie, T. Helleday, *Chem. Eur. J.* **2015**, *21*, 7394-7398.
40. G. A. Russell, G. Kaupp, *J. Am. Chem. Soc.* **1969**, *91*, 3851-3859.
41. A. D. Becke, *J. Chem. Phys.* **1993**, *98*, 5648-5652.
42. *Gaussian 09, Revision D.01*, M. J. Frisch, G. W. Trucks, H. B. Schlegel, G. E. Scuseria, M. A. Robb, J. R. Cheeseman, G. Scalmani, V. Barone, B. Mennucci, G. A. Petersson, H. Nakatsuji, M. Caricato, X. Li, H. P. Hratchian, A. F. Izmaylov, J. Bloino, G. Zheng, J. L. Sonnenberg, M. Hada, M. Ehara, K. Toyota, R. Fukuda, J. Hasegawa, M. Ishida, T. Nakajima, Y. Honda, O. Kitao, H. Nakai, T. Vreven, J. A. Montgomery, Jr., J. E. Peralta, F. Ogliaro, M. Bearpark, J. J. Heyd, E. Brothers, K. N. Kudin, V. N. Staroverov, T. Keith, R. Kobayashi, J. Normand, K. Raghavachari, A. Rendell, J. C. Burant, S. S. Iyengar, J. Tomasi, M. Cossi, N. Rega, J. M. Millam, M. Klene, J. E. Knox, J. B. Cross, V. Bakken, C. Adamo, J. Jaramillo, R. Gomperts, R. E. Stratmann, O. Yazyev, A. J. Austin, R. Cammi, C. Pomelli, J. W. Ochterski, R. L. Martin, K. Morokuma, V. G. Zakrzewski, G. A. Voth, P. Salvador, J. J. Dannenberg, S. Dapprich, A. D. Daniels, O. Farkas, J. B. Foresman, J. V. Ortiz, J. Cioslowski, D. J. Fox, *Gaussian, Inc., Wallingford CT*, **2013**.

Chapter 3

Photophysical, Aggregation, Electrochemical and Halochromic Behavior of PNI

Abstract: PNI displays a wide (FWHM = 2964 cm^{-1}) and strong absorption spectrum (ε = 33390 $M^{-1}cm^{-1}$) in chloroform with maxima at 632 nm. Monomeric form of the dye has a low photoluminescence quantum yield of 0.003 in THF. At higher concentrations the dye can form aggregate in DMSO solution. Aggregation is also induced in a binary solvent mixture due to the ambipolar property of the dye. In a solvent system of THF/*n*-hexane aggregation results into fluorescence enhancement by 6 fold compared to the monomeric dye. PNI undergoes oxidation and reduction at 0.30 V and –0.58 V (vs Fc/Fc^{+}), respectively, in chloroform. It also exhibits reversible halochromism in acidic medium.

3.1 Introduction

The historic dye indigo had been used as source of blue color over the centuries.[1] In recent times its applications extended to many other fields including organic electronics, pigments for contact lenses etc. Because of widespread application of indigo, various derivatives of the dye have been prepared and used. The multifaceted applications of indigo lies on its low acute toxicity[2], significant chemical stability and high photo-stability.[3] Unsurprisingly, the photochemical properties of indigo have been studied extensively in both solid and solution state to gain a deeper insight of its structural behaviors.[4] Additionally, there were significant numbers of theoretical considerations.[5] The *trans*-planar structure of the dye with cross conjugated donor (=NH) and acceptor (=CO) as the chromophoric core plays a significant role in determining the photophysical as well as aggregation outcome of the dye. The absorption behavior of indigo is also dependent on solvent polarity as well as state of the dye. In gas phase, indigo exhibits red color with absorption maxima at 540 nm. The dilute solution of the dye shows blue color in chloroform (605 nm). The absorption maxima further red shifted in ethanol. In the solid state, indigo displays absorption maxima at 700 nm.[6] Aggregation along with intermolecular H-bonds results into such huge bathochromic shifts.[7]

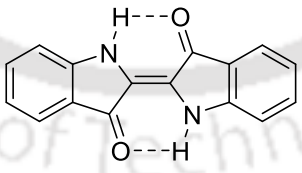

Figure 1. Intramolecular H-bonding in *trans*-planar H-chromophore of indigo.

The distinctive blue color of indigo dye is a result of its *trans*-planar cross-conjugated H-chromophore. In both solution and solid state, the dye stays in the *trans*-form. The impressive light fastness of the dye is reinforced by strong intra-molecular H-bonding between the electron donor (-NH) and the electron acceptor (carbonyl). Upon photo-irradiation, the S_1-

excited state undergoes rapid interconversion back to its ground state.[8] This fast process of non-radiative energy release utilizes excited state proton transfer mechanism and also accounts for the low photoluminescence emission of the dye.[9] Indigo and its derivatives are excellent choice for molecular self-assembly processes using intermolecular forces like H-bonding, π-π stacking etc. Indigo forms aggregate in solution state at very large concentrations.[10] Some derivatives show additional functionalities like crystallization induced enhanced emission. N,N'-disubstituted indigoid modified with ^{t}BOC groups forms ultrasonication induced crystalline aggregates in THF-water mixtures. This well-defined microcrystalline structure shows enhanced emission.[11] Compounds with such aggregation-induced emission (AIE) and/or crystallization-induced emission (CIE) behavior are important material for many applications like fluorescence-based sensing, bioimaging, light-emitting devices and other optoelectronic devices.[12] The redox-chemistry of indigo plays an important role in its vat dyeing process. [13] Reduction of indigo to its water soluble leuco-form is the most important step involved in vat dyeing. Application of this vat-solution to the fabric followed by aerial oxidation of the leuco-form back to indigo produces indigo-dyed clothes.[14] This requirement of reduction and subsequent re-oxidation demands proper understanding of the redox properties of indigo for efficient industrial scale application.[15] Cyclic voltammetry (CV) scans of indigo thin-films prepared via sublimation of the dye onto electrode surfaces shows a two-electron reduction to dianionic leucoindigo, utilized as the first step in textile dying. Similar to the reduction process, indigo exhibits a two-electron reversible oxidation. The HOMO and LUMO bandgap from CV is calculated to be 1.7 eV with an oxidation potential of 0.6 V (vs. Ag/AgCl) and reduction potential of -1.1 V (vs. Ag/AgCl).[16] The reversible oxidation and reduction of indigo also holds the key to its application as ambipolar charge transport material. Another intriguing aspect of indigoid chemistry is based on the

behavior of the compounds in variant pH of the system. Studies have shown that, effect of pH on the outcome of indigo coloration is quite noticeable depending upon the nature of fiber used.[17] Halochromism is also prominent in mono/di-imine indigoids.[18]

Unique photophysical, electrochemical and aggregation properties of indigo have been utilized in various types of applications. Molecular properties of many other indigoids were explored in detail. Since PNI is different in many aspects in comparison to indigo, it would be interesting to explore various molecular behaviors of PNI. Photophysical properties of PNI are a curious case of investigation, especially due to its existence in mono-enol form (Figure 2). The molecular structure of PNI gives room for investigation of excited state intramolecular proton transfer (ESIPT). PNI is an ambipolar dye on account of polar chromophoric core embedded in between two non-polar naphthyl rings. The dye also contains H-bond donor and acceptor moieties. Self-assembly process of the dye by utilizing either π-π interaction or intermolecular H-bonding or a combination of both is another topic of interest. The presence of four functional groups (-NH, =O, -OH, =N-) in the H-chromophore provides room to investigate the effect of change in pH. All these possibilities were explored in and summarized in this chapter.

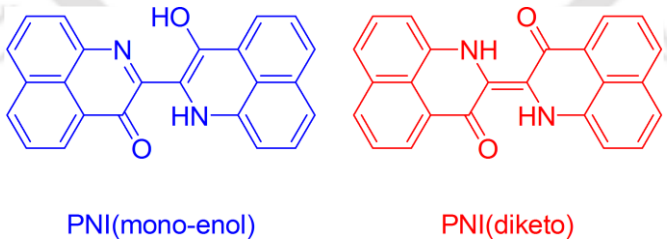

Figure 2. Different isomers of PNI.

The absorption behavior of the dye was explored in different solvents to see its potential for ESIPT process. Photoluminescence property was measured and compared with indigo. Electrochemical property was investigated in detail. Various self-assembly processes involving the dye were explored by changing solvent polarity. Many different kinds of

aggregates were produced in different solvent combinations. However, the most interesting case was the aggregation in THF/n-hexane (1:9). In that specific solvent-system the dye undergoes aggregation and shows aggregation induced enhanced emission (AIEE) phenomenon. Halochromism was successfully realized by treatment of the dye with strong acids like CF_3CO_2H, HCl etc. The changes were investigated by absorption, emission and ^1H NMR spectroscopy.

3.2 Photophysical behaviors of PNI

UV-vis absorption and emission behavior of PNI were recorded in chloroform and compared with indigo for priliminary notions.

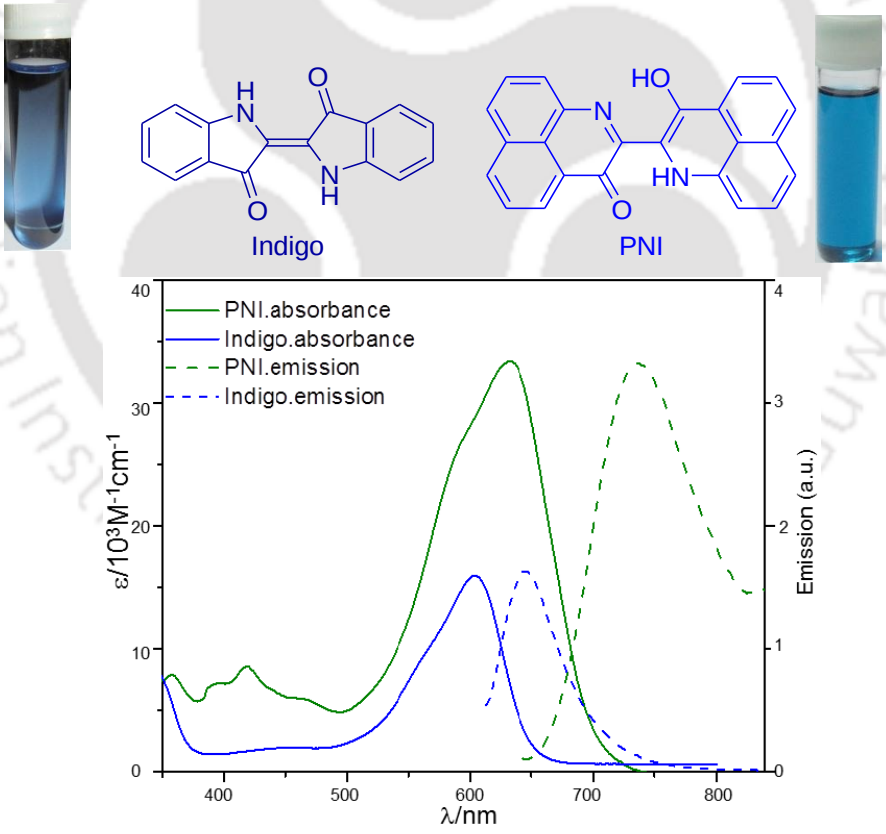

Figure 3. Top left: solution of indigo in chloroform; top middle: structures of indigo (diketo form) and PNI (mono-enol form); top right: solution of PNI in chloroform; bottom: absorption and emission spectra of PNI and indigo in $CHCl_3$.

As expected, changes in the electronic and steric surrounding of the chromophore were very much affective in its photophysical behaviors.[19] Compared to indigo[20], PNI shows a wider absorption band as full width at half maxima of the dye (2964 cm^{-1}) was found to be more than that of indigo (2210 cm^{-1}). Additionally, the absorption maxima show a bathochromic shift by 29 nm. Steady state emission of PNI in chloroform occurs in the near infra-red (NIR) region. The spectrum appears as a broad emission band with maxima at 736 nm. The Stokes shift of PNI was calculated to be 2235 cm^{-1} and significantly higher than that of indigo (1080 cm^{-1}, $CHCl_3$) (Figure 3). All the photophysical features of PNI and its comparison with indigo are shown in Table 1.

Table 1. Photophysical properties of PNI and indigo in $CHCl_3$.

Compound	λ_{abs}(nm)	λ_{em}(nm)	ε ($M^{-1}cm^{-1}$)	Stokes shift (cm^{-1})	FWHM (cm^{-1})
PNI	632	736	33390	2235	2964
Indigo	603	645	15940	1080	2201

The primary difference between the known indigoids with PNI lies in its structural constitution of four different functional groups (-OH, -NH, =N-, C=O) in the central chromophore unit. These four functional groups are connected in a cross conjugated fashion embedded into *peri*-positions of two naphthyl rings. Such specific arrangement of the functional groups is anticipated to undergo ESIPT[21] under suitable solvent polarity. The dye may switch to di-keto isomer depending upon solvent's polarity. UV-vis absorption spectra were measured in various solvents (Figure 4) to detect such change.

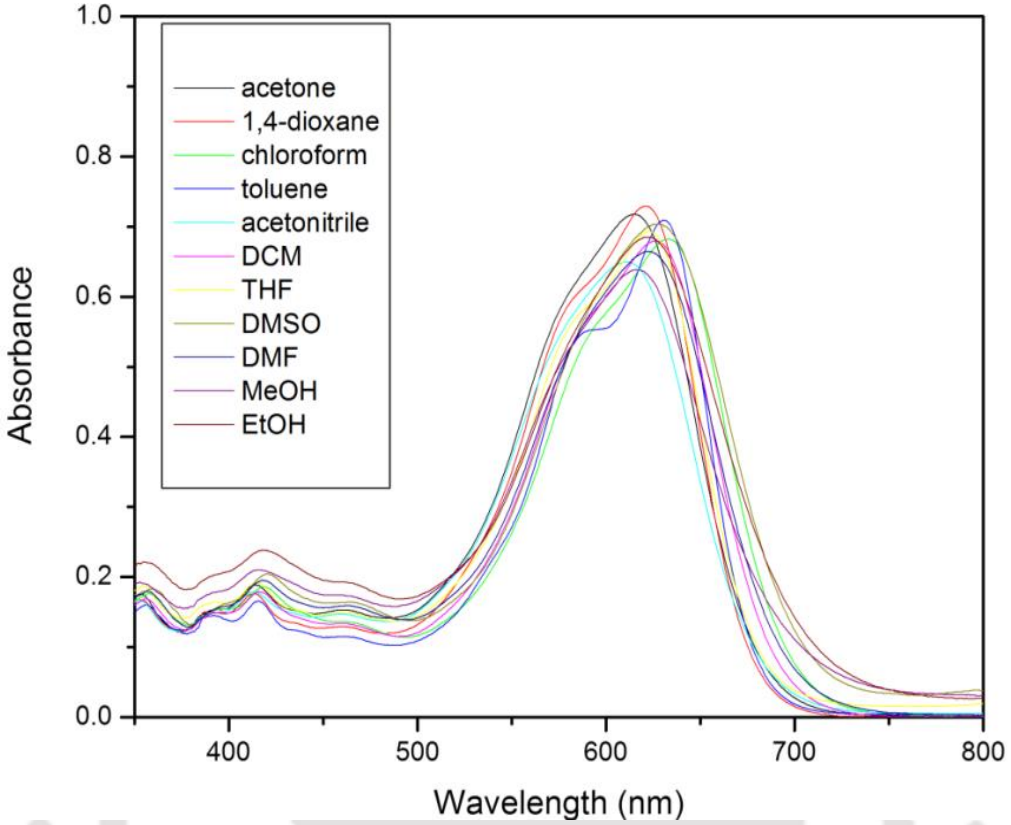

Figure 4. Normalised absorption spectra of PNI in different solvents.

The basic characteristic of the absorption bands remained the same despite changing solvent polarities (Figure 4). No significant changes in the spectra besides shift in absorption maxima were observed. The dye shows blue color in acetonitrile with absorption maxima at 611 nm, and changes to turquoise color in chloroform with maxima at 632 nm. Additional changes were detected when less polar solvents like 1,4-dioxane, toluene was used. The spectra became vibronically resolved in those solvent. Lack of intermolecular H-bonding with the specified solvents possibly caused such changes. To rule out any other possibility, specially the presence of di-keto form, ^{1}H NMR of the dye was recorded in benzene. The proton resonances of PNI supported a mono-enol isomer with twelve different aromatic protons for the naphthalene rings. PNI thus exists in mono-enol form in all solvents under the studied experimental condition.

Table 2. Absorption maxima for PNI in different solvents.

Solvent	**λ_{max} (nm)**
Acetone	615
1,4-Dioxane	621
chloroform	632
Toluene	631
Acetonitrile	611
Dichloromethane	626
Tetrahydrofuran	623
DMSO	626
DMF	622
Methanol	617
Ethanol	622

Steady state emission of PNI occurred in the near infra-red (NIR) region (Figure 5). The photoluminescence spectrum appears as a broad emission band with maxima varying from 736 nm in $CHCl_3$ to 706 nm in THF. The relative fluorescence quantum yield of PNI was measured in THF and found to be 0.003 with respect to 0.001 of indigo in DMF. The low quantum yield is also common in phenyl analogue compounds. A combination of proton transfer as well as intramolecular motion around the central single-bond may lead to such low emission efficiency.

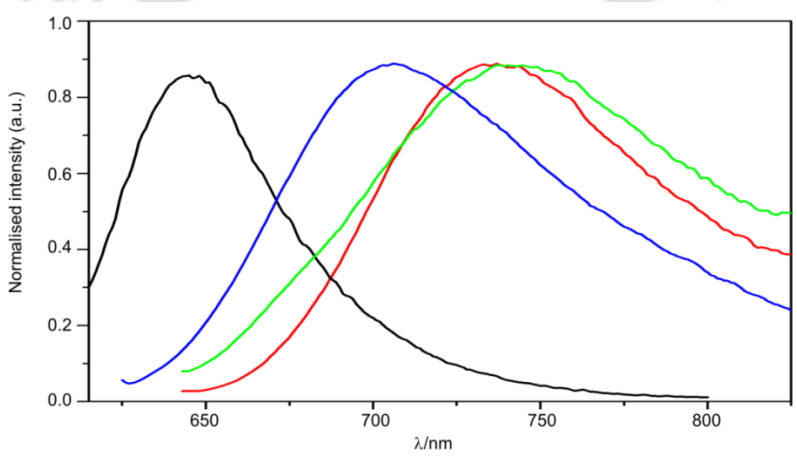

Figure 5. Photoluminescence spectra (293 K) of indigo (black) in chloroform, PNI in chloroform (red), acetonitrile (green), and THF (blue). Spectra were recorded after excitation at their respective absorption maxima.

3.3 Aggregation behavior of PNI

PNI is an ambipolar dye, with non-polar naphthalene rings connected at their sterically crowded 1,8-*peri* positions by the polar chromophore core. The functional groups in the molecule will prefer polar solvents, while naphthalene rings tend to avoid the same. This structural feature of the dye was an excellent tool for imposing molecular self-assembly process, as the intermolecular forces in act can be controlled by simply changing the solvent polarity. PNI, like indigo has the possibility for intermolecular H-bonding along with π-π stacking via the aromatic fragments. A combination of these forces would lead not only aggregation of the dye, but also restriction in molecular motions. Such changes can alter photophysical behavior of the dye significantly (Figure 6). Accordingly, aggregation behavior of PNI was explored by varying solvent polarity as well as concentration.

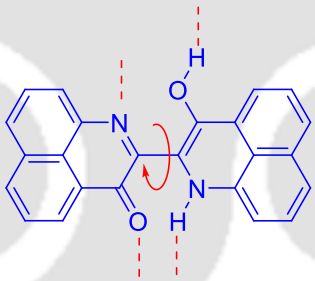

Figure 6. Structural scopes in mono-enol PNI towards aggregation via restriction in intramolecular motion and extension of intermolecular H-bonding.

The absorption spectra of the dye remained the same when measured in chloroform at different concentrations starting from $1x10^{-5}$ M to $1x10^{-3}$ M. As shown in Figure 7, the absorption spectra at different concentration remained the same with maxima at 632 nm. Lack of noticeable changes in absorption features, suggested the existence of monomeric PNI under the experimental concentrations.

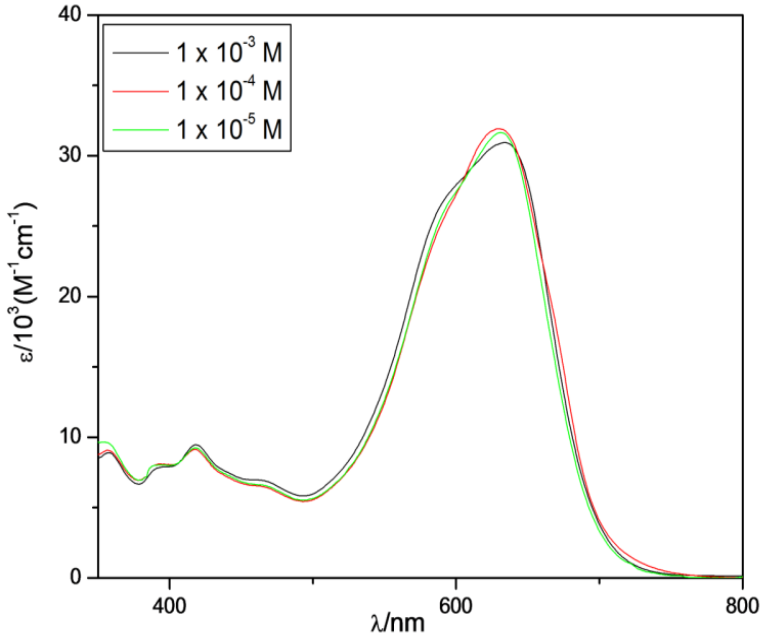

Figure 7. Concentration dependent UV-vis absorption spectrum of PNI in $CHCl_3$.

Similar results were obtained in DMSO (Figure 8) at akin concentration. Absorption behavior could not be detected at higher concentration due to the limitations with the available instrumental set up.

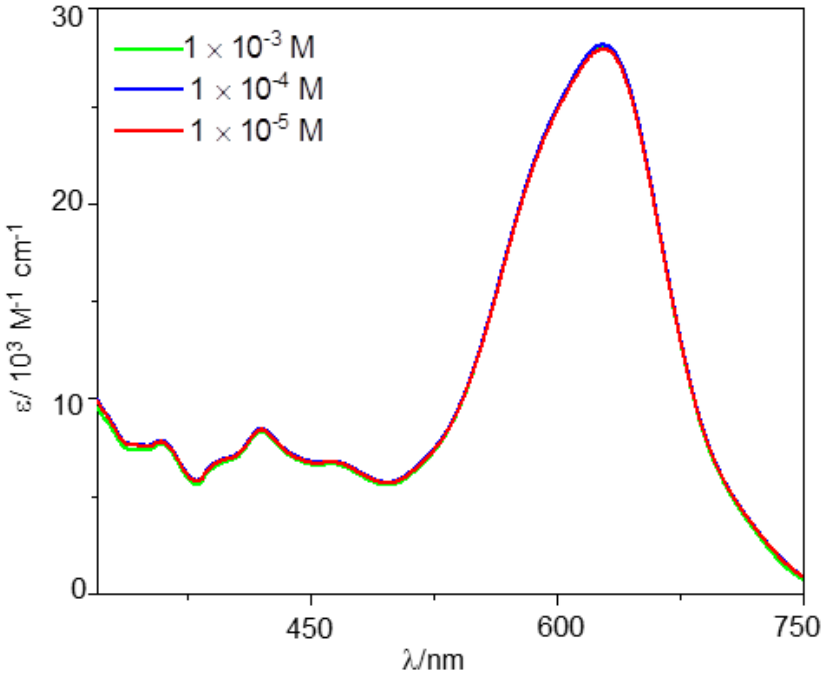

Figure 8. Concentration dependent UV-vis spectra of PNI in DMSO.

However, the effect of concentration change could be detected with the help of ^{1}H NMR spectroscopy. High solubility of PNI in DMSO fulfilled the demands. The dye remained as monomer up to 9.0 mmolL $^{-1}$ concentrations but produced aggregates at elevated concentration (20 mmolL^{-1}). The change in magnetic resonances at various concentrations is shown in Figure 9. Compared to the sharp aromatic proton signals of the monomeric dye, aggregation resulted into a broad ^{1}H NMR spectrum.

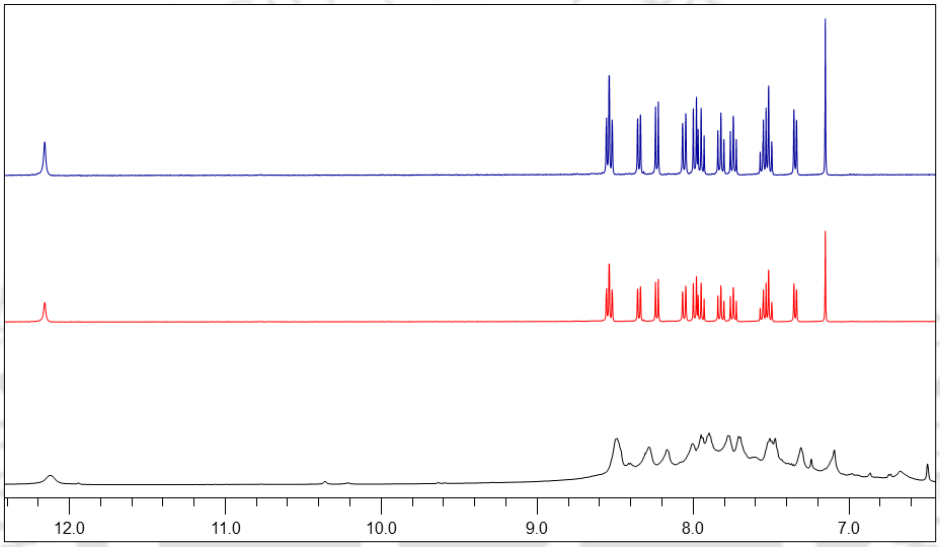

Figure 9. ^{1}H NMR (400 MHz, 295 K) spectra of PNI in DMSO-d_6 at various concentrations. c ≈ 2.9 mmolL $^{-1}$ (blue), ≈ 9.0 mmolL $^{-1}$ (red), ≈ 20 mmolL $^{-1}$ (black).

Formation of PNI aggregates was also evidenced from microscopic techniques. The FESEM image of a drop-casted solution of PNI in DMSO showed the formation of aggregated architectures (Figure 10). As witnessed from the reported experiment, PNI has tendency to go through self-assembly process under specific condition and demands deeper insight. A major problem of the self-assembly process of PNI in DMSO was high concentration demands, which prevented its photophysical investigations at specified concentration.

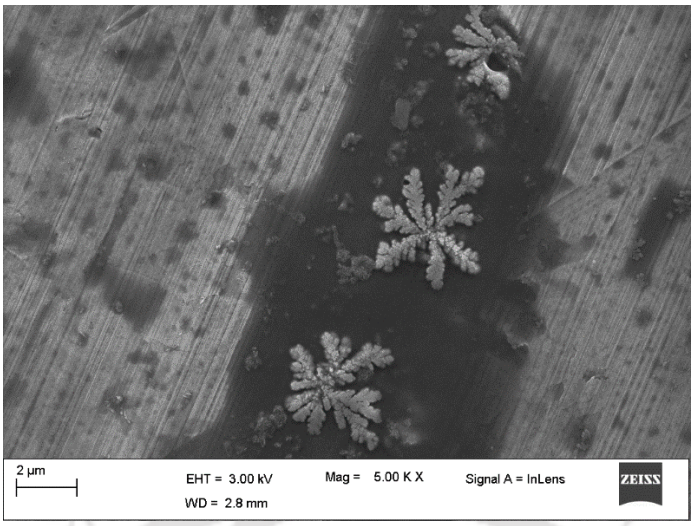

Figure 10. FESEM image of PNI-aggregate formed in DMSO. Image was captured after drop-casting a solution of the aggregate.

To overcome the barrier of high concentration, the possibility of self-assembly was investigated using different solvent systems. PNI is an ambipolar dye and its aggregation behavior is susceptible to change with variation of solvent polarity. The functional groups in the molecule prefer to interact with polar solvents, while naphthalene rings avoid the same. On the other hand, non-polar solvents interact with naphthalene rings and avoid the chromophore. Keeping these facts in mind, solvent assisted aggregation behavior of PNI was studied in two different ways. At first effect of increasing polarity was studied by adding water to a DMSO solution of the dye. Secondly, the nature of aggregation was investigated upon decreasing the solvent polarity by adding *n*-hexane to a THF solution of PNI.

To study the effect of increasing polarity on aggregation of PNI, the dye was dissolved in DMSO and subsequently water was added into the solution to gradually increase the polarity. The obtained solutions were monitored using UV-vis absorption spectroscopy. It was indeed possible to detect the occurrence of PNI self-assembly process at a considerably low concentration of 5×10^{-6} molL^{-1} in a solvent mixture of DMSO and H_2O. With the increase in solvent polarity via addition of water, the absorption co-efficient at the maxima

gradually decreased. A stark difference was visible when volume fraction of water (f_w) reached to 0.5. The intensity at the maxima decreased significantly along with the appearance of red shifted shoulder. The trends continued in similar fashion at higher f_w. The effect of increased polarity at various f_w is summarized in (Figure 11). Besides diminished extinction co-efficient at absorption maxima and shoulder at longer wavelength, there occurred changes near the blue-violet region (400-450 nm).

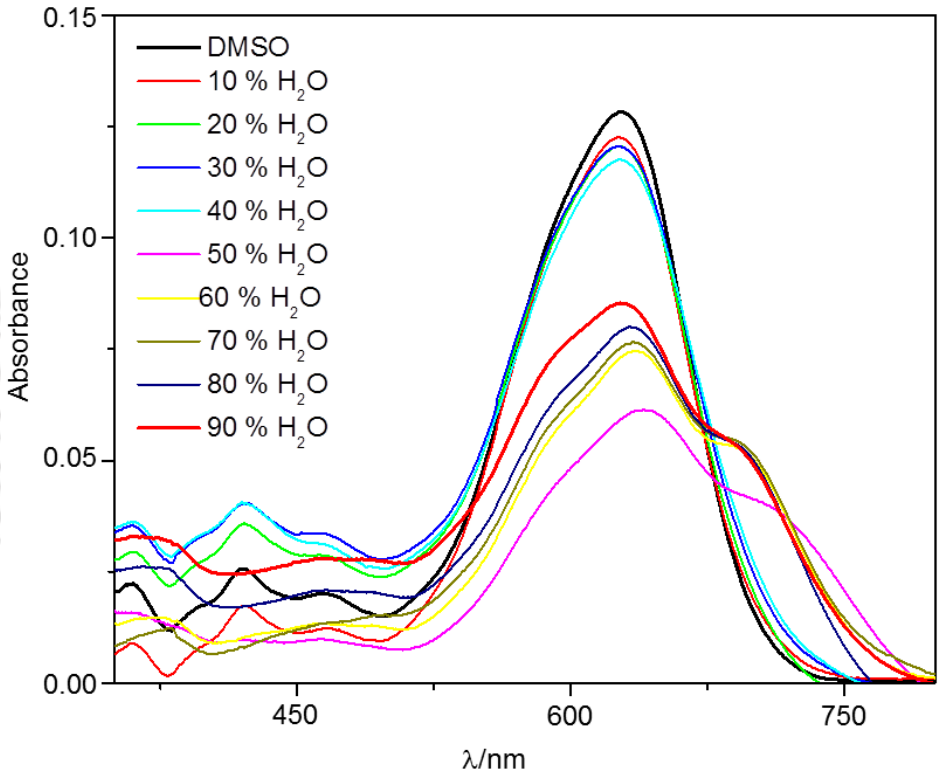

Figure 11. Absorption spectra (293 K) of PNI ($c \approx 5 \times 10^{-6}$ molL^{-1}) in DMSO (black) and in mixtures of DMSO-water (v/v = 9:1 to 1:9).

The formation of aggregates was also confirmed from microscopic images. FESEM image (Figure 12). of a drop-casted solution of PNI in DMSO-water (v/v =1/9) showed stacking of multiple layers without having any regularity. The unfavorable hydrophobic interactions at high f_w possibly caused such aggregation. With increase in fraction of water the unwanted interactions between the water molecules and hydrophobic naphthalene rings on PNI

increased. To avoid such interactions, PNI reduced the naphthalene surfaces via aggregation. After confirming self-assembly process of PNI at relatively low concentration, photoluminescence property was investigated at the f_w at aggregation occurred. Unfortunately, the emission of PNI quenched completely in the aggregated form in binary solvent systems. Via aggregation PNI increased the favorable interactions between water molecules and the polar functional groups. Such interaction possibly led to photoluminescence quenching of PNI via vibrational energy transfer to water molecules.

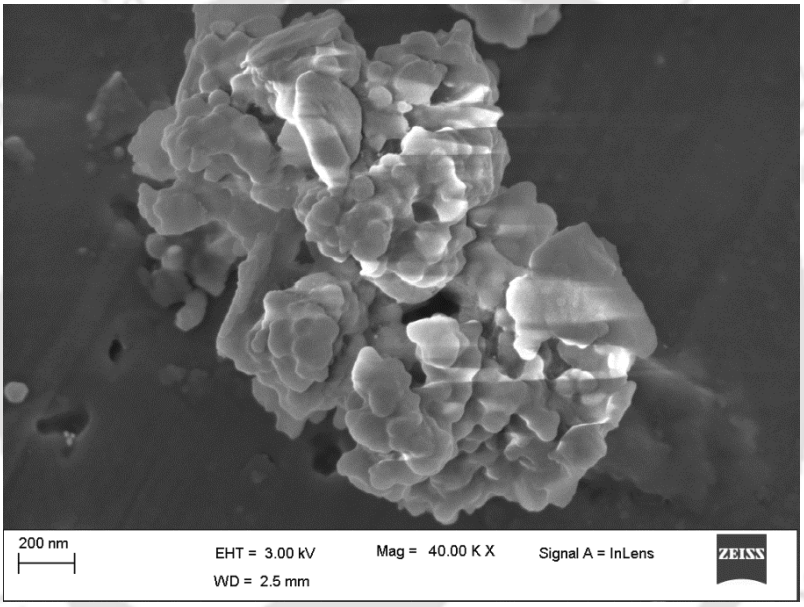

Figure 12. FESEM image of aggregate of PNI in DMSO/water (v/v = 1:9). Image was captured after drop-casting a solution of the aggregate.

As established from the above mentioned investigation, self-assembly process of PNI was possible at low concentration in binary solvent systems. The solvent system also allowed photophysical property studies in details. The effect of increased polarity of solvent system led to quenching of PNI emission. In the next set of experiments, the objective was to check the effect of decreased polarity of the solution. In this set of experiments polarity of the system was lowered by gradual addition of *n*-hexane to a THF solution of PNI and the process was studied using various spectroscopic techniques. Notable changes were observed

in the absorption behavior of the dye when volume fraction of *n*-hexane (f_h) reached to 0.9 (Figure 13).

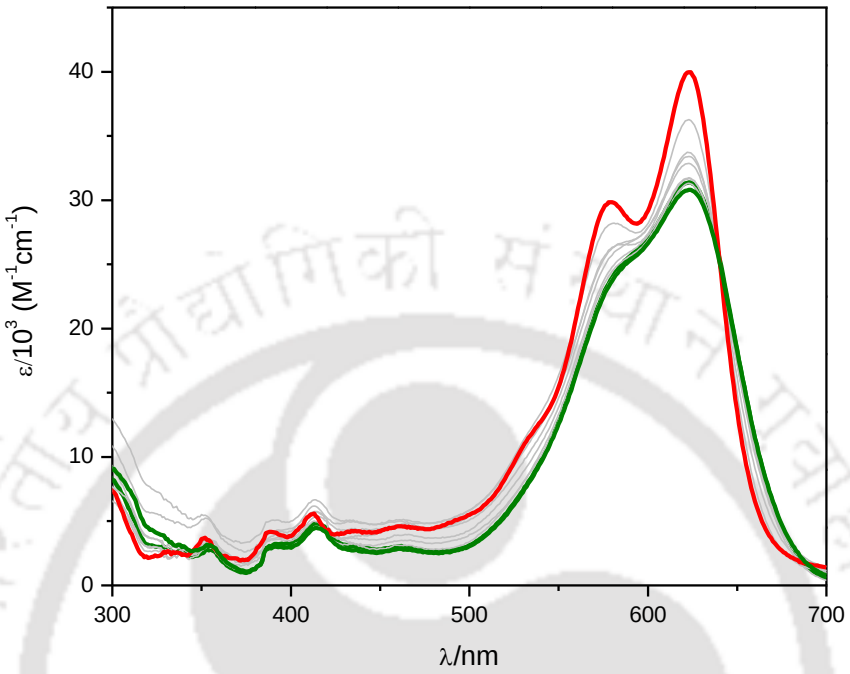

Figure 13. Absorption spectra (293 K) of PNI (c ≈ 3 × 10^{-6} $molL^{-1}$) in THF (olive) and in mixture (red) of THF/n-hexane (v/v = 1:9). Spectra in grey color are associated with intermediate fraction of *n*-hexane.

The characteristic broad absorption spectrum became vibronically resolved with increase in f_h. Molar extinction coefficient also gradually enhanced with decrease in solvent polarity. Restriction in intramolecular motion via aggregation possibly caused such spectral changes. The morphology of the aggregates was investigated in the solid using microscopic imaging technique. The recorded FESEM image of drop-casted solution of PNI in THF/*n*-hexane (v/v = 1:9) revealed the formation of well-defined microcrystalline cuboid architectures (Figure 14). The length of such cuboids extended up to micrometer.

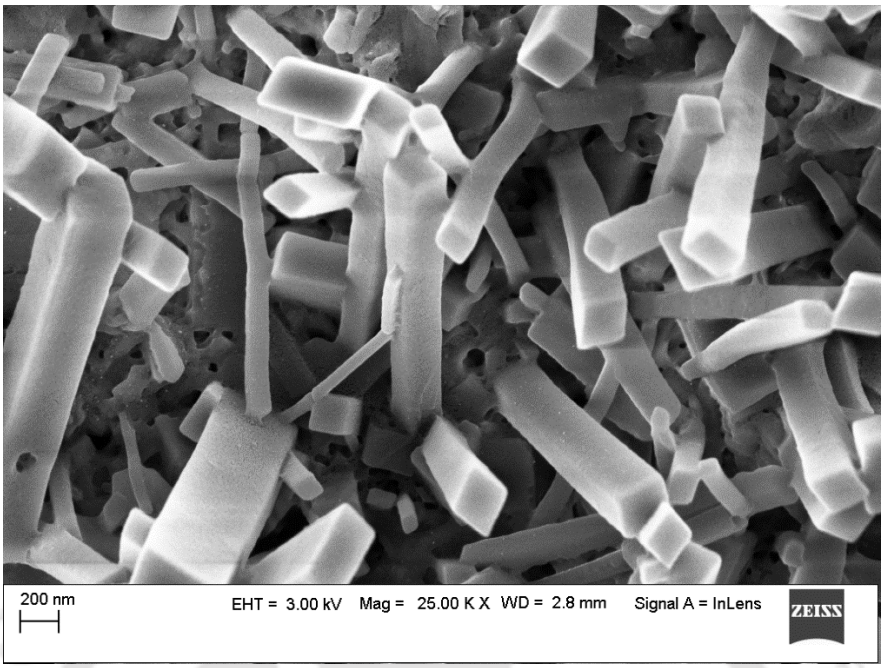

Figure 14. FESEM image of aggregate of PNI in THF/*n*-hexane (v/v = 1:9). Image was captured after drop-casting a solution of the aggregate.

The aggregation process was analyzed in the solid state using IR spectroscopy. Monomeric and aggregated PNI were obtained in their solid state by slow evaporation of a THF and a THF/*n*-hexane (v/v = 1:9) solution of the dye. IR spectra of the two samples were recorded using their respective KBr pellets. Significant changes were observed at around 1384, 1399, 1424, 1571 and 1621 cm^{-1} as shown in Figure 15. Compared to the broad peaks in the monomer, the aggregated state possessed sharp peaks in the mentioned values. From the analytical and spectroscopic measurement it was confirmed that self-assembly of PNI resulted in forming a rigid molecular network. Such rigidification via restriction in intramolecular motions gave rise to isolated absorption peaks.

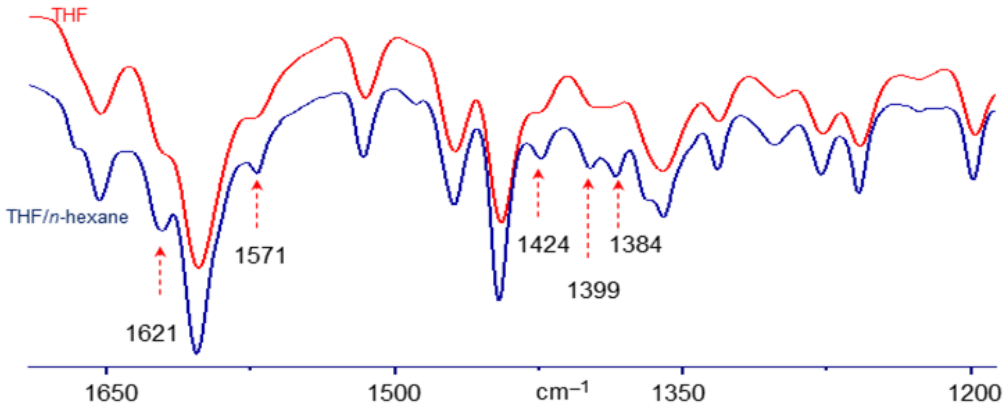

Figure 15. Partial IR (KBr) spectra of monomeric (red) and aggregated (blue) PNI. The monomeric and the aggregated solid of PNI were prepared by room temperature evaporation of solution of the dye in THF and in mixture of THF/*n*-hexane (v/v = 1:9) respectively.

The effect of solvent polarity upon the aggregation behavior of PNI was also investigated using ^{1}H NMR spectroscopy, recorded for PNI solutions with variable solvent combinations with different polarity indices. ^{1}H NMR of PNI in three different solvent combinations viz. C_6D_6:THF (1:2), C_6D_6 and C_6D_6:*n*-hexane (1:1) were recorded (Figure 16). Distinct alterations in all the proton signals were noticed with variation in polarity. For example, going from the most polar solvent system C_6D_6-THF to least polar system C_6D_6/*n*-hexane the N-H signal followed an up field shift of 0.43 ppm. These observations confirmed self-assembly processes at low polar solvent system.

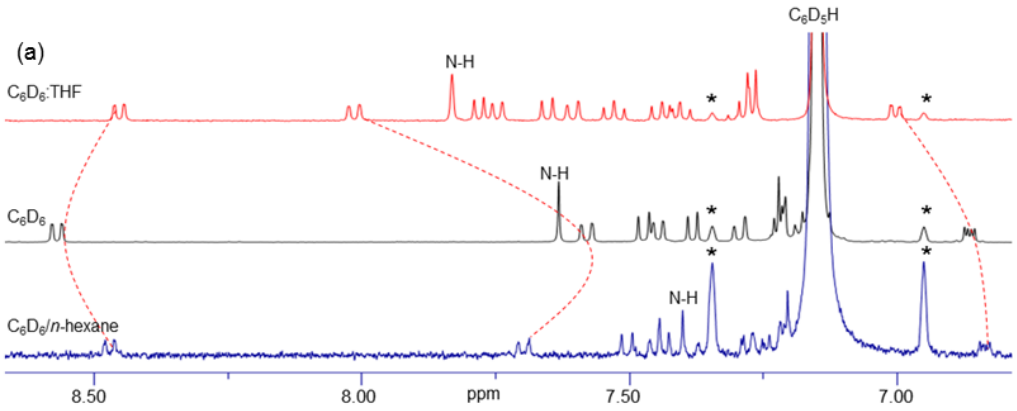

Figure 16. ^{1}H NMR (400 MHz, 295 K) spectra of PNI in C_6D_6 (black), THF/C_6D_6 (red) and *n*-hexane/C_6D_6 (blue); satellite peaks are marked with asterisks.

PNI was found to be emissive in the solvent mixtures of THF and *n*-hexane. With decrease in solvent polarity, by adding *n*-hexane to THF solution of the dye, emission intensity gradually increased (Figure 17). In addition to enhanced emission, there occurred significant change in the emission behavior. The maxima experienced gradual blue shift and appeared at 656 nm in f_h= 0.9. Compare to the monomer, the shift was about 50 nm. Due to such hypsochromic shift, the Stokes shift also gradually decreased. Diminished Stokes shift further supported the rigidification of structure via aggregation.

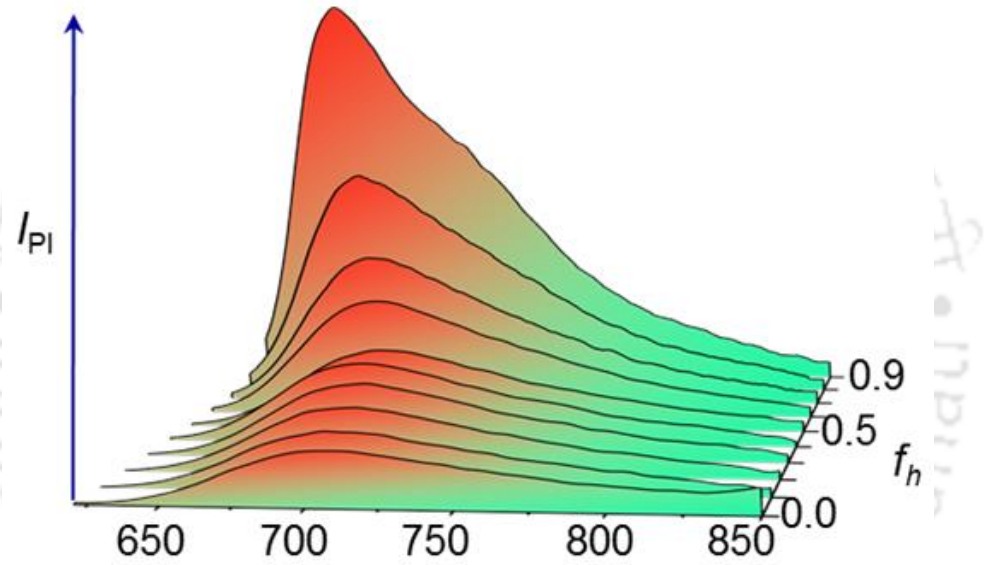

Figure 17. Photoluminescence of PNI in different mixtures of THF and n-hexane with f_h = 0.0, 0.1, 0.2 … 0.9. Here, f_h = fraction of n- hexane.

By comparing relative emission quantum yields at various solvent systems, the dye was found to be in excess of 6 fold more emissive than that of monomer. These observations confirmed aggregation induced enhancement of photoluminescence of PNI upon lowering the solvent polarity. Figure 18a shows the enhancement in photoluminescence of PNI from monomer to its aggregates. The AIEE process was also evident in the photographic documentation of the aggregates in their respective solutions (Figure 18b).

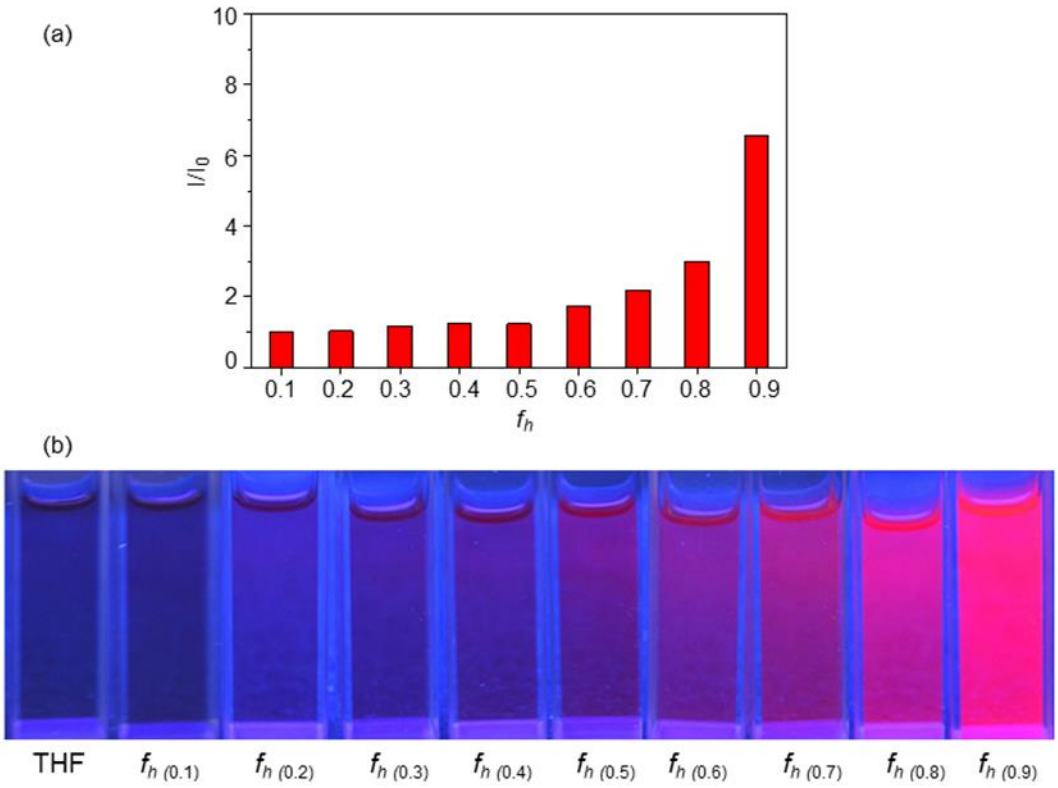

Figure 18. (a) Photoluminescence enhancement of PNI with increase in fraction of n-hexane (f_h). (b) Digital photograph of solution of PNI in THF and in different f_h. The photograph was captured after excitation with 365 nm UV lamp.

Since PNI showed AIEE, the self-assembly process must be explained with appropriate model. The observation can be rationalized in the following way. With decrease in solvent polarity, the unfavorable interaction between nonpolar hexane molecules and the polar functional groups of PNI increases. To avoid such interactions intermolecular H-bonding took place resulting in the formation of one dimensional (1D) sheet-like morphology. Further masking of the chromophore part took place via brick wall type stacking of the sheets. These two proceedings combined produced 3D cuboid architectures. The overall process is summarized in Figure 19. At first, intermolecular H-bonding provided growth in y-direction, while growth in x and z-direction was caused by brick wall type stacking. As the number of molecule in each 1D-sheet can vary, as well as the number of sheets in each stacking

arrangement, in the microscopic image cuboid structures of variable dimensions were observed.

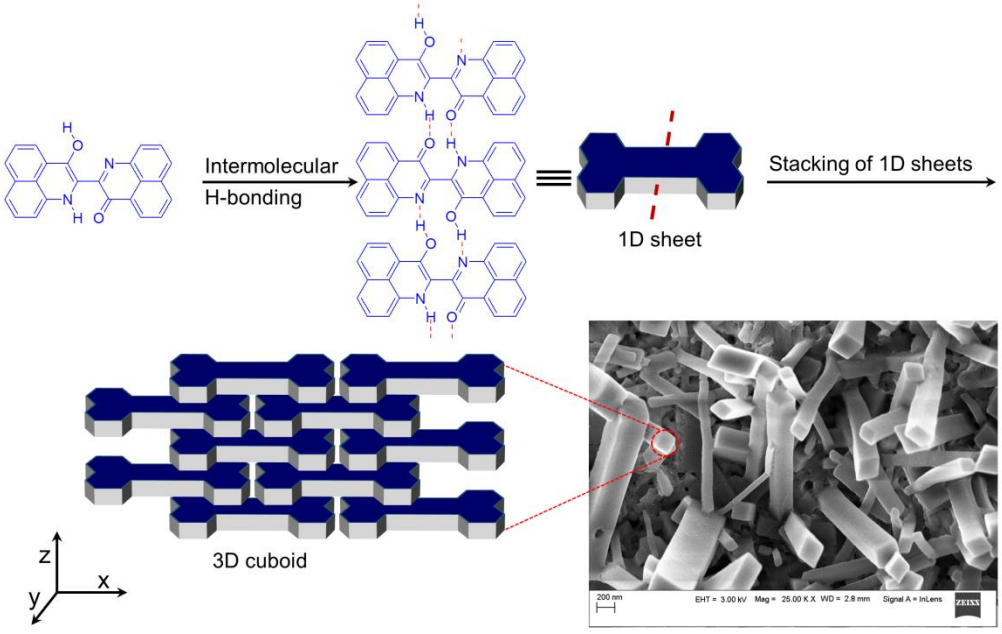

Figure 19. Self-assembly process of PNI via intermolecular H-bonding followed by brick-wall type stacking in THF/*n*-hexane (v/v = 1/9).

3.4 Cyclic voltammetry of PNI

Proper understanding of redox behaviors of a molecule is necessary to explore its potentials for various applications.[22] In a molecule, oxidation involves removal of electron from HOMO, while addition of electron in the LUMO causes reduction. Measurement of redox potential thus provides valuable information about location of HOMO-LUMO energy level and the band gap. Cyclic voltammetry (CV) method can be used to calculate the redox potentials E_{red} and E_{ox}. In the measurement ferrocence was used as a reference to calculate the energy of the HOMO and LUMO levels.

The energy levels were calculated using the following empirical equations:

$$E\ (HOMO) = -e\ [E_{ox}^{onset} + 4.4]$$

$$E\ (LUMO) = -e\ [E_{red}^{onset} + 4.4]$$

Where, E (HOMO) = Energy of highest occupied molecular orbital.

E (LUMO) = Energy of lowest unoccupied molecular orbital.

E_{ox}^{onset} = Onset oxidation potential in eV.

E_{red}^{onset} = Onset reduction potential in eV.

And 4.4eV is the redox potential of the internal reference ferrocene.

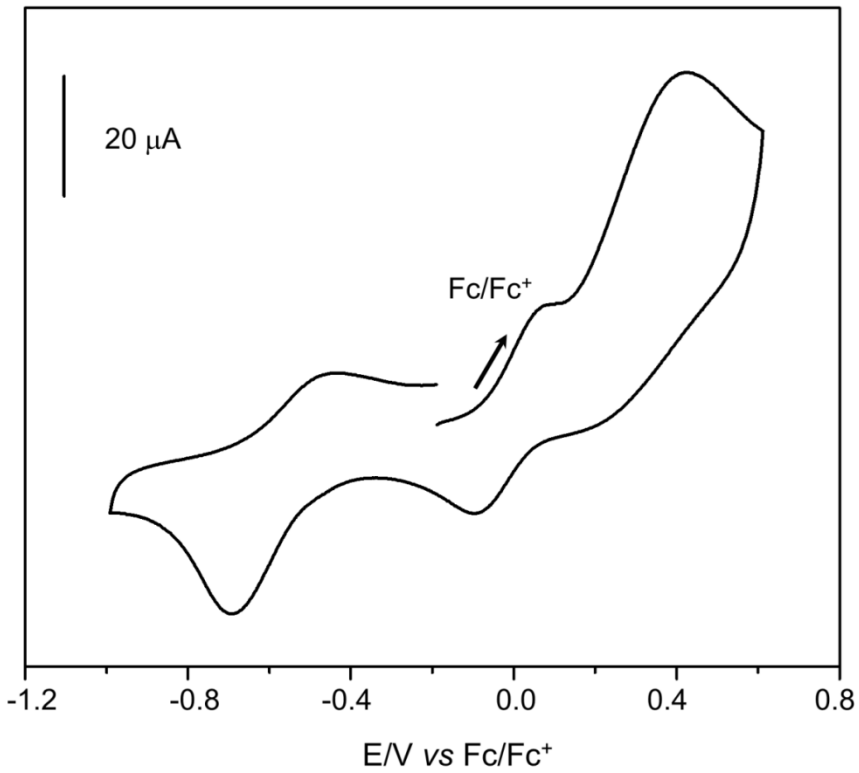

Figure 20. Cyclic voltammogram of PNI in chloroform.

The CV experiment was carried out using a 2.7 $x10^{-3}$ M solution of the dye with $n$$Bu_4NClO_4$ (0.3 M) as electrolyte against a Ag/AgCl reference electrode, Pt wire as auxiliary electrode, 3 mm glassy carbon disk as working electrode, and ferrocene as internal standard with scan rate of 200 mVs^{-1}. In a $CHCl_3$ solution, the dye undergoes a quasi-reversible oxidation and

reversible reduction at 0.30 V and –0.58 V with respect to ferrocene (Fc/Fc^+) as an internal reference (Figure 20). The electrochemical features were very much similar to that of indigo. However, both redox processes were found to be easier in PNI than indigo. From the obtained electrochemical data, the energy gap between the HOMO and the LUMO was calculated to be 0.88 eV. The redox properties of mono-enol PNI were also compared with the theoretical report on diketo-PNI by Zhang and his co-workers. [23] According to their calculation, the HOMO-LUMO gap was found to be 1.5 eV. The differences can be attributed to the different molecular structure as well as the gap between computation and experiments.

3.5 Halochromism

A material that responds to change in pH of the solution by changing the color is called a halochromic material.[24] Application of this kind of molecule ranges from pH indicators to determine the pH of an unknown solution. A halochromic substance contains functional group(s) that forms chemical bond to existing proton(s) or hydroxide ion(s) in solution upon a change in pH of the solution. These new chemical bond formation results into a change in the delocalization of the electron density finally affecting its absorption behaviour and presents a different color to the observer. The isolated form of PNI contains four functional groups (=CO, -NH-, -OH, -N=) accessible to change in pH in its solution (Scheme 1).

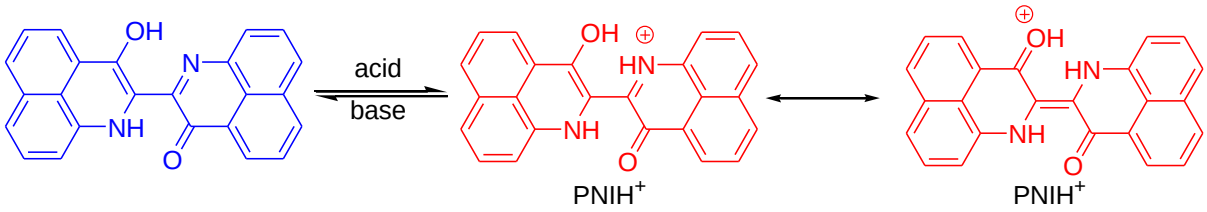

Scheme 1. Halochromism of PNI.

Taking advantage of these structural features, halochromism[25] was installed in PNI and the processes were monitored using UV-vis spectroscopy. Halochromism of PNI was studied in acidic pH. Upon addition of trifluoroacetic acid to a solution of PNI in chloroform its absorption maxima experienced a bathochromic shift from 632 nm to 698 nm with increased molar absorptivity (ε = 67965 $M^{-1}cm^{-1}$). The spectrum also became vibronically resolved. Such bathochromic shift associated with protonation is a known phenomenon in indigoid chemistry.[26] The acidification also led to quenching of PNI emission.

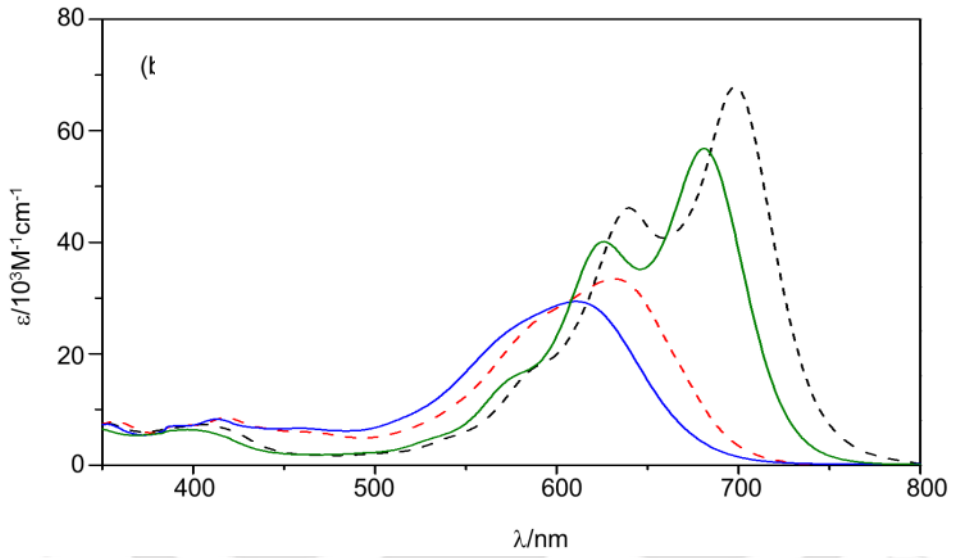

Figure 21. Absorption spectra (293 K, c ≈ 10^{-5} $molL^{-1}$) of PNI in chloroform (red, dash), acetonitrile (blue, solid), and $PNIH^+$ in chloroform (black, dash), acetonitrile (olive, solid).

Another significance of this process was its reversible nature. The initial spectrum can be recovered simply by addition of base. Halochromism of the dye was also prominent in other solvent (acetonitrile) as well as in presence of different acids (acetic acid, HCl). Sulfuric acid was avoided as it is known to produce sulfonated product in analogous dye.[24] In acetonitrile halochromism was detectable even in bare eyes as the color changed from blue to turquoise. The spectroscopic signature in acetonitrile with all other acids was similar to that one observed in chloroform with trifluoroacetic acid (Figure 21). The effect of proton on PNI was

also studied by ^{1}H NMR spectroscopy, which further supported the halochromism process. In acidic medium, formation of mono-protonated form the dye was evident from its ^{1}H NMR in CD_3CN.

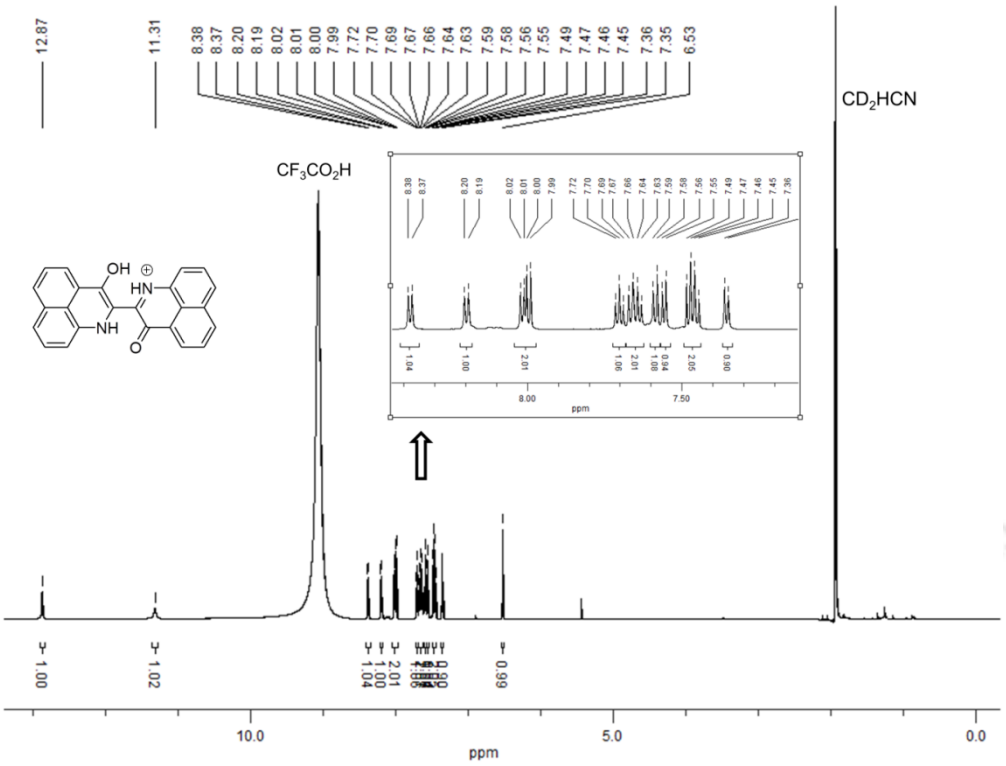

Figure 22. ^{1}H NMR spectrum of $PNIH^{+}\bullet CF_3CO_2^{-}$ (600 MHz, CD_3CN, 295K). Expanded aromatic region is shown in inset. Measurement was done by adding 20μL of trifluoroacetic acid to a solution of PNI (3.00 mg) in CD_3CN (0.5 mL).

The proton resonance spectra of $PNIH^{+}$ in CD_3CN (Figure 22) displayed three characteristic singlet at 6.53, 11.31 and 12.87 ppm assigned to O-H, N-H and proton at imine nitrogen. These signals were accompanied by twelve aromatic hydrogens indicating the structural integrity of the dye under acidic pH.

Experimental details of halochromism

In a typical experiment, 2.7 mL ($c \approx 1 \times 10^{-5}$ molL^{-1}) of PNI solution (in chloroform or acetonitrile) was loaded into a cuvette (1 cm path length) and titrated with acid

(CF_3CO_2H, CH_3CO_2H and HCl) and changes were monitored using UV-vis spectroscopy. Complete protonation of PNI was obvious from fading of absorbance maxima of the dye to result in new absorption behaviour. Dissociation of acid in organic solvents is not quantitative.

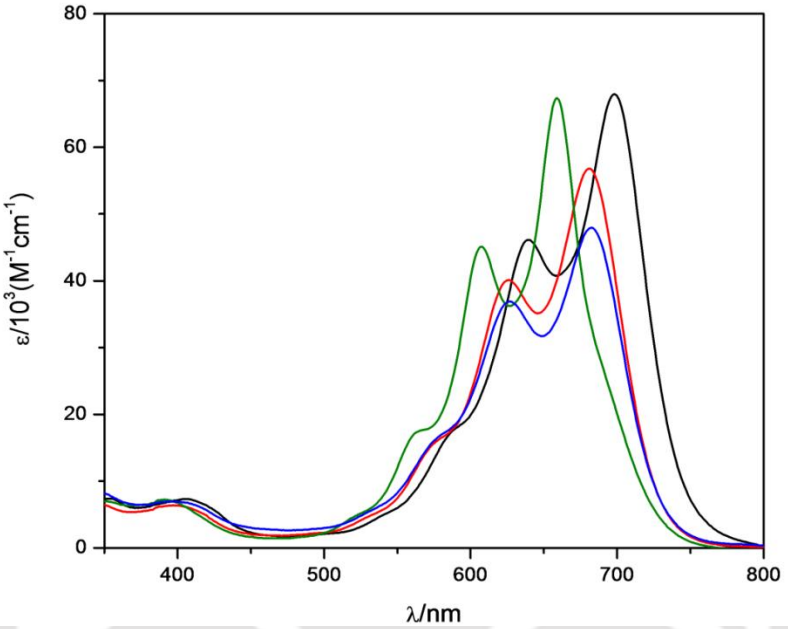

Figure 23. Absorption spectra (293 K) of $PNIH^+ \bullet CF_3CO_2^-$ in chloroform (black) and acetonitrile (red), $PNIH^+ \bullet CH_3CO_2^-$ in acetonitrile (blue) and $PNIH^+ \bullet Cl^-$ in acetonitrile (olive). Respective acids were added till complete protonation of PNI. Initial concentration of PNI solution = 1 x 10^{-5} $molL^{-1}$.

Because of it different volumes of acid viz. 50 μL for CF_3CO_2H, 900 μL for CH_3CO_2H, 10 μL for 0.3 M HCl in MeCN were needed. The deprotonation of $PNIH^+ \bullet CF_3CO_2^-$ in chloroform was accomplished by treatment with aqueous NH_4OH (or NaOH) followed by subsequent separation of organic layer. In acetonitrile, base (aqueous NH_4OH or NaOH) was added to the solution and filtered. After treatment with base, the respective solutions were checked by UV-vis spectroscopy. The absorption spectra of PNI and deprotonated $PNIH^+ \bullet X^-$ (X = CF_3CO_2, Cl) were found to be alike. This experiment established reversibility of the procedure.

3.8 Conclusion

In summary PNI exhibits wider and stronger (ε = 33390 $M^{-1}cm^{-1}$) absorption band than indigo with bathochromically shifted maxima (632 nm in chloroform). The diketo isomer of the dye was not detected with solvatochromic UV-vis studies. It's a dye with emission in the NIR region and a low quantum yield of 0.03 in solvents like THF, $CHCl_3$ etc. Aggregation of the dye was successfully achieved by controlling the polarity of the solvents as well the dye concentration. In a non-polar solvent combination of THF/*n*-hexane the dye exhibits AIEE. PNI undergoes oxidation and reduction at 0.30 V and –0.58 V (vs Fc/Fc^+), respectively, in chloroform. Both the reduction and oxidation processes are facile than that of indigo. Due to its distinct structural feature PNI also shows reversible halochromism upon protonation, marked by red shifted, vibronically resolved absorption maxima.

3.9 References

1. B. Schaefer, *Natural Products in the Chemical Industry* **2014**, *XVIII*, 13-22, ISBN: 978-3-642-54460-54466.
2. K. H. Ferber, *J. Environ. Pathol. Toxicol. Oncol*. **1987**, *7*, 73-83.
3. (a) I. Iwakura, A. Yabushita, T. Kobayashi, *Chem. Lett.* **2009**, *38*, 1020-1021; (b) R. Giustetto, O. Wahyudi, I. Corazzari, F. Turci, *Appl. Clay Sci.* **2011**, *52*, 41-50; (c) N. D. Bernardino, S. Brown-Xu, T. L. Gustafson, D. L. A. de Faria, *J. Phys. Chem. C* **2016**, *120*, 21905-21914.
4. (a) G. M. Wyman, B. M. Zarnegar, *J. Phys. Chem.* **1973**, 77, 831-837; (b) J. S. Sexias de Melo , R. Rondão , H. D. Burrows , M. J. Melo , S. Navaratnam , R. Edge , G. Voss , *Chemphyschem* **2006**, *7*, 2303-2311; (c) M. M. Sousa, C. Miguel, I. Rodrigues, A. J. Parola, F. Pina, J. S. Seixas de Melo, M. J. Melo, *Photochem. Photobiol. Sci.* **2008**, *7*, 1353-1359.
5. (a) G. Cui, W. Thiel, *Phys. Chem. Chem. Phys.* **2012**, *14*, 12378-12384; (b) M. Moreno, J. M. Ortiz-Sánchez, R. Gelaberta, J. M. Lluchac, *Phys. Chem. Chem. Phys.* **2013**, *15*, 20236-20246; (c) C. Ma, H. Li, Y. Yang, D. Li, Y. Liu, *Chem. Phys. Lett.* **2015**, *638*, 72-77.
6. (a) S. E. Sheppard, P. T. Newsome, *J. Am. Chem. Soc*. **1942**, *64*, 2937-2946; (b) M. Wyman, J. Weinstein, *J. Org. Chem*. **1956**, *78*, 2387-2390; (c) M. Klessinger, W. Lüttke, *Tetrahedron* **1963**,

19, 315-335; (d) A. R. Monahan, J. E. Kuder, *J. Org. Chem.* **1972**, *37*, 4182-4184; (e) L. Serrano-Andrés, B. Roos, *Chem. Eur. J.* **1997**, *3*, 717-725.

7. D. Jacquemin, J. Preat, V. Wathelet, E. A. Perpète, *J. Chem. Phys.* **2006**, *124*, 74104.
8. (a) T. Kobayashi , P. M. Rentzepis , *J. Chem. Phys.* **1979**, *70*, 886-892; (b) I. Iwakura, A. Yabushita, T. Kobayashi, *Chem. Phys. Lett.* **2010**, *484*, 354-357; (c) J. Pina, D. Sarmento, M. Accoto, P. L. Gentili, L. Vaccaro, A. Galvão, J. S. Sexias de Melo, *J. Phys. Chem. B* **2017**, *121*, 2308-2318.
9. (a) J. S. Seixas de Melo, A. P. Moura, M. J. Melo, *J. Phys. Chem. A* **2004**, *108*, 6975-6981; (b) R. Rondão, J. Seixas de Melo, F. A. Schaberle, G. Voss, *Phys. Chem. Chem. Phys*. **2012**, *14*, 1778-1783.
10. C. Miliani, A. Romani, G. Favaro, *Spectrochem. Acta A* **1998**, *54*, 581-588.
11. C. Yang, Q. T. Trinh, X. Wang, Y. Tang, K. Wang, S. Huang X. Chen, S. H. Mushrifa, M. Wang, *Chem. Commun*. **2015**, *51*, 3375-3378.
12. R. Hu , N. L. C. Leung, B. Z. Tang , *Chem. Soc. Rev.* **2014**, *43*, 4494-4562.
13. (a) J. R. McKee, M. Zanger, *J. Chem. Educ.* **1991**, *68*, 242-244; (b) J. N. Chakraborty, *Fundamentals and Practices in Colouration of Textiles, Chapter 8- Dyeing with vat dye*, **2014,** 88-108; (c) A. Gürses, M. Açıkyıldız, K. Güneş, M. S. Gürses, *Historical development of colourants, Chapter 2-Dyes and Pigments: Their Structure and Properties* **2016**, 13-29.
14. J. N. Chakraborty, R. B. Chavan, *Indian J. Fibre Text.* **2004**, *39*, 100-109.
15. L. Saikhao, J. Setthayanond, T. Karpkird, T. Bechtold, P. Suwanruji, J. Clean. Prod. **2018**, *197*, 106-113.
16. (a) E. O. Reyes-Salas, J. A. Manzanilla-Cano, M. H. Barceló-Quintal, J. Ramírez-Balderas, *Electrochemistry* **2004**, *37*, 463-472; (b) L. Leonat, G. Sbârcea, I. V. Brânzoi, *U. P. B. Sci. Bull. Series B.* **2013**, *75*, 111-118.
17. G. A. Baig, *Ind. J. Fib. Text. Res.* **2012**, *37*, 265-272.
18. E. C. Nicholls-Allison, G. Nawn, B. O. Patrick, R. G. Hicks, *Chem. Commun.* **2015**, *51*, 12482-12485.
19. J. S. Seixas de Melo, R. Rondão, H. D. Burrows, M. J. Melo, S. Navaratnam, R. Edge, G. Voss, *ChemPhysChem* **2006**, *7*, 2303-2311.
20. A. Amat, F. Rossi, C. Miliani, A. Sgamellotti, S. Fantacci, *J. Mol. Struct.* **2011**, *993*, 43-51.
21. (a) Y. Matsumoto, T. Ebata, N. Mikami, *J. Phys. Chem. A* **2002**, *106*, 5591-5599; (b) J. Lee, C. H. Kim, T. Joo, *J. Phys. Chem. A* **2013**, *117*, 1400-1405.
22. N. Elgrishi, K. J. Rountree, B. D. McCarthy, E. S. Rountree, T. T. Eisenhart, J. L. Dempsey, *J. Chem. Edu*. **2018**, *95*, 197-206.
23. S. -F. Zhang, X. -K. Chen, J. -X. Fan, A. -M. Ren, *Org. Electron.* **2015**, *24*, 12-25.

24. S. P. Zanotto, M. Scremin, C. Machado, M. C. Rezende, *J. Phys. Org. Chem.* **1993**, *6*, 637-641.

25. (a) P. Singh, A. Baheti, K. R. J. Thomas, *J. Org. Chem.* **2011**, *76*, 6134-6145; (b) K. Cai, Q. Yan, D. Zhao, *Chem. Sci.* **2012**, *3*, 3175-3182; (c) K. Matsui, Y. Segawa, K. Itami, *Org. Lett.* **2012**, *14*, 1888-1891; (d) Z. Yao, X. Hu, B. Huang, L. Zhang, L. Liu, Y. Zhao, H. -Chen Wu, *ACS Appl. Mater. Interfaces* **2013**, *5*, 5783-578; (e) P. K. Kundu, G. L. Olsen, V. Kiss, R. Klajn, *Nat. Commun.* **2014**, *5*, 3588; (f) H. T. Black, I. Pelse, R. M. W. Wolfe, J. R. Reynolds, *Chem. Commun.* **2016**, *52*, 12877-12880.

26. E. C. Nicholls-Allison, G. Nawn, B. O. Patrick, R. G. Hicks, *Chem. Commun.* **2015**, *51*, 12482-12485.

Chapter 4

Self-sorted co-assembly of PNI and 1,8-naphthalimide based dye

Abstract: Self-sorting in self-assembly processes is an excellent tool for synthesis of complex structures with desired functionalities from a multicomponent mixture. Using PNI as one of the molecules in a two-component mixture, social self-sorting was utilized to prepare co-aggregates with 1,8-naphthalimide based dyes. The obtained co-aggregate of PNI with NH_2-NMI showed mutual enhancement of emission. In addition to effective amalgamation of self-sorting and AIEE, the co-aggregate enabled energy transfer from the imide to PNI. The heteromeric aggregate was dual emissive in nature.

4.1 Introduction

4.1.1 Self-assembly

Self-assembly is a process of spontaneous organization of species into defined patterns, arrangements or structures without guidance or control from an outside source.[1] It allows formation of organized-assembly based on the information encoded in individual components which determine the interactions among them. The design of components that organize themselves into desired arrangements and functions is the important aspect for applications of self-assembly. Self-assembly is a unique phenomenon and takes place at molecular, mesoscopic, and macroscopic scales.[2] The arrangement of solar system is also an example of self-assembly process. Many biological systems are based on the process. A classic example is the case of tobacco mosaic virus.[3] The self-assembly process was recognised in chemistry in the early 1960s after the discovery of "crown ethers", "spherands" and "cryptands", by Pedersen[4], Cram[5], and Lehn[6] respectively (Figure 1). Further development and contribution in the field by them was recognised and awarded with Nobel Prize in Chemistry in 1987. The discovery also led to the generation of new branch, "supramolecular chemistry".

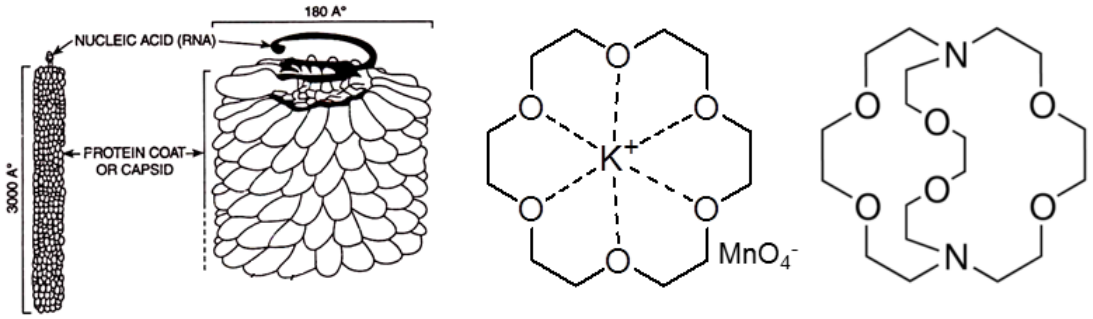

a. Tobacco mosaic virus (TMV) b. $KMNO_4$. 18-crown-6 c. Cryptands-2.2.2

Figure 1. Early discoveries of self-assembly processes in biological and molecular level**.**

In the molecular level self-assembly involves noncovalent interactions like hydrogen bonding[7], metal-ligand interactions[8], electrostatic interactions[9], π-π stacking[10] and

solvophobic effects[11] (Figure 2). Some weak covalent interactions like reversible imine formation,[12] boronic ester formation[13] etc. also involve in self-assembly process. Utilizing these tools a wide variety of self-assembled architectures have been reported.

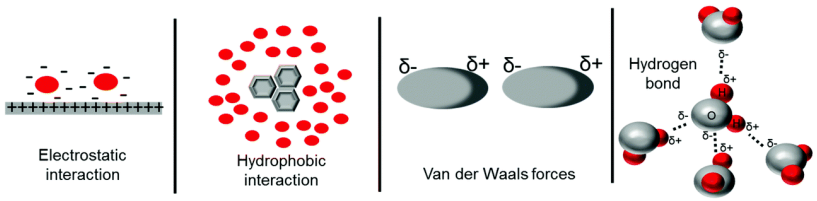

Figure 2. Non-covalent interactions involved in molecular self-assembly.

Contrary to the traditional organic chemistry, self-assembly process allows quick access to large molecular structures, necessary for many applications. Furthermore, the generated assembly exhibits new properties which are not observe in the monomeric level. Some of the common supramolecular systems are vesicles,[14] liquid crystal phases,[15] and Langmuir mono-layers by surfactant molecules.[16] Unsurprisingly, the self-assembly process has been studied extensively over the last 4-5 decades. Self-assembled nano materials have been used for a very wide range of applications in material sciences, electronic devices, biomedical sciences, information technologies, and environmental sciences. For example, gold nanoparticles have been used for biosensing.[17] Micelles and vesicles are attractive objects for catalysis as they tend to mimic liposomes and cells.[18] MOFs have attracted a lot of attention in the field of environmental sciences.[19] Their intrinsic porosity along with their stability in organic solvents has promoted them as suitable tools for heterogeneous catalysis.[20] Chiral MOFs have been used for asymmetric catalysis.[21] Development of conducting organic materials via self-assembly leads to formation of a huge library of conducting nanotubes, nanowires and nano sheets.[22]

4.1.2 Self-sorting in self-assembly

Most of the self-assembly processes studied in the laboratory are based on single components. Hence, artificial self-assembly processes lack diversity in comparison to the biological counterpart comprising of multiple different parts. The artificial self-assemblies should be prepared using multiple different entities. Self-sorting process provides solution to the above mentioned problem. The self-sorting in self-assembly is as the phenomena of high fidelity molecular recognition within a complex mixture.[27] The fact is well evident in Nature and builds the foundation of existence of life. For instance, the formation of the DNA double helix occurs via base-pairing (sorting) of complementary nitrogenous bases (adenine-thymine (A-T) and cytosine-guanine (C-G)).[23] These high-fidelity recognition events are keys to the storage of genetic information used in the development and functioning of living organisms. Formation of heterodimers composed of two different proteins through self-discrimination of equals, and the simultaneous recognition of complementary units is another example of efficient self-sorting in nature. Finally, formation of cell, also known as the functional basic unit of life occurs through self-sorting of such above mentioned macromolecules. And, within the cell, multiple levels of compartmentalization arising from the self-sorting of its molecular constituents allow the synchronicity of all the functional architectures acting independently. This outstanding selectivity in nature makes possible the existence of life.[24]

The message from the Nature has been replicated by the scientific community. The sorting phenomenon has been utilized in the artificial self-assembly process. The self-sorting in artificial self-assembly was first investigated by Prof. J. M. Lehn and his co-workers in mixtures of different helical-metal complexes (Scheme 1).[25] They demonstrated the co-self-assembly process in a mixture of two *tris*-bipyridine ligands in the presence of Ni(II) and Cu(I) ions into selective double and triple helicates in quantitative yields. Recognition of the

Ni(II) and Cu(I) ions by the respective ligands were evident from the mass spectrometric and ^{1}H NMR experiments, cancelling out the formation of crossover, mixed or undesired species. This remarkable observation was initially labelled as "self-recognition, or recognition of like from unlike and self-from nonself",[25] to explain the preferential binding ignoring other species in the solution.

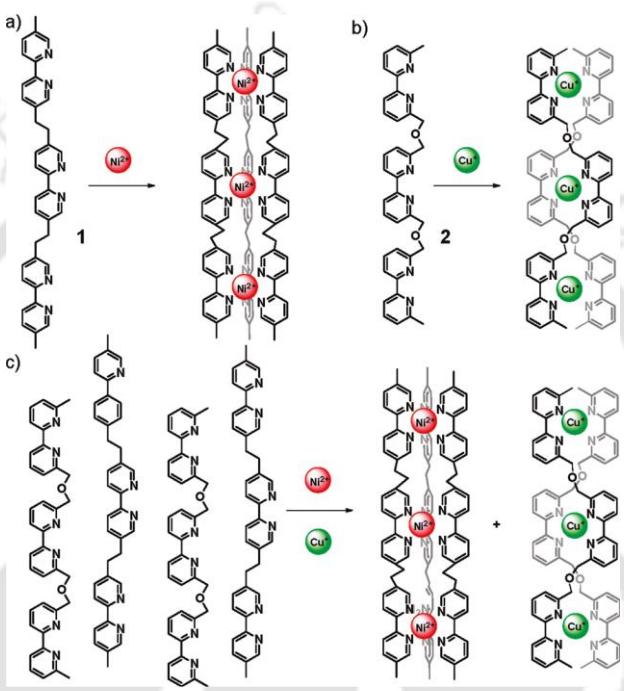

Scheme 1. First example of molecular recognition via metal-ligand interactions by Lehn and his co-workers.

Now, the term self-recognition has been replaced by the more general term "self-sorting" to describe such selective molecular recognition in multicomponent mixtures based on a suggestion of Isaacs and co-workers.[26,27] Depending upon the type of assemblies formed by the components in a mixture, it can result into either "narcissistic" self-sorting[28] or "social" self-sorting[29] (Figure 3). The former is a result of molecular affinity towards like molecules, whereas binding between unlike molecules results into the later.

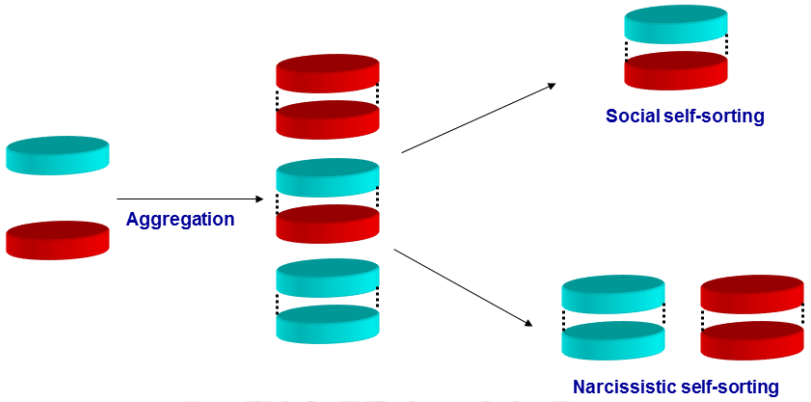

Figure 3. Self-sorting in a two-component system.

Following the footsteps of Lehn and other pioneers in the field of molecular self-sorting, supramolecular chemists have been exploring self-sorting in complex molecular mixtures to achieve a huge library of structurally diverse aggregate(s). Because of its potential to form numerous supramolecular structures with varying outcomes, social self-sorting has been growing as a fascinating research field among the scientists over the last few decades.[30] Discrete supramolecular structures[31], extended supramolecular aggregates[32] or gel-phase materials[33] in organic solvents have been prepared utilizing self-sorting phenomenon. Successful implementation of this process has been also realized in aqueous medium from binary mixtures of amphiphilic oligophenylenes[34], perylene bisimides[35], peptides[36], bisurea bolaamphiphiles[37] or cyclodextrins[38]. Apart from structural diversity some supramolecular aggregates are reported to have successful installation of new functionalities like machinery works.[39] This concept has also been extended towards molecular cybernetics[40]. In terms of structural complexity, the on-going work in social self-sorting is quite effective. In few instances are there, when functional improvements (like emission enhancement) got incorporated into the resultant aggregate.

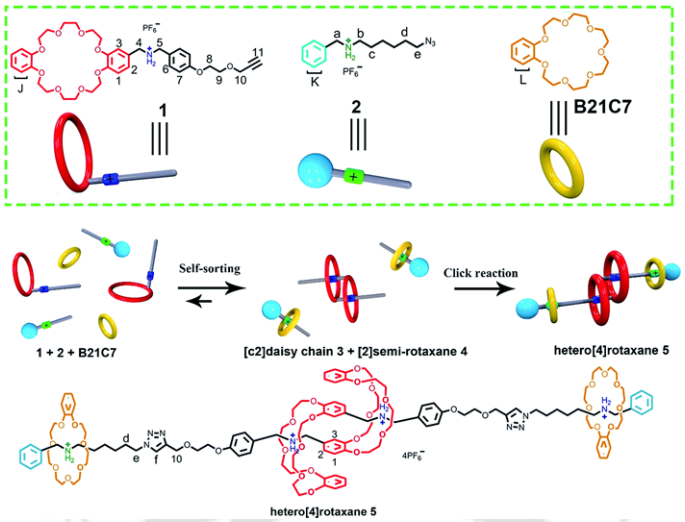

Figure 4. Schematic representation of an one-pot the preparation of hetero[4]rotaxane5 using a three-component modularized self-sorting system.[41]

For example in 2015, Peter J. Stang reported two multicomponent tetragonal prismatic supramolecular coordination complexes (SCC) to show enhanced emission upon molecular aggregation. Similar enhancement of fluorescence emission was also reported in other SCCs.[42] Fascinated by the possibility of diverse structures as well as functionalities to be installed in PNI-associated co-aggregates, this chapter is a stepping stone towards the same.

4.1.3 Objectives

The main objective of this chapter is to prepare various heteromeric aggregates via self-sorting. Because of the diverse range of interesting properties, as described in previous chapter, PNI has been used as one partner of the libraries. The other partner was decided by the guiding principle of self-sorting. The existence of geometrical complementarity of the chemical entities by means of size and shape is a vital criterion to form strong intermolecular interactions as illustrated by the lock-and-key-principle. In metal-coordination systems, for instance, ligands with different size, shape, or rigidity can self-sort into distinct supramolecular architectures in the presence of a metal ion. The social self-sorting process in

two-component library is often observed by preventing homomeric aggregation of one via steric control.[43] Utilizing a similar approach, two naphthalimide based dyes, H-NMI and NH_2-NMI (Figure 5), were designed. The bulky aromatic group was introduced at the imide position to prevent homomeric aggregation of the naphthalimide based dyes. The objective of this chapter was to generate various self-sorted aggregates of PNI and the naphthalimides. The possibility of Förster resonance energy transfer (FRET)[44] was also aimed to investigate as there were spectral overlap between the absorbance of PNI and the emission of NH_2-NMI. The imide dye NH_2-NMI does not show AIEE alone. However, it was targeted to induce the same via restriction of rotation of the amino group in the self-sorted co-aggregate of PNI and NH_2-NMI.

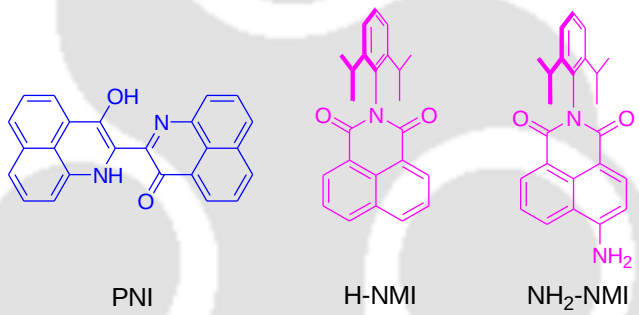

Figure 5. Structures of molecules used for social self-sorting.

4.2 Result and discussion

4.2.1 Co-aggregate of PNI and H-NMI

To fulfil the objective, the imide based dye was prepared and characterized according literature reports.[45] Before investigating two-component self-sorting process, the self-assembly capability of H-NMI was investigated. PNI shows AIEE in THF/n-hexane, and for comparison the same solvent system was used for investigations involving H-NMI. The imide based dye H-NMI exhibited absorption maxima at 343 nm (Figure 6) in a solvent

mixture of THF/*n*-hexane (v/v = 1:9). The spectral feature of the dye remained the same at various concentrations ranging from 1×10^{-3} M to 5×10^{-5} M. The absorption behaviors at various concentrations, as seen in Figure 6, supported that under the specified solvent system homomeric aggregation of H-NMI was not favorable.

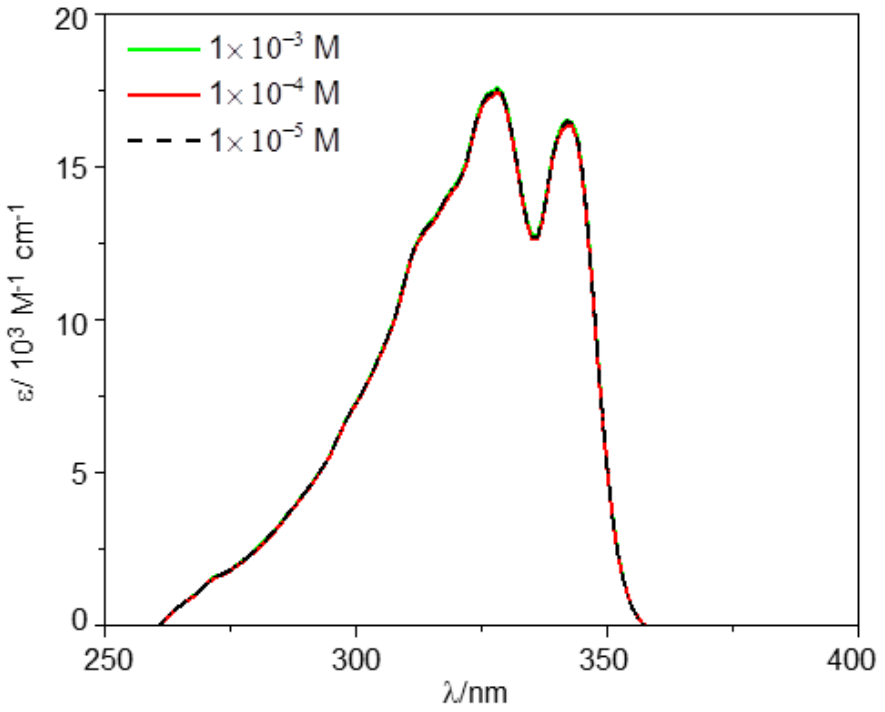

Figure 6. Absorption spectra (293 K) of H-NMI at various concentrations in THF/*n*-hexane (v/v = 1:9) mixture.

Based on the observation, co-assembly process of PNI and H-NMI was studied. This was done by preparing library of PNI and H-NMI at different molar ratios in THF/*n*-hexane (v/v = 1:9). Five different libraries were generated by taking PNI and H-NMI in 10:n (n = 1, 2,..5) molar ratio.

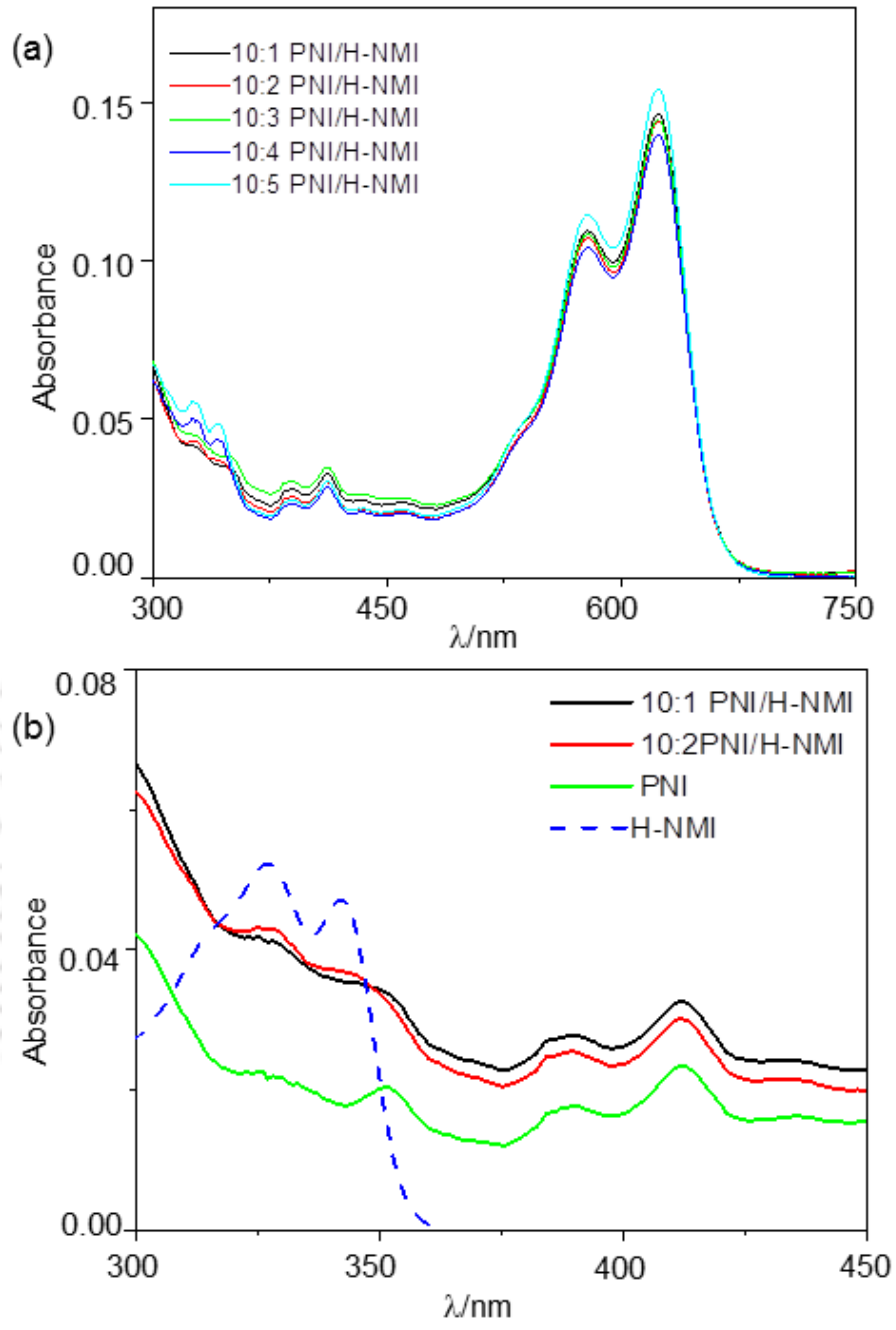

Figure 7. (a) Absorption spectra (293 K) of heteromeric aggregates of PNI and H-NMI in THF/*n*-hexane (v/v = 1:9) mixture. (b) Partial absorption spectra of homomeric aggregate of PNI (green, solid), heteromeric aggregates (red and black solid), and H-NMI (blue dash) in THF/*n*-hexane (v/v = 1:9).

The co-assemblies were prepared by dissolving PNI and H-NMI in THF, followed by addition of *n*-hexane. The resultant co-self-assembly processes were analysed by UV-vis spectroscopy. All the libraries displayed vibronically resolved spectra, suggesting aggregation (Figure 7). Significant changes were noticed in between 300-450 nm, suggesting

involvement of H-NMI in the co-assembly process. Substantial changes were also noticed in the PNI behaviour around this region. Moreover, the absorption spectra of the resultant aggregate were found to be different than the mathematical summation of the spectra of self-assembled PNI and monomeric H-NMI (Figure 7b). All these observations pointed towards exclusive formation of heteromeric aggregate excluding the possibility of a mixture of monomeric H-NMI and homomeric PNI-aggregate. Exclusive formation of the co-aggregate was also evident from the FESEM images of libraries (Figure 8). To prepare the respective sample for microscopic imaging a solution of co-aggregate was prepared by mixing a 3×10^{-6} M solution of PNI with appropriate amount of H-NMI in 10:2 molar ratio in THF/*n*-hexane (v/v = 1:9).

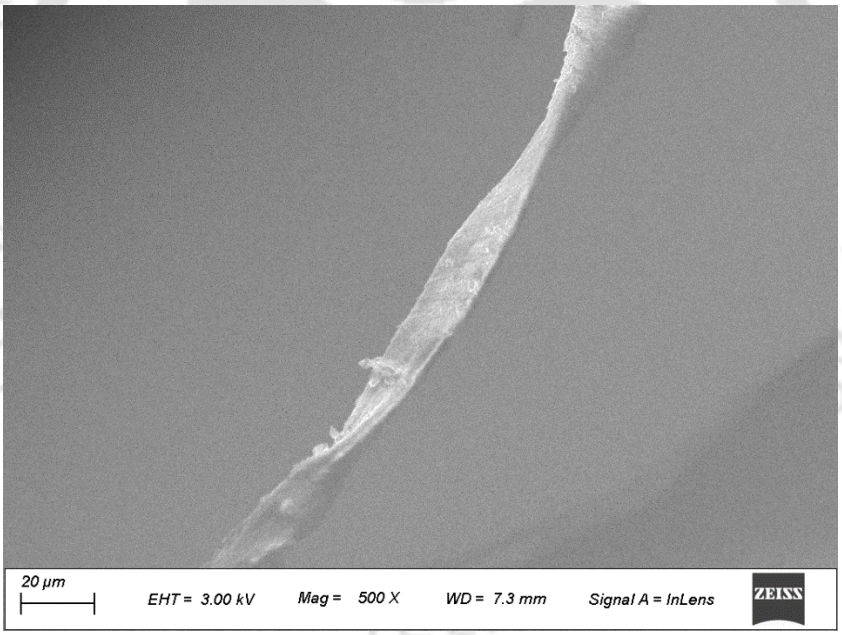

Figure 8. FESEM image of co-aggregate of PNI and H-NMI in THF/*n*-hexane (v/v = 1:9).

The obtained solution was then drop-casted followed by overnight room temperature drying. Unlike the sharp crystalline cuboids in PNI self-assembly, ribbon shaped uniform morphologies were observed. The dimension of the ribbon shaped architecture was few microns in length. Contrary to the distinctive 3D- nature of the homomeric PNI aggregate,

heteromeric aggregates were 2D in nature. Both the dimension and the ubiquity of the obtained morphology supported the assumptions made from the absorption behavior of the same. This was followed by investigation of photoluminescence behavior of PNI and the naphthalimide in the co-aggregate. The resultant co-aggregate was found to be emissive. Although photoluminescence of PNI was clearly enhanced compared to its monomeric form, H-NMI remained non-emissive (Figure 9a). The rigid structure of the naphthalimide limited its scope for aggregation induced enhanced emission. A comparison of photoluminescence spectra of PNI in different co-aggregates showed blue-shifted emission maxima with almost six fold increase in emission intensity (Figure 9b).

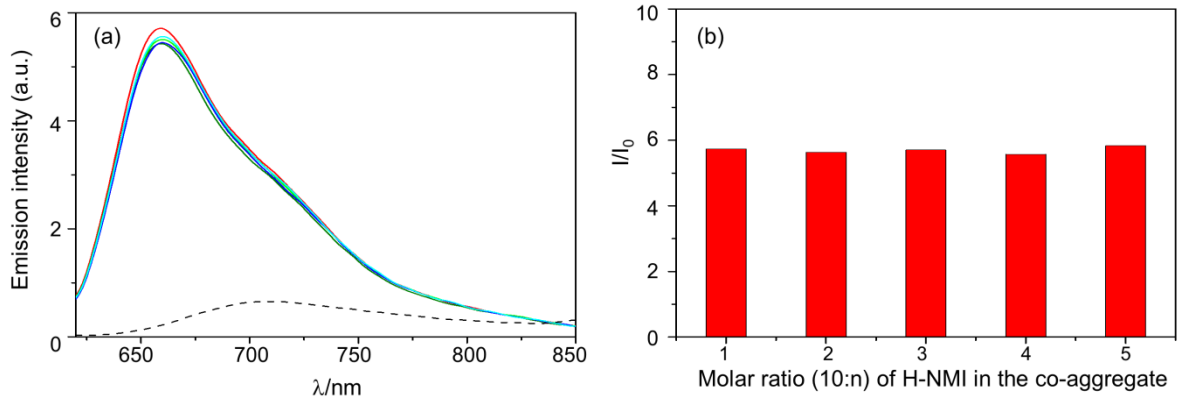

Figure 9. (a) Photoluminescence spectra (293 K) of monomeric PNI (black dash) in THF and aggregated PNI (colored) in the co-self-assembly with H-NMI in THF/*n*-hexane (v/v = 1:9) at different molar ratios (PNI:H-NMI = 10:n; n=1,2,..5). (b) Photoluminescence enhancement of PNI in the co-aggregate with H-NMI at different molar ratio of the imide.

4.2.2 Co-aggregate of PNI and NH_2-NMI

The prime objective of this chapter was to successfully install emission enhancement in all the components of a self-sorted co-assembly. In the co-aggregate of PNI and H-NMI, the former showed the expected emission enhancement. But by virtue of its structural rigidity, H-NMI remained non-emissive. Therefore in the next set of experiments a less rigid molecule NH_2-NMI[46] was used. Installation of the amino group at 4-position of the naphthyl ring was done to achieve enhanced emission via rotational restriction[47] upon the amino group in the resultant co-aggregate. At the beginning photophysical investigations were done to exclude the possibility of homomeric aggregate of NH_2-NMI in a solvent mixture of THF/*n*-hexane (v/v = 1:9). The naphthalimide based dye exhibited broad absorption maxima at 410 nm. The characteristic of its absorption behavior remained same at various concentrations ranging from 1×10^{-3} M to 1×10^{-6} M (Figure 10). Based on this, the possibility of homomeric aggregation of NH_2-NMI under the specified solvent system was canceled out.

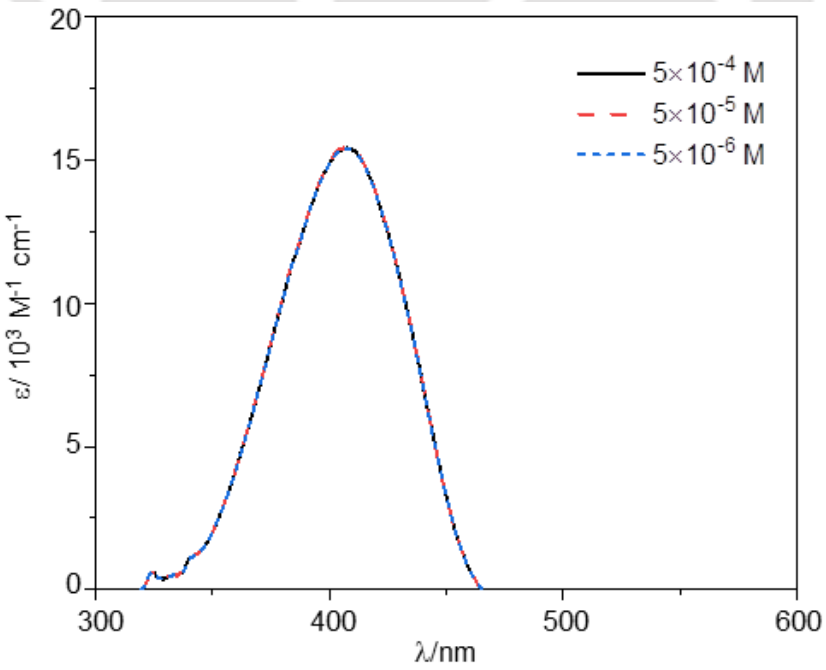

Figure 10. Absorption spectra (293 K) of NH_2-NMI at various concentrations in THF/*n*-hexane (v/v =1:9) mixture.

To study the social self-sorting process, PNI and NH_2-NMI were mixed in a 10:n (n = 1, 2,..5) molar ratio in THF, followed by addition of *n*-hexane to make the final f_h to 0.9. UV-vis absorption spectra of the resultant mixture displayed vibronically resolved absorption maxima for PNI (Figure 11a).

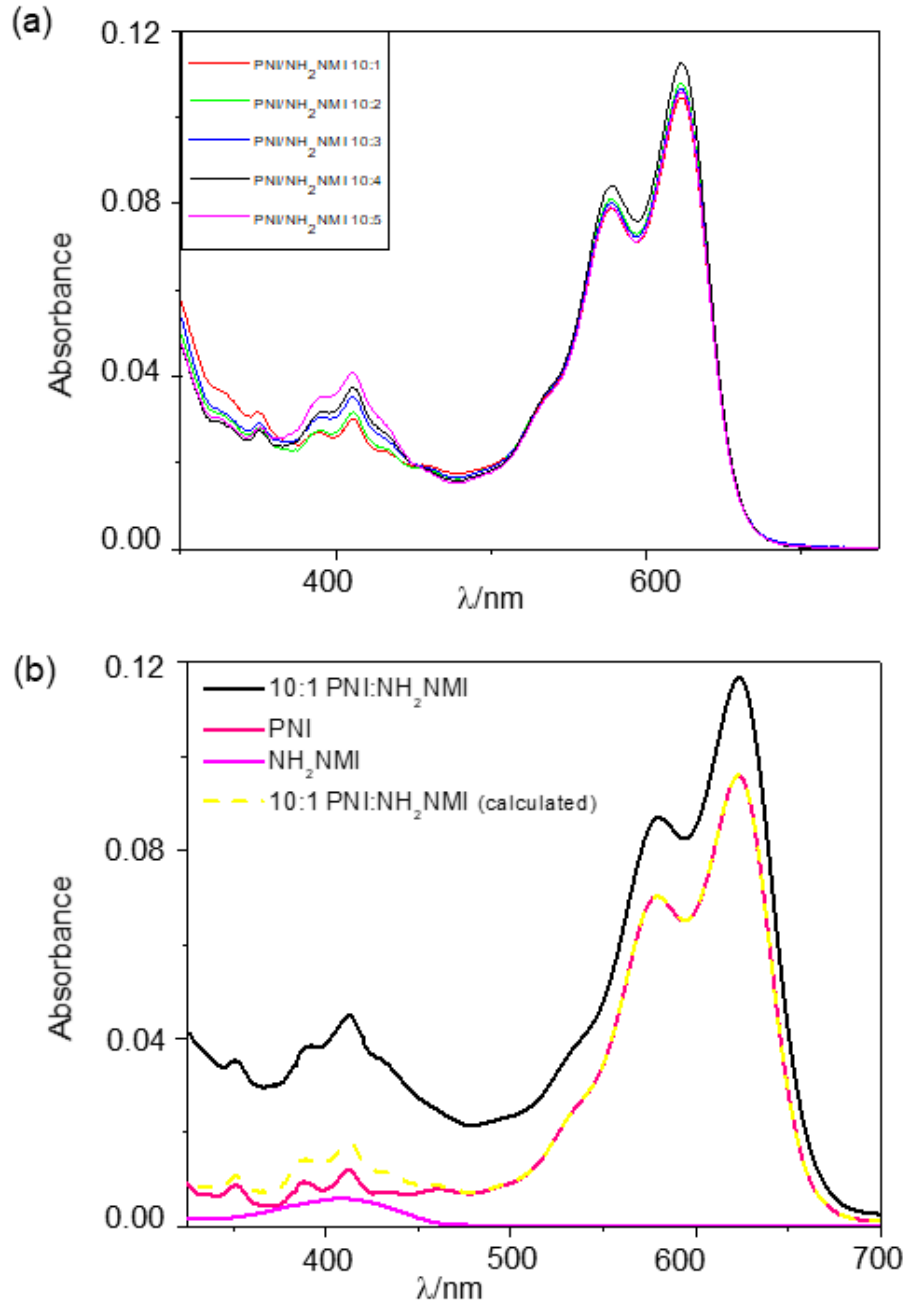

Figure 11. (a) Absorption spectra (293 K) of heteromeric aggregates of PNI and NH_2-NMI in THF/*n*-hexane (v/v = 1:9) mixture. (b) Experimental vs. calculated spectra for co-aggregate of PNI/NH_2-NMI.

Increase in molar absorptivity at the absorption maxima of NH_2-NMI was also noticeable in the mixture. Similar to the observations for PNI/H-NMI co-aggregate, the absorption spectra of the resultant mixture were found to be different than the mathematical summation of the spectra of self-assembled PNI and NH_2-NMI (Figure 11b). FESEM image of a PNI/NH_2-NMI (10:1 molar ratio) co-aggregate was recorded, which showed exclusive formation of ribbon-shaped morphology as shown in Figure 12. The observation is similar to that one observed with the other imide based dye. It reinforced the existence of social self-sorting in a mixture of PNI and NH_2-NMI. The obtained morphologies of these co-aggregates were clear indicators for opportunity of structural tuning of the hetero-aggregates vs. the homo-aggregate.

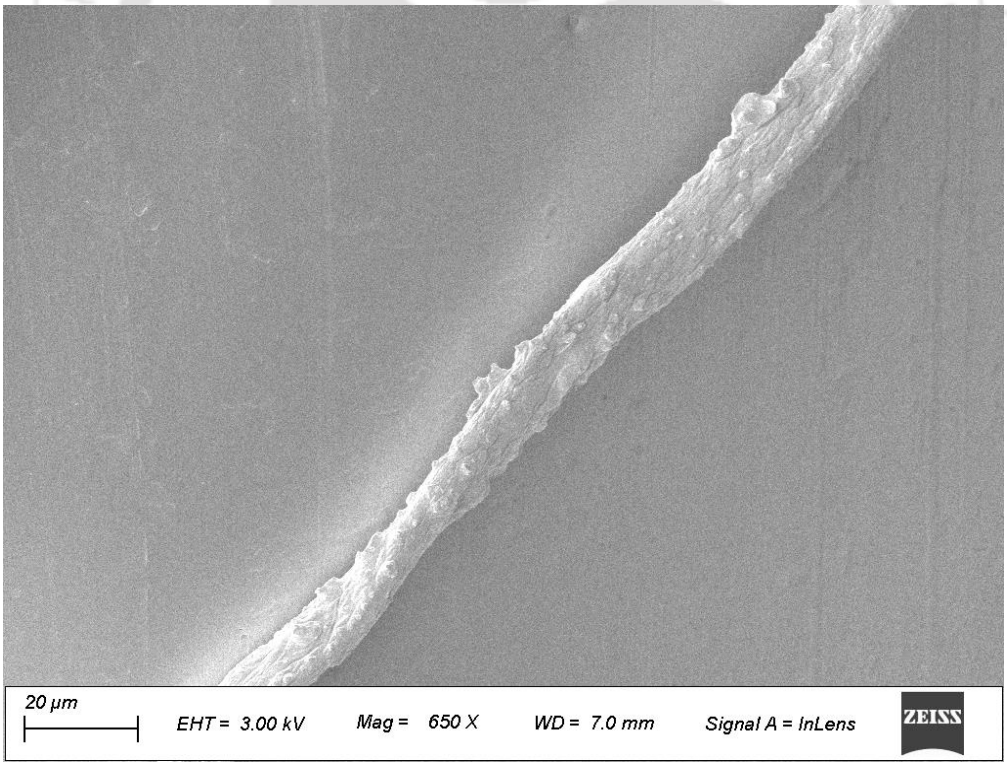

Figure 12. FESEM image of co-aggregate of PNI and NH_2-NMI in THF/*n*-hexane (v/v = 1:9).

Formation of ribbon-shaped morphologies in the co-aggregates of PNI with NMIs can be explained considering the figurative model shown in Figure 13. Partial insertion of the imide

molecules from the naphthyl part into the 1D-sheets of H-bonded PNI molecules would form a long continuous structure. Bulkiness of the di-isopropylphenyl substituent in the imide molecule would prevent successive stacking of the same. This would lead towards steric adjustments inserting the flexibility and results into spiral features as seen the 2D-architechtures.

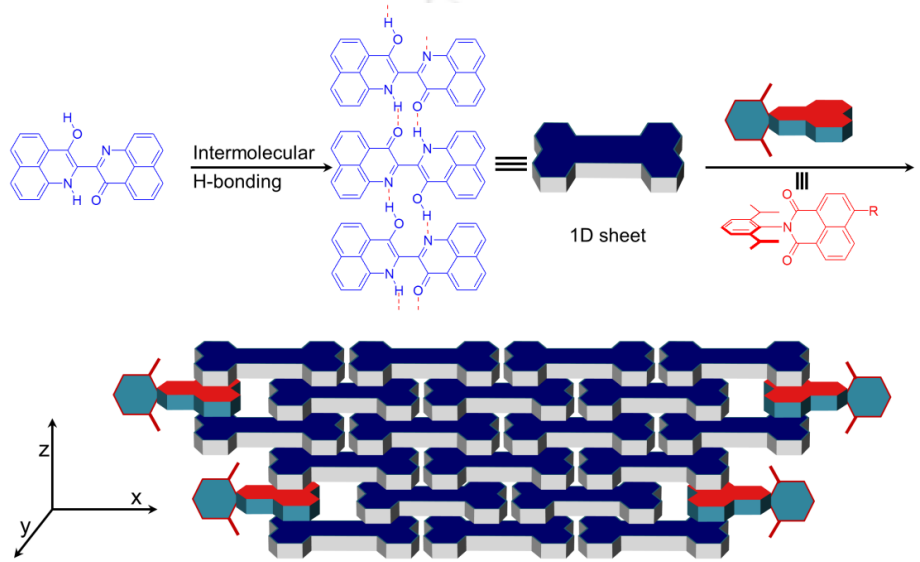

Figure 13. Co-self-assembly process of PNI and 1,8-substituted naphthalimide derivatives. Sandwiching of imide in between PNI caused restricted growth in x-direction, leading to 2D ribbon-shaped aggregate.

Photoluminescence measurement for PNI in its different co-aggregates with NH_2-NMI displayed emission enhancement similar to its homo-aggregate as well as its co-aggregates with H-NMI. Upon excitation of the co-aggregate solution at 610 nm, a blue-shifted emission maximum with increase in emission intensity was observed (Figure 14a). Mathematical comparison of emission intensity in the co-aggregates the monomeric form revealed more than five-fold enhancement in the photoluminescence intensity (Figure 14b).

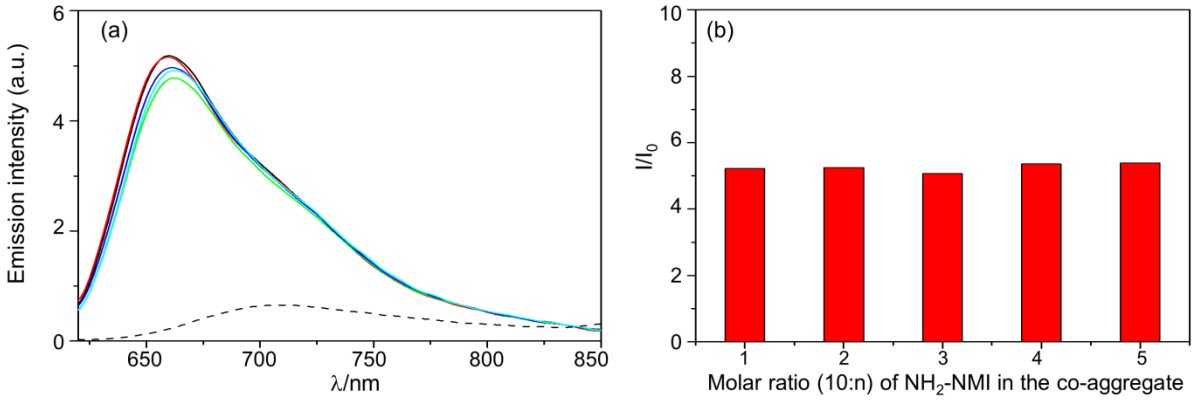

Figure 14. (a) Photoluminescence spectra (293 K) of monomeric PNI (black dash) in THF and aggregated PNI (colored solid) in the co-self-assembly with NH_2-NMI in THF/*n*-hexane (v/v = 1:9). (b) Photoluminescence enhancement of PNI in the co-aggregate with NH_2-NMI at different molar ratio of the imide.

To study the effect of co-aggregation upon photoluminescence of NH_2-NMI, emission spectra of co-aggregate solutions were recorded after excitation at 410 nm. As evident from Figure 15a, emission enhancement occurred for the naphthalimide in its co-aggregate with PNI. Calculations revealed a 1.28 fold increase in emission intensity and are represented in Figure 15b. Further confirmation on this was attained from time-resolved photoluminescence spectroscopy of the naphthalimide. The imide showed an improved lifetime of 8.84 ns in the co-assembled aggregate from 8.24 ns in monomer.

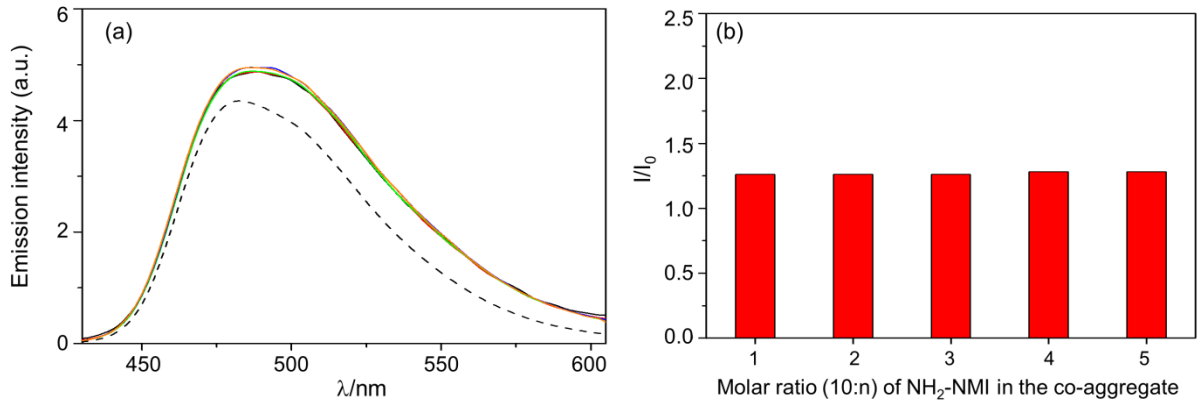

Figure 15. (a) Photoluminescence spectra (293 K) of NH_2-NMI as monomer (black dash) and as co-aggregate with PNI (colored) in THF/*n*-hexane (v/v = 1:9). (b) Photoluminescence enhancement of NH_2-NMI in the co-aggregate with PNI at different molar ratio of the imide.

This established successful association of social self-sorting with AIEE for all the participating molecules and the target of designing mutually benefitted co-assembly was fulfilled. Analysis of photophysical spectra obtained for the dyes showed that there is a region of spectral overlap between the NH_2-NMI emission band and the PNI absorption band (Figure 16). This indicated a probability for energy transfer from the imide to PNI.

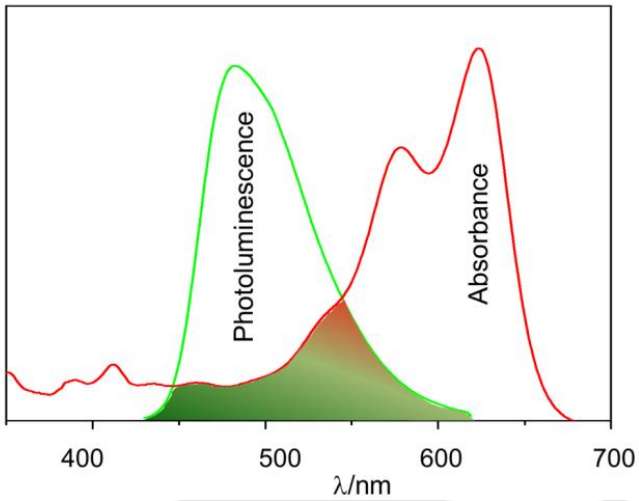

Figure 16. Spectral overlap between the emission of NH_2-NMI and the absorption of PNI.

To study the energy transfer process steady-state emission of PNI in the co-aggregate was recorded after exciting the same at the absorption maxima of NH_2-NMI. Upon excitation at 410 nm, emission enhancement of PNI at its maxima 657 nm was prominent compared to the emission from its homomeric aggregate. The increase in emission intensity in the hetero-aggregate can be attributed to Förster resonance energy transfer (FRET) from the imide to PNI (Figure 17).

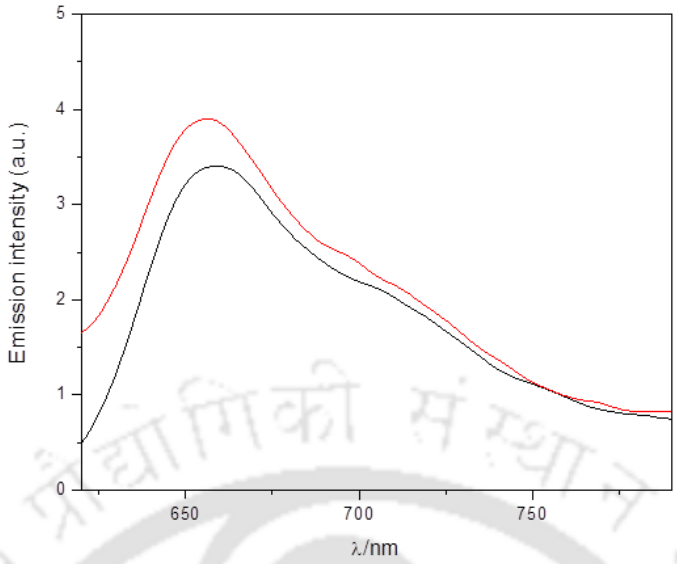

Figure 17. Photoluminescence spectra (293 K) of PNI in the heteromeric aggregate (red, PNI/NH_2-NMI 10:4) and in the homomeric aggregate (black) in THF/*n*-hexane (v/v = 1:9).

However, the energy transfer process was not very efficient. This resulted in formation of a dual emissive[48] aggregate when excited at 410 nm (Figure 18). The relative intensities of the emission maxima were found to be reliant on molar ratios of the dyes in the co-aggregate mixture. It presents an excellent scenario for selective control upon the dual-emission to obtain required intensities for photoluminescence based applications.[49]

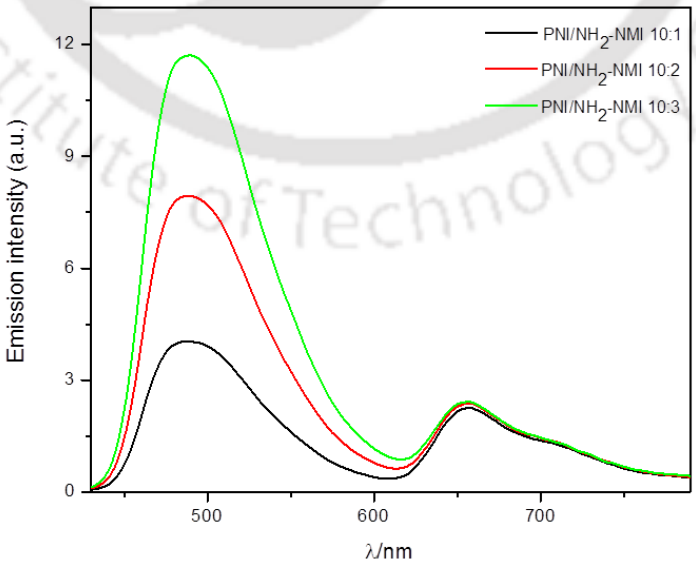

Figure 18. Dual-emissive spectra (293 K) of co-aggregates of PNI and NH_2-NMI in THF/*n*-hexane (v/v = 1:9).

4.3 Conclusion

In summary, PNI undergoes social self-sorting with both H-NMI and NH_2-NMI in a solvent mixture of THF/*n*-hexane (v/v = 1:9). In case of PNI/H-NMI co-aggregate, emission enhancement was observed for PNI while H-NMI remained non-emissive. But, mutual enhancement of emission was achieved in the co-aggregate between NH_2-NMI and PNI. Increments in steady state emission intensities were calculated to be 28% for the imide and more than 400% for PNI. In addition to successful merger of social self-sorting with AIEE, spectral overlap between the emission of NH_2-NMI and the absorption of PNI enabled FRET from the imide to PNI. The resultant co-aggregate of PNI/NH_2-NMI was also dual emissive in nature when excited at 410 nm. Such vibrant features obtained due to self-sorting holds the possibility of adding advantages in many applications that requires proper tuning of photophysical behavior. The photophysical characteristics of the multi-component assemblies (broad absorption band with emission in the NIR region) can also be useful for efficient light-energy harvesting.[50]

4.4 References

1. G. M. Whitesides, B. Grzybowski, *Science*, **2002**, *295*, 2418-2421.
2. G. M. Whitesides, M. Boncheva, *Proc. Natl. Acad. Sci. U. S. A.* **2002**, *99*, 4769-4774.
3. A. Klug, *Angew. Chem. Int. Ed.* **1983**, *22*, 565-569.
4. C. J. Pedersen, *Angew. Chem. Int. Ed.* **1988**, *27*, 1021-1027.
5. D. J. Cram, *Angew. Chem. Int. Ed.* **1988**, *27*, 1009-1020.
6. J. -M. Lehn, *Angew. Chem. Int. Ed.***1988**, *27*, 89-112.
7. (a) K. A. Jolliffe, P. Timmerman, D. N. Reinhoudt, *Angew. Chem. Int. Ed.* **1999**, *38*, 933-937; (b) Y. G. Ma, S. V. Kolotuchin, S. C. Zimmerman, *J. Am. Chem. Soc.* **2002**, *124*, 13757-13769.
8. (a) D. L. Caulder, K. N. Raymond, *Angew. Chem. Int. Ed*. **1997**, *36*, 1440-1442; (b) J. R. Nitschke, *Acc. Chem. Res*. **2006**, 40, 103-112; (c) M. Schmittel, K. Mahata, *Chem. Commun*. **2010**, *46*, 4163-4165; (d) K. Mahata, M. Schmittel, *Beilstein J. Org. Chem*. **2011**, *7*, 1555-1561.
9. W. Jiang, H. D. F. Winkler, C. A. Schalley, *J. Am. Chem. Soc.* **2008**, *130*, 13852-13853.

10. A. D. Shaller, W. Wang, H. Y. Gan, A. D. Q. Li, *Angew. Chem. Int. Ed.* **2008**,*47*, 7705-7709.

11. (a) B. Bilgicer, X. Xing, K. Kumar, *J. Am. Chem. Soc.* **2001**, *123*, 11815-1116; (b) N. A. Schnarr, A. J. Kennan, *J. Am. Chem. Soc.* **2003**, *125*, 667-671.

12. (a) C. D. Meyer, C. S. Joinera, J. F. Stoddart, *Chem. Soc. Rev*. **2007**, *36*, 1705-1723; (b) S. M. Oburn, D. C. Swenson, S. V. S. Mariappan, L. R. MacGillivray, *J. Am. Chem. Soc.* **2017**, *139*, 8452-8454

13. (a) R. Nishiyabu, Y. Kubo, T. D. James, J. S. Fossey, *Chem. Commun.* **2011**, *47*, 1124-1150; (b) S. D. Bull, M. G. Davidson, J. M. H. van den Elsen, J. S. Fossey, A. T. A. Jenkins, Y. -B. Jiang, Y. Kubo, F. Marken, K. Sakurai, J. Zhao, T. D. James, *Acc. Chem. Res.* **2013**, *46*, 312-326; (c) K. Ono, Y. Tohyama, T. Uchikura, Y. Kikuchi, K. Fujii, H. Uekusa, N. Iwasawa, *Dalton Trans.* **2017**, *46*, 2370-2376.

14. (a) C. Huang, D. Quinn, Y. Sadovsky, S. Suresh, K. J. Hsia, *Proc. Nat. Acad. Sci.* **2017**, *114*, 2910-2915; (b) A. R. Sapala, S. Dhawan, V. Haridas, *RSC Adv*. **2017**, *7*, 26608-26625.

15 F. J. M. Hoeben, I. O. Shklyarevskiy, M. J. Pouderoijen, H. Engelkamp, A. P. H. J. Schenning, P. C. M. Christianen, J. C. Maan, E. W. Meijer, *Angew. Chem. Int. Ed.* **2006**, *45*, 1232-1236.

16.(a) M. Gomez, J. Li, A. E. Kaifer, *Langmuir* **1991**, *7*, 1797-1806; (b) Y. -L. Lee, A. Dudek, T. -N. Ke, F. -W. Hsiao, C. -H. Chang, *Macromolecules* **2008**, *41*, 5845-5853.

17. (a) J. Lei, H. Ju, *Chem. Soc. Rev*. **2012**, *41*, 2122-2134; (b) K. B. Cederquist, S. O. Kelley, *Curr. Opin. Chem. Biol.* **2012**, *16*, 415-421.

18. S. R. K. Minkler, B. H. Lipshutz , N. Krause, *Angew. Chem. Int. Ed.* **2011**, *50*, 7820-7823.

19. X. Chen, Y. Wang, Q. Liu, Z. Zhang, C. Fan, L. He, *Angew. Chem. Int. Ed*. **2006**, *45*, 1759-1762.

20. A. Corma, H. García, F. X. Llabrès i Xamena, *Chem. Rev.* **2010**, *110*, 4606-4655.

21. Wu, C. He, J. Wang, X. Peng, X. Li, Y. An, C. Duan, *J. Am. Chem. Soc* **2012**, *134*, 14991-14999.

22. (a) S. S. Babu, S. Prasanthkumar, A. Ajayaghosh, *Angew. Chem. Int. Ed.* **2012**, *51*, 1766-1776; (b) E. Moulin, F. Niess, M. Maaloum, E. Buhler, I. Nyrkova, N. Giuseppone, *Angew. Chem. Int. Ed*. **2010**, *49*, 6974-6978; (c) E. Moulin, F. Niess, G. Fuks, N. Jouault, E. Buhler, N. Giuseppone, *Nanoscale* **2012**, *4*, 6748-6751.

23. (a) J. D. Watson, F. C. H. Crick, *Nature* **1953**, *171*, 737-738; (b) U. H. Bscher, G. Maga, Curr. *Opin. Chem. Biol*. **2011**, *15*, 627-635.

24. A. Nikoubashman, F. Schmid, *Nat. Chem*. **2019**, *11*, 298-300.

25. R. Kramer, J. M. Lehn, A. Marquisrigault, *Proc. Nat. Acad. Sci. U.S.A.* **1993**, *90*, 5394-5398.

26. P. Mukhopadhyay, A. X. Wu, L. Isaacs, *J. Org. Chem*. **2004**, 69, 6157-6164.

27. A. Wu, L. Isaacs, *J. Am. Chem. Soc*. **2003**, *125*, 4831-4835.

28. P. N. Taylor, H. L. Anderson, *J. Am. Chem. Soc*. **1999**, *121*, 11538-11545.

29. A. Shivanyuk, J. Rebek Jr., *J. Am. Chem. Soc.* **2002**, *124*, 12074 -12075.

30. (a) M. M. Safont-Sempere, G. Fernández, F. Würthner, *Chem. Rev*. **2011**, *111*, 5784-5814; (b) M. J. Mayoral, C. Rest, J. Schellheimer, V. Stepanenko, G. Fernández, *Chem. Eur. J.* **2012**, *18*, 15607–15611.

31. (a) D. Ajami, M. P. Schramm, A. Volonterio, J. Rebek, Jr., *Angew. Chem. Int. Ed.* **2007**, *46*, 242–247; (b) Y. Rudzevich, V. Rudzevich, F. Klautzsch, C. A. Schalley, V. Bçhmer, *Angew. Chem. Int. Ed.* **2009**, *48*, 3867-3871; (c) D. Ajami, J.-L. Hou, T. J. Dale, E. Barrett, J. Rebek Jr., *Proc. Nat. Acad. Sci. U. S. A.* **2009**, *106*, 10430-10434.

32. (a) G. B. W. L. Ligthart, H. Ohkawa, R. P. Sijbesma, E. W. Meijer, *J. Am. Chem. Soc.* **2005**, *127*, 810-812; (b) P. Jonkheijm, N. Stutzmann, Z. Chen, D. M. de Leeuw, E. W. Meijer, A. P. H. J. Schenning, F. Würthner, *J. Am. Chem. Soc.* **2006**, *128*, 9535-9540; (c) A. Ajayaghosh, C. Vijayakumar, V. K. Praveen, S. S. Babu, R. Varghese, *J. Am. Chem. Soc.* **2006**, *128*, 7174-7175; (d) T. Maeda, Y. Furusho, S.-I. Sakurai, J. Kumaki, K. Okoshi, E. Yashima, *J. Am. Chem. Soc.* **2008**, *130*, 7938-7954; (e) J. -Y. Wang, J. Yan, L. Ding, Y. Ma, J. Pei, *Adv. Funct. Mater*. **2009**, *19*, 1746-1752; (f) R. Bhosale, J. Míšek, N. Sakai, S. Matile, *Chem. Soc. Rev*. **2010**, *39*, 138-149; (g) A. Jain, K. V. Rao, U. Mogera, A. A. Sagade, S. J. George, *Chem. Eur. J.* **2011**, *17*, 12355-12361; (h) B. Zheng, F. Wang, S. Dong, F. Huang, *Chem. Soc. Rev*. **2012**, *41*, 1621-1636.

33. (a) S. Ghosh, X. -Q. Li, V. Stepanenko, F. Würthner, *Chem. Eur. J*. **2008**, *14*, 11343-11357; (b) J. R. Moffat, D. K. Smith, *Chem. Commun*. **2009**, 316–318; (c) M. R. Molla, A. Das, S. Ghosh, *Chem. Eur. J*. **2010**, *16*, 10084-10093; (d) A. Das, S. Ghosh, *Chem. Commun*. **2011**, *47*, 8922-8924; (e) S. S. Babu, S. Prasanthkumar, A. Ajayaghosh, *Angew. Chem. Int. Ed.* **2012**, *124*, 1800-1810.

34. (a) J. -H. Ryu, M. Lee, *J. Am. Chem. Soc.* **2005**, *127*, 14170-14171; (b) E. Lee, J. -K. Kim, M. Lee, *J. Am. Chem. Soc*. **2009**, *131*, 1824-18243; (c) H.-J. Kim, T. Kim, M. Lee, *Acc. Chem. Res.* **2011**, *44*, 72-82.

35. (a) X. Zhang, Z. Chen, F. Würthner, *J. Am.Chem. Soc.* **2007**, *129*, 4886-4887; (b) X. Zhang, S. Rehm, M. M. Safont-Sempere, F. Würthner, *Nat. Chem*. **2009**, *1*, 623-629; (c) K. Mahata, P. D. Frischmann, F. Würthner, *J. Am. Chem. Soc*. **2013**, *135*, 15656-15661.

36. (a) D. M. Ryan, T. M. Doran, B. L. Nilsson, *Langmuir* **2011**, *27*, 11145-11156; (b) R. J. Swanekamp, J. T. M. DiMaio, C. J. Bowerman, B. L. Nilsson, *J. Am. Chem. Soc.* **2012**, *134*, 5556-5559.

37. (a) A. Pal, S. Karthikeyan, R. P. Sijbesma, *J. Am. Chem. Soc*. **2010**, *132*, 7842-7843; (b) A. Pal, P. Besenius, R. P. Sijbesma, *J. Am. Chem. Soc*. **2011**, *133*, 12987-12989.

38. N. Tomimasu, A. Kanaya, Y. Takashima, H. Yamaguchi, A. Harada, *J. Am. Chem. Soc*. **2009**, *131*, 12339-12343.

39. (a) S. De, S. Pramanik, M. Schmittel, *Angew. Chem., Int. Ed.* **2014**, *53*, 14255-14259; (b) M. Schmittel, *Chem. Commun.* **2015**. *51*, 14956-14968; (c) P. Waelés, B. Riss-Yaw, F. Coutrot, *Chem. Eur. J.* **2016**, *22*, 6837-6845. (d) I. Paul, A. Goswami, N. Mittal, M. Schmittel, *Angew. Chem. Int. Ed.* **2018**, *57*, 354-358. (e) L. Zhiquan, H. Xie, S. E. Border, J. Gallucci, R. Z. Pavlović, J. D. Badjić, *J. Am. Chem. Soc.* **2018**, *140*, 11091-11100.

40. M. Schmittel, *Isr. J. Chem.* **2018**, *58*, 1-13.

41. X. Fu, Qi Zhang, S.-J. Rao, D. -H. Qu, H. Tiana, *Chem. Sci.* **2016**, *7*, 1696-1701.

42. (a) X. Yan, T. R. Cook, P. Wang, F. Huwang, P. J. Stang, *Nat. Chem.* **2015**, *7*, 342-348; (b) L. J. Chen, Y. -Y. Ren, N. -W. Wu, B. Sun, J. -Q. Ma, L. Zhang, H Tan, M. Liu, X. Li, H. -B. Yang, *J. Am. Chem. Soc.* **2015**, *137*, 11725-11735. (c) A. Chowdhury, P. Howlader, P. S. Mukherjee, *Chem. Eur. J.* **2016**, *22*, 7468-7478. (d) M. L. Saha, X. Yan, P. J. Stang, *Acc. Chem. Res.* **2016**, *49*, 2527-2549.

43. K. Mahata, M. Schmittel, *J. Am. Chem. Soc.* **2009**, *131*, 16544-16554.

44. R. M. Clegg, *Curr. Opin. Biotechnol.* **1995**, *6*, 103-110.

45. T. Weil, E. Reuther, K. Müllen, *Angew. Chem. Int. Ed.* **2002**, *41*, 1900-1904.

46. A. Boehm, H. Schmeisser, S. Becker, K. Müllen, *Ger. Offen.* **2001**, DE 19940708 A1 20010301.

47. Y. Hong, J. W. Y. Lam, B. Z. Tang, *Chem. Commun.* **2009**, 4332-4353.

48. X. Chen, Z. He, F. Kausar, G. Chen, Y. Zhang, W. Z. Yuan, *Macromolecules* **2018**, *51*, 9035-9042.

49. (a) J. Coppeta, C. Rogers, *Exp Fluids*. **1998**, *25*, 1-15; (b) G. T. Hanson, T. B. McAnaney, E. S. Park, M. E. P. Rendell, D. K. Yarbrough, S. Chu, L. Xi, S. G. Boxer, M. H. Montrose, S. J. Remington, *Biochemistry* **2002**, *41*, 15477-15488; (c) Q. Guan, R. Su, M. Zhang, R. Zhang, W. Li, D. Wang, M. Xu, L. Fei, Q. Xu, *New J. Chem*. **2019**, *43*, 3050-3058.

50. (a) R. Ziessel, A. Harriman, *Chem. Commun*. **2011**, 47, 611-631; (b) C. Kreisbeck, A. Aspuru-Guzik, *Chem. Sci.* **2016**, *7*, 4174-4183; (c) T. Mirkovic, E. E. Ostroumov, J. M. Anna, R. V. Grondelle, Govindjee, G. D. Scholes, *Chem. Rev.* **2017**, *117*, 249-293.

Chapter 5

Derivatives of *peri*-Naphthoindigo

Abstract: Utilization of PNI as ligand has been demonstrated by preparing palladium complex of the same. The dye acts as bidentate ligand form stable 2:1 (PNI:Pd(II)) complex. The palladium complex (**PNI**)$_2$Pd was characterized by mass spectrometry and ^{1}H NMR spectroscopy. Connectivity of the ligand was established from DFT-calculation. Attempts to install aliphatic substitution at the chromophore towards mono or di-substitution were unsuccessful. Under the reaction condition, the dye underwent decomposition to form N-substituted lactam. However, derivatization of PNI at the naphthalene rings was found to be successful. DibromoPNI was prepared from 1-bromonaphthalene in three steps. Halo-substitution in the naphthyl rings lowered solubility of the dye in common organic solvents. Photophysical properties showed red-shifted absorption and emission maxima. The new dye was halochromic in acidic medium similar to PNI.

5.1 Introduction

Due to the applications in multifaceted areas and huge socio-economic impact, the historical dye indigo is one of the most important dyes recognized by the scientific community. In the century-old journey of indigoid-chemistry, immense amounts of research effort have been carried out to realize ring[1]- and N-substituted[2] indigos. Indigo has also been utilized as ligands for metal-complexes.[3] The manipulation at the carbonyl, led to the generation of wide variety of nindigos, which are also known to coordinate with wide variety of metal complexes.[4] Derivatization also caused change in properties like photophysical behavior, solubility in common organic solvents and electrochemistry of the dye. Modifications done at the peripheral positions of the phenyl rings, amine proton with different alkyl/aryl/ acyl groups or conversion of carbonyl to imine resulted in enhanced solubility of the dye. For example, dialkylated-indigo at 5,5'-positions with propyl and butyl group shows solubility in chloroform and 1,2-dichlorobenzene, which are 65-89 times higher as compared to the parent indigo.[5] N-substituted indigoids are strong photoluminiscent molecules. This derivatization also led to other exciting properties like facile photoswitching and higher thermal stability of the Z-isomer. Enhanced solubility of N,N'-disubstituted indigoids with di-*tert*-butyldicarbonate group was useful for simplistic construction of indigo-based solar-cells.[6] Similarly, introduction of strong electron withdrawing substituents at the phenyl rings result in a lower LUMO energy of the indigo core to yield stable n-type semiconductors.[7] All together, these modifications amplified the scope of application and the so-called vat dye got attention from the fields of modern age like organic photovoltaic,[8] molecular switches[9] etc. As the scope and applications of indigo-derivatives is manifold, the modification of PNI is an attractive topic of research. Duo to the presence of mono-enol isomer and many different positions in the naphthyl rings, the room for structural tuning of PNI is even greater than

indigo. Without doing structural change, utilization of PNI as ligand is a good option to explore the chemistry of PNI. Derivatizations at the chromophore, either at the alcohol or at the amine, and at the naphthyl rings are also appealing.

The presence of four different functional groups in PNI makes it an interesting case for metal complexation. It can be utilized either as a bidentate or a bis(bidentate) ligand. Depending upon the nature of combination of the bidentate part, many isomers are possible. The molecule can serve as neutral bidentate ligand via coordination of imine and carbonyl, mono anionic via a combination of secondary amine and imine. Coordination through alcohol and imine is also reasonable. All the probabilities have been summarized in Figure 1.

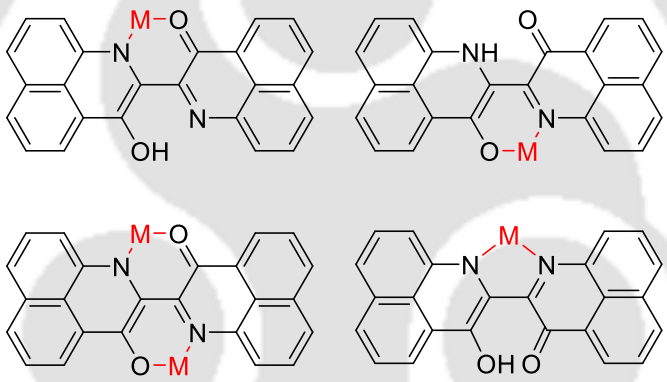

Figure 1. Available co-ordination sites of PNI.

The chromophoric unit of PNI contains two acidic protons, associated with the alcohol and the secondary amine group. Using accessible modes of substitution these protons can be replaced by numerous alkyl, aryl and/or acyl fragments. This type of substitution can give access to a variety of mono- and di-substituted PNIs (Figure 2a). Another class of PNI-derivatives can be prepared by modifications at the naphthyl rings. Various electron rich as well as electron deficient functional groups can be installed in the naphthyl rings on the basis of electronic and steric factor of individual position. Depending upon the position, number

and nature of substituent involved a diverse collection of compounds can be prepared (Figure 2b).

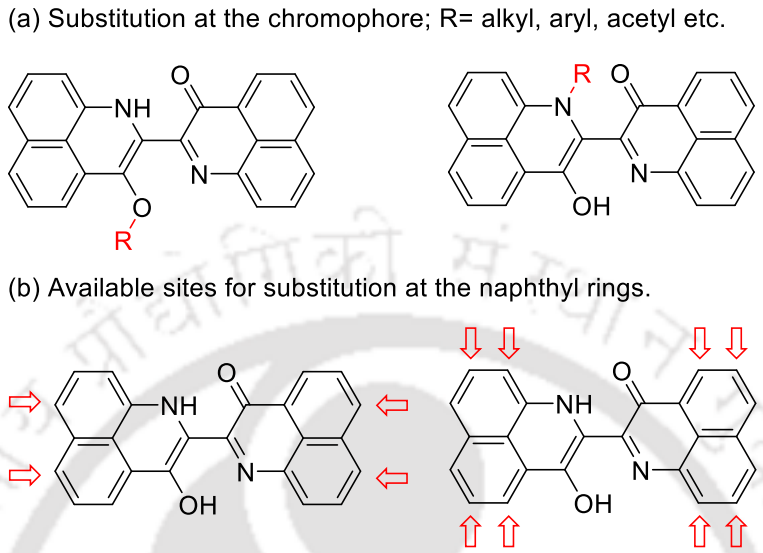

Figure 2. Different modes of substitutions possible at PNI.

5.1.1 Objectives

On account of these possibilities, attempts were made to synthesize a ring substituted PNI, a chromophore-substituted PNI, and a PNI-Pd(II) complex. This chapter is a brief discussion of these synthetic attempts and their respective outcomes. First, a Pd(II) complex was prepared by reacting PNI with the Pd(II)-precursor bis(acetonitrile)dichloropalladium(II). The synthesized complex was characterized using a combination of analytical techniques viz. HRMS, NMR etc. To comprehend the effect of metallation, photophysical properties were investigated. Various efforts were done to introduce substitution at the chromophore. Instead of the desired product, attempted reaction conditions lead to decomposition of PNI into an N-substituted lactam. Introduction of bromo-substitution at the naphthyl rings was accomplished to get dibromoPNI. This structural modification led to a new dye with lower energy absorption maxima than PNI. Similar to the parent dye, this red emissive derivative was also found to be halochromic in acidic condition.

5.2 Metal coordination

5.2.1 Synthesis and characterization

Applicability of PNI as ligand was tested by checking its coordination behavior. As an initiative palladium was used as metal. To prepare a Pd (II)-complex of the dye, PNI was treated with the metal precursor *bis*(acetonitrile)dichloropalladium(II).[10] Upon treatment with 0.5 equivalents of the metal precursor under atmospheric condition, the turquoise color solution of PNI in DCM turned into a green solution which eventually precipitate as green-solid (Scheme 1). The observation remained the same in THF. Reactions at different temperature, from room temperature to refluxing condition, did not produce unlike product(s). The precipitate obtained was filtered off, washed with *n*-hexane and cold DCM and dried under vacuum to get the PNI-Pd complex.

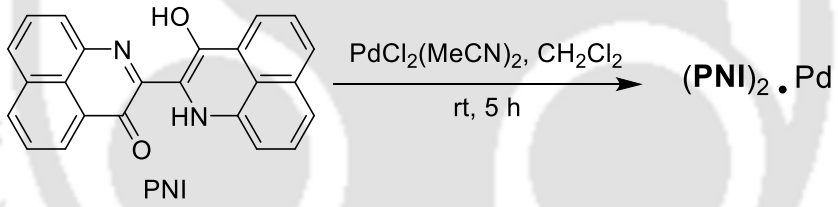

Scheme 1. Synthetic scheme for PNI-Pd complex.

The complex was first analyzed using mass spectrometry. HRMS data (Figure 3) of the green solid suggested the formation of a 2:1 (PNI:Pd) complex. Mass spectrum showed a peak at m/z = 872.0907, which can be assigned to the (**PNI**)$_2$Pd in which two protons are replaced by sodium.

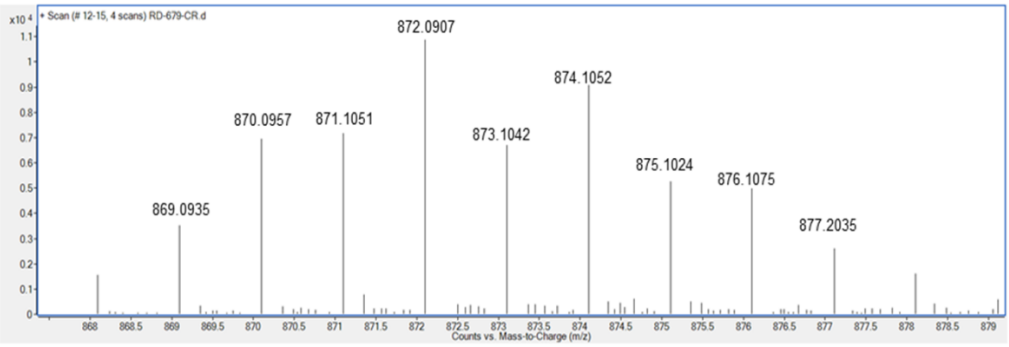

Figure 3. HRMS data of PNI:Pd complex.

After getting initial idea about the nature of palladium complex of PNI, further analysis was done using ^{1}H-NMR spectroscopy. The complex is less soluble than the ligand in chloroform. However, the solubility is sufficient for ^{1}H-NMR characterization of the complex. The proton-resonance spectra (Figure 4-top) of (**PNI**)$_2$Pd showed 12-types of magnetically isolated aromatic protons along with a sharp singlet corresponding to NH proton. Single set of protons confirmed the presence of only one complex and excluded any possibility of multiple isomers for (**PNI**)$_2$Pd. Compared to the ligand PNI, the proton signals of the complex experienced downfield shift. The least shielded proton in PNI appears at 8.62 ppm, while in the complex the same shifted to 10.21 ppm. The free N-H protons experienced a downfield shift of 1.82 ppm (7.21 ppm in PNI vs. 9.03 ppm in (**PNI**)$_2$Pd).

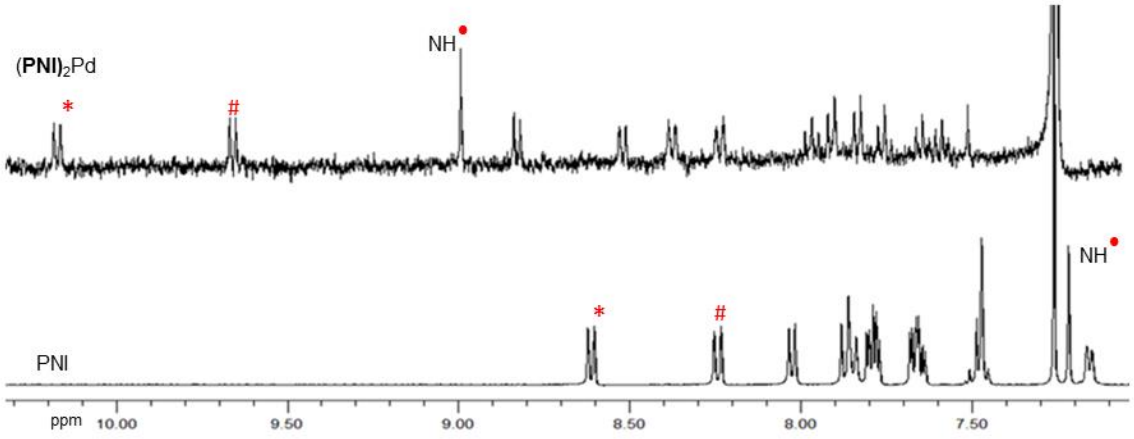

Figure 4. ^{1}H-NMR spectra (400 MHz, 298 K) of PNI (bottom) and its palladium complex (top) in $CDCl_3$.

Such drastic changes in proton resonances are not due to simple coordination. There is probably some structural change happened after the complex formation. Solid state structure could explain the phenomenon. However, all efforts to grow single crystal suitable for X-ray diffraction were turned out to be unsuccessful. Solubility of (**PNI**)$_2$Pd is not sufficient for its characterization using ^{13}C-NMR spectroscopy. The effect of metallation was also investigated using infrared spectroscopy. IR spectrum of the complex (Figure 5) was recorded in a KBr pellete and comparison was done with that of PNI. The bonding character in the metal complexes can be deduced by looking into change in the position of peaks, appearance of new peaks, splitting of peaks into multiplates and change in relative intensities. The effect of coordination was observed as a decrease in intensity of the peaks around 3600 cm^{-1}, which is associated generation of anion via loss of acidic proton.[11] In principle it may either be N-H or the hydroxy proton. Since the ^{1}H NMR suggested the presence of N-H group, the decrease intensity at 3600 cm^{-1} must be associated with loss of hydroxyl proton. Additionally, significant changes in terms of intensity, position and appearance of new peaks were observed in the range 1000-1600 cm^{-1}. In the free ligand the absorption bands in this region are attributed to multiple connectivities including C=O, C=N, C-O, C-N, C=C.

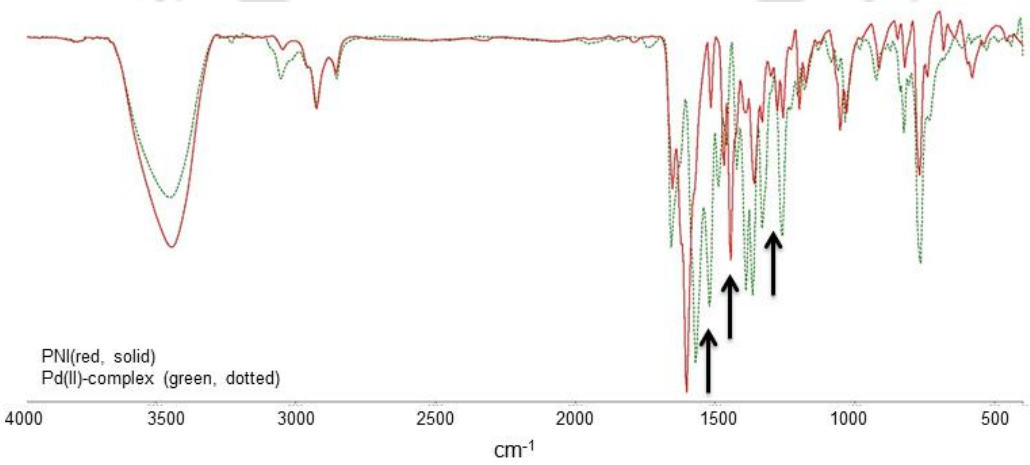

Figure 5. IR(KBr) spectra of PNI (solid, red) and 2PNI:1Pd complex (dotted, green) dye.

In principle, several isomers are possible for the (**PNI**)$_2$Pd complex. However, some of them can be ruled out from the observation noticed in various analytical techniques. Presence of a sharp singlet for N-H proton in the ^{1}H-NMR of (**PNI**)$_2$Pd, ruled out its involvement in the coordination. Decrease in IR peak intensity at around 3600 cm^{-1} suggested the loss of hydroxy proton, i.e. generation of anion for coordination. Mass analysis suggested that PNI acts as mono-anionic bidentate ligand. After ruling out the possibilities from various analytic techniques, the only remaining isomers are possible via N,O$^-$-coordination and shown in Figure 6 as Pd1 and Pd2. To justify the conclusions from analytical measurements, theoretical calculation was done for (**PNI**)$_2$Pd. In absence of a solid state structure and with possibility of multiple isomers, theoretical investigation was indeed needed to find the exact connectivity of PNI with palladium. Besides **Pd1** and **Pd2**, two more isomers were considered with mono-anionic bidentate nature of the ligand. The single point energy calculation in vacuo was performed with M06 DFT functional using a 6-31G(d) atomic basis set in Gaussian 09.[12] From the energy minimized structure, the isomer **Pd2** (Figure 6) was found to be of lowest energy. As expected, **Pd3** and **Pd4** were found to be energetically unfavorable. According to calculations the complex has a square planar geometry with *cis*-conformation through the hydroxyl and tertiary amine of the chromophore core.

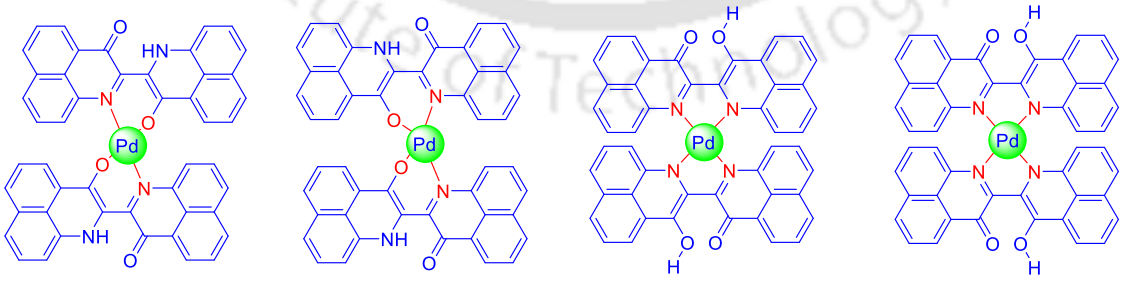

Figure 6. Possible structures for PNI:Pd (2:1) complex.

The Pd-O and Pd-N bond lengths are calculated to be 2.0497 Å and 2.0461 Å respectively with bond angles of 84.83° for O-Pd-N connectivity, 98.91° for N-Pd-N connectivity and 91.46° for O-Pd-O connectivity. Another notable change in the cis isomer was loss of planarity of PNI. Significant twisting occurred around the central single-bond. However, the distortion causes co-facial π-π stacking between naphthalene rings of two different PNI molecules. Such arrangement gives extra stability to **Pd2** over **Pd1**. The theoretical calculation also explains the huge downfield shift of the proton signals in the NMR spectrum. DFT calculation also explains the observation in infrared spectroscopy. It is suggested that when a metal ion combines with a ligand to form a co-ordination complex, its vibrational spectra is also expected to change. The change in the vibration can be related to molecular symmetry or with the change in the individual frequency. As seen in the energy optimized structure, PNI attains distortion from planarity in the complex. And the overall change in geometry as well as electron density has an effect on the absorption patterns for all the connectivity especially in the chromophoric core. These changes were evident in the IR-spectrum of the complex. So, changes in the range of 100-1600 cm^{-1} can be attributed to effect of change in overall charge distribution and orientation in the chromophoric part of the ligand. The IR spectrum of the complex also supports the fact that the basic structure of PNI was intact as seen from all the signature peaks. Therefore, based on theoretical investigation along with ^{1}H-NMR spectroscopy suggested **Pd2** was obtained from reacting PNI with bis(acetonitrile)dichloropalladium(II) (Figure 7).

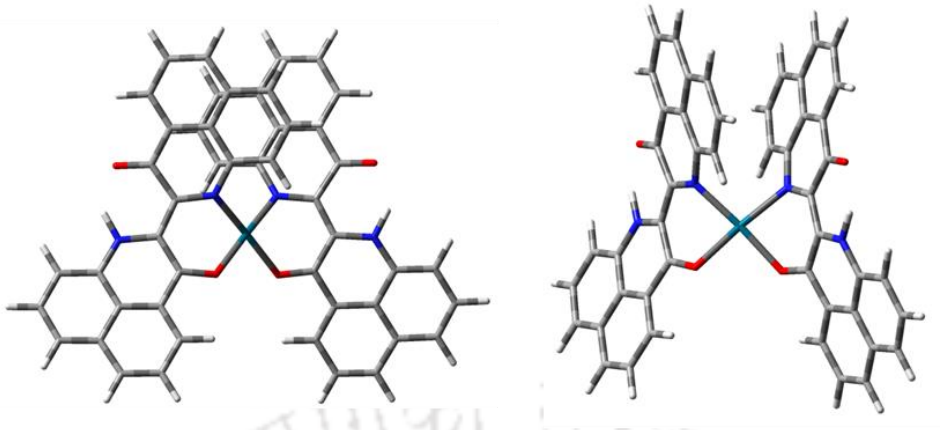

Figure 7. Energy optimized structure for **Pd2**.

5.2.2 Photophysical properties of $(PNI)_2Pd$

Coordination with metal caused substantial change in the structural part of PNI, which was evidenced from experimental and theoretical investigations. The appearance of the complex is also distinguished from the ligand. The palladium-complex $(\mathbf{PNI})_2Pd$ is green in chloroform, while PNI is turquoise in color. To check the effect of co-ordination on its photophysical behavior, UV-vis absorption spectra of the complex was recorded in chloroform. PNI exhibits its signature absorption maxima at 410 and 632 nm

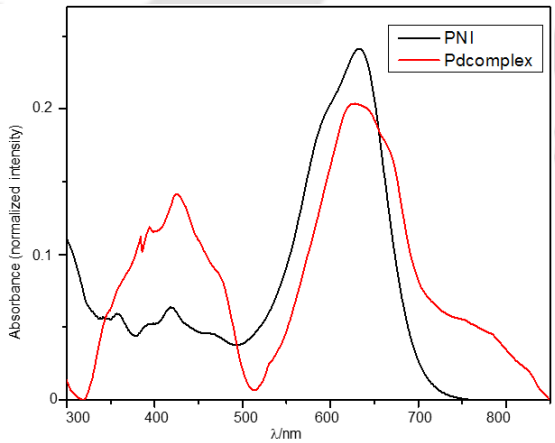

Figure 8. Normalized absorption spectra of PNI (black) and PNI:Pd (2:1) complex (red).

However, the intensity at lower energy decreased and the opposite phenomenon was observed at higher energy maxima. Additional signature was noticed in terms of shoulder in

the region of 700-800 nm. The absorption spectrum of the complex (Figure 8) showed significant broadening compare to the free PNI. Broadening of peak was due to the loss of rigidity of the structure, while other changes in the absorption pattern arise because of change in electronic distribution combined with charge transfer processes in the molecule. Metallation also resulted into fluorescence quenching for the ligand.

5.3 Substitution at the chromophore

Substitution at the chromophore is an interesting case of investigation. Depending on the nature of substitution, N-substituted (**1**) or O-substituted (**2**) product may produce. As a starting point for substitution at the chromophore, various alkyl groups were targeted to incorporate. To realize such PNI-derivatives, a THF solution of the dye was treated with methyl iodide in presence of K_2CO_3. The reaction was continued at room temperature for 1 h and monitored with thin-layer chromatography. But, the reaction was found to be unsuccessful. Modifications were attempted by changing the base, solvent, and reaction condition as well as reaction atmosphere (Scheme 2).

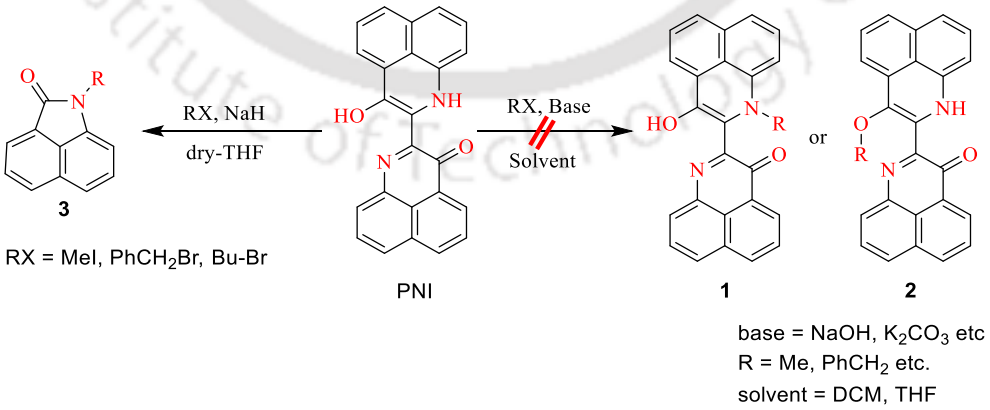

Scheme 2. Synthetic route towards core-substituted PNI.

While in most of the cases the reactant PNI was found to be intact, utilization of strong base NaH in dry THF was found to be different as there occurred consumption of PNI within 3 h. The color of the reaction mixture changed from turquoise to red. After exposing the reactants to the specific condition for overnight, the crude mixture was isolated and separated using column chromatography. The isolated compound was characterized using mass spectrometry and ^{1}H-NMR spectroscopy. HRMS data showed an intense peak at m/z = 184.0759, which neither match with mono methylated nor with dimethylated derivative of PNI. Critical analysis of the data revealed that the detected mass value is corresponding to protonated n-methylated lactam **3**. Further structural proof for **3** was obtained from a combination of ^{1}H and ^{13}C NMR measurements.

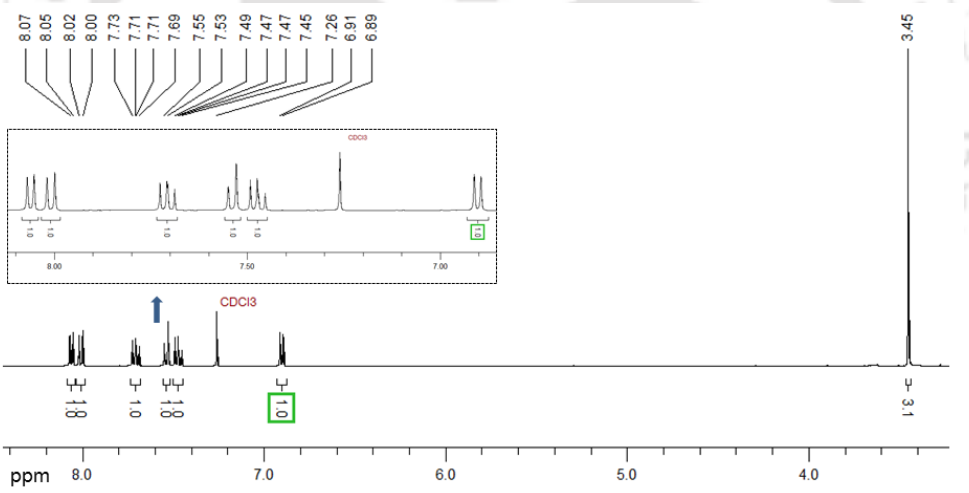

Figure 9. ^{1}H-NMR spectrum of compound **3** isolated from reaction scheme 3.

The proton resonance of the compound (Figure 9) showed six different aromatic protons along with a signal for methyl protons. ^{13}C NMR spectrum showed the presence of twelve magnetically isolated carbons in the compound. Most notable one was observed at 168.2 ppm, which is associated with the carbonyl. The structure **3** was unambiguously established from X-ray analysis. Based on these observations, it was clear that instead of the targeted compounds **1** and/or **2**, under the specified reaction condition, PNI underwent dissociation to

form N-methyllactam (**3**) (Scheme 2). Similar observations were noticed in case of butyl bromide and benzyl bromide.

Dissociation of indigoid compounds under various conditions is a common phenomenon. For instance, indigo undergoes oxidative dissociation in DCM to form isatin, anthranilic acid, tryptanthrin etc.[13] The decomposition pathway of PNI to lactam can be compared with the generation of anthranilic acid from indigo. Similar to the phenyl analogue, PNI produced an amine and carboxylic acid groups which subsequently cyclized to produce lactam under the reaction condition (Scheme 3). The observation is thus not unusual. As the attempted reaction procedures were unsuccessful to generate the desired derivatives of PNI, these targets would provide a fascinating synthetic challenge for further expansion of PNI-chemistry.

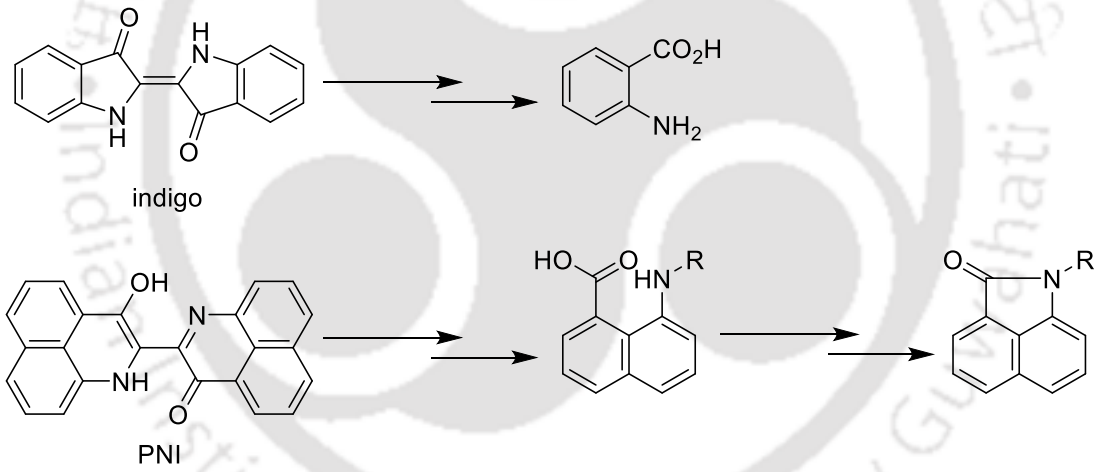

Scheme 3. Analogy between decomposition pathways of indigo and PNI

5.4 Substitution at the naphthyl rings

5.4.1 Synthesis and characterization of dibromo-PNI

The absence of symmetry in the PNI molecule due to four different functional groups in the chromophore generates different electronic scenarios in the two naphthyl rings. This differences in the naphthyl rings may lead to a complicated mixture of multiple compounds, if aromatic substation is attempted with PNI itself. Therefore, to prepare dibromoPNI (**7**) Scheme 4 was adopted as the synthetic route.

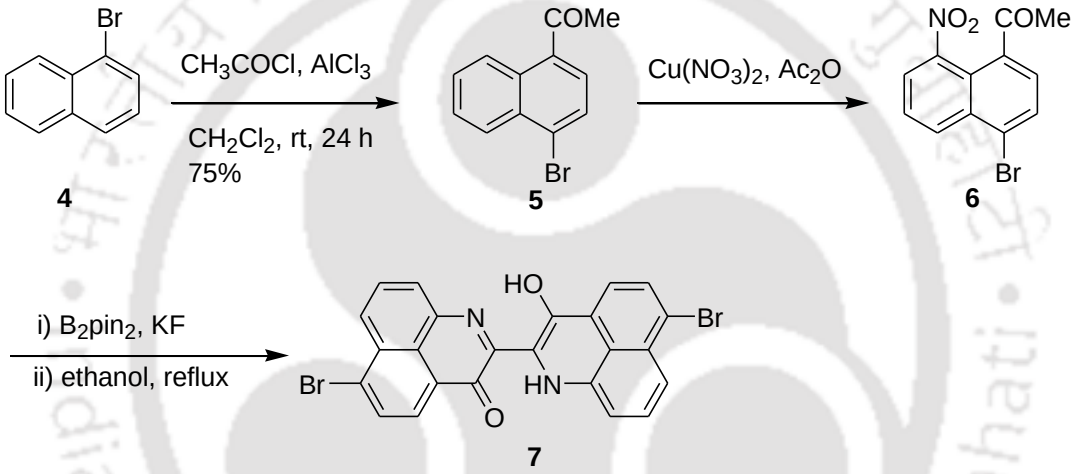

Scheme 4. Synthesis route for dibromoPNI.

To prepare the desired compound, precursor 4-bromo-8-nitro-1-acetylnaphthalene (**6**) was prepared from 1-bromonaphthalene in two steps. Following a reported procedure, compound **4** was reacted with acetyl chloride in presence of aluminium chloride. The resultant mixture of acylated products was purified using column chromatography to obtain the desired product **5** in 75% yield.[14] Nitration of **5** in presence of $Cu(NO_3)_2/Ac_2O$ in dichloromethane furnished a mixture of 5-nitro and 8-nitro derivatives. Chromatographic separation produced the required 8-nitro derivative **6** in 45% yield. [15]

The precursor **6** was then treated with *bis*-(pinacolato)diboron and KF in ethanol under aerobic condition. After continuing the reaction for 16 h, the crude mixture was isolated and

purified by column chromatography. The resulted dark turquoise solid was less soluble in common organic solvents compared to PNI. This limited scope for identification of the compound using solution state NMR spectroscopy. But, high resolution mass spectrometry (HRMS) of the compound from a very dilute acetonitrile solution using electrospray ionazation (ESI) method showed a peak at m/z = 504.9372 (Figure 10). This peak was associated with the dehydroxy-form of the dye ([M-OH] + H^+). Experimental and simulated isotropic distribution also matched with the assigned compound. This established a successful synthetic for dibromoPNI **7**.

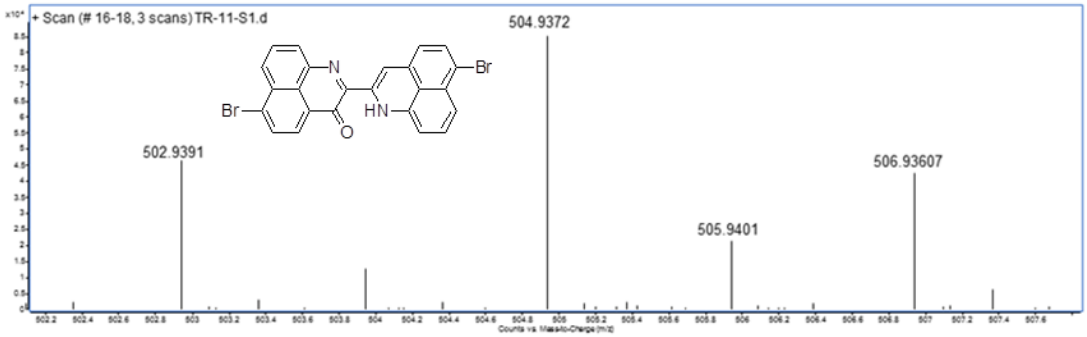

Figure 10. HRMS data of dibromoPNI.

5.4.2 Photophysical Properties

UV/vis absorption and emission behavior of dibromoPNI were recorded in chloroform and compared with that of the parent dye (Figure 11). In chloroform, dibromoPNI demonstrates very strong (ε = 42194 $M^{-1}cm^{-1}$) absorption with maxima at 642 nm. As expected, substitution at the napthyl rings imparts changes in electronic distribution and the effect is visible in its photophysical behaviors. Compared to PNI (632 nm, $CHCl_3$), the dihalo-derivative shows a red shifted absorption maxima by 10 nm. A similar behavior was observed in the steady state emission spectra. In chloroform, the halo-substituted PNI exhibits a low intensity emission band with maxima at 753 nm. The stoke shift of the dye was calculated to

be 2295 cm^{-1}. The Full width at half maxima of the absorption spectrum was calculated to be 2755 cm^{-1}.

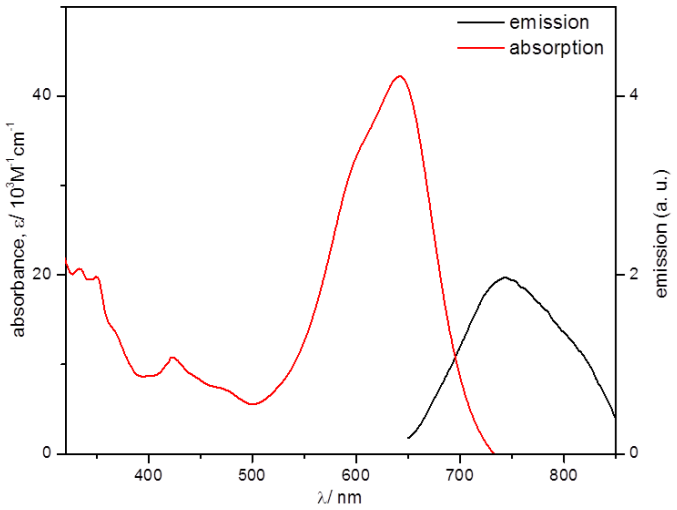

Figure 11. UV-vis absorption and emission spectra of dibromoPNI (THF, 293 K).

5.4.3 Halochromism

The dibromo-derivative of PNI showed similar halochromic behavior under acidic pH. To study the halochromic behavior of the dye, 2.7 mL ($c \approx 1 \times 10^{-5}$ $molL^{-1}$) of dibromo-PNI solution (in chloroform) was loaded into a cuvette (1 cm path length) and titrated with acid (CF_3CO_2H) and changes were monitored using UV-vis spectroscopy. Upon addition of organic acid to a solution of compound **7** in chloroform, the absorption maxima experienced a bathochromic shift of 17 nm (643 nm in **7** vs 660 nm in protonated **7**) with increased molar absorptivity (ε = 82392 $M^{-1}cm^{-1}$). Similar to the PNI, the spectrum become vibronically resolved (Figure 12) after protonation. The acidification also led to quenching of emission. The halochromism process was found to be reversible as in the case of PNI.

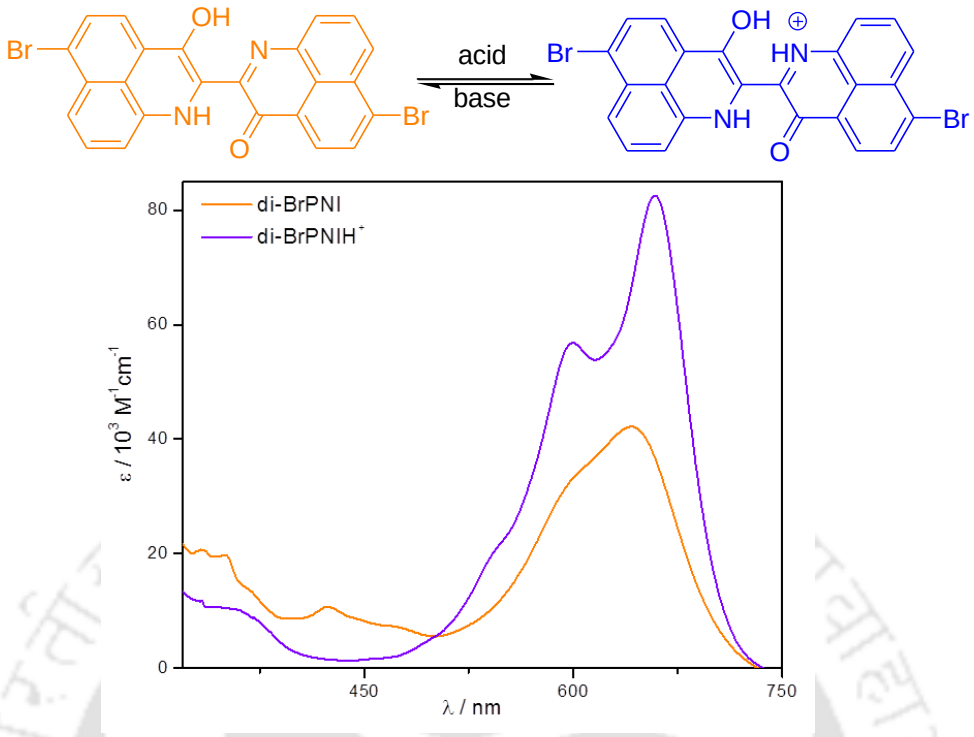

Figure 12. Top: halochromism of dibromoPNI; bottom: absorption spectra of dibromoPNI (orange) and dibromoPNIH$^+$ (blue) in THF (293 K).

5.5 Conclusion

In summary, PNI was found to be a strong bidentate ligand and produced 2:1 (PNI:Pd) complex. The coordination compound was characterized using mass spectrometry and ^{1}H-NMR spectroscopy. Though four different isomeric-complexes are possible, one isomer was exclusively produced in the reaction. Theoretical investigation along with ^{1}H-NMR spectroscopy suggested **Pd2** to be the most stable structure. Compared to PNI, the complex shows red shifted and broadened absorption behavior. The emission property of PNI was found to be quenched completely upon metal-coordination. Alkylation of PNI was attempted with various alkyl halides. Most of the reactions were found to be unfruitful. Instead of the desired N-alkylated and/or O-alkylated product(s), decomposition of PNI was observed when NaH was used as base. Characterization of the dissociation product confirmed formation of

N-substituted lactam. Such kind of dissociation is common in indigoids under various conditions. Effect of substitution in the naphthalene rings was explored by targeting synthesis of dibromo-PNI. Bromo substitution at the naphthyl rings further decreased the compound solubility and limited its characterization by NMR spectroscopy. However, its structure was established by HRMS and IR spectroscopy. Compared to PNI, the substituted dye exhibited red shifted absorption maxima (642 nm) in chloroform. The substituted dye was also found to be halochromic. Spectral patterns are similar to the parent PNI molecule. Bromo substituted PNI exhibited photoluminescence in the NIR region with maxima at 753 nm (chloroform).

5.6 References

1. (a) T. M. Ivanova, G. M. Ostapchuk, L. B. Shagalov, V. N. Berdyugin, *Chem. Heterocycl. Compd.* **1981**, *17*, 360-363; (b) J. R. Bailey, J. Travis, *Dyes Pigments* **1985**, *6*, 135-154; (c) J. H. Porada, D. Blunk, *J. Mater. Chem.* **2010**, *20*, 2956–2958; (d) C.-Y. Huang, A. Bonasera, L. Hristov, Y. Garmshausen, B. M. Schmidt, *J. Am. Chem. Soc.* **2017**, *139*, 15205-15211.
2. (a) J. Abe, Y. Nagasawa, H. Takahashi, *J. Chem. Phys.* **1989**, *91*, 3431-3434; (b) H. Bauer, K. Kowski, H. Kuhn, W. Liittke, Paul Rademacher, *J. Mol. Struct.* **1998**, *445*, 277-286; (c) Y. Matsumoto, H. Tanaka, *Heterocycles* **2003**, *60*, 1805-1810; (d) C. Yang, Q. T. Trinh, X. Wang, Y. Tang, K, Wang, S. Huang, X. Chen, S. H. Mushrif, M. Wang, *Chem. Commun.* **2015**, *51*, 3375-3378.
3. (a) J. -Y. Wu, C. -H. Chang, P. Thanasekaran, C. -C. Tsai, T. -W. Tseng, G. -H. Lee, S. -M. Peng, K. -L. Lu, *Dalton Trans.* **2008**, 6110-6112; (b) G. Nawn, K. M. Waldie, S. R. Oakley, B. D. Peters, D. Mandel, B. O. Patrick, R. McDonald, R. G. Hicks, *Inorg. Chem.* **2011**, *50*, 9826-9837; (c) G. Nawn, S. R. Oakley, M. B. Majewski, R. McDonald, B. O. Patrick, R. G. Hicks, *Chem. Sci.* **2013**, *4*, 612-621; (d) M. Chatterjee, P. Ghosh, K. Beyer, A. Paretzki, J. Fiedler, W. Kaim, G. K. Lahiri, *Chem. Asian J.* **2018**, *13*, 118-125.
4. (a) K. Fries, G. Fink, *Ber. Dcsch. Ges.* **1908**, *41*, 4271-4284; (b) G. M. Wyman, B. M. Zarnegar, J. Phys. Chem., 1977, 77, 831-837; (c) K. Hoffmann, P. Mayera, H. Dube, *Org. Biomol. Chem.* **2019**, *17*, 1979-1983.

5. M. Watanabe, N. Uemura, S. Ida, H. Hagiwara, K. Goto, T. Ishihara, *Tetrahedron* **2016**, *72*, 4280-4287.
6. E. D. Głowacki, G. Voss, K. Demirak, M. Havlicek, N. Sünger, A. C. Okur, U. Monkowius, J. Gąsiorowski, L. Leonat, N. S. Sariciftci, *Chem. Commun.* **2013**, *49*, 6063-6065.
7. I. V. Klimovich, L. I. Leshanskaya, S. I. Troyanov, D. V. Anokhin, D. V. Novikov, A. A. Piryazev, D. A. Ivanov, N. N. Dremova, P. A. Troshin, *J. Mater. Chem. C* **2014**, *2*, 7621-7622.
8. (a) P. Venkatachalam, N. G. Joby, N. Krishnakumar, *Sol-Gel. Sci. Techno.* **2013**, *67*, 618-628; (b) B. He, A. B. Pun, D. Zherebetskyy, Y. Liu, F. Liu, L. M. Klivansky, A. M. Mcgough, B. A. Zhang, K. Lo, T. P. Russell, L. Wang, Y. Liu, *J. Am. Chem. Soc.* **2014**, *136*, 15093-15101; (c) C. Guo, J. Quinn, B. Sun, Y. Li, *J. Mater. Chem. C* **2015**, *3*, 5226-5232; (d) J. Zhu, T. Li, K. Shi, J. Wang, Y. Lin, G. Yu, X. Zhan, *J. Polym. Sci. A* **2018**, *56*, 213-220.
9. (a) Y. Matsumoto, H. Tananka, *Heterocycles* **2003**, *60*, 1805-1810; (b) C. Y. Huang, A. Bonasera, L. Hristov, Y. Garmshausen, B. M. Schmidt, D. Jacquemin, S. Hecht, *J. Am. Chem. Soc*. **2017**, *139*, 15205−15211 ; (c) C. Petermayer, H. Dube, *Acc. Chem. Res.* **2018**, *51*, 1153-1163.
10 K. Tsutsumi, K. Itagaki, K. Nomura, *ACS Omega* **2017**, *2*, 3886-3900.
11. (a) W. Beck, C. Schmidt, R. Wienold, M. Steimunn, B. Wagner, *Angew. Chem. Int. Ed.* **1989**, *28*, 1529-1531; (b) J. Coates, *Interpretation of Infrared Spectra, a Practical Approach, R.A. Meyers (Ed.), Encyclopedia of Analytical Chemistry, John Wiley & Sons Ltd, Chichester* **2000**, 10815-10837.
12. M. J. Frisch, G. W. Trucks, H. B. Schlegel, G. E. Scuseria, M. A. Robb, J. R. Cheeseman, G. Scalmani, V. Barone, B. Mennucci, G. A. Petersson, H. Nakatsuji, M. Caricato, X. Li, H. P. Hratchian, A. F. Izmaylov, J. Bloino, G. Zheng, J. L. Sonnenberg, M. Hada, M. Ehara, K. Toyota, R. Fukuda, J. Hasegawa, M. Ishida, T. Nakajima, Y. Honda, O. Kitao, H. Nakai, T. Vreven, J. A. Montgomery, Jr., J. E. Peralta, F. Ogliaro, M. Bearpark, J. J. Heyd, E. Brothers, K. N. Kudin, V. N. Staroverov, T. Keith, R. Kobayashi, J. Normand, K. Raghavachari, A. Rendell, J. C. Burant, S. S. Iyengar, J. Tomasi, M. Cossi, N. Rega, J. M. Millam, M. Klene, J. E. Knox, J. B. Cross, V. Bakken, C. Adamo, J. Jaramillo, R. Gomperts, R. E. Stratmann, O. Yazyev, A. J. Austin, R. Cammi, C. Pomelli, J. W. Ochterski, R. L. Martin, K. Morokuma, V. G. Zakrzewski, G. A. Voth, P. Salvador, J. J. Dannenberg, S. Dapprich, A. D. Daniels, O. Farkas, J. B. Foresman, J. V. Ortiz, J. Cioslowski, D. J. Fox, *Gaussian 09, Revision D.01, Gaussian Inc. Wallingford CT,* **2013**.
13. P. Novotná, J. J. Boon, J van der Horst, V. Pacáková, *Color. Technol*. **2003**, *119*, 121-127.
14. E. Dixon, A. Fischer, F. P. Robinson, *Can. J. Chem.* **1981**, *59*, 2629-2641.
15. S. D. Barker, K. Wilson, R. K. Norris, *Aus. J. Chem.* **1995**, *48*, 1969-1979.

Chapter 6

Conclusion and Future Prospective

6.1 Conclusion

In summary, PNI was successfully synthesized and characterized for the first time. Change in surrounding of chromophore marks huge difference in property as well as in synthetic difficulty. The common synthetic methods known for indigo did not work for PNI. On the other hand, indigo cannot be prepared by the method describes for PNI. Unlike indigo, PNI exists in mono-enol form and has better solubility in common organic solvents. PNI has stronger and wider absorption than indigo. Due to distinct structural features, PNI shows halochromism upon protonation. The process is marked by bathochromically shifted maxima (by 66 nm) with increase in colour intensity. The dye produced cuboid architecture via self-assembly process in THF/n-hexane (1:9 v/v). A combination of intermolecular H-bonding and π-π stacking caused such aggregation. Due to the restriction in intramolecular motion, emission intensity was enhanced by 500% in the aggregate. PNI formed co-aggregate with H-NMI, NH_2-NMI and Ph-NMI. In the co-assembly of NH_2-NMI and PNI, successful merger of AIEE and social self-sorting was observed. Pd-complex of PNI was prepared and characterized. Structural optimization was done using DFT calculation. After metallation, the absorption maxima shifted to the longer wavelength. Structural modification at the chromophore of PNI was attempted in vain. However, substitution at the naphthalene ring was found to be successful. Bromination causes decreased solubility and red shifted absorption maxima. Similar to PNI, brominated PNI is also halochromic in nature.

6.2 Future prospective

The dyeing potential of PNI will be explored. Because of narrow HOMO-LUMO gap, the dye could be used as material for organic electronics. The concept of amalgamation of AIEE

and social self-sorting can be used in opto-electronic device like OLED. This model can be useful for efficient energy harvesting due to greater coverage of the solar spectrum via multi-component assembly and energy funneling. The coordination behaviour of the dye will be extended to other metals. Brominated PNI will be explored as precursor for polymerization. Installation of different functional group at the naphthalene rings would also present a promising research topic.

Chapter 7

Experimental Section

7.1 General information

7.1.1 Instrumentation and methods

IR-spectroscopy

Infra-red (IR) spectra were collected as a film on KBr pellets using Perkin-Elmer FT-IR spectrometer and frequencies are presented in reciprocal centimetre (cm^{-1}).

Mass-spectroscopy

High resolution mass spectrometry (HRMS) measurements were done with Agilent QTOF 6520 mass spectrometer using electrospray ionization (ESI) mode. Isotopic distributions of the mass were calculated using Agilent Mass Hunter Data analysis (version 8.0.8208.0) software.

^{1}H- and ^{13}C-NMR spectroscopy

^{1}H and ^{13}C NMR and ^{1}H-^{1}H COSY NMR spectra were recorded using either Bruker AscenedTM 400 MHz NMR spectrometer or Bruker Avance III 600 MHz NMR spectrometer using the deuterated solvent as the lock and residual solvent as the internal reference. The chemical shifts were reported in δ (ppm) relative to the residual protonated solvent peak of the deuterated solvent ($CDCl_3$: δ_H = 7.26 ppm, δ_C = 77.0 ppm; CD_3CN: δ_H = 1.94 ppm, δ_C = 1.24 ppm; DMSO-*d*$_6$ δ_H =2.50 ppm, δ_C = 39.4 ppm; Benzene-*d*$_6$: δ_H = 7.15 ppm). NMR measurements were carried out at 295 K. The following abbreviations were utilized to describe peak patterns: s = singlet, d = doublet, t = triplet, q = quartet, dd = doublet of doublet, dt = doublet of triplet, ddd = doublet of doublet of doublet, m = multiplet, and br = broad. The numbering of the carbon atoms of the molecular formulas shown in the Experimental Section is only used for the assignments of the NMR signal and is not in accordance with the IUPAC nomenclature rules.

UV/Vis spectroscopy

The UV-Vis absorption spectra were recorded on Perkin-Elmer Lmabda-25 and Lambda-35 UV spectrophotometers at 293 K. Depending upon concentrations, samples were loaded either in 1 mm or in 10 mm path length quartz UV-cuvette.

Photoluminescence spectroscopy

Photoluminescence (PL) spectra were recorded on a Horiba Fluoromax-4 spectrofluorometer. A 10 mm × 10 mm quartz cuvette was used for the solution spectra at 293 K. The spectra were corrected using the correction factor implemented in the software.

Refractive index measurement

Refractive index values of solvents (THF, *n*-hexane and mixtures of THF/*n*-hexane) required for calculation of relative quantum yield was recorded on Anton-paar Abbemat 3100 Compact Refractometer at 293 K.

Time resolved fluorescence spectroscopy

The time-resolved fluorescence was recorded in a time-correlated single photon counting (TCSPC) setup (Horiba Instruments) using a picosecond laser diode (Horiba Instruments) of 405 nm excitation wavelength. FWHM of the setup was typically ~90 ps. The fluorescence decays were fitted using DAS6 software (Horiba Instruments). The fluorescence transients were recorded by keeping the analyzer at the magic angle (55^{o}) with respect to the polarizer.

Microscopic imaging

Microscopic images were recorded either on FESEM Sigma 300 or FESEM Gemini 300 microscope. Samples were prepared by drop-cast method from the respective solvent system and followed by room temperature evaporation for 10-16 h.

Cyclic voltametry

The cyclic voltammetry (CV) measurements of PNI were performed in a standard three-electrode set-up (glassy carbon disk as working electrode (3.0 mm diameter), Pt wire as auxiliary electrode and Ag/AgCl as reference electrode) using PGSTATE101 potentiostate from Metrohm© and the corresponding software NOVA 1.11. The experiments were carried out on a 2.7 x 10^{-3} M solution of the dye in dry chloroform with 0.3 M *n*-Bu_4NClO_4 as supporting electrolyte under N_2 atmosphere. The potentials were calculated based on an internally added standard ferrocene ($E_{1/2}$ = +4.4 eV vs Ag/AgCl).

Photoluminescence quantum yield

Relative quantum yield (QY) of PNI was measured in deoxygenated and dry THF against using the following equation.[3]

$$\Phi^{i} = \frac{F^{i} f_{s} n_{i}^{2}}{F^{s} f_{i} n_{s}^{2}} \Phi^{s}$$

where Φ^{i} and Φ^{s} are the photoluminescence QY of the sample and that of the standard, respectively; F^{i} and F^{s} are the integrated intensities (areas) of sample and standard spectra, respectively ; fx is the absorption factor ($fx = 1 - 10^{-Ax}$, where A = absorbance); the refractive indices of the sample and reference solution are n_i and n_s, respectively. Indigo was used as reference ($\Phi^{s} = 0.0023$ in DMF).[4]

Calculation of emission enhancement in PNI self-assembly

The photoluminescence enhancement at various f_h were calculated by using the formula,

$$\mathbf{I/I_0 = \Phi_{fh}/\Phi_{THF}}.$$

Where, I = Photoluminescence intensity of PNI at various f_h.

I_0 = Photoluminescence intensity of PNI in THF.

Φ_{fh} = Relative photoluminescence quantum yield at various f_h.

Φ_{THF} =Relative photoluminescence quantum yield of PNI in THF.

Calculation of emission enhancement for PNI in PNI/NMI co-aggregate

Emission enhancement was then calculated using the following formulae,

$$\mathbf{I/I_0 = (F^{fh}/F^{THF})(\eta_{fh}^{2}/\eta_{THF}^{2})}$$

Where F^{fh} = Integrated area of emission spectra of PNI in heteromeric aggregate.

F^{THF} = Integrated area of emission spectra of PNI in THF.

η_{fh} and η_{THF}= refractive indices of the respective solvents.

Calculation of emission enhancement for NH_2-NMI in PNI/NH_2-NMI co-aggregate

The Photoluminescence enhancement was calculated using the formulae,

$$\mathbf{I/I_0 = (F_{co\text{-}aggregate}/F_{monomer}).}$$

Where, $F_{co\text{-}aggregate}$ = Integrated area of emission spectra for NH_2-NMI in co-aggregate.

$F_{monomer}$ = Integrated area of emission spectra for monomeric NH_2-NMI.

For comparison, photoluminescence spectra obtained were divided by appropriate factors to keep NH_2-NMI concentration same in all co-aggregate solutions.

7.1.2 Materials, Chemicals and Reagents

Chemicals

The starting materials and reagents were purchased from commercial chemical suppliers (Acros, Merck, HiMedia, Aldrich, Fluka, Alfa Aesar, S. D. Fine-Chem Limited, Loba Chemie or Chempur) and were used without further purification. Deuterated solvents ($CDCl_3$: 99.8 atom % D; CD_3CN: 99.8 atom % D; acetone-d_6: 99.9 atom % D; DMSO-d_6: 99.9 atom % D; C_6D_6: 99.6 atom % D) and potassium bromide (FT-IR grade) were procured from Sigma Aldrich. HPLC and UV grade solvents were purchased from either Merck or Spectrochem. Silica gel for column chromatography (60-120 mesh) was procured from Spectrochem. Analytical thin layer chromatography (TLC) plate (silica gel 60 F254) was purchased from Merck.

Chromatography

Chromatographic purifications were performed on Silica gel 60 (60-230 mesh). Thin layer chromatography was carried out on Merck silica gel plates (60F-254) and visualized under 254 nm or 365 nm UV-light.

7.2 Synthesis

Synthesis of 8-nitro-1-naphthaldehyde (chapter 2, compound 3)

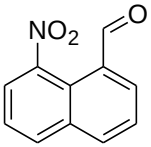

A homogenous slurry of KNO_3 (5.055g, 50 mmol) and 96% H_2SO_4 (2.033ml, 47.5 mmol) in 20 mL DCM was cooled in an ice-bath. To this in-situ nitrating mixture, a solution of 1-naphthaldehyde (1 ml, 7.36 mmol) in 20 ml DCM was slowly added followed by room temperature stirring for 4 hours. The reaction was quenched by adding 50 ml 10% aq. Na_2SO_4. Organic layer was separated and further washed with another 50 ml of 10% aq. Na_2SO_4 and 50 ml brine. The collected organic layer was then dried over anhydrous Na_2SO_4 and solvent was removed under reduced pressure to obtain the crude mixture. Purification was done by column chromatography using 15% DCM- Hexane as eluent with silica gel as the stationary phase.[1]

Yield: 0.540 mg (2.68 mmol, 36%).

HRMS (ESI) *m/z* [($C_{11}H_7NO_3$) + H^+] : calculated: 202.0504, experimental: 202.0509

^{1}H NMR (400 MHz, $CDCl_3$, δ ppm): 7.66 (t, *J* = 8.4 Hz, 1H), 7.76 (t, *J* = 8.4 Hz, 1H), 8.12-8.17 (m, 4H).

Synthesis of 8-iodo-1-naphthoic acid (chapter 2, compound 18)

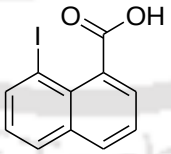

To a solution of 1,8-naphthalic anhydride (1.00 g, 5.04 mmol) in 30 ml 0.5 M aq. NaOH, 1 ml of glacial acetic acid was slowly added. To this, an aq. solution of HgOAc (1.600 g, 5.04 mmol) was added and the reaction mixture was refluxed for 30 min. another 2 ml of glacial acid acid was added followed by 24 h reflux for complete discharge of CO_2. The reaction was

1. P. Strazzolini, A. G. Giumanini, A. Runcio, *Tetrahedron Lett.* **2001**, *42*, 1387-1389.

cooled down with an ice bath, and the obtained ppt. was filtered out and washed with water. The obtained white ppt. was used for the next step.[2]

To a solution of 3.320 g (20.0 mmol) of potassium iodide in 25 mL of water, anhydro-8-(hydroxymercuri)-1-naphthoic acid (1.850 g, 5 mmol). After dissolution, 1.270 g (5 mmol) of iodine was added and the reaction mixture was heated at reflux for 15 h. The solution was cooled to ambient temperature and a brown precipitate was filtered out. To the filtrate was added 1.00 g (10 mmol) of sodium thiosulfate in 9 mL of H_2O to destroy excess iodine and the solution was acidified by the drop wise addition of conc. HCl. The crude acid was filtered out, dissolved in hot acetone and concentrated *in vacuum*. Recrystallization from $CHCl_3$ gave 8-iodo-1-naphthoic acid as a white solid.[3]

Yield: 0.80 g (52%)

^{1}H NMR (400 MHz, $CDCl_3$) δ ppm: 7.21 (t, *J* = 8.0 Hz, 1H), 7.52 (t, *J* = 8.0 Hz, 1H), 7.90-7.94 (m, 3H), 8.27(d, *J* = 8.0 Hz, 1H).

Synthesis of 1,8-Naphtholactam (chapter 2, compound 19)

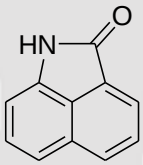

1.00 g (5.05 mmol) of 1,8-naphthalic anhydride, 0.350 g (5.05 mmol) of hydroxylamine hydrochloride and 7ml of 4-picoline were charged in the reactor and heated while stiffing. The reaction was conducted under reflux for 1 h, followed by cooling to 80 °C. Then 1.92 g (10.1 mmol) of *p*-toluenesulfonyl chloride was added to the reaction system. After addition, the temperature was raised and the reaction was carried out under reflux for 1 h, followed by cooling. The reaction mixture was poured into ice-water and stirred to precipitate crystals, which were collected by filtration. The crystals were transferred to a beaker and washed successively with 100 ml of a sodium hydrogencarbonate aqueous solution and 100 ml of water, followed by filtration. The whole amount of this intermediate, 25 ml of ethanol and 25

2. R. J. Bailey, P. J. Card, H. Shechter, *J. Am. Chem. Soc*. **1983**,*105*, 6096-6103.
3. J. L. Wiley, V. J. Smith, J. Chen, B. R. Martin, J. W. Huffman, *Bioorg. Med. Chem.* **2012**, *20*, 2067-2081.

ml of water were put in a reactor and stirred. Then 50 ml of a 3 M aqueous solution of sodium hydroxide was added drop wise to the mixture. Thereafter, the mixture was heated to refluxing temperature, at which the reaction was carried out for 3 h while distilling off ethanol. After completion of the reaction, the reaction mixture was cooled and acidified with of concentrated hydrochloric acid. The precipitated crystals were collected by filtration, washed with water, and dried to give the title compound.[4]

Yield: 630 mg (75 %).

HRMS (ESI) *m/z* [$((C_{11}H_7NO) + H^+]$: calculated: 170.1873, experimental: 170.0676

^{1}H NMR (**400 MHz, $CDCl_3$)** δ ppm: 6.98 (d, 1H), 7.71 (t, 1H), 7.57 (d, 1H), 7.75 (t, 1H), 8.06 (d, 1H), 8.09 (d, 1H), 2.17 (s, NH).

Synthesis of lactam ester (chapter 2, compound 21)

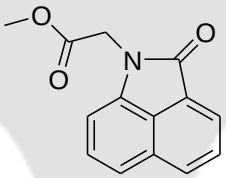

A DMF solution of 1,8-naphthholactam (450 mg, 2.65 mmol), methyl chloroacetate (339 mg, 3.12 mmol), potassium carbonate (717 mg, 5.18 mmol) and potassium iodide (5 mg) was heated at 130°C for 5 h. The reaction was quenched by adding into ice-water extracted with ethyl acetate (3 x 30 ml) three times. The organic layer was then washed with brine and DI water to remove the DMF. The combined organic layer was dried over anhydrous sodium sulfate and filtered. After evaporating the solvent, the residue was purified by column chromatography.[4]

Yield: 380 mg (60 %).

^{1}H NMR (400 MHz, $CDCl_3$) δ ppm: 3.74 (s, 3H), 4.67 (s, 2H), 6.81 (d, *J* = 8.0 Hz, 1H), 7.43 (dd, *J* = 8.0 Hz, 1H), 7.52 (d, *J* = 8.0 Hz, 1H), 7.69 (dd, *J* = 8.0 Hz, 1H), 8.00 (d, *J* = 8.0 Hz, 1H), 8.05 (d, *J* =8.0 Hz, 1H).

4. J. Nei, D. –D. Dong, Y. Zhang, T. –Y Wang, W. Liu, S. –Z. Yi, *Asian J. Chem.* **2014**, *26*, 7329-7336.

Synthesis of lactam acid (chapter 2, compound 22)

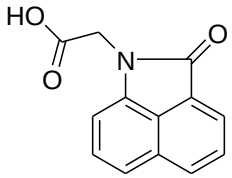

A solution of the lactam-ester (350 mg, 1.45 mmol) in 20 ml ethanol, added with 10 ml 5 M aq. NaOH was refluxed for 12 h. Ethanol was removed via distillation and the obtained aqueous part was acidified with conc. HCl. The yellow ppt. obtained was washed with water and dried under vacuum.

Yield: 280 mg (90 %)

HRMS (ESI) *m/z* [$((C_{13}H_9NO_3) + H^+]$: calculated: 228.0661, experimental: 228.0634

^{1}H NMR (**400 MHz, $CDCl_3$)** δ ppm: 8.22 (d, *J* = 8.0 Hz, 1H), 8.11 (d, *J* = 8.0 Hz, 1H), 7.81 (dd, *J* = 8.0 Hz, 1H), 7.66 (d, *J* = 8.0 Hz, 1H), 7.53 (dd, *J* = 8.0 Hz, 1H), 7.19 (d, *J* = 8.0 Hz, 1H), 4.69 (s, NH).

Synthesis of 8-Nitro-1-acetylnaphthalene (chapter 2, compound 27)

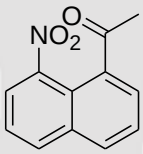

A suspension of $Cu(NO3)_2.3H_2O$, (5.00 g, 20.69 mmol) in 40 ml acetic anhydride was cooled in an ice bath. With constant stirring, a solution of 1-acetylnaphthalene (1 ml, 6.58 mmol) in 40 ml acetic anhydride was slowly added followed by room temperature stirring. After stirring for 10 h at room temperature, the reaction mixture was poured into de-ionized (DI) water, and extracted with diethyl ether (3 x 30 ml) three times. The organic layer was then washed with brine and DI water. The combined organic layer was dried over anhydrous sodium sulfate and filtered. After evaporating the solvent, the residue was purified by column chromatography on silica gel with ethyl acetate in hexane (starting with 10 % upto 25 %) as an eluent to give the title compound as a yellow solid.[5]

Yield: 900 mg (63 %)

HRMS (ESI) *m/z* [$((C_{12}H_8NO_3) + H]^+$: calculated:216.0661, found: 216.0681

5. S. D. Barker, K. Wilson, R. K. Norris, *Aust. J. Chem.* **1995**, *48*, 1969-1979.

^{1}H NMR (400 MHz, $CDCl_3$) δ ppm: 2.75 (s, 3H), 7.59-7.66 (m, 2H), 7.91 (d, *J*=4.0 MHz, 1H), 8.03 (d, *J*=8.0 MHz, 1H), 8.09-8.11 (m, 2H).

Synthesis of *Peri*-Naphthoindigo (PNI)

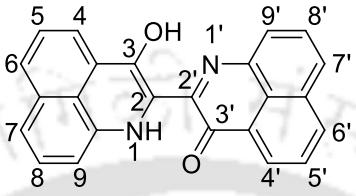

PNI (mono-enol)

Potassium fluoride (406 mg, 6.99 mmol) was added to a solution of 8-nitro-1-acetylnaphthalene (300 mg, 1.39 mmol) and bis-(pinacolato)diboron (708 mg, 2.79 mmol) in ethanol (15 mL). The reaction mixture was refluxed for 16 h in aerial condition. After removal of solvent, the crude mixture was washed with water (3 x 10 mL), cold ethanol (3 x 10 mL) and diethyl ether (3 x 10 mL). The resultant solid was purified by column chromatography using dichloromethane/hexane (1:2 to 2:1) as eluent. PNI was received as blue-green solid.

Yield 113 mg (45 %);

^{1}H NMR (400 MHz, $CDCl_3$) δ 7.16 (d, ^3J = 8.0 Hz, 1H, 9-H), 7.22 (s, 1H, N-H), 7.45-7.52 (m, 2H, 7-, 8-H), 7.66 (dd, ^3J = 8.0 Hz, ^3J = 8.0 Hz, 2H, 5-, 8'-H), 7.79 (dd, ^3J = 8.0 Hz, ^3J = 8.0 Hz, 1H, 5'-H), 7.79 (d, ^3J = 8.0 Hz, 1H, [4/6/7'/9']-H), 7.85 (d, ^3J = 8.0 Hz, 1H, [4/6/7'/9']-H), 7.87 (d, ^3J = 8.0 Hz, 1H, [4/6/7'/9']-H), 8.03 (d, ^3J = 8.0 Hz, 1H, [4/6/7'/9']-H), 8.24 (d, ^3J = 8.0 Hz, 1H, [4'/6']-H), 8.61 (d, ^3J = 8.0 Hz, 1H, [4'/6']-H), 12.49 (br, O-H) ppm

13C NMR (150 MHz, CDCl3) δ 90.8, 107.9, 119.7, 121.1, 122.9, 125.1, 126.5, 126.7, 127.3 (2C), 128.0, 128.1, 128.6, 129.3, 129.4, 130.4, 132.9, 134.2, 135.7, 138.4, 144.0, 153.1, 156.0, 179.5 ppm;

HRMS (ESI):*m/z* calcd for $[C_{24}H_{14}N_2O_2 + H]^+$ 363.1128, experimental: 363.1142.

IR (KBr) 582, 684, 740, 767, 778, 822, 848, 915, 1030, 1053, 1068, 1175, 1198, 1257, 1277, 1331, 1359, 1398, 1424, 1445, 1468, 1516, 1571, 1602, 1621, 1653, 1665, 2920, 3046, 3434 cm^{-1};

Synthesis of Indigo

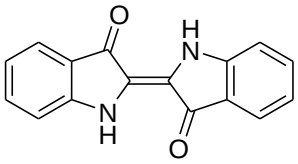

To a solution of 2-nitrobenzaldehyde (1 g, 3.31 mmol) in 10 ml acetone, Taken in a 50-mL single-neck round-bottom flask, an aqueous solution of NaOH (10 %, 2 ml) was added. Followed, the reaction was added with 3 ml water and stirred at room temperature for 8 h. The reaction mixture was purged with air and cooled in an ice-bath. Indigo ppt was collected using vacuum filtration and washed with distilled water, ethanol and diethyl ether successively.[6]

Yield: 0.63 g (62.8 %)

Synthesis of H-NMI (chapter 4)

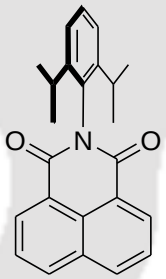

A mixture of 1,8-naphthalic anhydride (1.00 g, 5.02 mmol) and 2,6-diisopropylaniline (3 ml, 15.06 mmol) was refluxed in acetic acid (25 ml) for 12 h. reaction was quenched by adding ice-water (150 ml). The ppt formed was filtered off and washed with water. The resultant solid was purified by column chromatography using 10% ethyl acetate-hexane solvent system. The final product was received as white solid.[7]

Yield: 1.25 g (70 %)

HRMS (ESI):*m/z* calcd for $[C_{24}H_{21}NO_2 + H]^+$ 358.1807, experimental: 358.1829

6. A. Baeyer, V. Drewsen, Ber. Dtsch. Chem. Ges. 1882, 15, 2856-2864.

7. T. Weil, E. Reuther, K. Müllen, *Angew. Chem. Int. Ed.* **2002**, *41*, 1900-1904.

Synthesis of NH_2-NMI (chapter 4)

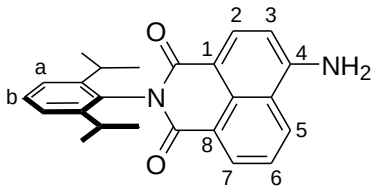

A mixture of 4-nitro-imide (550 mg, 1.367 mmol), $SnCl_2.2H_2O$ (1.542 g, 6.83 mmol), 0.10 ml of conc. HCl were taken refluxed in 15 ml ethanol for 18 h. The yellow ppt. obtained upon cooling the reaction mixture, was filtered out, washed with aqueous Na_2CO_3 and dried under vacuum to obtain the imide as light-yellow solid.

Yield: 360 mg (71 %)

HRMS (ESI) m/z calcd for $[C_{24}H_{24}N_2O_2 + H]^+$ 373.1915, found: 373.1955;

^{1}H NMR (600 MHz, DMSO-*d*$_6$) δ ppm: 1.03-1.04 (m, 12H, methyl-H), 2.60 (m, 2H, C-H), 6.89 (d, ^3J = 8.4 Hz 1H, 3-H), 7.28 (d, ^3J = 7.8 Hz, 2H, a-H), 7.40 (t, ^3J = 7.8 Hz, 1H, b-H), 7.60 (s, 2H, N-H), 7.69 (dd, ^3J = 8.2 Hz, ^3J = 7.6 Hz, 1H, 6-H), 8.23 (d, ^3J = 8.4 Hz, 1H, 2-H) 8.47 (d, ^3J = 7.6 Hz, 1H, 5-H), 8.70 (d, ^3J = 8.2 Hz, 1H, 7-H).

^{13}C NMR (150 MHz, DMSO-*d*$_6$) δ ppm: 23.5, 28.4, 107.1, 108.3, 119.5, 121.6, 123.4, 124.1, 128.6, 129.8, 130.3, 131.5, 131.9, 134.4, 145.3, 153.1, 163.1, 164.1.

Synthesis of $(PNI)_2Pd$ (chapter 5)

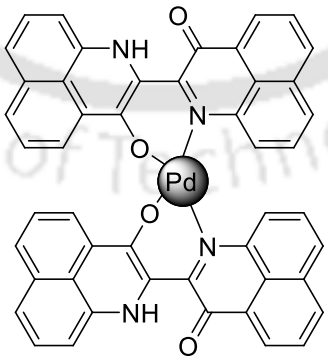

To a solution of PNI (20.0 mg, 0.055 mmol) in 10 ml DCM, 7.0 mg (0.0275 mmol) of $PdCl_2(CH_3CN)_2$ was added portion wise. The reaction mixture was stirred at room temperature for 5 h. The green ppt. obtained was filtered out and washed with 25 ml cold

hexane and 10 ml cold DCM. The resultant solid was dried under high vacuum to obtain the pure compound.

Yield: 16 mg (72 %)

HRMS: (ESI) m/z [((PNI)$_2$Pd) – OH))+ 2Na]$^+$: calculated:872.0992, experimental: 872.0907

^{1}H NMR (400 MHz, CDCl$_3$) δ ppm :7.60 (t, J = 8.0 Hz, 1H), 7.65 (t, J = 8.0 Hz, 1H), 7.76 (t, J = 8.0 Hz, 1H), 7.83 (d, J = 8 Hz, 1H), 7.91 (d, J = 8 Hz, 1H), 7.98 (t, J = 8.0 Hz, 1H), 7.65 (t, J = 8.0 Hz, 1H), 7.60 (t, J = 8.0 Hz, 1H), 8.84 (d, J = 8.0 Hz, 1H), 9.02 (s, 1H, NH) 9.71 (d, J = 8.0 Hz, 1H), 10.20 (d, J = 8.0 Hz, 1H).

IR (KBr) 736.41, 765.1, 823.9, 923.0, 1034.4, 1259.8, 1330.8, 1365.08, 1388.2, 1421.6, 1462.6, 1488.02,1518.4, 1568.3,1655.9, 2853.3, 2922.0, 3050.3, 3446.3 cm^{-1}.

Synthesis of N-methyl lactam (chapter 5)

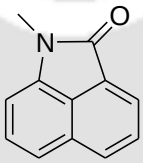

Hexane triturated NaH (55 mg, 1.38 mmol) was loaded into argon filled 2-neck round bottom flask followed by PNI (100 mg, 0.27 mmol). The reaction vessel was cooled with ice-bath and dry THF (5 ml) was added. CH_3I (0.17 ml, 2.75 mmol) was added as THF solution (5ml). At reflux temperature the reaction was continued for 12 h. after cooling down in an ice bath, reaction was quenched by slow addition of water and extracted with DCM (3 x 30 ml) three times. The organic layer was then washed with brine and DI water. The combined organic layer was dried over anhydrous sodium sulfate and filtered. After evaporating the solvent, the residue was purified by column chromatography on silica gel using DCM-hexane (starting with 25 % upto 50 %) as eluent to give the title compound as a yellow solid.

Yield: 27 mg (53 %)

HRMS: (ESI) m/z]$^+$: [($C_{12}H_9NO$) + H^+] calculated:, experimental: 184.0759

^{1}H NMR (400 MHz, $CDCl_3$) δ ppm: 3.45 (s, 3H), 6.89 (d, J = 8.0 Hz, 1H), 7.45 (t, J = 8.0 Hz, 1H), 7.53 (d, J = 8.0 Hz, 1H), 7.71 (t, J = 8 Hz, 1H), 8.00 (d, J = 8 Hz, 1H), 8,.05 (d, J = 8.0 Hz, 1H).

^{13}C NMR (75.5 MHz, $CDCl_3$) δ ppm: 26.3, 104.6, 120.3, 124.2, 125.1, 126.8, 128.6, 128.5, 129.0, 130.7, 140.1, 168.2.

Synthesis of 5-Bromo-1-acetylnaphthalene (chapter 5, compound 5)

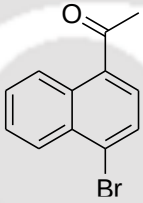

To an ice-cold suspension of $AlCl_3$ (7.17 g, 53.82 mmol) in 50 ml DCM, acetyl chloride (5.12 ml, 71.71 mmol) was added and stirred for 15 min. To this homogenous slurry, a solution of 1-bromonaphthalene (5 ml, 35.88 mmol) in 50 mL of DCM was added. The reaction was stirred at ambient temperature for 15 h. The reaction mixture was poured over ice and concentrated HCl, extracted with DCM, washed with $NaHCO_3$ and brine. After drying over anhydrous sodium sulphate, the solution was concentrated in vacuo and purified by chromatography (ethyl acetate/hexane, 1 % to 5%) to give 1-acetyl-4-bromonaphthalene as a brown oil.[8]

Yield: 6.7 g (75 %)

HRMS (ESI) *m/z* [($C_{12}H_9OBr$) + H^+] : calculated:248.9915, experimental: 248.9395

^{1}H NMR (400 MHz, $CDCl_3$) δ ppm: 2.73 (s, 3H), 7.64-7.66 (m, 2H), 7.73 (d, J = 8.0 Hz, 1H), 7.82 (d, J = 8.0 Hz, 1H), 8.31-8.34 (m, 1H), 8.70-8.73 (m, 1H).

Synthesis of 5-bromo-8-nitro-1-acetylnaphthalene (chapter 5, compound 6)

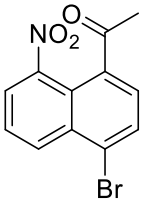

8. E. Dixon, A. Fischer, F. P. Robinso, *Can. J. Chem.* **1981**, 2629-2641.

A suspension of $Cu(NO_3)_2.3H_2O$, (4.00 g, 16.55 mmol) in 40 ml acetic anhydride was cooled in an ice bath. With constant stirring, a solution of 4-bromo1-acetylnaphthalene (1.00 g, 4.5 mmol) in 40 ml acetic anhydride was slowly added followed by room temperature stirring. After stirring for 10 h at room temperature, the reaction mixture was poured into de-ionized (DI) water, and extracted with diethyl ether (3 x 30 ml) three times. The organic layer was then washed with brine and DI water. The combined organic layer was dried over anhydrous sodium sulfate and filtered. After evaporating the solvent, the residue was purified by column chromatography on silica gel with ethyl acetate in hexane (starting with 10 % upto 25 %) as an eluent to give the title compound as a yellow solid.

Yield: 529 mg (45 %)

HRMS (ESI) *m/z* $[(C_{12}H_8NO_3Br) + H^+]$: calculated: 293.9766, found: 293.9459

Synthesis of dibromoPNI (chapter 5, compound 7)

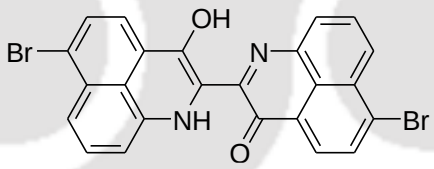

Potassium fluoride (400 mg, 6.85 mmol) was added to a solution of 4-bromo-8-nitro-1-acetylnaphthalene (400 mg, 1.36 mmol) and bis-(pinacolato)diboron (690 mg, 2.72 mmol) in ethanol (15 mL). The reaction mixture was refluxed for 16 h in aerial condition. After removal of solvent, the crude mixture was washed with water (3 x 10 mL), cold ethanol (3 x 10 mL) and diethyl ether (3 x 10 mL). The resultant solid was purified by column chromatography using dichloromethane/hexane (1:2 to 2:1) as eluent. dibromoPNI was received as blue-green solid.

Yield: 240 mg (35 %).

HRMS (ESI) *m/z* $[((C_{24}H_{12}N_2O_2Br_2) – OH) + H]^+$: calculated: 504.9316, found: 504.9372.

7.3 Spectra

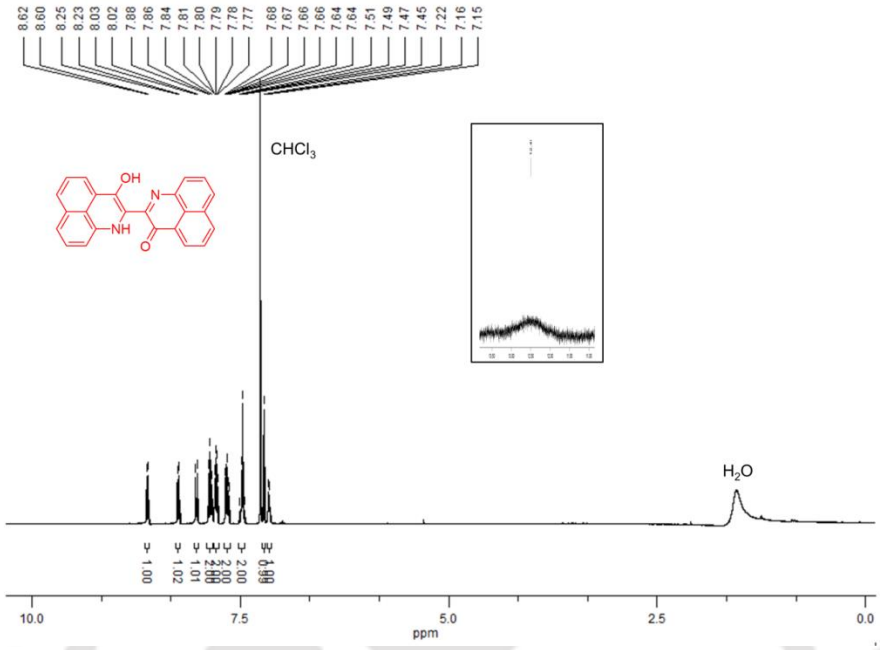

Figure 1.[1]H NMR spectrum of **PNI** (mono-enol) (400 MHz, $CDCl_3$, 295K). Hydroxy proton is shown in inset.

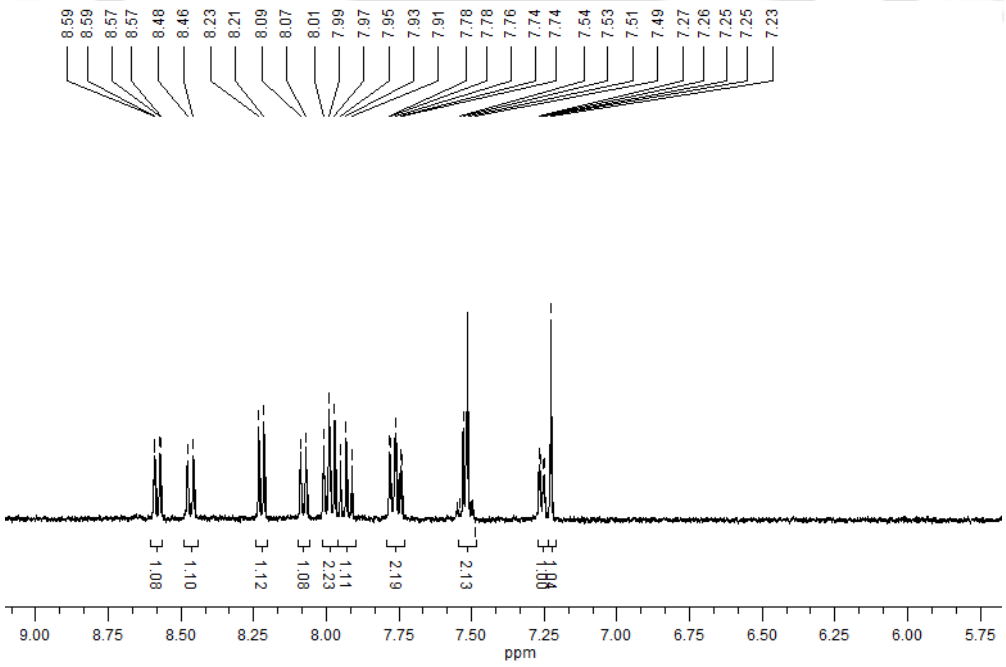

Figure 2. [1]H NMR spectrum of **PNI** (mono-enol) (400 MHz, acetone-d_6, 295K).

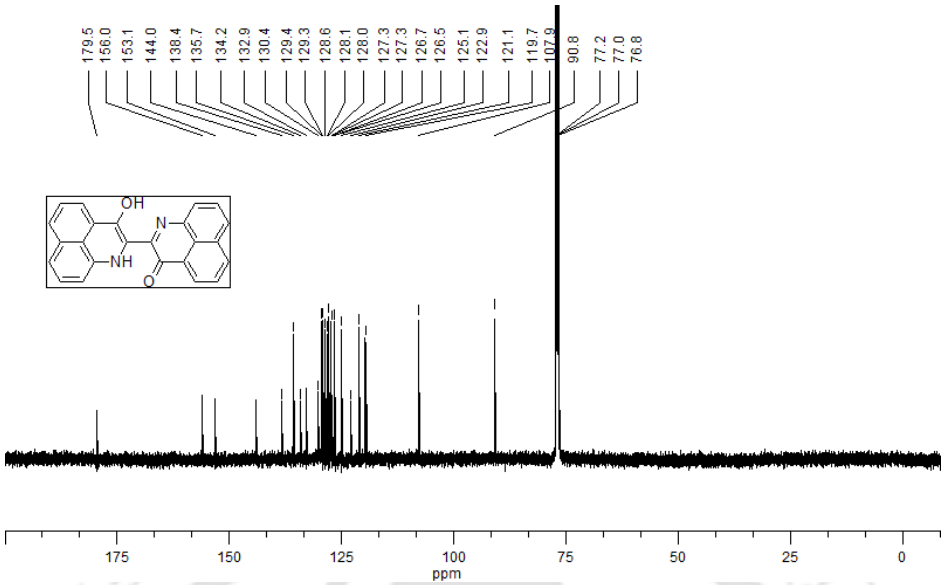

Figure 3. ^{13}C NMR spectrum of **PNI** (150 MHz, $CDCl_3$, 295K).

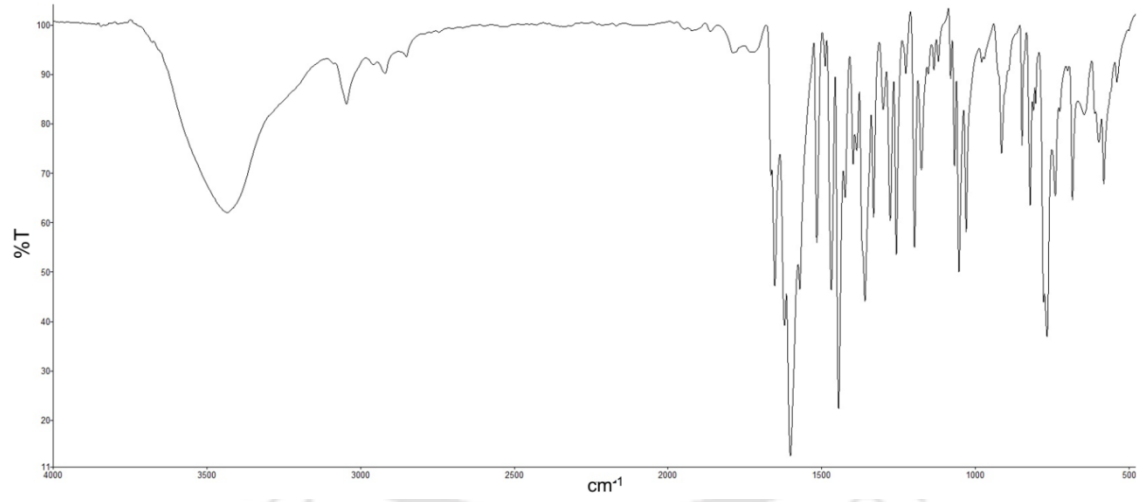

Figure 4. IR (KBr) spectrum of **PNI**.

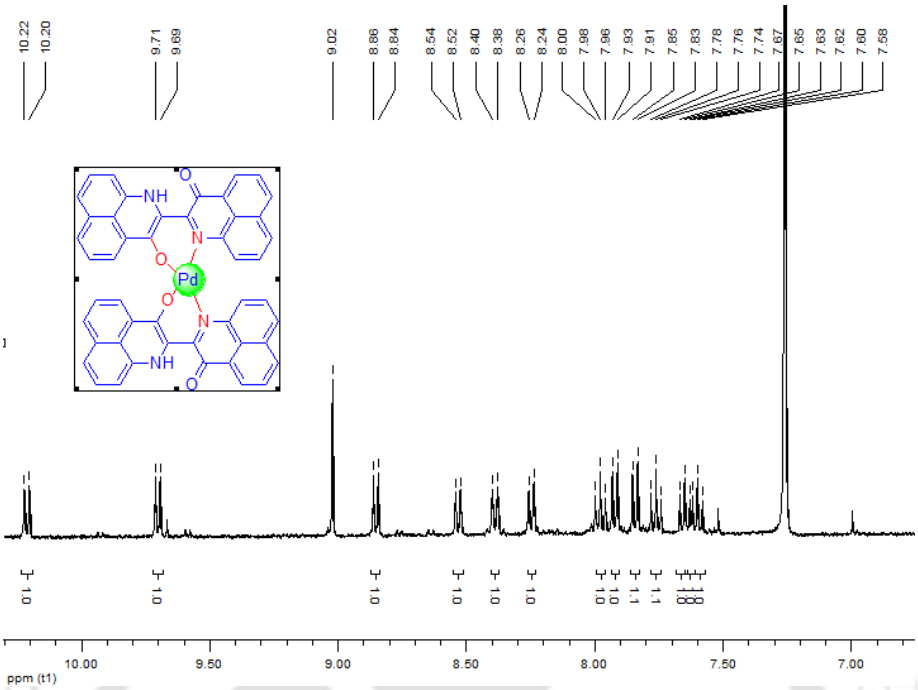

Figure 5. .[1]H NMR spectrum of **(PNI)$_2$Pd** (400 MHz, $CDCl_3$, 295K).

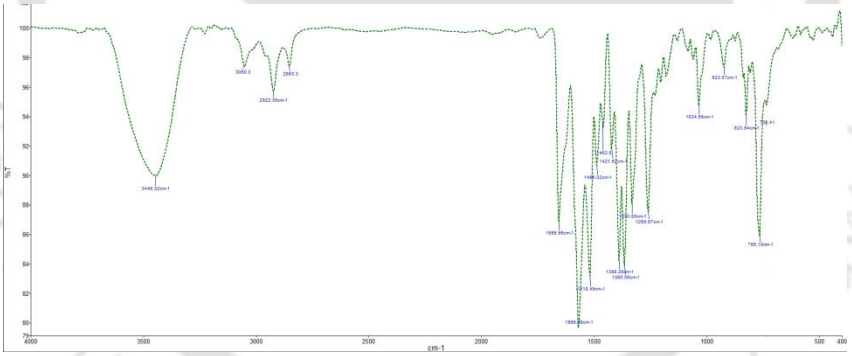

Figure 6. IR (KBr) spectrum of **(PNI)$_2$Pd**.

Annexure

Publications

1. R. J. Das, K. Mahata, "Mutualistic Benefit in the Self-sorted Co-aggregates of peri-Naphthoindigo and a 4-Amino-1,8-Naphthalmide Derivative," *Soft Matter.*, **2019**, *15*, 5282-5286.

2. R. J. Das, K. Mahata, "Synthesis, Photophysical, Electrochemical, and Halochromic Properties of peri-Naphthoindigo," *Org. Lett.*, **2018**, *20*, 5027-5031.

Oral/poster presentation at conference

1. National Conference on Recent Advances in Chemistry (RAC 2019), Department of chemistry, NIT Meghalaya.

2. FICS 2018, Department of chemistry, IIT Guwahati.

3. Chemconvene 2017, Department of chemistry, IIT Guwahati.

Organic LETTERS

Letter

Cite This: Org. Lett. 2018, 20, 5027−5031

pubs.acs.org/OrgLett

Synthesis, Photophysical, Electrochemical, and Halochromic Properties of *peri*-Naphthoindigo

Rashmi J. Das and Kingsuk Mahata*

Department of Chemistry, Indian Institute of Technology Guwahati, Guwahati 781039, India

Supporting Information

ABSTRACT: A facile synthesis of *peri*-naphthoindigo (PNI) was reported for the first time from simple precursor. Installation of a chromophore at the *peri*-position of naphthalene is very unique in terms of synthetic challenges and properties. PNI exists in monoenol form, undergoes halochromism in acidic medium, and displays a wide and strong absorption band (ε = 33390 $M^{-1}cm^{-1}$) with maxima at 632 nm (chloroform). The dye undergoes oxidation and reduction at +0.30 and −0.58 V (vs Fc/Fc^{+}), respectively, in chloroform.

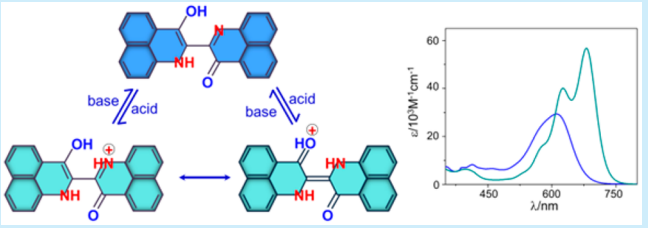

peri-Naphthoindigo (PNI), with potential applications in diverse areas, is an organic dye containing cross-conjugated donor−acceptor (H-chromophore) sandwiched between two naphthalene rings through the *peri*-positions (Figure 1). The

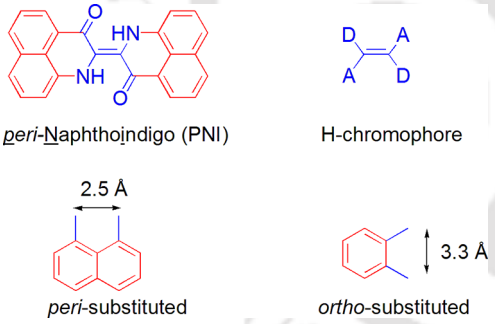

Figure 1. Structure of PNI, H-chromophore, and steric scenarios at the *ortho*- and *peri*-positions.

structure of PNI was proposed for the first time in 1977 by Nathan et al. in a patent claiming it to be a candidate for solar energy applications.[1] A recent theoretical study by Ren and co-workers emphasized PNI as a promising ambipolar organic semiconductor.[2] However, to date, there is no report about the synthesis and properties of this fascinating molecule. On the contrary, analogous compounds with the H-chromophore installed between two *ortho*-substituted benzene rings, namely indigoids, have extensively been studied in the literature. For example, indigo and analogous compounds have been used as vat dye, food colorants, pigments for contact lenses, ambipolar organic semiconductors, and ligands for various metal complexes.[3,4] Thioindigo,[5] *peri*-naphthothioindigo,[6] N,N′-disubstituted indigos,[7] and hemiindigos[8] are known to show photochromic behavior.[9] Hemithioindigos[10] are promising tools in the competitive field of molecular machines.[11]

The unavailability of synthetic methods for PNI can be attributed to different steric scenarios at the *ortho*- vs *peri*-positions. The spatial distance between two *ortho*-protons in an aromatic ring is 3.3 Å, whereas *peri*-protons are separated only by 2.5 Å in naphthalene.[12] Inspired by this fascinating molecule, we accepted the synthetic challenge and herein report for the first time the synthesis, characterization, and photophysical properties of PNI. We have also demonstrated halochromism[13] of the new dye by protonation. Contrary to theoretical predication, PNI exists in monoenol form.

Our pursuit toward PNI was initiated by following Baeyer−Drewsen method for indigo synthesis (Scheme 1a).[14] 1-Naphthaldehyde was nitrated to prepare main precursor **2**,[15]

Scheme 1. Unsuccessful Attempts for the Preparation of PNI

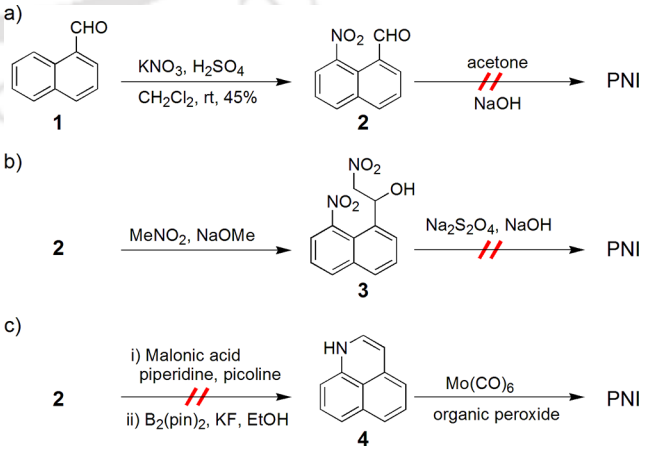

Received: July 12, 2018
Published: August 8, 2018

DOI: 10.1021/acs.orglett.8b02178
Org. Lett. 2018, 20, 5027−5031

which was treated with acetone in the presence of aqueous NaOH to afford PNI. The cross-aldol reaction and subsequent dimerization process was found to be unsuccessful. Rather, a complicated mixture of multiple compounds was received. Changes in base, temperature, strength of base, and sequence of addition were done to overcome the challenge. However, this did not improve the situation either. All efforts to purify the reaction mixture were found to be fruitless.

The Harley-Mason[16] method was employed in our next attempt to prepare PNI, and the synthetic route is summarized in Scheme 1b. The Henry reaction was carried out by treating **2** with nitromethane in the presence of sodium methoxide. The reaction was found to be ineffective. Different conditions were attempted by changing base and temperature. Despite various modifications, crude yield was limited to 20% only. Isolation of pure product from the nitroaldol reaction was difficult, and the crude mixture containing **3** was treated with alkaline sodium dithionite solution to yield PNI. This synthetic route was also found to be unsuccessful. Our next attempt was to prepare compound **4** and subsequent treatment with $Mo(CO)_6$ and organic peroxide to yield PNI via an oxidative coupling reaction.[17] The synthetic method is described in Scheme 1c. Compound **2** was treated with malonic acid followed by B_2pin_2 in the presence of KF for the preparation of **4**.[18] However, the reaction gave a complex mixture without the desired one.

After exhausting several methods known for the preparation of indigo, we followed a new approach to synthesize PNI. Recently, Song et al.[18] reported that 2-nitrostyrene could be converted into indole by using B_2pin_2 and KF under inert conditions. We anticipated a similar cyclization reaction on the enol form of **6** leading to **7** (Scheme 2). Accordingly, precursor

Scheme 2. Synthetic Route of PNI

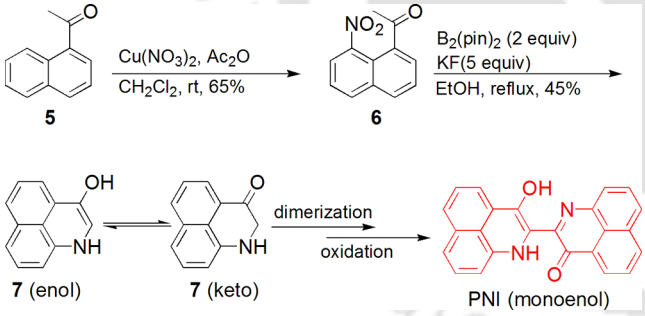

6 was prepared following a known method[15b] and refluxed in ethanol in the presence of B_2pin_2 and KF under inert atmosphere (Scheme 2). Instead of the isolation of **7**, a dark greenish-blue color was received after exposing the reaction mixture overnight. The crude mixture was separated by column chromatography and thoroughly characterized by high-resolution mass spectrometry (HRMS), 1D and 2D NMR, and infrared (IR) spectroscopy.

The HRMS spectrum (see Supporting Information) of the dark turquoise solid showed a peak at m/z = 363.1142, which is assigned to protonated PNI. One additional peak was observed at m/z = 347.1179 after fragmentation. The signal is associated with PNI after cleavage of the hydroxy group from the monoenol isomer (Scheme 2). PNI has better solubility in common organic solvent than that of indigo dye. It was indeed possible to record ^1H and ^{13}C NMR in $CDCl_3$. The proton resonance of PNI showed 12 multiplets in the aromatic region along with a sharp singlet at 7.22 ppm and a broad peak at 12.49 ppm (Figure S1). No other peak was noticed in between 0.00 and 13.00 ppm. This can be explained by considering the monoenol form of PNI, in which all aromatic protons are magnetically different. The sharp singlet at 7.22 ppm is assigned to N−H, while a broad peak is attributed to hydroxyl proton. Absence of signal for aliphatic proton established the involvement of methyl group in the reaction via enolization and subsequent conversion into endocyclic double bond. In order to eliminate possibility of merger of any peak with residual chloroform, ^1H NMR was recorded in acetone-d_6 (Figure S2). The spectrum was found to be similar to the one recorded in $CDCl_3$. Connectivity among the multiplets was verified by $^1H-^1H$ correlation spectroscopy (COSY). The COSY spectrum and cross peak correlation among the multiplets is shown in Figure 2. A doublet at 7.16 ppm is

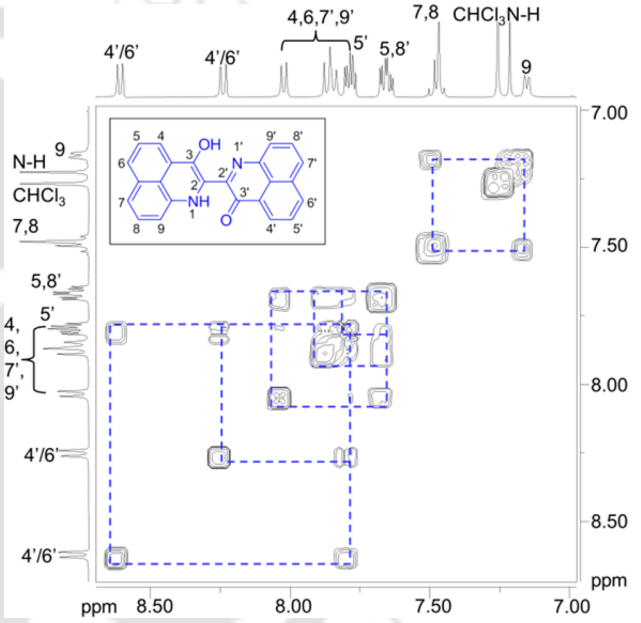

Figure 2. $^1H-^1H$ COSY (400 MHz, 295 K) spectrum of PNI in $CDCl_3$.

assigned to C9-H. The magnetic resonance of C7,8-H was observed together as multiplet at 7.45−7.52 ppm. The low-field doublets at 8.24 and 8.61 ppm are associated with C4′,6′-H. Their correlated cross peak was observed as doublet of doublets (dd) at 7.79 ppm and attributed to C5′-H. Signals for the remaining two benzene rings were observed as four doublets at 7.79, 7.85, 7.87, and 8.03 ppm (4,6,7′,9′-H) and two dd at 7.66 ppm (5,8′-H). Their cross peak correlation was also found to be in agreement with the structure. Further proof of the proposed structure was received from ^{13}C NMR (Figure S4). Twenty-four peaks were observed in between 90.8 and 179.5 ppm. The downfield signal at 179.5 ppm is assigned to the carbonyl group. The presence of the keto group was also confirmed by IR spectroscopy (Figure S9). The stretching vibration of C=O was detected near 1602 cm^{-1}. The broad signal at 3440 cm^{-1} with a shoulder can be associated with the stretching vibration of N−H and O−H. Comparison with the IR frequency of indigo dye (Figure S10) showed a notable difference at around 1172, 1126, 1067, 712, and 563 cm^{-1}, all of which are characteristic of five-membered rings in indigo.[19] Complete disappearance of the peaks around 1126, 712, and

DOI: 10.1021/acs.orglett.8b02178
Org. Lett. 2018, 20, 5027−5031

563 cm^{-1} and very weak signals at around 1172 and 1067 cm^{-1} suggested the absence of a five-membered ring in PNI. A very weak signal at around 1068 cm^{-1} can be attributed to the rocking vibration of C═O. All other signals associated with aromatic C−C, C−H, endocyclic double bond, C−N, and N−H appeared in line with that of indigo dye. To gain insight into the geometry of PNI, solid-state structures would be undoubtedly desirable. Unfortunately, all efforts directed toward the generation of diffractable single crystals proved to be unsuccessful.

The formation of PNI occurred through a series of reaction and was dependent on several factors. Hence, attention was given to various parameters to receive optimum yield. Our initial goal was to carry out cyclization of **6** and isolate **7**. However, under the reaction conditions, **7** underwent dimerization (Figure S8) and subsequent oxidation (possibly during work up) leading to PNI. Such dimerization and oxidation is indeed known in indigo prepration.[20] Since oxidation is an important step in the sequence, we also carried out the reaction under open air atmosphere as well as in pure oxygen. The yield was improved significantly from 21% under N_2 atmosphere to 65% in air. However, the yield was decreased to 12% in pure oxygen. A similar trend was noticed in case of indigo synthesis.[20] We performed the reaction by changing base, solvent and other conditions (Table S1). The best outcome (65%) was achieved when ethanol was used as solvent and KF as base in air. Other bases like NaOH and ^{t}BuOK produced PNI in negligible yield. The aldol reaction was possibly the major reaction in the presence of NaOH. The best result in alcohol can be attributed to stabilization of the enol form of **6**. The other vital step in the synthesis is B_2pin_2-mediated cyclization of **6** to **7**. Different reagents,[21] known for similar cyclization, were employed. However, reaction of **6** with $P(OEt)_3/K_2CO_3$ at 170 ^{o}C did not produce PNI. The reagents and conditions for PNI production were found to be very specific. Treatment of *o*-nitroacetophenone with B_2pin_2 and KF in ethanol did not produce indigo at all. A different steric scenario at the *peri*-position compared to the *ortho*-position was possibly the reason for such an outcome.[12] This also explains our initial failure described in Scheme 1.

Photophysical properties of PNI were investigated and summarized in Table 1. The solution of PNI in chloroform exhibits turquoise color, and the absorption spectrum (Figure 3b) features a broad maximum at around 632 nm with a very strong allowed transition (ε = 33390 M^{-1} cm^{-1}). Compared to indigo, PNI exhibits wider absorption as full width at half maxima of the dye (2964 cm^{-1}) was found to be more than that of indigo (2210 cm^{-1}). Furthermore, the absorption maxima shows bathochromic shift by 29 nm (Table 1). The absorption property of PNI in chloroform remained the same even at various concentrations (1 × 10^{-3} mol L^{-1} to 1 × 10^{-5} mol L^{-1}), ruling out the possibility of any aggregation (Figure S12). Solvent-dependent investigation showed (Figure S11) absorption maxima ranging from 611 nm (MeCN, blue in color) to 632 nm ($CHCl_3$). However, the spectral characteristic remained same, excluding the existence of diketo isomer. Photoluminescence spectrum of PNI in chloroform (Figure S15) showed broad emission with maxima at around 736 nm and Stokes shift of 2235 cm^{-1}, which was found to be longer than that of indigo (1080 cm^{-1}). The relative photoluminescence quantum yield of PNI was measured to be 0.003 in THF. The low quantum yield is common in phenyl analogue compounds.[22]

Table 1. Photophysical Properties of PNI, Indigo, and PNIH$^+$

compd	solvent	λ_{abs} [a] (nm)	λ_{em} [b] (nm)	ε [c] ($M^{-1}cm^{-1}$)
PNI	$CHCl_3$	632	736	33390
PNI	CH_3CN	611	739	29390
indigo	$CHCl_3$	603	645	15940
$PNIH^+$	$CHCl_3$	698		67965
$PNIH^+$	CH_3CN	681		56815

[a]Absorption maxima. [b]Emission maxima. [c]Molar absorption coefficient at experimental λ_{abs}.

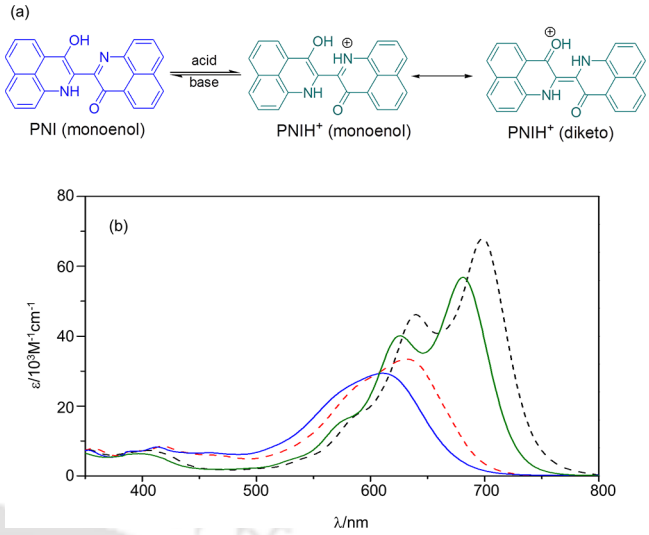

Figure 3. (a) Halochromism of PNI. (b) Absorption spectra (293 K, $c \approx 10^{-5}$ mol L^{-1}) of PNI in chloroform (red, dash), acetonitrile (blue, solid), and $PNIH^+$ in chloroform (black, dash), acetonitrile (olive, solid).

Redox properties of PNI were investigated in chloroform by cyclic voltammetry technique. The dye undergoes oxidation and reduction at +0.30 V and −0.58 V (vs Fc/Fc^+), respectively (Figure S16). The electrochemical features are similar to that one observed for indigo in thin film.[23] However, both redox processes are easier in case of PNI. From the electrochemical data, the energy gap between highest occupied molecular orbital (HOMO) and lowest unoccupied molecular orbital (LUMO) was measured to be 0.88 eV.

Taking advantage of the structural feature of monoenol PNI, halochromism[13] was installed, and the process was monitored by UV−vis spectroscopy. Upon addition of trifluoroacetic acid to a solution of PNI in chloroform, absorption maxima (Figure 3b, Table 1) shifted bathochromically to 698 nm with an increase in color intensity (ε = 67965 M^{-1} cm^{-1}). Such bathochromic shift associated with protonation is known in indigo[24] and other dyes.[13a] The protonation process is reversible and the initial spectrum can be recovered simply by addition of base (NaOH, NH_4OH). The halochromism process was observed in other solvent (acetonitrile) as well as in the presence of different acids (acetic acid, HCl). Sulfuric acid was avoided as it is known to produce sulfonated product in analogous dye.[24] In acetonitrile, halochromism was visible even in naked eye as color changed from blue to turquoise. The spectroscopic signature (Figure 3b) was similar to that one observed in chloroform. Structure of the protonated dye

DOI: 10.1021/acs.orglett.8b02178
Org. Lett. 2018, 20, 5027−5031

($PNIH^+$) was confirmed by ^1H NMR spectroscopy. Proton resonance of $PNIH^+$ in CD_3CN (Figure S5) displayed three singlet at 6.53, 11.31, and 12.87 ppm (associated with O−H, N−H, and proton at imine nitrogen) along with signals for 12 aromatic hydrogens. The protonated PNI was found to be nonemissive.

In summary, we have successfully reported for the first time the synthesis and characterization of PNI from a simple precursor. A change in the surroundings of the chromophore marks a huge difference in property as well as in synthetic difficulty. The common synthetic methods known for indigo did not work for PNI. On the other hand, indigo cannot be prepared by the method described for PNI. The dye exists in monoenol form, possibly due to better conjugation than the diketo isomer, and has good solubility in common organic solvents. PNI has a strong and wide absorption band. PNI shows halochromism upon protonation. The process is marked by bathochromically shifted maxima (by 66 nm) with an increase in color intensity. Because of the diverse chemistry of naphthalene, PNI will give new dimension to the indigoids' chemistry and the reversible halochromism will contribute significantly to stimuli-responsive molecular switches.[25]

■ ASSOCIATED CONTENT

Supporting Information

The Supporting Information is available free of charge on the ACS Publications website at DOI: 10.1021/acs.orglett.8b02178.

Synthetic details; NMR, HRMS, IR, absorption, photoluminescence spectra, etc. (PDF)

■ AUTHOR INFORMATION

Corresponding Author

*E-mail: kingsuk@iitg.ac.in.

ORCID

Kingsuk Mahata: 0000-0001-8453-2650

Notes

The authors declare no competing financial interest.

■ ACKNOWLEDGMENTS

R.J.D. thanks IIT Guwahati for a fellowship. We thank the Department of Chemistry and the Central Instrumental Facility (CIF), Indian Institute of Technology Guwahati, for various instrumental facilities.

■ REFERENCES

(1) Nathan, R. A.; Schwerzel, R. E.; Adelman, A. H.; Wyant, R. E. U.S. Patent 4004572, 1977.

(2) Zhang, S.-F.; Chen, X.-K.; Fan, J.-X.; Ren, A.-M. *Org. Electron.* **2015**, *24*, 12−25.

(3) (a) Ferber, K. H. *J. Environ. Pathol., Toxicol. Oncol.* **1987**, *7*, 73−83. (b) Irimia-Vladu, M.; Głowacki, E. D.; Troshin, P. A.; Schwabegger, G.; Leonat, L.; Susarova, D. K.; Krystal, O.; Ullah, M.; Kanbur, Y.; Bodea, M. A.; Razumov, V. F.; Sitter, H.; Bauer, S.; Sariciftci, N. S. *Adv. Mater.* **2012**, *24*, 375−380. (c) Głowacki, E. D.; Voss, G.; Sariciftci, N. S. *Adv. Mater.* **2013**, *25*, 6783−6800. (d) Newsome, A. G.; Culver, C. A.; van Breemen, R. B. *J. Agric. Food Chem.* **2014**, *62*, 6498−6511. (e) Gsänger, M.; Bialas, D.; Huang, L.; Stolte, M.; Würthner, F. *Adv. Mater.* **2016**, *28*, 3615−3645. (f) Jiang, Y.; Gao, Y.; Tian, H.; Ding, J.; Yan, D.; Geng, Y.; Wang, F. *Macromolecules* **2016**, *49*, 2135−2144. (g) Jiang, Y.; Zheng, X.; Deng, Y.; Tian, H.; Ding, J.; Xie, Z.; Geng, Y.; Wang, F. *Angew. Chem., Int. Ed.* **2018**, *57*, 10283−10287.

(4) (a) Wu, J.-Y.; Chang, C.-H.; Thanasekaran, P.; Tsai, C.-C.; Tseng, T.-W.; Lee, G.-H.; Peng, S.-M.; Lu, K.-L. *Dalton. Trans.* **2008**, 6110−6112. (b) Bhattacharya, D.; Chang, C.-H.; Cheng, Y.-H.; Lai, L.-L.; Lu, H.-Y.; Lin, C.-Y.; Lu, K.-L. *Chem. - Eur. J.* **2012**, *18*, 5275−5283. (c) Mondal, P.; Das, A.; Lahiri, G. K. *Inorg. Chem.* **2016**, *55*, 1208−1218. (d) Mondal, P.; Chatterjee, M.; Paretzki, A.; Beyer, K.; Kaim, W.; Lahiri, G. K. *Inorg. Chem.* **2016**, *55*, 3105−3116. (e) Konarev, D. V.; Zorina, L. V.; Khasanov, S. S.; Shestakov, A. F.; Fatalov, A. M.; Otsuka, A.; Yamochi, H.; Kitagawa, H.; Lyubovskaya, R. N. *Inorg. Chem.* **2018**, *57*, 583−589. (f) Chatterjee, M.; Ghosh, P.; Beyer, K.; Paretzki, A.; Fiedler, J.; Kaim, W.; Lahiri, G. K. *Chem. - Asian J.* **2018**, *13*, 118−125.

(5) (a) Friedländer, P. *Ber. Dtsch. Chem. Ges.* **1906**, *39*, 1060−1069. (b) Dinescu, L.; Lemieux, R. P. *Adv. Mater.* **1999**, *11*, 42−45. (c) Jacquemin, D.; Preat, J.; Wathelet, V.; Fontaine, M.; Perpète, E. A. *J. Am. Chem. Soc.* **2006**, *128*, 2072−2083. (d) Rondão, R.; Seixas de Melo, J. S. *J. Phys. Chem. C* **2013**, *117*, 603−614. (e) Dittmann, M.; Graupner, F. F.; Maerz, B.; Oesterling, S.; de Vivie-Riedle, R.; Zinth, W.; Engelhard, M.; Lüttke, W. *Angew. Chem., Int. Ed.* **2014**, *53*, 591−594. (f) Boice, G.; Patrick, B. O.; McDonald, R.; Bohne, C.; Hicks, R. *J. Org. Chem.* **2014**, *79*, 9196−9205.

(6) (a) Irie, M.; Ishida, H.; Tsujioka, T. *Jpn. J. Appl. Phys.* **1999**, *38*, 6114−6117. (b) Cherepy, N. J.; Sanner, R. D. *Opt. Mater.* **2006**, *28*, 1350−1354.

(7) (a) Giuliano, C. R.; Hess, L. D.; Margerum, J. D. *J. Am. Chem. Soc.* **1968**, *90*, 587−594. (b) Nuñez, A.; Hollebeek, T.; Labes, M. M. *J. Am. Chem. Soc.* **1992**, *114*, 4925−4926. (c) Farka, D.; Scharber, M.; Głowacki, E. D.; Sariciftci, N. S. *J. Phys. Chem. A* **2015**, *119*, 3563−3568. (d) Huang, C.-Y.; Bonasera, A.; Hristov, L.; Garmshausen, Y.; Schmidt, B. M.; Jacquemin, D.; Hecht, S. *J. Am. Chem. Soc.* **2017**, *139*, 15205−15211.

(8) Petermayer, C.; Thumser, S.; Kink, F.; Mayer, P.; Dube, H. *J. Am. Chem. Soc.* **2017**, *139*, 15060−15067.

(9) Petermayer, C.; Dube, H. *Acc. Chem. Res.* **2018**, *51*, 1153−1163.

(10) (a) Wiedbrauk, S.; Maerz, B.; Samoylova, E.; Reiner, A.; Trommer, F.; Mayer, P.; Zinth, W.; Dube, H. *J. Am. Chem. Soc.* **2016**, *138*, 12219−12227. (b) Kink, F.; Collado, M. P.; Wiedbrauk, S.; Mayer, P.; Dube, H. *Chem. - Eur. J.* **2017**, *23*, 6237−6243. (c) Huber, L. A.; Hoffmann, K.; Thumser, S.; Böcher, N.; Mayer, P.; Dube, H. *Angew. Chem., Int. Ed.* **2017**, *56*, 14536−14539. (d) Zweig, J. E.; Newhouse, T. R. *J. Am. Chem. Soc.* **2017**, *139*, 10956−10959.

(11) (a) Kay, E. R.; Leigh, D. A.; Zerbetto, F. *Angew. Chem., Int. Ed.* **2007**, *46*, 72−191. (b) Coskun, A.; Banaszak, M.; Astumian, R. D.; Stoddart, J. F.; Grzybowski, B. A. *Chem. Soc. Rev.* **2012**, *41*, 19−30. (c) Erbas-Cakmak, S.; Leigh, D. A.; McTernan, C. T.; Nussbaumer, A. L. *Chem. Rev.* **2015**, *115*, 10081−10206. (d) Leigh, D. A. *Angew. Chem., Int. Ed.* **2016**, *55*, 14506−14508.

(12) Balasubramaniyan, V. *Chem. Rev.* **1966**, *66*, 567−641.

(13) (a) Singh, P.; Baheti, A.; Thomas, K. R. J. *J. Org. Chem.* **2011**, *76*, 6134−6145. (b) Cai, K.; Yan, Q.; Zhao, D. *Chem. Sci.* **2012**, *3*, 3175−3182. (c) Matsui, K.; Segawa, Y.; Itami, K. *Org. Lett.* **2012**, *14*, 1888−1891. (d) Kundu, P. K.; Olsen, G. L.; Kiss, V.; Klajn, R. *Nat. Commun.* **2014**, *5*, 3588. (e) Maeda, T.; Würthner, F. *Chem. Commun.* **2015**, *51*, 7661−7664. (f) Black, H. T.; Pelse, I.; Wolfe, R. M. W.; Reynolds, J. R. *Chem. Commun.* **2016**, *52*, 12877−12880.

(14) Baeyer, A.; Drewsen, V. *Ber. Dtsch. Chem. Ges.* **1882**, *15*, 2856−2864.

(15) (a) Spiteller, G.; Derkosch, J. *Monatsh. Chem.* **1959**, *90*, 634−644. (b) Barker, S. D.; Wilson, K.; Norris, R. K. Aust. *Aust. J. Chem.* **1995**, *48*, 1969−1979. (c) Strazzolini, P.; Giumanini, A. G.; Runcio, A. *Tetrahedron Lett.* **2001**, *42*, 1387−1389.

(16) Harley-Mason, J. *J. Chem. Soc.* **1950**, 2907.

(17) (a) Yamamoto, Y.; Inoue, Y.; Takaki, U.; Suzuki, H. *Bull. Chem. Soc. Jpn.* **2011**, *84*, 82−89. (b) Watanabe, M.; Uemura, N.; Ida, S.; Hagiwara, H.; Goto, K.; Ishihara, T. *Tetrahedron* **2016**, *72*, 4280−4287.

(18) Yang, K.; Zhou, F.; Kuang, Z.; Gao, G.; Driver, T. G.; Song, Q. *Org. Lett.* **2016**, *18*, 4088−4091.
(19) (a) Baran, A.; Fiedler, A.; Schulz, H.; Baranska, M. *Anal. Methods* **2010**, *2*, 1372−1376. (b) Amat, A.; Rosi, F.; Miliani, C.; Sgamellotti, A.; Fantacci, S. *J. Mol. Struct.* **2011**, *993*, 43−51.
(20) Russell, G. A.; Kaupp, G. *J. Am. Chem. Soc.* **1969**, *91*, 3851−3859.
(21) Llona-Minguez, S.; Desroses, M.; Ghassemian, A.; Jacques, S. A.; Eriksson, L.; Isacksson, R.; Koolmeister, T.; Stenmark, P.; Scobie, M.; Helleday, T. *Chem. - Eur. J.* **2015**, *21*, 7394−7398.
(22) de Melo, J. S. S.; Rondão, R.; Burrows, H. D.; Melo, M. J.; Navaratnam, S.; Edge, R.; Voss, G. *ChemPhysChem* **2006**, *7*, 2303−2311.
(23) Klimovich, I. V.; Leshanskaya, L. I.; Troyanov, S. I.; Anokhin, D. V.; Novikov, D. V.; Piryazev, A. A.; Ivanov, D. A.; Dremova, N. N.; Troshin, P. A. *J. Mater. Chem. C* **2014**, *2*, 7621−7631.
(24) Nicholls-Allison, E. C.; Nawn, G.; Patrick, B. O.; Hicks, R. G. *Chem. Commun.* **2015**, *51*, 12482−12485.
(25) Klajn, R. *Chem. Soc. Rev.* **2014**, *43*, 148−184.

DOI: 10.1021/acs.orglett.8b02178
Org. Lett. 2018, 20, 5027−5031

Soft Matter

PAPER

View Article Online
View Journal | View Issue

Cite this: *Soft Matter*, 2019, **15**, 5282

Mutualistic benefit in the self-sorted co-aggregates of *peri*-naphthoindigo and a 4-amino-1,8-naphthalimide derivative†

Rashmi Jyoti Das and Kingsuk Mahata *

Received 4th March 2019,
Accepted 6th June 2019

DOI: 10.1039/c9sm00454h

rsc.li/soft-matter-journal

Photoluminescence enhancement for all the members of a self-sorted co-aggregate was observed for the first time by successfully amalgamating AIEE and social self-sorting. Intermolecular H-bonding and π–π stacking were utilised to prepare several co-aggregates of *peri*-naphthoindigo (PNI) and a 4-amino-1,8-naphthalimide derivative dye, NH_2-NMI. In the heteromeric aggregates, photoluminescence intensities were increased by 28% for the imide and more than 400% for PNI. Due to spectral overlap between the emission of the imide and the absorption of PNI, energy transfer took place from the former to the latter. The heteromeric aggregates are dual emissive and the relative intensities of the emissions can easily be tuned by varying the stoichiometry of the dyes.

Introduction

Social self-sorting[1] or high fidelity non-self-recognition is a universal phenomenon that has multifaceted appearances in Nature. In chemistry, social self-sorting is defined as a process in which two or more different molecules prefer to assemble with other(s) instead of themselves. Such a specific co-assembly process provides an opening to structural diversity in the resultant aggregate(s). Unsurprisingly, social self-sorting has been a topic of research among scientists over the last few decades.[1–5] The principle has been exploited to fabricate a wide variety of multi-component complex molecular architectures.[2–7] Considering structural diversity, the research in social self-sorting has been quite successful. But, the functional aspect of the self-sorting algorithm is still very inadequate. Only in recent years, Schmittel[8] and others[9] utilised the sorting protocol to assemble various molecular machines. The concept of self-sorting has also been extended to molecular cybernetics[10] and light emitting materials. In an exciting paper, Stang *et al.* showed that the photoluminescence property of a molecule was significantly enhanced in heteromeric aggregates compared to the monomeric form.[11] Similar observations were reported by a few other groups.[12,13] These examples are promising, but the numbers are still very low. Furthermore, there is no example where photoluminescence intensities have been increased for all the components of co-aggregates prepared by social self-sorting, although in social networking practiced in Nature, every participating member benefits.[14] Molecular social self-sorting thus requires additional dimensions to enhance its diversity and application potential.

Photoluminescence enhancement of a molecule occurs when contributions from nonradiative decay pathways are reduced. This is normally done by imposing a restriction in molecular rotation and/or vibration through aggregation or crystallisation. Photoluminescence enhancement due to restriction in intramolecular motion is a well-known phenomenon and the concept has been studied extensively over the last two decades.[15,16] The principle of aggregation-induced enhanced emission (AIEE) has been utilised in diverse areas including bioscience, energy, medicine, optics and electronics.[17] Judicious application of the AIEE concept in social self-sorting would lead to enhancement of emission of all the entities involved in a co-assembly. However, amalgamation of these two independent concepts needs masterful design. Every component involved in a co-aggregate generated *via* the social self-sorting process should have provision for photoluminescence enhancement in the aggregate. Successful installation of the two independent concepts would give another benefit in terms of Förster resonance energy transfer (FRET), if there is spectral overlap between the absorbance of one component and emission of the other.

To observe a photoluminescence enhancement in a self-sorted multi-component co-assembly, we decided to use *peri*-naphthoindigo (PNI) as one partner (Chart 1). PNI is an ambipolar dye in which four functional groups are sandwiched between two naphthalene rings *via peri*-positions. Although the structure of the dye was proposed several decades ago in a patent,[18] its synthesis was reported recently for the first time by us.[19] Unlike the anticipated

Department of Chemistry, Indian Institute of Technology Guwahati, Assam 781039, India. E-mail: kingsuk@iitg.ac.in

† Electronic supplementary information (ESI) available: NMR, absorption, and photoluminescence spectra, FESEM images. See DOI: 10.1039/c9sm00454h

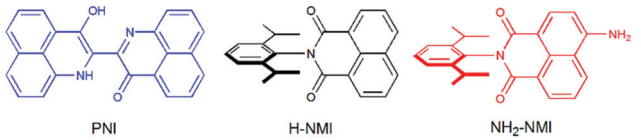

Chart 1 Structures of molecules used for co-assembly processes.

diketo isomer,[18,20] PNI exists in monoenol form. Due to the special structural feature, PNI has potential to show emission enhancement in the aggregated form. Another reason to choose PNI is its unique photophysical properties. The dye emits in the near-infrared region with the maximum at 736 nm (in $CHCl_3$). Enhancement of emission in the bio-optical region is very much in demand for various applications.[21] PNI also absorbs in a broad region, which gives it a good chance to fulfil criteria for the FRET process. The second partner for the co-assembly process must be complementary to PNI. Accordingly, we chose two naphthalene monoimide based dyes, H-NMI and NH_2-NMI (Chart 1). In this communication, we have explored various social self-sorting processes involving the dyes and reported for the first time the mutual enhancement of emission in the self-sorted co-aggregates of NH_2-NMI and PNI. In the heteromeric aggregates of the two dyes, emissions were increased by more than 5 times for PNI and 1.28 fold for the imide. Additionally, energy transfer took place from the imide to PNI.

Results and discussion

We first explored the self-assembly process of PNI by varying solvent polarity as well as concentration. PNI was found to be in the aggregated form in DMSO only at a very high concentration ($c \approx 20$ mmol L^{-1}). Switching from the monomer to the aggregate could be detected using ^{1}H NMR spectroscopy (Fig. S3, ESI†). But, it was not possible to observe the change by UV-vis spectroscopy (Fig. S7, ESI†). The high concentration demand limited our scope for photophysical property investigations. To overcome this problem, we considered a solvent system in which self-assembly is possible even at a very low concentration. As PNI is an ambipolar dye, its aggregation property can easily be tuned by changing the solvent polarity. The functional groups in the molecule do not like nonpolar solvents, while naphthalene rings avoid polar solvents. We investigated the effect of increased polarity by dissolving the dye in DMSO and subsequently adding water into the solution. It was indeed possible to observe the self-assembly process at a very low concentration ($c \approx 5 \times 10^{-6}$ mol L^{-1}) in a mixture of DMSO and H_2O (v/v = 1 : 9). Aggregate formation in the solution was confirmed by UV-vis spectroscopy. A red shifted shoulder at 690 nm along with diminished molar extinction coefficient at the maximum (632 nm) proved the self-assembly process (Fig. S8, ESI†). To avoid unfavourable interactions between the hydrophobic naphthalene rings of PNI and water molecules, aggregation occurred even at a low concentration. Emission of PNI was found to be quenched completely in the DMSO–water mixture. Vibrational energy transfer to water molecules probably diminished the emission. As our goal was to observe a photoluminescence enhancement,

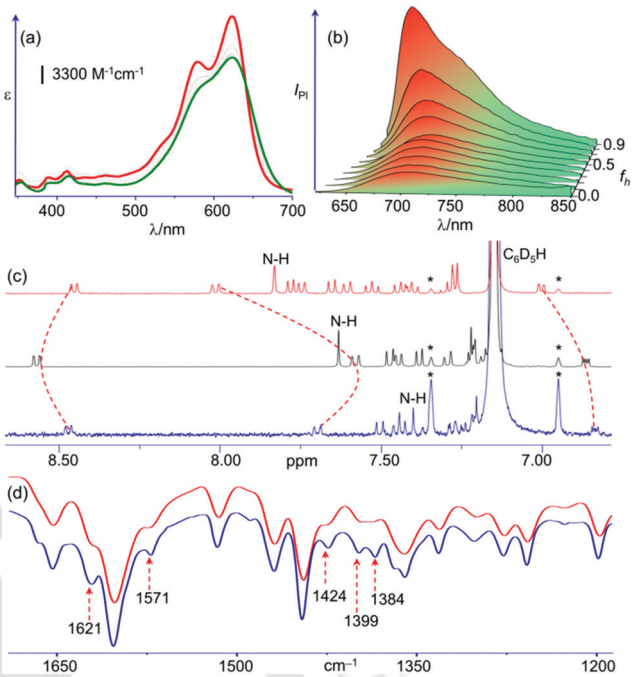

Fig. 1 (a) Absorption spectra of PNI in THF (green) and in a mixture (red) of THF/*n*-hexane (v/v = 1 : 9). (b) Photoluminescence (Pl) spectra of PNI in THF and in mixtures of THF and *n*-hexane. Emission maximum gradually blue shifted with an increase in f_h. (c) ^{1}H NMR (400 MHz, 295 K) spectra of PNI in C_6D_6 (black), THF/C_6D_6 (red) and *n*-hexane/C_6D_6 (blue); satellite peaks are marked with asterisks. (d) Comparison of IR spectra of PNI monomer (red) and aggregate (blue).

a different solvent combination was needed. In the next set of experiments, we reduced the polarity of the solvent by gradual addition of *n*-hexane to a THF solution of PNI and the process was investigated using UV-vis spectroscopy. The absorption spectra became vibronically resolved when the volume fraction of *n*-hexane (f_h) reached 0.9 (Fig. 1a). Additionally, there was an increase in molar extinction coefficient at the absorption maximum. A restriction in intramolecular motion through aggregation possibly caused such changes. UV-vis absorption property investigations (Fig. S12, ESI†), at different concentrations (1×10^{-6} mol L^{-1} to 1×10^{-3} mol L^{-1}) in THF/*n*-hexane (v/v = 1 : 9), suggested the formation of larger aggregates at higher concentration, marked by a decreased molar extinction co-efficient. Unlike the studies mentioned earlier, the PNI-aggregate was found to be emissive in a mixture of THF and *n*-hexane. A comparison of photoluminescence properties of PNI in different fractions of THF and *n*-hexane is shown in Fig. 1b. With an increase in f_h, emission intensity gradually increased, and at $f_h = 0.9$, a more than 6 fold enhancement was recorded. The observations confirmed the aggregation-induced photoluminescence enhancement of PNI. In addition to the amplified photoluminescence, there was a gradual hypsochromic shift of the emission maximum with an increase in f_h. Such a decrease in Stokes shift also supported rigidification of the structure *via* aggregation. The self-assembly process of PNI was further established from ^{1}H NMR investigations. We measured the ^{1}H NMR spectra of PNI in three different solvent systems, C_6D_6 : THF (v/v = 1 : 2), C_6D_6 and C_6D_6 : *n*-hexane (v/v = 1 : 1). Almost all the

proton signals changed with variation in polarity (Fig. 1c). For example, the N–H signal experienced an upfield shift of 0.43 ppm going from the most polar solvent combination C_6D_6-THF to the least polar system C_6D_6/*n*-hexane. All these observations confirmed the aggregation process of PNI. The self-assembly process was further corroborated using infrared (IR) spectroscopy. For the same purpose, bulk solid and ordered aggregates of PNI were isolated by evaporating THF and THF/*n*-hexane (v/v = 1 : 9) solutions of the dye. The IR spectra of the two samples were notably different (Fig. 1d). Significant changes were observed at around 1384, 1399, 1424, 1571 and 1621 cm^{-1}. Peaks were broad in the bulk solid, but became sharp in the ordered aggregates. Powder X-ray diffraction (PXRD) patterns of the two different solids were compared to see the differences in intermolecular arrangement. The presence of more signals in the PXRD pattern (Fig. S6, ESI†) of the solid generated from THF/*n*-hexane (v/v = 1 : 9) confirmed the existence of highly ordered intermolecular arrangements *via* the self-assembly process. The nature of the morphology generated in the self-assembly process was investigated by field emission scanning electron microscopy (FESEM). The FESEM image of the aggregate on a surface, prepared by drop-casting a solution of PNI in THF/*n*-hexane (v/v = 1 : 9), showed the formation of well-defined microcrystalline cuboid architectures (Fig. 2). The height and width of the cuboids were found to be in the range of 50–500 nm. In length, the aggregates were extended up to several microns. The self-assembly process can be explained by considering intermolecular H-bond formation and subsequent stacking. With a decrease in solvent polarity, unfavorable interactions between the polar functional groups and non-polar solvents increased. To avoid the same, intermolecular H-bonding took place resulting in the formation of a one dimensional (1D) sheet-like morphology. The chromophore part was further masked by a brick wall type stacking of the sheets, producing 3D cuboid architectures. The overall process is summarised in Fig. 2.

Our next objective was to prepare a self-sorted co-aggregate of PNI and naphthalene monoimide H-NMI (Chart 1).[22] In a two-component system, self-sorting is often enabled by installing steric control, which prevents homomeric aggregation of one and forces the other partner to produce a heteromeric assembly.[23] We followed a similar strategy here. A bulky group was introduced into the imide position in H-NMI to prevent homomeric aggregate formation of the same. We checked the self-assembly potential of H-NMI in solution and monitored the process using UV-vis spectroscopy. The naphthalimide displayed absorption maximum at 343 nm in THF/*n*-hexane (v/v = 1 : 9) and the spectra remained the same even at various concentrations (Fig. S10, ESI†), suggesting the inability of H-NMI towards self-aggregation in the specified solvent system. We then investigated the co-self-assembly process of the imide with PNI. To obtain the heteromeric aggregate, PNI and H-NMI were mixed in a 10 : *n* (*n* = 1, 2,. . .,5) molar ratio in THF, followed by addition of *n*-hexane to make the final f_h 0.9. Similar to the self-aggregation of PNI, the absorption spectrum of the co-assembly process was found to be vibronically resolved (Fig. 3a). But, a major change was noticed between 300 and 450 nm (Fig. 3a). Besides an increase in molar absorptivity near the absorption maximum of H-NMI, there occurred significant changes around the absorption of PNI. Furthermore, the absorption spectrum of the co-assembly process appeared to be different than the mathematical summation of the spectra of self-assembled PNI and monomeric H-NMI, which confirmed the formation of a heteromeric aggregate and excluded the possibility of a mixture of monomeric H-NMI and the homomeric PNI-aggregate. A FESEM image (Fig. 3b) of the co-assembly process shows a ribbon-shaped aggregate, which was generated *via* sandwiching of H-NMI into the 1D sheets of PNI (Fig. S27, ESI†). The heteromeric aggregates were found to be several hundred micrometres long. The uniform morphology confirmed the exclusive formation of heteromeric aggregates. Photoluminescence of PNI in the co-assembly process was increased in a similar fashion as observed in the case of homomeric aggregation (Fig. S16, ESI†). The heteromeric aggregates can be prepared either in a single step, as mentioned above, or in a stepwise manner by adding NMI to the self-assembled PNI in THF/*n*-hexane (v/v = 1 : 9). The outcomes were found to be the same in both cases. The naphthalimide remained non-emissive in the monomeric form as well as in the aggregate. Because of the very rigid structure of H-NMI, there was no scope for emission enhancement and the outcome was indeed unsurprising. To observe an emission enhancement for every component, modification was needed for the imide.

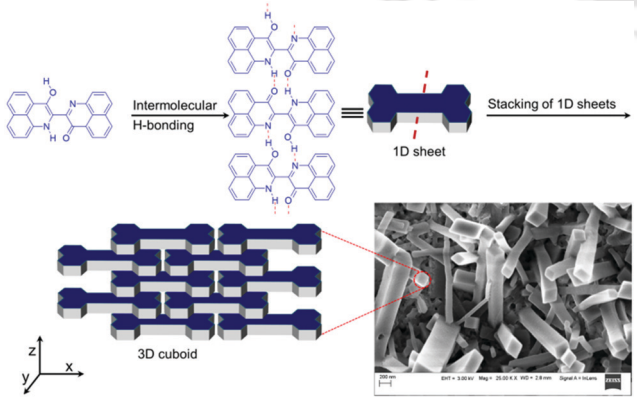

Fig. 2 Stepwise self-assembly process of PNI along with FESEM image of the aggregates.

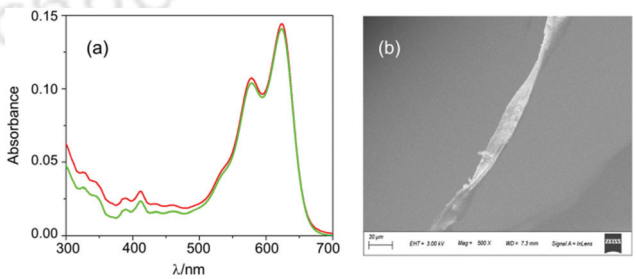

Fig. 3 (a) Experimental (red) and hypothetical (green) absorption spectra of a co-aggregate of PNI and H-NMI (10 : 2 molar ratio). Hypothetical spectrum was calculated by adding absorption spectra of homomeric aggregate of PNI and monomeric H-NMI in 10 : 2 molar ratio. (b) FESEM image of heteromeric aggregate of PNI and H-NMI.

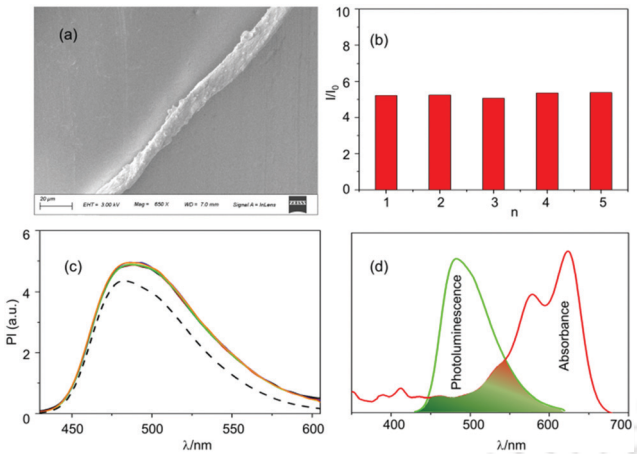

Fig. 4 (a) FESEM image of heteromeric aggregate of PNI and NH_2-NMI. The sample was prepared by mixing PNI and NH_2-NMI in a 10 : 1 molar ratio. (b) Photoluminescence enhancement of PNI in the co-aggregates (PNI/NH_2-NMI = 10 : *n*). (c) Photoluminescence spectra of NH_2-NMI in monomer (black, dashed) and in co-aggregates (coloured, solid) in THF/*n*-hexane (v/v = 1 : 9). (d) Spectral overlap between the emission spectrum of NH_2-NMI (green) and the absorption spectrum of PNI (red).

To achieve our final goal, the mutual enhancement of emission for every component in a social self-sorting process, we introduced an amino group at the 4-position of naphthalimide and prepared NH_2-NMI (Chart 1).[24] The amino group was incorporated for two reasons. Restriction in rotation of the amino group might give enhanced emission in the resultant co-aggregate. Spectral overlap between the emission of NH_2-NMI and the absorption of PNI would give a chance for energy transfer. Concentration dependent studies of the imide did not result in any change in absorption spectra (Fig. S11, ESI†). Investigation of the co-assembly process of NH_2-NMI with PNI revealed a similar outcome, *i.e.* the formation of ribbon-shaped heteromeric aggregates (Fig. 4a) *via* self-sorting. Time-resolved photoluminescence spectroscopy revealed an improved lifetime, from 8.24 ns in the monomer to 8.84 ns in the co-assembled aggregate, for the imide dye. A comparative study of photoluminescence intensity showed a 1.28-fold enhancement for NH_2-NMI and more than 5-fold enhancement for PNI in the co-assembled aggregate (Fig. 4b and c). We then focused on the FRET process in the co-aggregate as there is spectral overlap between the emission of the imide and the absorption of PNI (Fig. 4d). The energy transfer process was investigated by exciting at the absorption maximum of NH_2-NMI and recording the steady-state emission of PNI. It was indeed possible to detect enhanced emission of PNI at 657 nm after excitation of the heteromeric aggregate at the absorption maximum of the imide (410 nm). It is necessary to mention that the homomeric aggregate of PNI shows weak emission after excitation at 410 nm. This observation proved the successful energy transfer from the imide to PNI (Fig. S19, ESI†). However, the FRET process was not quantitative and dual emission was observed after excitation at 410 nm. The relative intensities of the dual emission can easily be tuned simply by changing the stoichiometry of the dyes (Fig. S20, ESI†).

Conclusions

In summary, we have successfully amalgamated AIEE and social self-sorting. Both the imides, H-NMI and NH_2-NMI, can exclusively form heteromeric aggregates with PNI *via* a sorting process. But, the perfect pair for the merger of AIEE and social self-sorting was NH_2-NMI and PNI. Photoluminescence intensities were increased by up to 28% for the imide and more than 400% for PNI in the co-assemblies of the two dyes. Although PNI can exhibit AIEE alone, NH_2-NMI needs support from PNI to enhance its photoluminescence intensity. Due to spectral overlap between the emission of NH_2-NMI and the absorption of PNI, energy transfer took place from the former dye to the latter. This model can be useful for efficient energy harvesting due to greater coverage of the solar spectrum *via* multi-component assembly and energy funneling.[25] The dual emissive nature of the co-aggregates of PNI and NH_2-NMI will be useful for various photoluminescence-based applications.

Conflicts of interest

The authors declare no competing financial interests.

Acknowledgements

We thank the Science and Engineering Research Board, Government of India for financial support (SB/FT/CS-184/2013). RJD thanks IIT Guwahati for her doctoral fellowship. We are grateful to the Department of Chemistry and the Central Instrumental Facility, Indian Institute of Technology Guwahati, for various instrumental facilities.

References

1 (*a*) A. Wu and L. Isaacs, *J. Am. Chem. Soc.*, 2003, **125**, 4831–4835; (*b*) L. Isaacs, *Acc. Chem. Res.*, 2014, **47**, 2052–2062.
2 (*a*) P. Mukhopadhyay, A. Wu and L. Isaacs, *J. Org. Chem.*, 2004, **69**, 6157–6164; (*b*) N. Tomimasu, A. Kanaya, Y. Takashima, H. Yamaguchi and A. Harada, *J. Am. Chem. Soc.*, 2009, **131**, 12339–12343; (*c*) W. Jiang, Q. Wang, I. Linder, F. Klautzsch and C. A. Schalley, *Chem. – Eur. J.*, 2011, **17**, 2344–2348; (*d*) M. J. Mayoral, C. Rest, J. Schellheimer, V. Stepanenko and G. Fernández, *Chem. – Eur. J.*, 2012, **18**, 15607–15611; (*e*) L. Li, H.-Y. Zhang, J. Zhao, N. Li and Y. Liu, *Chem. – Eur. J.*, 2013, **19**, 6498–6506; (*f*) K. Han, D. Go., T. Tigges, K. Rahimi, A. J. C. Kuehne and A. Walther, *Angew. Chem., Int. Ed.*, 2017, **56**, 2176–2182; (*g*) S. Díaz-Cabrera, Y. Dorca, J. Calbo, J. Aragó, R. Gómez, E. Ortí and L. Sánchez, *Chem. – Eur. J.*, 2018, **24**, 2826–2831; (*h*) H. M. Coubrough, S. C. C. van der Lubbe, K. Hetherington, A. Minard, C. Pask, M. J. Howard, C. F. Guerra and A. J. Wilson, *Chem. – Eur. J.*, 2019, **25**, 785–795.
3 (*a*) R. Joseph, A. Nkrumah, R. J. Clark and E. Masson, *J. Am. Chem. Soc.*, 2014, **136**, 6602–6607; (*b*) T. Rama, A. Blanco-Gómez, I. Neira, O. Domarco, M. D. García, J. M. Quintela and C. Peinador, *Chem. – Eur. J.*, 2017, **23**, 16743–16747;

(*c*) Y.-S. Wang., T. Feng., Y.-Y. Wang, F. E. Hahn and Y.-F. Han, *Angew. Chem., Int. Ed.*, 2018, **57**, 15767–15771; (*d*) M. Raeisi, K. Kotturi, I. del Valle, J. Schulz, P. Dornblut and E. Masson, *J. Am. Chem. Soc.*, 2018, **140**, 3371–3377.

4 (*a*) S. Klotzbach and F. Beuerle, *Angew. Chem., Int. Ed.*, 2015, **54**, 10356–10360; (*b*) D. Beaudoin, F. Rominger and M. Mastalerz, *Angew. Chem., Int. Ed.*, 2017, **56**, 1244–1248.

5 (*a*) M. M. Safont-Sempere, G. Fernández and F. Würthner, *Chem. Rev.*, 2011, **111**, 5784–5814; (*b*) L. E. Buerkle and S. J. Rowan, *Chem. Soc. Rev.*, 2012, **41**, 6089–6102; (*c*) M. L. Saha, S. Neogi and M. Schmittel, *Dalton Trans.*, 2014, **43**, 3815–3834; (*d*) Q. Ji, R. C. Lirag and O. Š. Miljanić, *Chem. Soc. Rev.*, 2014, **43**, 1873–1884; (*e*) Z. He., W. Jiang and C. A. Schalley, *Chem. Soc. Rev.*, 2015, **44**, 779–789; (*f*) W. M. Bloch and G. H. Clever, *Chem. Commun.*, 2017, **53**, 8506–8516; (*g*) N. Sinha and F. E. Hahn, *Acc. Chem. Res.*, 2017, **50**, 2167–2184; (*h*) L. R. Holloway, P. M. Bogie and R. J. Hooley, *Dalton Trans.*, 2017, **46**, 14719–14723; (*i*) F. Beuerle and B. Gole, *Angew. Chem., Int. Ed.*, 2018, **57**, 4850–4878; (*j*) M. Mastalerz, *Acc. Chem. Res.*, 2018, **51**, 2411–2422.

6 (*a*) A. Wu, A. Chakraborty, J. C. Fettinger, R. A. Flowers II and L. Isaacs, *Angew. Chem., Int. Ed.*, 2002, **41**, 4028–4031; (*b*) W. Jiang, H. D. F. Winkler and C. A. Schalley, *J. Am. Chem. Soc.*, 2008, **130**, 13852–13853; (*c*) K. Osowska and O. Š. Miljanić, *J. Am. Chem. Soc.*, 2011, **133**, 724–727; (*d*) S. Onogi, H. Shigemitsu, T. Yoshii, T. Tanida, M. Ikeda, R. Kubota and I. Hamachi, *Nat. Chem.*, 2016, **8**, 743–752; (*e*) H. A. M. Ardoña, E. R. Draper, F. Citossi, M. Wallace, L. C. Serpell, D. J. Adams and J. D. Tovar, *J. Am. Chem. Soc.*, 2017, **139**, 8685–8692; (*f*) P. Pramanik, D. Ray, V. K. Aswal and S. Ghosh, *Angew. Chem., Int. Ed.*, 2017, **56**, 3516–3520; (*g*) W. Drożdż, C. Bouillon, C. Kotras, S. Richeter, M. Barboiu, S. Clément, A. R. Stefankiewicz and S. Ulrich, *Chem. – Eur. J.*, 2017, **23**, 18010–18018; (*h*) E. R. Cross, S. Sproules, R. Schweins, E. R. Draper and D. J. Adams, *J. Am. Chem. Soc.*, 2018, **140**, 8667–8670.

7 (*a*) S. Ulrich and J.-M. Lehn, *J. Am. Chem. Soc.*, 2009, **131**, 5546–5559; (*b*) K. Mahata, M. L. Saha and M. Schmittel, *J. Am. Chem. Soc.*, 2010, **132**, 15933–15935; (*c*) A. M. Johnson and R. J. Hooley, *Inorg. Chem.*, 2011, **50**, 4671–4673; (*d*) M. L. Saha and M. Schmittel, *J. Am. Chem. Soc.*, 2013, **135**, 17743–17746; (*e*) T. K. Ronson, D. A. Roberts, S. P. Black and J. R. Nitschke, *J. Am. Chem. Soc.*, 2015, **137**, 14502–14512; (*f*) P. Howlader and P. S. Mukherjee, *Chem. Sci.*, 2016, **7**, 5893–5899.

8 (*a*) S. De, S. Pramanik and M. Schmittel, *Angew. Chem., Int. Ed.*, 2014, **53**, 14255–14259; (*b*) M. Schmittel, *Chem. Commun.*, 2015, **51**, 14956–14968; (*c*) S. K. Samanta, A. Rana and M. Schmittel, *Angew. Chem., Int. Ed.*, 2016, **55**, 2267–2272.

9 (*a*) P. Waelés, B. Riss-Yaw and F. Coutrot, *Chem. – Eur. J.*, 2016, **22**, 6837–6845; (*b*) L. Zhiquan, H. Xie, S. E. Border, J. Gallucci, R. Z. Pavlović and J. D. Badjić, *J. Am. Chem. Soc.*, 2018, **140**, 11091–11100.

10 M. Schmittel, *Isr. J. Chem.*, 2019, **59**, 197–208.

11 X. Yan, T. R. Cook, P. Wang, F. Huwang and P. J. Stang, *Nat. Chem.*, 2015, **7**, 342–348.

12 Q. Zhao, Y. Chen, S.-H. Li and Y. Liu, *Chem. Commun.*, 2018, **54**, 200–203.

13 (*a*) W.-C. Geng, Y.-C. Liu, Y.-Y. Wang, Z. Xu, Z. Zheng, C.-B. Yang and D.-S. Guo, *Chem. Commun.*, 2017, **53**, 392–395; (*b*) J.-Y. Chen, G. Kadam, A. Gupta, Anuradha, S. V. Bhosale, F. Zheng, C.-H. Zhou, B.-H. Jia, D. S. Dalal and J.-L. Li, *Chem. – Eur. J.*, 2018, **24**, 14668–14678.

14 D. Umberson and J. K. Montez, *J. Health Soc. Behav.*, 2010, **51**(suppl), S54–S66.

15 J. Luo, Z. Xie, J. W. Y. Lam, L. Cheng, H. Chen, C. Qiu, H. S. Kwok, X. Zhan, Y. Liu, D. Zhu and B. Z. Tang, *Chem. Commun.*, 2001, 1740–1741.

16 (*a*) Y. Hong, J. W. Y. Lam and B. Z. Tang, *Chem. Commun.*, 2009, 4332–4353; (*b*) Z. He, C. Ke and B. Z. Tang, *ACS Omega*, 2018, **3**, 3267–3277; (*c*) H.-T. Feng, Y.-X. Yuan, J.-B. Xiong, Y.-S. Zheng and B. Z. Tang, *Chem. Soc. Rev.*, 2018, **47**, 7452–7476.

17 (*a*) Z. Zhao, J. W. Y. Lam and B. Z. Tang, *J. Mater. Chem.*, 2012, **22**, 23726–23740; (*b*) Z. Chi, X. Zhang, B. Xu, X. Zhou, C. Ma, Y. Zhang, S. Liu and J. Xu, *Chem. Soc. Rev.*, 2012, **41**, 3878–3896; (*c*) J. Mei, Y. Hong, J. W. Y. Lam, A. Qin, Y. Tang and B. Z. Tang, *Adv. Mater.*, 2014, **26**, 5429–5479; (*d*) J. L. Banal, B. Zhang., D. J. Jones, K. P. Ghiggino and W. W. H. Wong, *Acc. Chem. Res.*, 2017, **50**, 49–57; (*e*) F. Hu, S. Xu and B. Liu, *Adv. Mater.*, 2018, **30**, 1801350; (*f*) G. Feng and B. Liu, *Acc. Chem. Res.*, 2018, **51**, 1404–1414; (*g*) J. Li and K. Pu, *Chem. Soc. Rev.*, 2019, **48**, 38–71.

18 R. A. Nathan, R. E. Schwerzel, A. H. Adelman and R. E. Wyant, *US Pat.*, 4004572, 1977.

19 R. J. Das and K. Mahata, *Org. Lett.*, 2018, **20**, 5027–5031.

20 S.-F. Zhang, X.-K. Chen, J.-X. Fan and A.-M. Ren, *Org. Electron.*, 2015, **24**, 12–25.

21 (*a*) J. O. Escobedo, O. Rusin, S. Lim and R. M. Strongin, *Curr. Opin. Chem. Biol.*, 2010, **14**, 64–70; (*b*) L. Yuan, W. Lin, K. Zheng, L. He and W. Huang, *Chem. Soc. Rev.*, 2013, **42**, 622–661; (*c*) Z. Guo, S. Park, J. Yoon and I. Shin, *Chem. Soc. Rev.*, 2014, **43**, 16–29; (*d*) H. Chen., B. Dong, Y. Tang and W. Lin, *Acc. Chem. Res.*, 2017, **50**, 1410–1422.

22 (*a*) T. Weil, E. Reuther and K. Müllen, *Angew. Chem., Int. Ed.*, 2002, **41**, 1900–1904; (*b*) F. Nolde, J. Qu, C. Kohl, N. G. Pschirer, E. Reuther and K. Müllen, *Chem. – Eur. J.*, 2005, **11**, 3959–3967; (*c*) W. Zhang, Y. Xu, M. Hanif, S. Zhang, J. Zhou, D. Hu, Z. Xie and Y. Ma, *J. Phys. Chem. C*, 2017, **121**, 23218–23223.

23 K. Mahata and M. Schmittel, *J. Am. Chem. Soc.*, 2009, **131**, 16544–16554, and references cited therein.

24 A. Boehm, H. Schmeisser, S. Becker and K. Müllen, *Ger. Offen.*, DE19940708 A1 20010301, 2001.

25 (*a*) R. Ziessel and A. Harriman, *Chem. Commun.*, 2011, **47**, 611–631; (*b*) C. Kreisbeck and A. Aspuru-Guzik, *Chem. Sci.*, 2016, **7**, 4174–4183; (*c*) T. Mirkovic, E. E. Ostroumov, J. M. Anna, R. van Grondelle, Govindjee and G. D. Scholes, *Chem. Rev.*, 2017, **117**, 249–293.